Identification of Novel Synaptic Components by Transcriptome Profiling of the Murine Neuromuscular Junction

Inauguraldissertation

zur
Erlangung der Würde eines Doktors der Philosophie
vorgelegt der
Philosophisch-Naturwissenschaftlichen Fakultät
der Universität Basel

von

Martin Weihrauch

aus Deutschland

Basel, 2019

Genehmigt von der Philosophisch-Naturwissenschaftlichen Fakultät
auf Antrag von

Prof. Dr. Christoph Handschin
Prof. Dr. Markus A. Rüegg

Basel, den 15.10.2019

Prof. Dr. Martin Spiess
Dekan der Philosophisch-Naturwissenschaftlichen Fakultät

Table of contents

Abstract

The neuromuscular junction (NMJ) has been studied for over a century, yet we still do not have a complete picture of all its structural and functional components, knowledge of which is paramount in devising treatment strategies for neuromuscular diseases. Previous microarray-based approaches aimed at elucidating novel NMJ components were hindered by technological limitations. Recent technological advancements propelled next-generation RNA-sequencing with its wider dynamic range to the forefront of transcriptome-level gene expression profiling.

We utilized laser-capture microdissection to isolate myonuclei underlying the NMJ combined with RNA-sequencing and successfully generated NMJ gene expression profiles of fast-twitch *extensor digitorum longus* (EDL) and slow-twitch *soleus* (SOL) muscles and identified a large number of potential novel NMJ genes. The expression levels of canonical NMJ genes were nearly identical between the EDL and SOL, which suggests that the core NMJ gene program might be well conserved between different skeletal muscle types. We used *in vivo* muscle electroporation to overexpress one of our candidate genes, the transcription factor T-box 21 (TBX21), in the *tibialis anterior* (TA) muscle and observed an increased density of postsynaptic acetylcholine receptors. TBX21 may thus represent a novel transcription factor contributing to the regulation of the NMJ gene program, with a role in postsynaptic sensitivity.

We also generated NMJ gene expression profiles of the TA muscle of 10-month-old ("young") and 30-month-old ("old") mice to investigate the effect of aging on the NMJ gene program. Strikingly, the NMJ gene program was remarkably stable, with nearly identical expression levels of canonical NMJ genes between young and old mice. This implies that age-related perturbations of the NMJ are likely caused by external factors, such as accumulated myofiber damage and changes in nerve input, rather than by gradual dysregulation of the NMJ gene program with increasing age. Our findings argue against the hypothesis that aging

leads to a broad deterioration of the NMJ gene program that would contribute to perturbations of NMJ structure and function.

Furthermore, functional annotation analysis of our different NMJ gene expression datasets strongly indicates the importance of an extensive number of hitherto unknown glycoproteins, as well as of posttranslational modifications, especially glycosylations, at the synaptic basal lamina. We highlight a set of candidate genes that encode for enzymes putatively involved in these processes at the NMJ, and which are potentially involved in the pathophysiology of neuromuscular diseases such as congenital myasthenic syndromes. This thesis expands our understanding of the complexity of the NMJ and lays the foundation for further research that will functionally characterize novel synaptic components and provide the basis for novel therapeutic treatment strategies.

List of Abbreviations

α-BTX	α-Bungarotoxin
AAV	Adeno-associated virus
ACHE	Acetylcholinesterase
AChR	Acetylcholine receptor
ActRII	Myostatin/activin type II receptor
AKT1S1/PRAS40	Proline-rich AKT1 substrate 1
Akt/PKB	Protein Kinase B; Serine-Threonine Protein Kinase
AMPK	AMP-activated protein kinase
APOE	Apolipoprotein E
APLP2	Amyloid beta (A4) precursor-like protein 2
AQP4	Aquaporin 4
ARHGEF3/XPLN	Rho guanine nucleotide exchange factor (GEF) 3
ATP	Adenosine triphosphate
ATPase	Adenosine triphosphate hydrolase
ATP5D	ATP synthase subunit delta, mitochondrial
ATAC-seq	Assay for Transposase-Accessible Chromatin using sequencing
autoLPC	Automated laser-pressure catapulting
BDNF	Brain-derived neurotrophic factor
BP	Biological process (Gene Ontology term)
B4GALNT3	Beta-1,4-N-acetyl-galactosaminyl transferase 3
BSA	Bovine serum albumin
CC	Cellular component (Gene Ontology term)
CCND1	Cyclin D1
cDNA	Complementary DNA
CHPF	Chondroitin polymerizing factor 1
CHPF2	Chondroitin polymerizing factor 2
CHRNE	Cholinergic receptor, nicotinic, epsilon polypeptide
CKMT2	Creatine kinase, mitochondrial 2

CMS	Congenital myasthenic syndrome
ColQ	Acetylcholinesterase collagenic tail peptide
CPM	Counts per million
CR	Caloric restriction
CRYM	Crystallin, mu
CSA	Cross-sectional area
CT	Control group
DAPI	4′,6-diamidino-2-phenylindole
DAVID	Database for Annotation, Visualization and Integrated Discovery
D-BSSE	Department of Biosystems Science and Engineering
DCN	Decorin
DEPTOR	DEP domain-containing mTOR-interacting protein
DGC	Dystrophin-associated glycoprotein complex
DAGK	Diacylglycerol kinase
DAGKZ	Diacylglycerol kinase zeta
DHPR	Dihydropyridine receptor
DLK1	Delta like non-canonical Notch ligand 1
DMD	Dystrophin
Dok-7/Dok7	Docking protein 7
DPAGT1	Dolichyl-phosphate (UDP-N-acetylglucosamine) N-acetylglucosaminephosphotransferase 1
DSHB	Developmental Studies Hybridoma Bank
ECM	Extracellular matrix
EDL	*Extensor digitorum longus* muscle
eGFP	Enhanced green fluorescent protein
EIF4E	Eukaryotic translation initiation factor 4E
EIF4EBP1/4E-BP1	Eukaryotic translation initiation factor 4E binding protein 1
EtOH	Ethanol
ETV5/ERM	ETS variant 5; Ets-Related Protein ERM
EX	Resistance-exercise group
FDR	False discovery rate

FNDC5	Fibronectin type III domain-containing protein 5
FoxO	Forkhead-box-protein
GABPα	GA repeat binding protein alpha
GABPβ	GA repeat binding protein beta
GAS	*Gastrocnemius* muscle
GC	Glucocorticoids
GDNF	Glial cell line derived neurotrophic factor
GEF	Guanine nucleotide exchange factor
GFPT1	Glutamine-fructose-6-phosphate transaminase 1
GO	PANTHER Gene Ontology Enrichment
GTP	Guanosine triphosphate
GTPase	Guanosine triphosphate hydrolase
H2-Aa	Histocompatibility 2, class II antigen A, alpha
HPRT	Hypoxanthine guanine phosphoribosyl transferase
HSPG	Heparan sulfate proteoglycan
HS6ST	Heparan sulfate 6-O-sulfotransferase (Drosophila)
HS6ST1	Heparan sulfate 6-O-sulfotransferase 1
HS6ST2	Heparan sulfate 6-O-sulfotransferase 2
IDH2	Isocitrate dehydrogenase 2, mitochondrial
IFITM10	Interferon induced transmembrane protein 10
IFN-γ	Interferon gamma
IGF-1	Insulin-like growth factor 1
IGF-2	Insulin-like growth factor 2
IGFBP2	Insulin-like growth factor binding protein 2
IL-1β	Interleukin-1 beta
IL-6	Interleukin-6
KEGG	Kyoto Encyclopedia of Genes and Genomes
LAT1/SLC7A5	Solute carrier family 7 (cationic amino acid transporter, y+ system), member 5
LC3	Microtubule-associated protein 1A/1B-light chain 3
logCPM	Log2-transformed counts per million

LPAAT	Lysophosphatidic acid acyltransferases
LRP4	Low-density lipoprotein receptor-related protein 4
MAFbx/Atrogin-1	F-box protein 32
MARP	Muscle ankyrin repeat protein
MAPKAP1/mSIN1	Mitogen-activated protein kinase associated protein 1
MDa	Megadalton
MDS	Multidimensional scaling
MF	Molecular function (Gene Ontology term)
MLST8	Mammalian lethal with SEC13 protein 8
MMP2	Matrix metallopeptidase 2
MND	Myonuclear domain
MPB	Muscle protein synthesis
MPS	Muscle protein breakdown
MSTN	Myostatin
mTOR	Mammalian/mechanistic target of rapamycin
mTORC1	Mammalian target of rapamycin complex 1
mTORC2	Mammalian target of rapamycin complex 2
MuRF1/TRIM63	Muscle RING finger 1
MuRF2/TRIM55	Muscle RING finger 2
MuSK	Muscle-specific tyrosine kinase
MyHC	Myosin heavy chain
NA	Numerical aperture
Na^+-K^+-ATPase	Sodium-potassium adenosine triphosphatase; sodium-potassium pump
NELL2	NEL-like 2
NES	Nestin
NF-κB	Nuclear factor kappa-light-chain-enhancer of activated B cells
NMJ	Neuromuscular junction
NRB1	NRB1, autophagy cargo receptor
NRF1/NFE2L1	Erythroid-derived 2-related factor 1
NSF	N-ethylmaleimide sensitive fusion protein

OGDH	Oxoglutarate dehydrogenase
PA	Phosphatidic acid
PBS	Phosphate-buffered saline
PDZRN3	PDZ domain-containing RING finger protein 3
PDZRN4	PDZ domain-containing RING finger protein 4
PCoA	Principal coordinate analysis
PFA	Paraformaldehyde
PLA	*Plantaris* muscle
PLCG1	Phospholipase C, gamma 1
PLD	Phospholipase D
PPARGC1A/PGC-1α	Peroxisome proliferative activated receptor, gamma, coactivator 1 alpha
PRR5/PROTOR1	Proline Rich 5; Protein Observed With Rictor-1
PRRL5/PROTOR2	Proline Rich 5 Like; Protein Observed With Rictor-2
qPCR	Semiquantitative real-time polymerase chain reaction
QUAD	*Quadriceps* muscle
RAP2A	Ras-related protein Rap-2a
RAPSYN	43 kDa receptor-associated protein of the synapse
RPTOR	Regulatory-associated protein of mTOR
RE	Resistance exercise
RHEB	Ras homolog enriched in brain
RICTOR	Rapamycin-insensitive companion of mTOR
RIN	RNA integrity number
RM	Rapamycin
RPS6	Ribosomal protein S6
RPS6KB1/p70S6K	Ribosomal protein S6 kinase, polypeptide 1
RWE	Resistance-wheel exercise
RYR1	Ryanodine receptor 1, skeletal muscle
SCN3B	Sodium channel, voltage-gated, type III, beta
SED	Sedentary control group
SERCA1	Sarco/endoplasmic reticulum Ca^{2+}-ATPase

SERPINB1A	Serine (or cysteine) peptidase inhibitor, clade B, member 1a
SMA	Spinal muscular atrophy
SMAD2/3	SMAD family member 2/3
SMARCD3/BAF60C	SWI/SNF related, matrix associated, actin dependent regulator of chromatin, subfamily d, member 3
SNTA1	Syntrophin alpha 1
SOL	*Soleus* muscle
SQSTM1/P62	Sequestosome 1
SULF2	Sulfatase 2
SWI/SNF	SWItch/Sucrose Non-Fermentable
TA	*Tibialis anterior* muscle
TBP	TATA box binding protein
TBX15	T-box 15
TBX21	T-box 21 (T-Bet)
TEAD	TEA domain family transcription factors
TELO2	Telomere maintenance 2
TID1/DNAJA3	Tumorous imaginal discs
TGF-β	Transforming growth factor beta
TNF-α	Tumor necrosis factor alpha (Cachexin)
TSC1	Tuberous sclerosis complex (TSC) subunit 1 (Hamartin)
TSC2	Tuberous sclerosis complex (TSC) subunit 2 (Tuberin)
TSC1/2	Tumor suppressor tuberous sclerosis complex TSC1-TSC2
TT	Transverse tubular system
TTI1	TELO2-interacting protein 1
UBR5	Ubiquitin protein ligase E3 component n-recognin 5
UBTF	Upstream binding transcription factor, RNA polymerase I
UQCRC2	Ubiquinol cytochrome c reductase core protein 2
UTRN	Utrophin
VTI	Vinculin-talin-integrin system
WWTR1/TAZ	WW domain containing transcription regulator 1
XPLN/ARHGEF3	Exchange factor found in platelets, leukemic, and neuronal tissues

YAP1	Yes-associated protein 1
YFP	Yellow fluorescent protein
YY1	YY1 transcription factor

1 General introduction

1.1 The musculoskeletal system

The musculoskeletal system provides stability, support, shape, and locomotion to the body. Skeletal muscles can voluntarily contract and enable movement by pulling on the bones of the skeleton, to which they attach via specialized connective tissue, the tendons. Unlike skeletal muscle, smooth muscle and cardiac muscle contract involuntarily. Smooth muscle is found within and in part composes the walls of blood vessels and of certain hollow organs of the body, such as the stomach and intestines.

Skeletal muscle and exercise in whole-body metabolism

Skeletal muscle is the largest organ of the human body and typically makes up around 40% of total body mass, but can reach levels of over 65% in professional male bodybuilders **(Spenst, Martin et al. 1993)**. Apart from its roles in posture and locomotion, skeletal muscle also contributes significantly to whole-body metabolism, with a particularly important role in glucose tolerance and insulin handling, as skeletal muscle is the predominant site of insulin-mediated glucose uptake after food consumption **(Stump, Henriksen et al. 2006)**. In fact, skeletal muscle insulin resistance likely is the primary defect in the development of type 2 diabetes mellitus **(Warram, Martin et al. 1990, DeFronzo and Tripathy 2009)**. Thus, maintaining normal insulin sensitivity is essential to remain metabolically flexible in times of energy surplus (more glucose-based fuel usage) and scarcity (more lipid-based fuel usage) **(Stump, Henriksen et al. 2006)**. Exercise improves metabolic control by acutely increasing glucose uptake into skeletal muscles and by priming muscle insulin sensitivity for up to two days following physical activity **(Richter, Garetto et al. 1982, Wojtaszewski, Hansen et al. 2000)**. Even a single bout of exercise can improve skeletal muscle insulin sensitivity in diabetic patients **(Devlin, Hirshman et al. 1987)**. In the basal state, skeletal muscle accounts for about 30% of the basal metabolic rate, but this contribution to whole-body energy use can rise significantly during strenuous exercise, and whole-body metabolic

rate may rise more than 20-fold **(Gaitanos, Williams et al. 1993)**. Thus, skeletal muscle evidently plays an important role in whole-body energy homeostasis and health status.

Skeletal muscle is an active endocrine organ and as such contributes to systemic signaling and inter-organ communication via the production and secretion of various myokines, which are peptides or proteins that may exert multiple autocrine, paracrine, and endocrine effects. Muscle contraction is thought to be a major regulator of myokine expression and release, but not all myokines respond to contraction **(Pedersen and Febbraio 2012)**. Some myokines work in autocrine or paracrine fashion within skeletal muscle itself and are not released into the circulation **(Whitham and Febbraio 2016)**. Interleukin-6 (IL-6) is the prototypical and first-identified myokine originally detected in blood samples of marathon runners post-race **(Ostrowski, Rohde et al. 1998)**. IL-6 is a myokine released from skeletal muscle during exercise and plays a role in glucose homeostasis and in stimulating hepatic glucose production **(Febbraio, Hiscock et al. 2004)**. Interest in myokines has risen sharply in recent years, which is understandable considering their potential therapeutic use in metabolic disease, which opens up novel pharmacological approaches and puts emphasis on exercise as an important treatment and disease-prevention strategy **(Benatti and Pedersen 2015, Gorgens, Eckardt et al. 2015, Schnyder and Handschin 2015)**.

Decorin (DCN), a small, leucine-rich dermatan sulfate proteoglycan, shows elevated levels upon muscle contraction in mice and humans. It is an exercise-regulated myokine secreted into circulation and is involved in a pro-hypertrophic response by binding directly to myostatin (MSTN) **(Kanzleiter, Rath et al. 2014)**. The myokine MSTN itself is a member of the transforming growth factor beta (TGF-β) superfamily expressed during skeletal muscle development and mainly exerts negative effects on skeletal muscle mass **(McPherron, Lawler et al. 1997)**. Decorin stimulates muscle cell differentiation, repair, and induces myogenic satellite cell proliferation by antagonizing TGF-β1 sensitivity **(Bianco, Fisher et al. 1990, Li, McFarland et al. 2008)**. Treatment with growth hormone, but not testosterone, increased circulating DCN levels in humans **(Bahl, Stone et al. 2018)**. Additionally, DCN plays a role in connective tissue formation in skeletal muscle and stimulates collagen

synthesis **(Vogel and Trotter 1987, Neame, Kay et al. 2000)**. Decorin also seems to play a role in metabolism, as feeding a high-fat diet to DCN-knockout mice lead to impaired glucose tolerance concomitant with a downregulation of genes involved in the organization of the extracellular matrix and in triglyceride biosynthesis, as well as an upregulation of adipose tissue genes. Consistently, adipose-tissue DCN levels were found to be elevated in obese adult humans after profound fat loss. Taken together, these observations establish DCN as a myokine with an important role in glucose tolerance maintenance **(Svard, Rost et al. 2019)**. Although DCN is secreted into circulation after exercise, it remains unclear whether increased circulatory levels, local production in the adipose tissue, or both, mediate these metabolic effects, and further research is required in this area.

Irisin is another recently identified myokine. It plays an important role in lipid metabolism through the browning of white adipose tissue **(Bostrom, Wu et al. 2012)**. Irisin arises through proteolytic cleavage from the fibronectin type III domain-containing protein 5 (FNDC5), a transmembrane protein that is expressed under regulation of the peroxisome proliferator-activated receptor γ coactivator 1α (PGC-1α). PGC-1α is a transcriptional co-activator readily inducible by exercise and exposure to cold, among other things, and is known for its distinctive effect on metabolism by greatly enhancing mitochondrial biogenesis **(Handschin and Spiegelman 2008, Zhang, Chang et al. 2015, Mattson, Moehl et al. 2018)**. Irisin is secreted into circulation upon exercise and leads to energy balance improvements. It might therefore find use as a possible treatment in metabolic disease and in counteracting systemic inflammation **(Lecker, Zavin et al. 2012, Polyzos, Anastasilakis et al. 2018)**. However, conflicting results in human studies preclude conclusions about irisins' effectiveness in white adipose tissue browning and further studies are warranted **(Elsen, Raschke et al. 2014)**.

Exercise-induced induction of PGC-1α and the concomitant release of irisin from skeletal muscle into the circulation induces brain derived neurotrophic factor (BDNF) production in different brain regions, linking exercise with beneficial neuroprotective effects and resilience to stress **(Wrann, White et al. 2013, Phillips, Baktir et al. 2014, Zhan, Huang et al. 2018)**. BDNF is also produced by skeletal muscle upon exercise, conferring

enhanced lipid oxidation via activation of AMP-activated protein kinase (AMPK), and thus belongs itself to the myokine family of proteins **(Matthews, Astrom et al. 2009)**. However, it appears that BDNF is not released into circulation in significant amounts, thus exerting its functions on skeletal muscle mainly in an autocrine/paracrine manner **(Schnyder and Handschin 2015)**. Furthermore, it has recently been shown (see **Appendix B)** that BDNF is a mediator of glycolytic fiber-type specification in mouse skeletal muscle **(Delezie, Weihrauch et al. 2019)**. Muscle-specific deletion of BDNF lead to reduced motor end plate volume and slower contractile properties of glycolytic fast-twitch muscles, such as the *extensor digitorum longus* muscle (EDL). Accordingly, muscle-specific overexpression of BDNF promoted a fast muscle-type gene program and lead to increased levels of the transcriptional regulators SWI/SNF-related matrix-associated actin-dependent regulator of chromatin subfamily D member 3 (SMARCD3; also known as BAF60C) and T-box 15 (TBX15), which control glycolytic muscle fiber identity **(Meng, Li et al. 2013, Lee, Singh et al. 2015, Delezie, Weihrauch et al. 2019)**. Mechanistically it is still unclear how exactly BDNF modulates SMARCD3, TBX15, and the fast fiber gene program, and further research is warranted.

Overall, skeletal muscle displays remarkable malleability in response to contractile activity, as well as nutritional- and health-status. It provides the body with a powerful means in metabolic control, and is involved in whole-body energy homeostasis and signaling via the expression and secretion of myokines. The importance and functionality of skeletal muscle evidently goes far beyond simple locomotion and even encompasses temperature control via shivering. The following sections will illustrate the immense ability of skeletal muscles to adapt to their environment and to the contractile and energetic demands placed on them.

Skeletal muscle plasticity

Skeletal muscle fibers, also called myofibers, within the same and between different muscles may differ in fiber type, with each type demonstrating distinct contractile and metabolic properties. This myofiber type heterogeneity facilitates contractile flexibility in different tasks, e.g. high-intensity contractions when lifting a heavy weight, or low-intensity contractions to maintain posture. Myofibers are highly plastic, as they are capable of changing in size as well as type in response to mechanical loading and neuromuscular activity **(Pette 2002)**. In general, two major types of myofibers are distinguishable through their predominantly oxidative or glycolytic metabolism and correspondingly their speed of contraction and resistance to fatigue **(Schiaffino, Hanzlikova et al. 1970)**. Predominantly slow-twitch, oxidative "type I" myofibers are rich in myoglobin, mitochondria and oxidative enzymes. Type I myofibers are optimally equipped for continuous and sustained contractions. Predominantly fast-twitch, glycolytic "type II" myofibers contain less mitochondria and rely more on glycolytic metabolism. Type II myofibers are optimally equipped for powerful, yet fatigable contractions. Depending on their characteristics and expression of different myosin heavy chain (MyHC) proteins, they can be subdivided into type IIA, type IIB, and type IIX. Type IIA myofibers possess intermediate contractile characteristics between type I and type II, and express MyHC-2A, while type IIB and type IIX fibers express MyHC-2B and MyHC-2X, respectively **(Schiaffino, Gorza et al. 1989)**. Fatigue-resistance and contractile characteristics of type IIX myofibers lie between type IIA and IIB **(Larsson, Edstrom et al. 1991)**. Notably, Type IIB myofibers are found in rodent, but not in human skeletal muscle **(Schiaffino and Reggiani 2011)**.

Myofiber heterogeneity is not limited to differences in contractile characteristics and metabolism alone. There is also a wide variability in terms of calcium handling in intracellular signaling and interrelated transmembrane ionic flux. For instance, muscle membrane excitability is a product of the abundance and activity state of sodium ion-channels. Sodium channel density is several times higher in fast-twitch myofibers, allowing them to respond to the high discharge rate of their associated motor neurons with powerful contractions **(Ruff and Whittlesey 1992)**. However, this large sodium ion influx rate may be in excess of what

the sodium-potassium-ion-pump (Na^+-K^+-ATPase) can handle, thus contributing to the high fatigability of fast-twitch myofibers. The Na^+-K^+-ATPase works to maintain the resting membrane potential by actively removing three intracellular sodium ions in exchange for two potassium ions, resulting in a negative net-charge change. Although fast myofibers contain a larger amount of Na^+-K^+-ATPase, its activity during repetitive stimulations is several times lower than in slow myofibers, contributing to their lower fatigue resistance **(Everts and Clausen 1992)**.

Intracellular cytosolic free calcium levels are tightly controlled in myofibers, as calcium may trigger muscle contraction by binding to troponin, but also may influence various protein activity states through phosphorylation events caused by calcium binding to calmodulin, a multifunctional intermediate calcium-binding messenger. Specific transporter proteins (i.e. Sarco/endoplasmic reticulum Ca^{2+}-ATPase (SERCA1)) and a generally larger volume of the sarcoplasmic reticulum enable a more efficient uptake of calcium ions in fast-twitch, type II myofibers **(Salviati, Sorenson et al. 1982, MacLennan, Brandl et al. 1987)**. Cytoplasmic calcium buffers, mitochondria, and the composition of the sarcolemma itself contribute to fine-tuned control of intracellular calcium concentration. Calcium transients reach a higher peak and decline approximately twice as fast in type II myofibers **(Liu, Carroll et al. 1997, Baylor and Hollingworth 2003)**. These calcium transient kinetics directly determine the shorter time to peak as well as half-relaxation time of fast myofiber twitch-contractions.

Calcium release from the sarcoplasmic reticulum into the cytosol occurs through specialized calcium-release channels, called ryanodine receptor 1 (RYR1), which are coupled to L-type voltage-gated calcium channels, called dihydropyridine receptors (DHPR) **(Rios and Brum 1987, Takeshima, Nishimura et al. 1989)**. DHPRs are found in the frequent invaginations of the sarcolemma, called the transverse tubular system (TT), which allows action potentials to travel towards the inner part of muscle cells **(Adrian, Costantin et al. 1969)**. Upon stimulation by action potentials, DHPRs facilitate activation of RYR1s and thus calcium release from the sarcoplasmic reticulum into the cytosol. This direct coupling between DHPRs and RYR1s ensures a fast and reliable release of calcium ions upon TT

depolarization by action potentials, ultimately causing muscle contraction **(Catterall 1991)**. Fast myofibers contain about twice as many RYR1s **(Franzini-Armstrong, Ferguson et al. 1988)**. Furthermore, slow myofiber DHPR-to-RYR1-ratio is lower **(Margreth, Damiani et al. 1993)**. Yet, intraluminal calcium levels may also influence RYR1 channel activity by facilitating binding of calmodulin and many other RYR1 modulators. Taken together, slow myofibers show reduced capacity of voltage-dependent calcium release due to a larger portion of DHPR-uncoupled RYR1s, which suggests that a greater emphasis is put on calcium-induced calcium release in slow versus fast myofibers, presumably mediated via calmodulin **(Tang, Sencer et al. 2002)**.

The capability of a myofiber to buffer calcium directly influences its calcium transient kinetics. Cytosolic calcium-buffering proteins include, but are not limited to, troponin, calmodulin, and parvalbumin. High levels of parvalbumin are found in type IIB and IIX myofibers, while it is much less abundant in type IIA and type I myofibers **(Celio and Heizmann 1982)**. Parvalbumin acts as a cytosolic calcium buffer in fast myofibers by quickly reducing cytosolic calcium levels after calcium release from the sarcoplasmic reticulum, and thus helps to enable faster twitch contractions by regulating relaxation speed **(Schwaller, Dick et al. 1999)**. Calmodulin also contributes to calcium buffering, and, like parvalbumin, is more abundant in fast myofibers, although to a lesser extent **(Campbell, Gordon et al. 2001)**. In conclusion, it is clear that myofiber type differences extend far beyond myofibrillar protein composition and metabolic enzyme expression, and that myofibers are flexibly fine-tuned to their exact functional demands.

Signaling pathways regulating skeletal muscle protein balance

The perpetual process of muscle protein synthesis (MPS) and breakdown (MPB) governs the maintenance of skeletal muscle mass. Under normal conditions, overall daily rates of MPS and MPB are roughly equal. A wide variety of extracellular stimuli influences this dynamic regulation, and can activate or inhibit distinct intracellular processes that alter protein balance within myofibers. Anabolic stimuli, such as insulin-like growth factor 1 (IGF-1), testosterone, insulin, and β2-adrenergic agonists, may tip protein balance within myofibers towards MPS, resulting in protein accretion **(Griggs, Kingston et al. 1989, Biolo, Declan Fleming et al. 1995, Glass 2005)**. For example, binding of IGF-1 and insulin to receptors in the muscle membrane activates signaling pathways mediated by protein kinase B (Akt/PKB) and mammalian target of rapamycin (mTOR), and thus promotes MPS and eventually myofiber hypertrophy **(Schiaffino and Mammucari 2011)**. In contrast, catabolic factors, such as glucocorticoids (GC) and a wide variety of pro-inflammatory cytokines (such as tumor necrosis factor alpha (TNF-α), interferon gamma (IFN-γ), interleukin-1 beta (IL-1β), and IL-6) may tip muscle protein balance towards breakdown and thus lead to muscle wasting **(Reid and Li 2001)**. In particular, GCs are elevated in many catabolic diseases, such as sepsis and cancer cachexia, in which they contribute to muscle wasting and functional decline, but are also elevated during physically and psychologically stressful conditions including fasting and exercise **(Bodine and Furlow 2015)**. Elevated circulating GC levels may perturb muscle protein balance two-fold, by decreasing MPS as well as by increasing MPB, which is a commonly occurring theme in perturbations of muscle protein balance **(Pereira and Freire de Carvalho 2011)**.

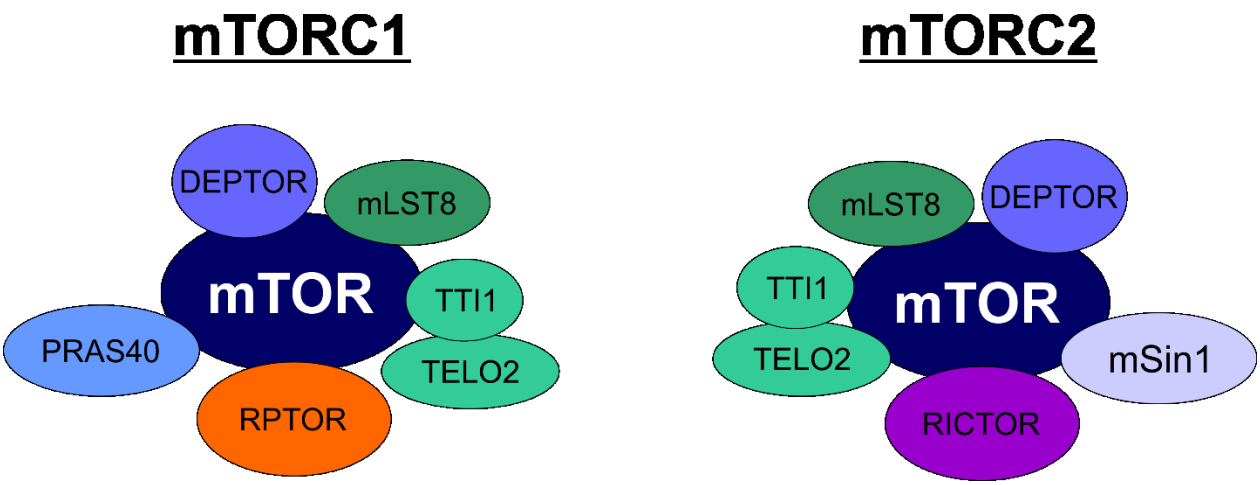

Figure 1-1. Schematic representations of mTOR complex 1 (mTORC1) and mTOR complex 2 (mTORC2).

The aforementioned mTOR signaling pathway exerts a large degree of influence on the maintenance of skeletal muscle mass **(Yoon 2017)**. Mammalian target of rapamycin is a highly conserved serine/threonine protein kinase capable of sensing a plethora of environmental cues and intracellular changes, such as amino acid and nutrient availability **(Sancak, Peterson et al. 2008, Sengupta, Peterson et al. 2010)**. It integrates these cues and influences a variety of cellular processes, most prominently cell growth and differentiation, but also plays a role in metabolism, autophagy and survival **(Dibble and Manning 2013)**. Mammalian target of rapamycin forms two structurally and functionally distinct complexes, the mTOR complex 1 (mTORC1), which is involved in anabolic processes like protein synthesis, and mTOR complex 2 (mTORC2), which governs other cellular processes, such as angiogenesis and for example regulates glucose uptake in response to insulin and in endurance exercise **(Inoki and Guan 2006, Ziegler, Hatch et al. 2016, Kleinert, Parker et al. 2017)**. While both mTORC1 and mTORC2 contain mTOR as their catalytic core, mTORC1 consists of the regulatory-associated protein of mTOR (RPTOR), the proline-rich AKT1 substrate 1 (AKT1S1; also known as PRAS40), the DEP domain-containing mTOR-interacting protein (DEPTOR), the complex of TELO2-interacting protein 1 (TTI1) and telomere maintenance 2 (TELO2), and the mammalian lethal with SEC13 protein 8 (MLST8). Mammalian target of rapamycin complex 2 shares DEPTOR, MLST8, and the TTI1-TELO2 complex with mTORC1, but instead of RPTOR contains the rapamycin-insensitive companion

of mTOR (RICTOR), the rho guanine nucleotide exchange factor (GEF) 3 (ARHGEF3; also known as XPLN), the proline rich 5 (PRR5; also known as PROTOR1) or the proline rich 5 like (PRR5L; also known as PROTOR2), and the mitogen-activated protein kinase associated protein 1 (MAPKAP1, also known as mSIN1) (**Figure 1-1**) **(Hara, Maruki et al. 2002, Jacinto, Loewith et al. 2004, Frias, Thoreen et al. 2006, Jacinto, Facchinetti et al. 2006, Pearce, Huang et al. 2007, Sancak, Thoreen et al. 2007, Peterson, Laplante et al. 2009, Kaizuka, Hara et al. 2010, Khanna, Fang et al. 2013)**.

Mammalian target of rapamycin complex 1 regulates mitochondrial oxygen consumption and oxidative capacity through cooperative activity modulation of the YY1 transcription factor (YY1) and of PGC-1α **(Cunningham, Rodgers et al. 2007)**. Perhaps unsurprisingly, resistance exercise (RE) activates mTORC1, which plays a fundamental role in the hypertrophic adaptive response of muscle **(Egan and Zierath 2013)**. Specifically, mTORC1 regulates muscle protein balance by activation of its downstream targets ribosomal protein S6 kinase, polypeptide 1 (RPS6KB1; also known as p70S6K) and eukaryotic translation initiation factor 4E binding protein 1 (EIF4EBP1; also known as 4E-BP1) **(Ma and Blenis 2009)**. The tumor suppressor tuberous sclerosis complex (TSC1/2) is formed by TSC complex subunit 1 (TSC1; also known as hamartin) and TSC complex subunit 2 (TSC2; also known as tuberin). The TSC1/2 complex acts as a guanosine triphosphate hydrolase (GTPase)-activating protein for the small GTPase ras homolog enriched in brain (RHEB), which facilitates upstream regulation of mTORC1. The TSC1/2 complex itself is regulated via Akt/PKB, which may phosphorylate TSC1/2 and thus inhibit its GTPase-activating function towards RHEB, leading to activation of RHEB **(Inoki, Li et al. 2003)**. Activated RHEB in turn activates mTORC1, which results in phosphorylation and thus activation of RPS6KB1 and EIF4EBP1, which in turn promote protein synthesis by activating ribosomal protein S6 (RPS6) and eukaryotic translation initiation factor 4E (EIF4E) **(Parmar and Tamanoi 2010)**. Protein kinase B (Akt/PKB) also inhibits mTORC1 independently of TSC1/2 by inducing the dissociation of AKT1S1 from mTORC1 through its phosphorylation **(Sancak, Thoreen et al. 2007, Wang, Harris et al. 2007)**. Mammalian target of rapamycin complex 1 activity is furthermore governed by a wide variety of influences from growth factors, amino acids, energy status, pro-inflammatory cytokines (i.e. TNF-α), hypoxia, to DNA damage and

many other inputs, which underlines the evident importance of this central growth pathway **(Brugarolas, Lei et al. 2004, Inoki and Guan 2006, Lee, Kuo et al. 2007)**.

The mTORC1 governs skeletal muscle size not only by facilitating increased MPS rates upon growth stimuli, but also plays a major role in regulating MPB. If the overall rate of MPB exceeds that of MPS, a muscle will shrink, or atrophy **(Sandri 2013)**. In times of low nutrient availability and upon other catabolic stimuli, such as physical inactivity, Akt/PKB is inactive and no longer inhibits TSC1/2, resulting in greater mTORC1 inhibition. Simultaneously, while forkhead-box-protein (FoxO)-family transcription factors are kept in an inactivated state in the cytosol when Akt/PKB is active, they become activated, enter the nucleus and become transcriptionally active upon Akt/PKB inhibition **(Sandri, Sandri et al. 2004)**. This contributes to muscular atrophy, as active FoxO-signaling increases ubiquitin-mediated proteolysis pathways, which occurs for example in insulin-deficient diabetes **(O'Neill, Bhardwaj et al. 2019)**. Apart from FoxO-family transcription factors, several other factors, collectively termed "Atrogenes", as these genes are involved in the induction of muscular atrophy, contribute to a negative muscle protein balance. The most prominent atrogenes are perhaps muscle ring finger 1 (MuRF1/TRIM63) and F-box protein 32 (MAFbx/Atrogin-1), both of which are E3 ubiquitin ligases enriched in muscle **(Bodine and Baehr 2014)**. Forkhead-box-protein signaling drives the overall MPB rate, presumably by the coordinated regulation of ubiquitin-proteasome mediated proteolysis and of autophagy, which it facilitates via the regulation of a large amount of different atrogenes **(Milan, Romanello et al. 2015, Taillandier and Polge 2019)**. A recently identified E3 ubiquitin ligase, ubiquitin protein ligase E3 component n-recognin 5 (UBR5), is inversely regulated compared to MuRF1 and MAFbx during atrophy, recovery from atrophy, as well as during hypertrophy. UBR5 becomes epigenetically altered via DNA-methylation events after human RE and retraining, indicating involvement of proteolytic activity in both anabolic as well as catabolic remodeling events **(Seaborne, Strauss et al. 2018, Seaborne, Hughes et al. 2019)**. Nevertheless, the coordinated crosstalk between autophagy and the ubiquitin-proteasome system in skeletal muscle atrophy is still incompletely understood and remains an active research topic **(Nam, Han et al. 2017)**.

Mechanical stimuli and resistance exercise in skeletal muscle hypertrophy

As established above, physical activity alters skeletal myofiber size, metabolism and structural properties, but also affects the entire body through endo and paracrine signaling. Yet, we lack a deeper understanding of how exactly mechanical stimuli mediate muscular hypertrophy. This still somewhat enigmatic process was termed "mechanotransduction". How does mechanotransduction allow muscle cells to convert mechanical stimuli into intracellular biochemical responses? How do muscle cells "sense" mechanical stimuli? What exactly comprises a mechanical stimulus capable of inducing hypertrophy? While the mTORC1-mediated increase in MPS was conclusively established as a key mechanism by which RE causes skeletal muscle hypertrophy, the initiating stimuli by which RE stimulates hypertrophy have remained elusive **(Bodine, Stitt et al. 2001, Marcotte, West et al. 2015)**. All of these questions remain to be answered conclusively, but recent research has revealed several potential routes by which muscle cells may integrate mechanical stimuli and respond with hypertrophy.

Normal levels of skeletal muscle mass are only maintained if normal levels of physical activity are adhered to, as severe muscular atrophy is evident upon immobilization **(Appell 1990)**. The force generated by a muscle contraction is transmitted to tendons and bones via longitudinal force transduction from one end of a myofiber to the other. However, there is also a lateral force component, which is transmitted from the force-generating sarcomeres through the sarcolemma and to the extracellular matrix via costameres **(Street 1983)**. Sarcomeres are the smallest functional units of myofibers. They form repeating units between two Z-lines, which themselves are dense protein discs acting as anchoring points for actin filaments. Costameres are structural-functional components of myofibers connecting the sarcomere to the cell membrane **(Pardo, Siliciano et al. 1983)**. They aid not only in lateral force transfer from sarcomeres to the extracellular matrix, but also in maintenance of sarcolemmal mechanical integrity **(Peter, Cheng et al. 2011)**. As the structural anchor of myofibrils inside myofibers, costameres may exert mechanosensory capabilities through their two major protein constituents, the dystrophin-associated glycoprotein complex (DGC) and the focal adhesion vinculin-talin-integrin system (VTI) **(Anastasi, Amato et al. 2003,**

Bamman, Roberts et al. 2018, Wackerhage, Schoenfeld et al. 2019). One prominent example is the costamere and primary DGC protein dystrophin, mutations of which cause severe muscular dystrophies such as Duchenne muscular dystrophy, in which irreparable myofiber damage accumulates **(Jaka, Casas-Fraile et al. 2015)**. Importantly, dystrophin levels decrease in aging skeletal muscle, causing increased susceptibility to mechanically induced damage **(Hughes, Wallace et al. 2015)**. While both the DGC and the VTI are attractive candidate mechanotransducers in skeletal muscle hypertrophy signaling, the exact way by which they may translate mechanical stimuli into biochemical signals requires further investigation.

The lipid second messenger phosphatidic acid (PA) may prove itself an intermediate mechanotransducer, as PA directly activates mTORC1 upon contractile activity **(Hornberger 2011, Jacobs, Goodman et al. 2014)**. Upon physical activity, diacylglycerol kinase zeta (DAGKZ) synthesizes PA via phosphorylation of diacylglycerol (**Figure 1-2**), thus suggesting DAGKZ to be a mechanosensitive enzyme capable of increasing PA levels and thereby activating mTORC1-mediated upregulation of protein synthesis **(You, Lincoln et al. 2014)**. Nevertheless, while oral PA feeding increases muscle mTORC1 activity and MPS rates, the exact mechanism by which mechanical load induces DGKZ activity is once again not really understood **(Mobley, Hornberger et al. 2015)**. Phosphatidic acid signaling can also be activated through the conversion of phosphatidylinositol 4, 5-bisphospate into PA, which is catalyzed by phospholipase Cγ1 (PLCG1). This conversion happens in a mechanosensitive way through attachment to the extracellular matrix, which can vary greatly in its stiffness, and also activates the Hippo signaling pathway with its effector proteins yes-associated protein 1 (YAP1) and its paralog WW domain containing transcription regulator 1 (WWTR1/TAZ) **(Meng, Qiu et al. 2018)**. Both YAP1 and WWTR1 are regulated by mechanical cues and mediate cellular responses to stiffness of the extracellular matrix **(Halder, Dupont et al. 2012)**. This regulation works through the activation of the ras-related protein Rap-2a (RAP2A), which itself is activated by low extracellular matrix stiffness and acts as an intracellular signal transducer for YAP1 and WWTR1 **(Meng, Qiu et al. 2018)**. Therefore, mechanical load may activate YAP1 and WWTR1 through PA-mediated RAP2A activation. Activated YAP1 and WWTR1 then increase levels of the high-affinity leucine

transporter LAT1 (also known as SLC7A5) mainly via co-activating TEA domain family transcription factors (TEAD), presumably sensitizing the contracting muscle to leucine-mediated mTORC1 activation **(Hansen, Ng et al. 2015, Dupont 2016)**. Extracellular matrix stiffness may also be affected by RE-induced myofiber and whole-muscle swelling, thus providing a potential mechanism by which mechanical stimuli influence cellular signaling pathways **(Farup, de Paoli et al. 2015, Wackerhage, Schoenfeld et al. 2019)**. Furthermore, it has recently been shown that YAP signaling, while functional, is constitutively active in the *mdx* mouse model for Duchenne muscular dystrophy and that this hyperactivation of YAP may render muscles unresponsive to mechanical load. This could be due to an increased state of "pre-stress" with increased cytoskeletal and extracellular matrix stiffness **(Iyer, Shah et al. 2019)**. Taken together, muscle contractile activity can increase PA production, which leads to mTORC1 activation through the Hippo signaling pathway with its effectors YAP1 and WWTR1 through activation of RAP2A. Yet, this once again illustrates intermediate mechanotransductive pathways, but does not reveal the primary mechanosensor itself, the identification of which remains to be achieved in future research efforts.

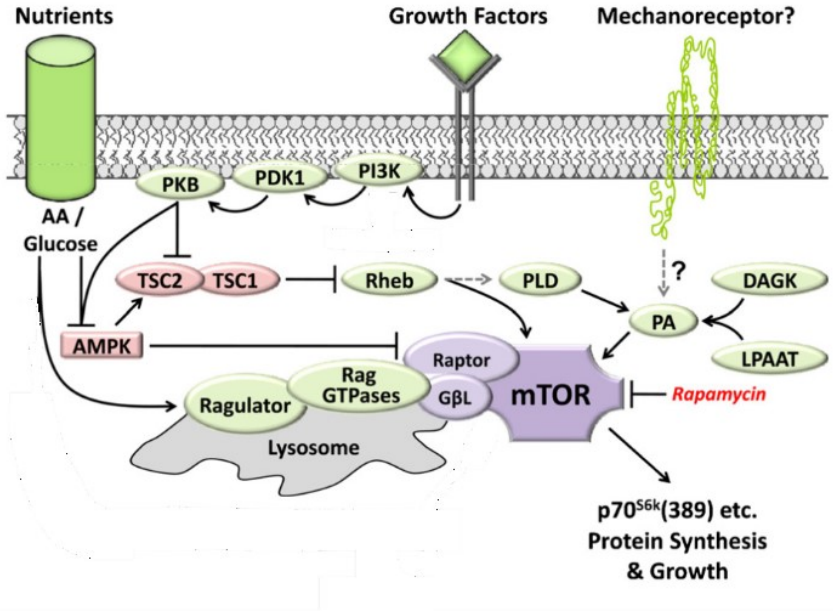

Figure 1-2. Mechanoregulation of mTORC1 activity via phophatidic acids. Diacylglycerol kinases (DAGKs), lysophosphatidic acid acyltransferases (LPAATs) and phospholipase D (PLD) synthetize phosphatidic acids (PAs) that in turn can activate mTORC1 signaling, influencing muscle protein synthesis. The exact mechanism by which a mechanical stimulus induces PA synthesis is still unknown. Adapted from **(Hornberger 2011)**.

Apart from costamere-based mechanotransduction through the DGC and VTI, titin has emerged as a potential mechanosensor during muscle contraction **(Kruger and Kotter 2016)**. Titin is the largest known protein and makes up around 10% of total muscle protein content, so an 80 kg adult human on average carries about 0.5 kg of it **(Labeit, Kolmerer et al. 1997)**. Titin is critical for muscle function, and mutations in its gene can cause various myopathies of skeletal and cardiac muscle **(Savarese, Sarparanta et al. 2016)**. The filamentous molecules of titin span from the Z-line to the M-line (which marks the middle of a sarcomere) of the sarcomeres, thus forming a third filament system next to actin and myosin. Therefore, titin plays an essential role for the structural integrity of the sarcomere and the passive tension response of a stretched myofiber. Different length-variants of titin are expressed between cardiac and skeletal muscle, providing an explanation for the ~10-fold difference in passive tension between these muscle types **(Linke, Popov et al. 1994)**. In skeletal muscles the so-called N2A titin isoform type is expressed in many muscle-specific splice variants, varies in its size between 3.3 and 3.7 MDa, and thus governs myofibrillar passive stiffness **(Neagoe, Opitz et al. 2003)**. In addition to its structural support and role in myofiber elasticity, titin contains a stretch-activated c-terminal kinase domain. When stretch is applied to titin, this pulls several amino acids out of its usually blocked ATP-binding pocket, thus allowing ATP to bind, causing autophosphorylation and the subsequent activation of titins' kinase domain **(Puchner, Alexandrovich et al. 2008)**. In its activated form, titin kinase interacts directly with the autophagy cargo receptor NBR1 (NBR1), which forms a signaling complex with the ubiquitin-binding protein sequestosome 1 (SQSTM1/p62) and muscle ring finger 2 (MuRF2/TRIM55). Titin-kinase-activated NBR1 then targets SQSTM1 to the sarcomere, where it in turn interacts with MuRF2 and potentially prevents its nuclear translocation and thus its negative impact on hypertrophic signaling, as mechanical inactivity induces nuclear translocation of MuRF2 **(Lange, Xiang et al. 2005)**. Furthermore, the titin-kinase-activated NBR1/SQSTM1-complex is involved in muscle protein balance and promotes proteasomal degradation by facilitating protein ubiquitination, as well as by targeting poly-ubiquitinated proteins to the autophagic protein turnover machinery via the autophagosomal membrane anchor microtubule-associated protein 1A/1B-light chain 3 (LC3) **(Pankiv, Clausen et al. 2007, Seibenhener, Geetha et al. 2007, Waters, Marchbank et al. 2009)**. Together, these findings suggest a way for titin to

"sense" mechanical stretch and to regulate protein turnover and gene expression in muscle cells. Titin thus serves as a candidate for pharmacological interventions aimed at ameliorating muscle loss in different disease conditions. Nevertheless, upon muscle contraction the forces acting on titin molecules actually decrease as it goes slack, calling into question its role as a true "mechanoreceptor".

Many more potential mechanosensors were recently investigated than described here, but the evidence remains mostly indirect and is difficult to interpret. It remains to be shown whether muscle cells actually have a unique mechanosensing system that goes beyond universal focal adhesion proteins such as costameres, which are present in most cell types and sense their mechanical surroundings. Resistance exercise provides a plethora of different kinds of stimuli that are difficult to isolate from one another. Knockout models of putative hypertrophy mediators are limited in their usefulness due to the knockout often causing myopathies and dystrophies, as the proteins in question are often required for normal muscle function. Targeted and inducible mouse models may help circumvent some of these limitations in future research.

Approaches to ameliorate progressive skeletal muscle wasting in disease

Various myopathies and diseases, such as Duchenne muscular dystrophy and cancer cachexia, lead to progressive skeletal muscle wasting and functional deterioration, which negatively influences quality of life and survival. Skeletal muscle mass losses incurred via certain muscular dystrophies or cancer-related mass losses are not always reversible via nutritional interventions or exercise alone **(Rybalka, Timpani et al. 2015, Bruggeman, Kamal et al. 2016, Ryder, Leadley et al. 2017, Schmidt, Rohm et al. 2018)**. Although moderate intensity exercise is generally regarded to be beneficial, it can sometimes even worsen the condition, i.e. due to structural instability of the sarcolemma or due to metabolic perturbations caused by disease **(Tisdale 1997, Siciliano, Simoncini et al. 2015, Chico, Ricci et al. 2017)**. Efforts so far have concentrated a lot on counteracting progressive skeletal muscle wasting by pharmacologically increasing muscle mass.

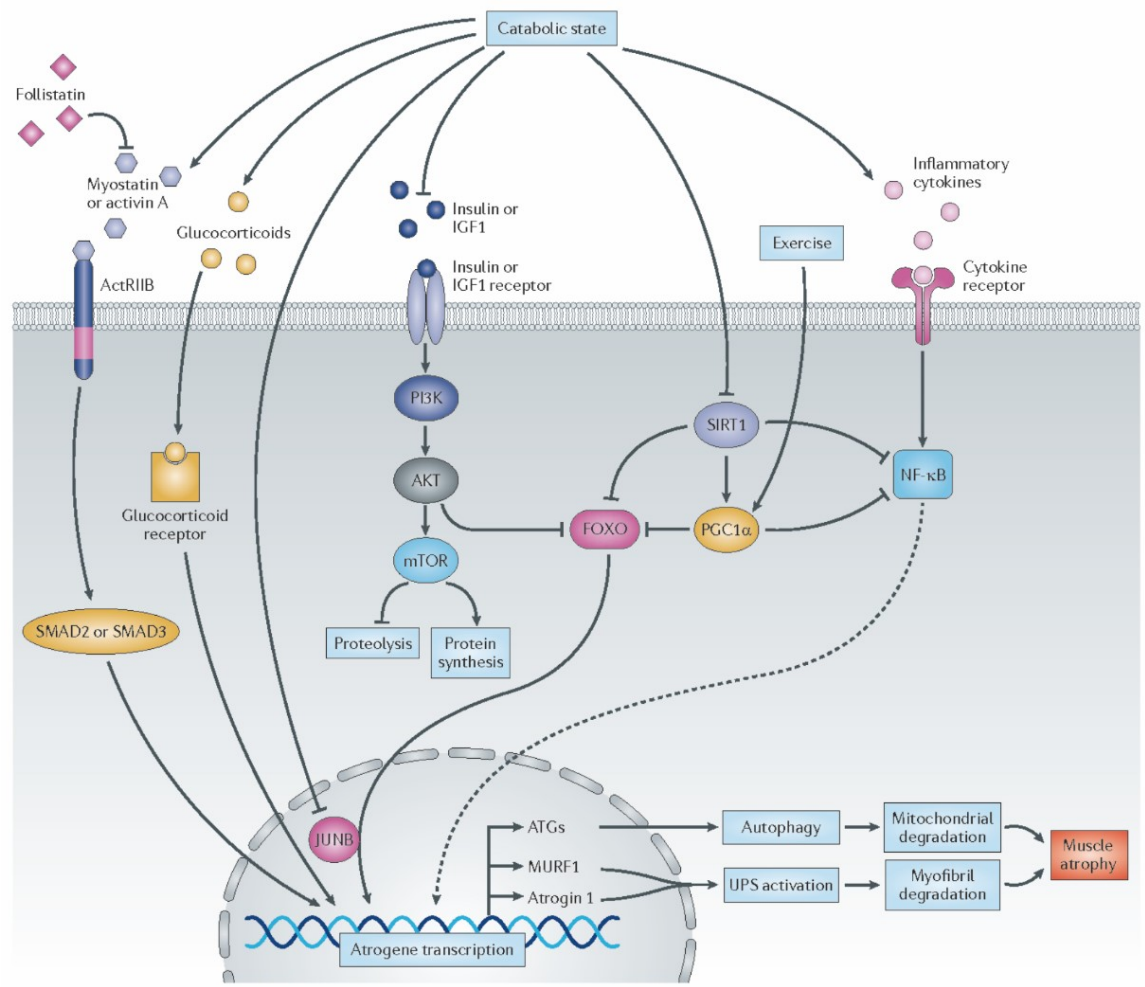

Figure 1-3. Atrophy signaling pathways. Atrogene expression can be induced via a variety of pathways upon a catabolic state. Activated ActRIIB-signaling is mediated via SMAD2/3 and regulates muscle mass via FoxO-dependent atrogene transcription. Glucocorticoids are catabolic factors that activate atrogene transcription upon binding glucocorticoid receptors, while inflammatory cytokines may act via cytokine receptors to influence atrogene expression via NF-κB. ActRIIB, activin receptor type IIB; NF-κB, nuclear factor-κB; Adapted from **(Cohen, Nathan et al. 2015)**.

Some recent approaches are targeting the myostatin/activin type II receptor (ActRII) pathway, which plays a major role in the regulation of skeletal muscle mass **(Lee and McPherron 2001, Souza, Chen et al. 2008)**. Activation of the ActRII complex on the muscle membrane induces SMAD family member 2/3-mediated transcription, which then leads to FoxO-dependent transcription (**Figure 1-3**). This ultimately results in increased muscle protein breakdown via the ubiquitin-proteasome system and autophagy **(Han, Zhou et al. 2013)**. The activation of SMAD2/3-mediated transcription furthermore leads to the

inhibition of muscle protein synthesis by suppressing Akt/PKB-signaling **(Sartori, Milan et al. 2009)**. Taken together, ActRII complex activation perturbs muscle protein balance and drives muscle wasting. Consequently, ActRII pathway interference has been considered in the treatment of muscular dystrophies with progressive muscle wasting resulting in weakness and frailty **(Amthor and Hoogaars 2012)**. Antibodies were devised that specifically block ActRIIs and prevent myostatin from binding. In doing so, dramatic increases in skeletal muscle mass beyond simple myostatin inhibition have been reported in mice **(Lach-Trifilieff, Minetti et al. 2014, Morvan, Rondeau et al. 2017)**. Furthermore, one of these antibodies, BYM338 (Bimagrumab), was reported to prevent glucocorticoid-induced atrophy and weakness in mice, highlighting the immense therapeutic potential of such agents **(Lach-Trifilieff, Minetti et al. 2014)**. BYM338 subsequently entered clinical trials and proved effective in increasing muscle mass and mobility in older adults with sarcopenia **(Rooks, Praestgaard et al. 2017)**. In a different approach of ActRII inhibition, an adeno-associated virus-mediated gene transfer improved muscle mass and absolute strength in a mouse model of mild spinal muscular atrophy (SMA), but did not prevent the reduction in motor units **(Liu, Hammers et al. 2016)**. Importantly, inhibition of the ActRII pathway with pharmacological means successfully counteracted progressive muscle wasting and prolonged lifespan in several animal models of disease **(Han, Zhou et al. 2013)**. However, while skeletal muscle mass and absolute contractile force were increased by inhibition of the ActRII pathway, the specific muscle contractile force did not improve accordingly, indicating that the obtained muscular hypertrophy, while beneficial in absolute terms, was not entirely functional **(Liu, Hammers et al. 2016)**.

The force-producing capability of a muscle is directly proportional to its size and in turn the cross-sectional area of its myofibers. Skeletal muscle hypertrophy may occur even in the absence of satellite cells, which are skeletal muscle stem cells capable of donating their nuclei via fusion to increase the myonucleic pool of myofibers **(Jackson, Mula et al. 2012, Murach, Fry et al. 2018)**. Individual myonuclei of a myofiber can only transcriptionally support a limited, but flexible amount of sarcoplasmic volume, termed their myonuclear domain (MND) **(Van der Meer, Jaspers et al. 2011, van der Meer, Jaspers et al. 2011, Kirby, Patel et al. 2016)**. Importantly, the size of individual MNDs in hypertrophic muscles

has significant effects on specific contractile force and myosin content. Fast-twitch myofibers (e.g. EDL muscle) were reported to have larger MNDs compared to slow-twitch myofibers (e.g. *Soleus* (SOL) muscle), which suggests that hypertrophying fast-twitch muscles might reach the upper limits of their MNDs relatively quickly **(Bruusgaard, Liestol et al. 2003, Qaisar, Renaud et al. 2012)**. The incorporation of additional myonuclei during *de novo* hypertrophy might consequently be crucial once the available MNDs are fully saturated **(Goh and Millay 2017)**. The apparent lack of proportional strength gains observed with ActRII-pathway inhibition may thus partly be explained by a lack of additional myonuclei contributed by satellite cells **(Qaisar, Renaud et al. 2012)**. Indeed, muscle hypertrophy driven by myostatin blockade requires little or no satellite cell activity **(Amthor, Otto et al. 2009)**. It therefore seems plausible that non-mechanically mediated skeletal muscle hypertrophy differs fundamentally from overload-induced hypertrophy **(Murach, Fry et al. 2018)**. The underlying molecular mechanisms that trigger muscular growth and the inevitable adverse effects of a general long-term ActRII-pathway inhibition, which is not limited to skeletal muscle, remain to be thoroughly investigated.

A lot of focus has been directed towards finding pharmacological means that counteract muscle mass losses incurred in different disease conditions, with the aim of ameliorating weakness and frailty, restoring locomotive autonomy, and improving quality of life in patients. Many such approaches, including the ones described here, successfully increase muscle mass and absolute muscle strength, but the obtained muscle mass often is not completely functional in terms of specific strength. This limits the therapeutic potential of such pharmacological interventions, as increasing muscular strength to ameliorate weakness is often the primary goal. Future research efforts should therefore focus on finding factors that better improve skeletal muscle force alongside muscle mass.

1.2 The neuromuscular system

Bodily movement, posture, and breathing are under the control of the neuromuscular system, which is composed of skeletal muscles, as well as a neural circuit consisting of sensory and motor neurons. The motor neurons of the neuromuscular system can be subdivided into alpha-, beta- and gamma-motor neurons, each type of which constitutes different structural and functional properties. Alpha motor neurons innervate extrafusal myofibers, which are responsible for muscle contraction, whereas gamma motor neurons innervate intrafusal myofibers of the muscle spindle, which is involved in proprioception **(Kroger 2018)**. Beta motor neurons innervate the intrafusal myofibers of the muscle spindles and additionally form collateral connections with extrafusal myofibers as well **(Adal and Barker 1965, Banks 1994)**. Importantly, the axons of all three types of motor neurons become myelinated, which dramatically increases their action potential transmission rates.

The neuromuscular system is functionally organized into so-called motor units. A motor unit comprises a particular (alpha-) motor neuron as well as all the myofibers it innervates. Individual motor neurons may differ substantially in their nerve impulse firing patterns. Motor units comprised primarily of slow-twitch, oxidative myofibers are characterized by a tonic low-frequency, long-lasting impulse activity, whereas motor units primarily comprised of fast-twitch, glycolytic fibers generally display a more phasic, high-frequency and short-duration impulse activity **(Hennig and Lomo 1985, Schiaffino and Reggiani 2011)**. The firing pattern of a motor units' motor neuron and the myofiber type of the fibers it innervates correspond well based on fatigue resistance **(Burke, Levine et al. 1973)**. It therefore seems likely that the nervous discharge pattern exerts strong, if not complete influence on myofiber type.

The neuromuscular junction (NMJ) is the interface at which motor neuron axons contact myofiber membranes and innervate them. Neuromuscular junctions are specialized, tripartite synapses consisting of the presynaptic motor nerve terminal, the perisynaptic basal lamina, and the postsynaptic specialization of the muscle membrane (**Figure 1-4**). While myofibers are wrapped by a basal lamina along their entire length, the perisynaptic part of

the basal lamina differs in its molecular composition, as it contains molecules secreted by both the muscle and the nerve **(Patton, Miner et al. 1997)**. The motor axon nerve terminal is capped by specialized glial cells, the so-called perisynaptic or terminal Schwann cells, which contribute to the organization of the NMJ **(Arbour, Vande Velde et al. 2017)**. The NMJ is additionally covered by one or several so-called kranocytes, which are fibroblast-like cells with a yet poorly defined role that extent their cytoplasmic processes over the entire synaptic endplate area **(Court, Gillingwater et al. 2008, Sugiura and Lin 2011)**. Synaptic transmission at the NMJ is extremely efficient and reliable. The amount of acetylcholine receptors (AChR) situated at the junctional fold shoulders of the deeply folded postsynaptic specialization of the muscle membrane, as well as the amount of acetylcholine vesicles released from the presynaptic nerve terminal per nerve impulse, are much greater than what would be necessary to cross the membrane potential threshold. This margin of safety, coined "safety factor", ensures reliable muscle contraction **(Wood and Slater 2001)**.

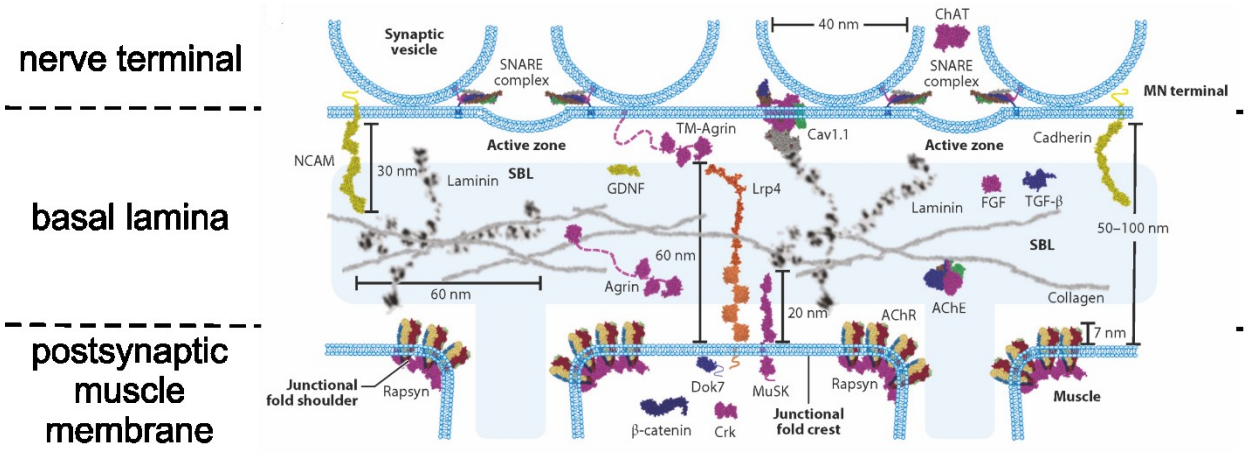

Figure 1-4. Schematic representation of the structure of the neuromuscular junction (NMJ). Adapted with minor modifications from **(Li, Xiong et al. 2018)**.

Fast-twitch type II and slow-twitch type I myofibers have developed structural and functional specializations of their NMJs. Postsynaptic fold density and concomitant voltage-gated sodium channel accumulation, along with absolute nerve terminal area are larger at NMJs of fast-twitch myofibers **(Milton, Lupa et al. 1992)**. The greater density of sodium channels enables fast-twitch fibers to respond to the fast firing rate of the corresponding

motor neuron, and results in powerful, but short-lived contractions. Yet, when normalized for fiber diameter, nerve terminal area is actually larger in slow-twitch fibers. Additionally, quantal content, the amount of neurotransmitter per synaptic vesicle, is larger at NMJs of fast-twitch fibers, yet slow-twitch fiber NMJs release far more vesicles per action potential **(Prakash, Miller et al. 1996)**. Thus, initial acetylcholine release upon stimulation is greater in fast fibers, and so is the endplate potential **(Reid, Slater et al. 1999)**. However, upon repeated stimulation, synaptic depression sets in, resulting in a reduction of synaptic vesicles released per stimulus and a pronounced decline in fast-fiber safety factor **(Gertler and Robbins 1978)**. The enzyme acetylcholinesterase (ACHE) quickly and efficiently breaks down acetylcholine into choline and acetate, thus removing it from the synaptic cleft to allow subsequent stimulations of the AChRs as well as preventing their over-activation. Importantly, fast myofiber NMJs contain about four times as much ACHE, presumably enabling faster stimulation patterns **(Pregelj, Trinkaus et al. 2007)**.

The Agrin/Lrp4/MuSK regulatory pathway in neuromuscular junction formation, structure and function

Skeletal myofibers are multinucleated syncytia and typically contain dozens, if not hundreds of myonuclei (muscle cell nuclei). Only a small subset of these aggregate directly underneath the NMJ, and express a distinct gene program **(Rossi, Vazquez et al. 2000, Ruegg 2005)**. These so-called fundamental myonuclei (**Figure 1-5**) presumably express most of the components necessary for the postsynaptic specializations of the myofiber membrane at the NMJ and expression of these components becomes silenced in extrajunctional myonuclei concomitant with innervation **(Schaeffer, de Kerchove d'Exaerde et al. 2001)**. An extensive body of research has elucidated many different signaling pathways that contribute to the regulation of the NMJ gene program and enable the various post – and pre-synaptic specializations of the NMJ. The clustering of AChRs at the junctional fold shoulders is one of the central processes that are under the regulation of many different pathways.

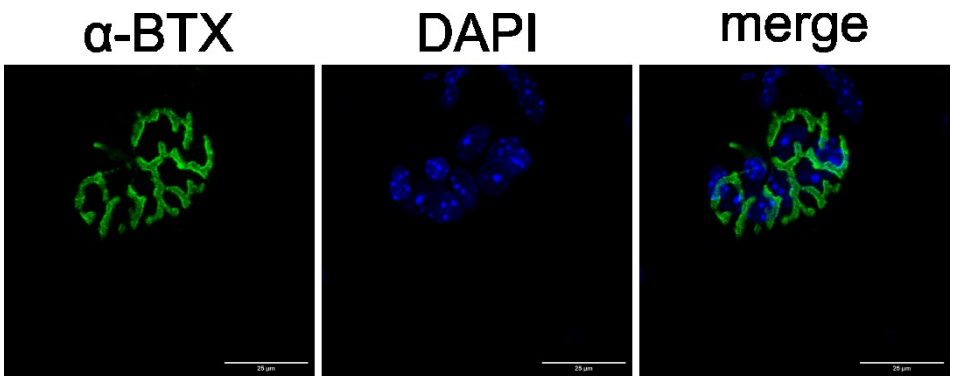

Figure 1-5. A small number of so-called fundamental myonuclei underlie the neuromuscular junction and express a distinct gene program compared with myonuclei elsewhere in a myofiber. α-BTX: α-Bungarotoxin staining postsynaptic acetylcholine receptors. **DAPI**: 4′,6-diamidino-2-phenylindole stains nuclei. **Merge**: Composite image. Scale bar: 25 μm.

Agrin is a heparan sulfate proteoglycan (HSPG) synthetized by motor neurons and is subsequently transported down the axon and released into the synaptic basal lamina of the NMJ, where it exerts its function and triggers postsynaptic differentiation, including AChR clustering **(Campanelli, Hoch et al. 1991, Ruegg, Tsim et al. 1992)**. Motor neuron-derived agrin is central to the most prominent regulatory nexus of AChR clustering at the NMJ, the complex of muscle-specific tyrosine kinase (MuSK) and low-density lipoprotein receptor-related protein 4 (Lrp4) (**Figure 1-6**). Lrp4 serves as a receptor for neural agrin, binding of which to Lrp4 triggers phosphorylation of MuSK and is essential during the earliest steps of NMJ assembly **(DeChiara, Bowen et al. 1996, Weatherbee, Anderson et al. 2006, Kim, Stiegler et al. 2008)**. Another essential process is the additional stabilization of MuSK by the muscle-specific adaptor protein docking protein 7 (Dok-7/Dok7) **(Okada, Inoue et al. 2006)**.

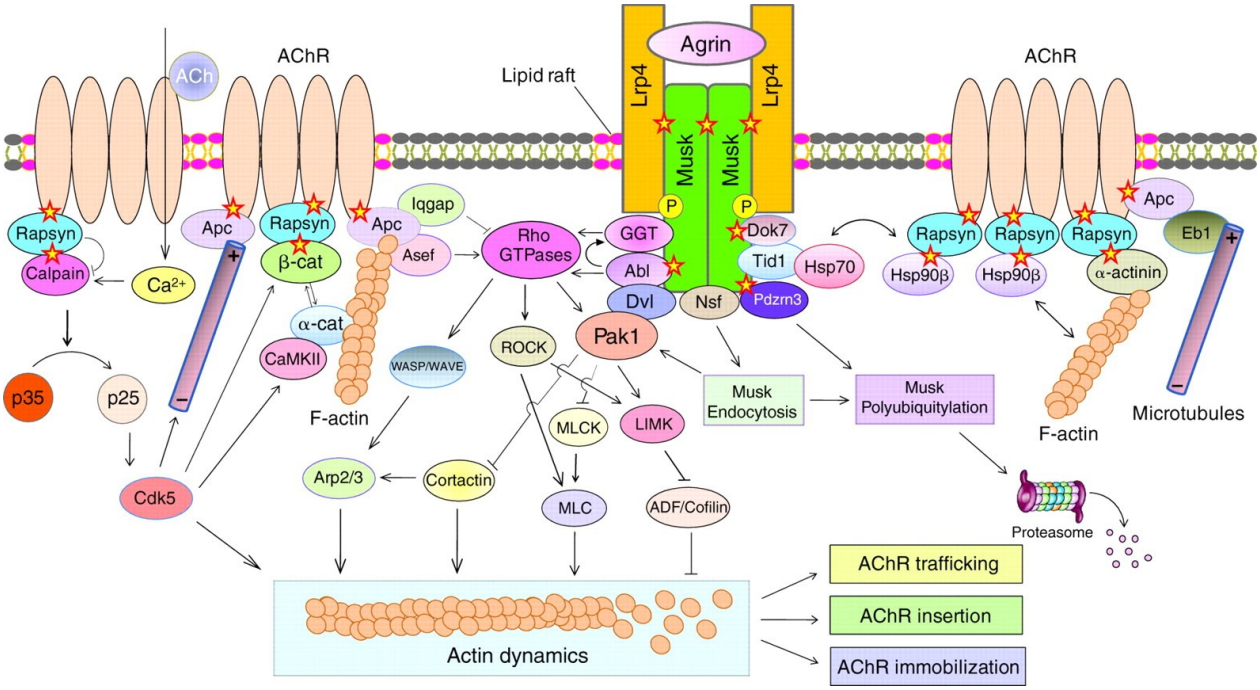

Figure 1-6. Motor neuron-derived agrin triggers a variety of intracellular signaling pathways regulating acetylcholine receptor clustering through the Lrp4-MuSK complex. Lrp4 serves as a receptor for agrin and triggers the phosphorylation of MuSK, which leads to Lrp4-MuSK dimerization. Dok-7 further stabilizes the phosphorylation of MuSK and a large variety of downstream signaling pathways is subsequently activated. Not all pathways illustrated here have been validated *in vivo*. Stars indicate protein-protein interactions. Adapted from **(Wu, Xiong et al. 2010)**.

A lack of agrin results in defective NMJs in loss-of-function mouse models, underlining the importance of this regulatory pathway in NMJ formation **(Gautam, Noakes et al. 1996)**. While agrin is also expressed by myofibers and by Schwann cells, which are located at the NMJ, neural agrin is several orders of magnitude more potent in inducing AChR clustering **(Reist, Werle et al. 1992, Gesemann, Denzer et al. 1995)**. A lack of MuSK results in highly branched motor neuron nerve terminals that innervate a much broader region, indicating that involvement of the Lrp4-MuSK-complex not only in post-, but also in pre-synaptic differentiation **(DeChiara, Bowen et al. 1996, Lin, Burgess et al. 2001, Yang, Arber et al. 2001)**.

The 43 kDa receptor-associated protein of the synapse (RAPSYN) is a synaptic peripheral membrane protein required for AChR clustering **(Gautam, Noakes et al. 1995)**. RAPSYN also stimulates MuSK activity by clustering it as well **(Gillespie, Balasubramanian et al. 1996)**. RAPSYN anchors AChRs in the synaptic fold shoulders by interacting with α-actinin and β-catenin, thus linking them to the postsynaptic actin cytoskeleton. While α-actinin is an actin crosslinker, β-catenin regulates α-catenin-dependent actin polymerization **(Yamada, Pokutta et al. 2005)**. Lack of either protein results in deficiencies of neural agrin-induced AChR clustering **(Apel, Roberds et al. 1995, Moransard, Borges et al. 2003, Zhang, Luo et al. 2007, Dobbins, Luo et al. 2008)**. MuSK, RAPSYN, and the dystrophin-associated glycoprotein complex (DGC) link the postsynaptic actin cytoskeleton to the synaptic basal lamina (**Figure 1-7**). The DGC consists of utrophin (UTRN; the synaptic homolog of dystrophin), which is linked to the actin cytoskeleton, three different groups of transmembrane proteins, namely the sarcoglycans, dystroglycan and sarcospan, as well as two groups of cytoplasmic proteins, the dystrobrevins and syntrophins **(Singhal and Martin 2011)**. Dystroglycan is posttranslationally cleaved into α- and β-dystroglycan **(Ibraghimov-Beskrovnaya, Ervasti et al. 1992)**. Importantly, α-dystroglycan becomes extensively glycosylated, and these modified sugar side-chains are required for the binding of α-dystroglycan to its numerous ligands at the synaptic basal lamina, including agrin, various laminins, perlecan, and neurexin **(Ervasti and Campbell 1993, Talts, Andac et al. 1999)**. Mutations of the various enzymes that are involved in the intricate glycosylation of α-dystroglycan can cause a variety of congenital myasthenic syndromes (CMS), which are a

class of inherited disorders of neuromuscular transmission characterized by early-onset fatigable muscle weakness **(Endo 2005)**. Genetic manipulations of the extent of glycosylation of α-dystroglcan provided further evidence for its stabilizing role at the NMJ, as well as the importance of glycosylation events for the structure and function of the synaptic basal lamina **(Hara, Balci-Hayta et al. 2011, Goddeeris, Wu et al. 2013)**. Apart from α-dystroglycan, many other proteins at the NMJ are glycosylated, including but not limited to agrin and MuSK, perlecan, and the AChRs themselves **(Martin and Sanes 1995, Martin, Scott et al. 1999, Yamaguchi 2002)**. The N-terminal extracellular domains of AChR subunits contain *N*-linked glycans, glycosylations of which ensure proper AChR assembly and folding **(Prives and Bar-Sagi 1983, Gehle, Walcott et al. 1997)**. While it has been established that specific glycans containing *β*-linked *N*-acetylgalactosamines are concentrated at the NMJ, the biological meaning of these highly diverse glycosylation events remains poorly understood and animal models investigating the impact of glycosylation events on NMJ structure and function are needed **(Herbst, Iskratsch et al. 2009)**.

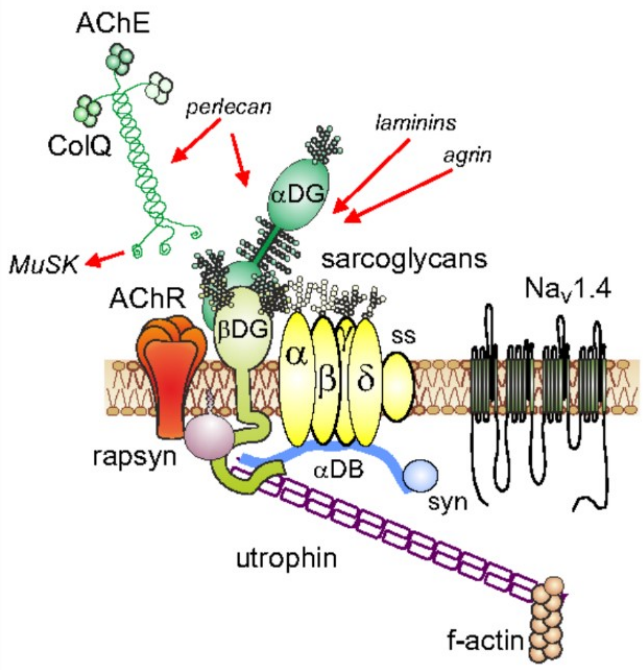

Figure 1-7. The dystrophin-associated glycoprotein complex (DGC) anchors important synaptic components of the basal lamina to the actin cytoskeleton. The extensively glycosylated α-dystroglycan (αDG) links its diverse binding partners within the synaptic basal lamina via the membrane-spanning β-dystroglycan (βDG) and cytoplasmic utrophin to the actin cytoskeleton (f-actin). Adapted from **(Tintignac, Brenner et al. 2015)**.

A lack of RAPSYN, similar to a lack of MuSK or agrin, results in AChR deficiencies **(Cossins, Burke et al. 2006)**. Mutations in the gene encoding for RAPSYN are causative for CMS, which often are treatable with cholinergic agonists **(Maselli, Dunne et al. 2003, Cossins, Burke et al. 2006, Milone, Shen et al. 2009)**. Similarly, mutations in Dok-7, Lrp4, MuSK or AChRs themselves may cause different kinds of CMS requiring different types of treatment **(Maselli, Arredondo et al. 2010, Rodriguez Cruz, Palace et al. 2014, Bevilacqua, Lara et al. 2017)**. Over 30 different CMS are recognized today (**Figure 1-8**), but we most likely still do not know more than half of the possible causative mutations of different NMJ components and identification of the disease-causing genes is crucial for determining optimal therapeutic measures **(Engel 2018)**.

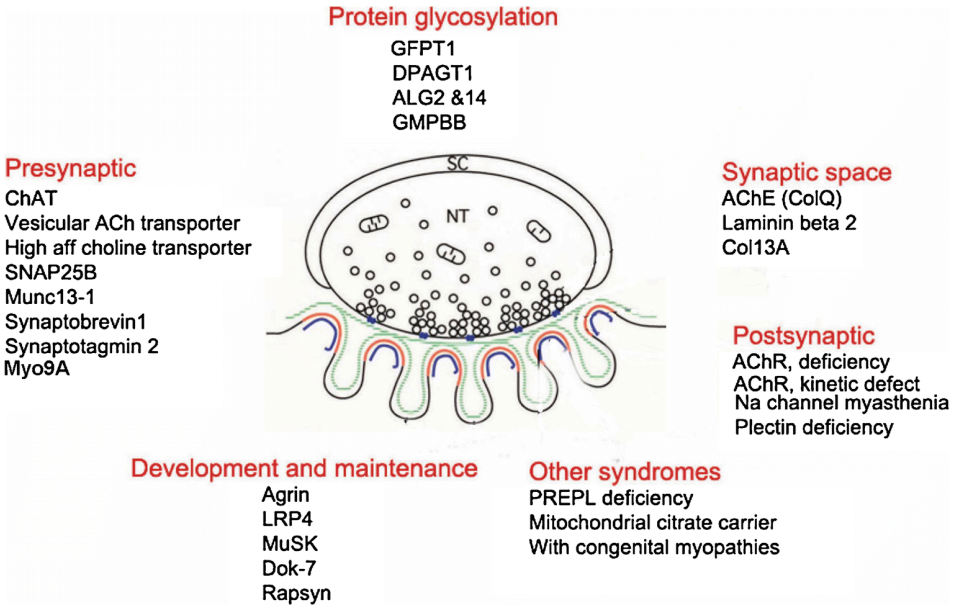

Figure 1-8. Currently identified congenital myasthenic syndromes. Adapted from **(Engel 2018)**.

In addition to the MuSK-activity regulation by agrin, Lrp4, Dok-7, and RAPSYN, MuSK also interacts with tumorous imaginal discs (TID1/DNAJA3). TID1 is necessary for Dok-7 binding to MuSK in response to neural agrin **(Linnoila, Wang et al. 2008)**. MuSK becomes rapidly internalized upon its activation, a process that is mediated by the direct interaction with the ATPase N-ethylmaleimide sensitive fusion protein (NSF) and is required for MuSK internalization **(Zhu, Yang et al. 2008)**. MuSK internalization can lead to its proteasomal

degradation mediated in part by the E3 ubiquitin ligase PDZ domain containing RING finger 3 (PDZRN3), which constitutes an important regulator of MuSK signaling contributing to precise and dynamic control of synaptic development **(Lu, Je et al. 2007)**.

Subsynaptic transcriptional regulation of the neuromuscular junction gene program

Genes coding for components of the NMJ often show nearly exclusive synaptic expression and become silenced in the extrasynaptic regions of a myofiber upon innervation. Site-directed mutagenesis of such synaptically expressed gene promotors revealed a six base pair DNA element conferring this synaptic specificity, the so-called N-box **(Koike, Schaeffer et al. 1995, Duclert, Savatier et al. 1996)**. Importantly, a point mutation in the N-box element of the acetylcholine receptor epsilon subunit (CHRNE) promotor was reported to cause congenital myasthenia due to reduced expression of CHRNE at the NMJ **(Nichols, Croxen et al. 1999, Ohno, Anlar et al. 1999)**. Moreover, subsynaptic expression of utrophin (UTRN) and acetylcholinesterase (ACHE) is also controlled by the presence of N-box elements in their respective gene promotors **(Gramolini, Angus et al. 1999, Khurana, Rosmarin et al. 1999)**. The mere presence of an N-box element in a genes' promotor is not sufficient to explain its targeted expression to the NMJ. Indeed, the N-box is a conserved ETS binding site and likely facilitates the binding of ETS-related transcription factors, the most prominent example being the growth-associated binding protein alpha (GABPα), which is required for postsynaptic differentiation *in vivo* **(Fromm and Burden 1998, Schaeffer, Duclert et al. 1998, Briguet and Ruegg 2000)**. Transcriptional activation of genes by GABPα via its ETS domain requires heterodimerization with the GABPβ subunit, the latter of which provides a nuclear localization sequence and a transcriptional activation domain **(LaMarco, Thompson et al. 1991, Sawa, Goto et al. 1996, Briguet and Ruegg 2000)**. However, enrichment of GABPα mRNA at the NMJ is relatively minor **(Schaeffer, Duclert et al. 1998)** and conditional inactivation of GABPα in skeletal muscle indicated that it is in fact dispensable for NMJ formation and subsynaptic gene expression **(Jaworski, Smith et al. 2007)**, or at the very least causes only minor structural and functional alterations of the NMJ **(O'Leary, Noakes et**

al. 2007). Taken together, these findings imply that GABPα most likely is not the central regulator of the NMJ gene program. Another ETS-related transcription factor, ETS variant 5 (ETV5/ERM) was found to facilitate the synapse-specific expression of many, but not all synaptic genes (**Figure 1-9**), although direct binding to the N-box element has not been confirmed as of yet **(Hippenmeyer, Huber et al. 2007)**. However, while ETV5 depletion caused synaptic defects and symptoms resembling that of congenital myasthenia, it did not lead to complete disruption of synaptogenesis, implying that ETV5 might act as a synaptic gene expression booster rather than being an all-or-nothing trigger. It is not clear how expression of ETV5 itself becomes subsynaptically restricted as its expression is independent of innervation status **(Hippenmeyer, Huber et al. 2007)**. The complete picture of how exactly the transcriptional regulation of the NMJ gene program is regulated still remains to be fully elucidated.

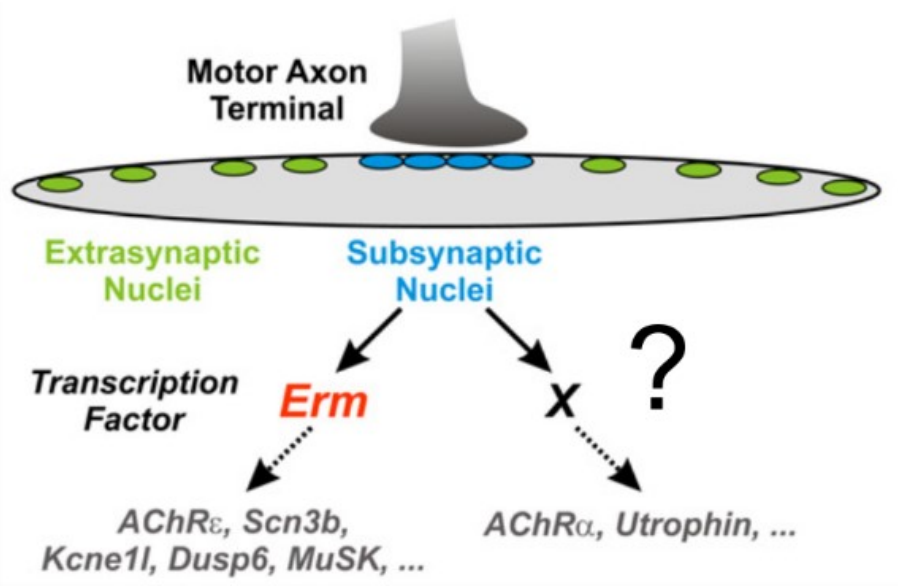

Figure 1-9. ETV5/Erm is partially in control of the subsynaptic gene program of the neuromuscular junction. There are at least two alternative transcriptional pathways involved in the regulation of subsynaptic gene expression. Erm regulates many, but not all subsynaptically expressed genes. Adapted with minor modifications from **(Hippenmeyer, Huber et al. 2007)**.

1.3 References

Adal, M. N. and D. Barker (1965). "Intramuscular Branching of Fusimotor Fibres." J Physiol **177**: 288-299.

Adrian, R. H., L. L. Costantin and L. D. Peachey (1969). "Radial spread of contraction in frog muscle fibres." J Physiol **204**(1): 231-257.

Amthor, H. and W. M. Hoogaars (2012). "Interference with myostatin/ActRIIB signaling as a therapeutic strategy for Duchenne muscular dystrophy." Curr Gene Ther **12**(3): 245-259.

Amthor, H., A. Otto, A. Vulin, A. Rochat, J. Dumonceaux, L. Garcia, E. Mouisel, C. Hourde, R. Macharia, M. Friedrichs, F. Relaix, P. S. Zammit, A. Matsakas, K. Patel and T. Partridge (2009). "Muscle hypertrophy driven by myostatin blockade does not require stem/precursor-cell activity." Proc Natl Acad Sci U S A **106**(18): 7479-7484.

Anastasi, G., A. Amato, G. Tarone, G. Vita, M. C. Monici, L. Magaudda, M. Brancaccio, A. Sidoti, F. Trimarchi, A. Favaloro and G. Cutroneo (2003). "Distribution and localization of vinculin-talin-integrin system and dystrophin-glycoprotein complex in human skeletal muscle. Immunohistochemical study using confocal laser scanning microscopy." Cells Tissues Organs **175**(3): 151-164.

Apel, E. D., S. L. Roberds, K. P. Campbell and J. P. Merlie (1995). "Rapsyn may function as a link between the acetylcholine receptor and the agrin-binding dystrophin-associated glycoprotein complex." Neuron **15**(1): 115-126.

Appell, H. J. (1990). "Muscular atrophy following immobilisation. A review." Sports Med **10**(1): 42-58.

Arbour, D., C. Vande Velde and R. Robitaille (2017). "New perspectives on amyotrophic lateral sclerosis: the role of glial cells at the neuromuscular junction." J Physiol **595**(3): 647-661.

Bahl, N., G. Stone, M. McLean, K. K. Y. Ho and V. Birzniece (2018). "Decorin, a growth hormone-regulated protein in humans." Eur J Endocrinol **178**(2): 145-152.

Bamman, M. M., B. M. Roberts and G. R. Adams (2018). "Molecular Regulation of Exercise-Induced Muscle Fiber Hypertrophy." Cold Spring Harb Perspect Med **8**(6).

Banks, R. W. (1994). "The motor innervation of mammalian muscle spindles." Prog Neurobiol **43**(4-5): 323-362.

Baylor, S. M. and S. Hollingworth (2003). "Sarcoplasmic reticulum calcium release compared in slow-twitch and fast-twitch fibres of mouse muscle." J Physiol **551**(Pt 1): 125-138.

Benatti, F. B. and B. K. Pedersen (2015). "Exercise as an anti-inflammatory therapy for rheumatic diseases-myokine regulation." Nat Rev Rheumatol **11**(2): 86-97.

Bevilacqua, J. A., M. Lara, J. Diaz, M. Campero, J. Vazquez and R. A. Maselli (2017). "Congenital Myasthenic Syndrome due to DOK7 mutations in a family from Chile." Eur J Transl Myol **27**(3): 6832.

Bianco, P., L. W. Fisher, M. F. Young, J. D. Termine and P. G. Robey (1990). "Expression and localization of the two small proteoglycans biglycan and decorin in developing human skeletal and non-skeletal tissues." J Histochem Cytochem **38**(11): 1549-1563.

Biolo, G., R. Y. Declan Fleming and R. R. Wolfe (1995). "Physiologic hyperinsulinemia stimulates protein synthesis and enhances transport of selected amino acids in human skeletal muscle." J Clin Invest **95**(2): 811-819.

Bodine, S. C. and L. M. Baehr (2014). "Skeletal muscle atrophy and the E3 ubiquitin ligases MuRF1 and MAFbx/atrogin-1." Am J Physiol Endocrinol Metab **307**(6): E469-484.

Bodine, S. C. and J. D. Furlow (2015). "Glucocorticoids and Skeletal Muscle." Adv Exp Med Biol **872**: 145-176.

Bodine, S. C., T. N. Stitt, M. Gonzalez, W. O. Kline, G. L. Stover, R. Bauerlein, E. Zlotchenko, A. Scrimgeour, J. C. Lawrence, D. J. Glass and G. D. Yancopoulos (2001). "Akt/mTOR pathway is a crucial regulator of skeletal muscle hypertrophy and can prevent muscle atrophy in vivo." Nat Cell Biol **3**(11): 1014-1019.

Bostrom, P., J. Wu, M. P. Jedrychowski, A. Korde, L. Ye, J. C. Lo, K. A. Rasbach, E. A. Bostrom, J. H. Choi, J. Z. Long, S. Kajimura, M. C. Zingaretti, B. F. Vind, H. Tu, S. Cinti, K. Hojlund, S. P. Gygi and B. M. Spiegelman (2012). "A PGC1-alpha-dependent myokine that drives brown-fat-like development of white fat and thermogenesis." Nature **481**(7382): 463-468.

Briguet, A. and M. A. Ruegg (2000). "The Ets transcription factor GABP is required for postsynaptic differentiation in vivo." J Neurosci **20**(16): 5989-5996.

Brugarolas, J., K. Lei, R. L. Hurley, B. D. Manning, J. H. Reiling, E. Hafen, L. A. Witters, L. W. Ellisen and W. G. Kaelin, Jr. (2004). "Regulation of mTOR function in response to hypoxia by REDD1 and the TSC1/TSC2 tumor suppressor complex." Genes Dev **18**(23): 2893-2904.

Bruggeman, A. R., A. H. Kamal, T. W. LeBlanc, J. D. Ma, V. E. Baracos and E. J. Roeland (2016). "Cancer Cachexia: Beyond Weight Loss." J Oncol Pract **12**(11): 1163-1171.

Bruusgaard, J. C., K. Liestol, M. Ekmark, K. Kollstad and K. Gundersen (2003). "Number and spatial distribution of nuclei in the muscle fibres of normal mice studied in vivo." J Physiol **551**(Pt 2): 467-478.

Burke, R. E., D. N. Levine, P. Tsairis and F. E. Zajac, 3rd (1973). "Physiological types and histochemical profiles in motor units of the cat gastrocnemius." J Physiol **234**(3): 723-748.

Campanelli, J. T., W. Hoch, F. Rupp, T. Kreiner and R. H. Scheller (1991). "Agrin mediates cell contact-induced acetylcholine receptor clustering." Cell **67**(5): 909-916.

Campbell, W. G., S. E. Gordon, C. J. Carlson, J. S. Pattison, M. T. Hamilton and F. W. Booth (2001). "Differential global gene expression in red and white skeletal muscle." Am J Physiol Cell Physiol **280**(4): C763-768.

Catterall, W. A. (1991). "Excitation-contraction coupling in vertebrate skeletal muscle: a tale of two calcium channels." Cell **64**(5): 871-874.

Celio, M. R. and C. W. Heizmann (1982). "Calcium-binding protein parvalbumin is associated with fast contracting muscle fibres." Nature **297**(5866): 504-506.

Chico, L., G. Ricci, O. D. C. M. Cosci, C. Simoncini and G. Siciliano (2017). "Physical exercise and oxidative stress in muscular dystrophies: is there a good balance?" Arch Ital Biol **155**(1-2): 11-24.

Cohen, S., J. A. Nathan and A. L. Goldberg (2015). "Muscle wasting in disease: molecular mechanisms and promising therapies." Nat Rev Drug Discov **14**(1): 58-74.

Cossins, J., G. Burke, S. Maxwell, H. Spearman, S. Man, J. Kuks, A. Vincent, J. Palace, C. Fuhrer and D. Beeson (2006). "Diverse molecular mechanisms involved in AChR deficiency due to rapsyn mutations." Brain **129**(Pt 10): 2773-2783.

Court, F. A., T. H. Gillingwater, S. Melrose, D. L. Sherman, K. N. Greenshields, A. J. Morton, J. B. Harris, H. J. Willison and R. R. Ribchester (2008). "Identity, developmental restriction and reactivity of extralaminar cells capping mammalian neuromuscular junctions." J Cell Sci **121**(Pt 23): 3901-3911.

Cunningham, J. T., J. T. Rodgers, D. H. Arlow, F. Vazquez, V. K. Mootha and P. Puigserver (2007). "mTOR controls mitochondrial oxidative function through a YY1-PGC-1alpha transcriptional complex." Nature **450**(7170): 736-740.

DeChiara, T. M., D. C. Bowen, D. M. Valenzuela, M. V. Simmons, W. T. Poueymirou, S. Thomas, E. Kinetz, D. L. Compton, E. Rojas, J. S. Park, C. Smith, P. S. DiStefano, D. J. Glass, S. J. Burden and G. D. Yancopoulos (1996). "The receptor tyrosine kinase MuSK is required for neuromuscular junction formation in vivo." Cell **85**(4): 501-512.

DeFronzo, R. A. and D. Tripathy (2009). "Skeletal muscle insulin resistance is the primary defect in type 2 diabetes." Diabetes Care **32 Suppl 2**: S157-163.

Delezie, J., M. Weihrauch, G. Maier, R. Tejero, D. J. Ham, J. F. Gill, B. Karrer-Cardel, M. A. Ruegg, L. Tabares and C. Handschin (2019). "BDNF is a mediator of glycolytic fiber-type specification in mouse skeletal muscle." Proc Natl Acad Sci U S A.

Devlin, J. T., M. Hirshman, E. D. Horton and E. S. Horton (1987). "Enhanced peripheral and splanchnic insulin sensitivity in NIDDM men after single bout of exercise." Diabetes **36**(4): 434-439.

Dibble, C. C. and B. D. Manning (2013). "Signal integration by mTORC1 coordinates nutrient input with biosynthetic output." Nat Cell Biol **15**(6): 555-564.

Dobbins, G. C., S. Luo, Z. Yang, W. C. Xiong and L. Mei (2008). "alpha-Actinin interacts with rapsyn in agrin-stimulated AChR clustering." Mol Brain **1**: 18.

Duclert, A., N. Savatier, L. Schaeffer and J. P. Changeux (1996). "Identification of an element crucial for the sub-synaptic expression of the acetylcholine receptor epsilon-subunit gene." J Biol Chem **271**(29): 17433-17438.

Dupont, S. (2016). "Role of YAP/TAZ in cell-matrix adhesion-mediated signalling and mechanotransduction." Exp Cell Res **343**(1): 42-53.

Egan, B. and J. R. Zierath (2013). "Exercise metabolism and the molecular regulation of skeletal muscle adaptation." Cell Metab **17**(2): 162-184.

Elsen, M., S. Raschke and J. Eckel (2014). "Browning of white fat: does irisin play a role in humans?" J Endocrinol **222**(1): R25-38.

Endo, T. (2005). "Aberrant glycosylation of alpha-dystroglycan and congenital muscular dystrophies." Acta Myol **24**(2): 64-69.

Engel, A. G. (2018). "Congenital Myasthenic Syndromes in 2018." Curr Neurol Neurosci Rep **18**(8): 46.

Ervasti, J. M. and K. P. Campbell (1993). "A role for the dystrophin-glycoprotein complex as a transmembrane linker between laminin and actin." J Cell Biol **122**(4): 809-823.

Everts, M. E. and T. Clausen (1992). "Activation of the Na-K pump by intracellular Na in rat slow- and fast-twitch muscle." Acta Physiol Scand **145**(4): 353-362.

Farup, J., F. de Paoli, K. Bjerg, S. Riis, S. Ringgard and K. Vissing (2015). "Blood flow restricted and traditional resistance training performed to fatigue produce equal muscle hypertrophy." Scand J Med Sci Sports **25**(6): 754-763.

Febbraio, M. A., N. Hiscock, M. Sacchetti, C. P. Fischer and B. K. Pedersen (2004). "Interleukin-6 is a novel factor mediating glucose homeostasis during skeletal muscle contraction." Diabetes **53**(7): 1643-1648.

Franzini-Armstrong, C., D. G. Ferguson and C. Champ (1988). "Discrimination between fast- and slow-twitch fibres of guinea pig skeletal muscle using the relative surface density of junctional transverse tubule membrane." J Muscle Res Cell Motil **9**(5): 403-414.

Frias, M. A., C. C. Thoreen, J. D. Jaffe, W. Schroder, T. Sculley, S. A. Carr and D. M. Sabatini (2006). "mSin1 is necessary for Akt/PKB phosphorylation, and its isoforms define three distinct mTORC2s." Curr Biol **16**(18): 1865-1870.

Fromm, L. and S. J. Burden (1998). "Synapse-specific and neuregulin-induced transcription require an ets site that binds GABPalpha/GABPbeta." Genes Dev **12**(19): 3074-3083.

Gaitanos, G. C., C. Williams, L. H. Boobis and S. Brooks (1993). "Human muscle metabolism during intermittent maximal exercise." J Appl Physiol (1985) **75**(2): 712-719.

Gautam, M., P. G. Noakes, L. Moscoso, F. Rupp, R. H. Scheller, J. P. Merlie and J. R. Sanes (1996). "Defective neuromuscular synaptogenesis in agrin-deficient mutant mice." Cell **85**(4): 525-535.

Gautam, M., P. G. Noakes, J. Mudd, M. Nichol, G. C. Chu, J. R. Sanes and J. P. Merlie (1995). "Failure of postsynaptic specialization to develop at neuromuscular junctions of rapsyn-deficient mice." Nature **377**(6546): 232-236.

Gehle, V. M., E. C. Walcott, T. Nishizaki and K. Sumikawa (1997). "N-glycosylation at the conserved sites ensures the expression of properly folded functional ACh receptors." Brain Res Mol Brain Res **45**(2): 219-229.

Gertler, R. A. and N. Robbins (1978). "Differences in neuromuscular transmission in red and white muscles." Brain Res **142**(1): 160-164.

Gesemann, M., A. J. Denzer and M. A. Ruegg (1995). "Acetylcholine receptor-aggregating activity of agrin isoforms and mapping of the active site." J Cell Biol **128**(4): 625-636.

Gillespie, S. K., S. Balasubramanian, E. T. Fung and R. L. Huganir (1996). "Rapsyn clusters and activates the synapse-specific receptor tyrosine kinase MuSK." Neuron **16**(5): 953-962.

Glass, D. J. (2005). "Skeletal muscle hypertrophy and atrophy signaling pathways." Int J Biochem Cell Biol **37**(10): 1974-1984.

Goddeeris, M. M., B. Wu, D. Venzke, T. Yoshida-Moriguchi, F. Saito, K. Matsumura, S. A. Moore and K. P. Campbell (2013). "LARGE glycans on dystroglycan function as a tunable matrix scaffold to prevent dystrophy." Nature **503**(7474): 136-140.

Goh, Q. and D. P. Millay (2017). "Requirement of myomaker-mediated stem cell fusion for skeletal muscle hypertrophy." Elife **6**.

Gorgens, S. W., K. Eckardt, J. Jensen, C. A. Drevon and J. Eckel (2015). "Exercise and Regulation of Adipokine and Myokine Production." Prog Mol Biol Transl Sci **135**: 313-336.

Gramolini, A. O., L. M. Angus, L. Schaeffer, E. A. Burton, J. M. Tinsley, K. E. Davies, J. P. Changeux and B. J. Jasmin (1999). "Induction of utrophin gene expression by heregulin in skeletal muscle cells: role of the N-box motif and GA binding protein." Proc Natl Acad Sci U S A **96**(6): 3223-3227.

Griggs, R. C., W. Kingston, R. F. Jozefowicz, B. E. Herr, G. Forbes and D. Halliday (1989). "Effect of testosterone on muscle mass and muscle protein synthesis." J Appl Physiol (1985) **66**(1): 498-503.

Halder, G., S. Dupont and S. Piccolo (2012). "Transduction of mechanical and cytoskeletal cues by YAP and TAZ." Nat Rev Mol Cell Biol **13**(9): 591-600.

Han, H. Q., X. Zhou, W. E. Mitch and A. L. Goldberg (2013). "Myostatin/activin pathway antagonism: molecular basis and therapeutic potential." Int J Biochem Cell Biol **45**(10): 2333-2347.

Handschin, C. and B. M. Spiegelman (2008). "The role of exercise and PGC1alpha in inflammation and chronic disease." Nature **454**(7203): 463-469.

Hansen, C. G., Y. L. Ng, W. L. Lam, S. W. Plouffe and K. L. Guan (2015). "The Hippo pathway effectors YAP and TAZ promote cell growth by modulating amino acid signaling to mTORC1." Cell Res **25**(12): 1299-1313.

Hara, K., Y. Maruki, X. Long, K. Yoshino, N. Oshiro, S. Hidayat, C. Tokunaga, J. Avruch and K. Yonezawa (2002). "Raptor, a binding partner of target of rapamycin (TOR), mediates TOR action." Cell **110**(2): 177-189.

Hara, Y., B. Balci-Hayta, T. Yoshida-Moriguchi, M. Kanagawa, D. Beltran-Valero de Bernabe, H. Gundesli, T. Willer, J. S. Satz, R. W. Crawford, S. J. Burden, S. Kunz, M. B. Oldstone, A. Accardi, B. Talim, F. Muntoni, H. Topaloglu, P. Dincer and K. P. Campbell (2011). "A dystroglycan mutation associated with limb-girdle muscular dystrophy." N Engl J Med **364**(10): 939-946.

Hennig, R. and T. Lomo (1985). "Firing patterns of motor units in normal rats." Nature **314**(6007): 164-166.

Herbst, R., T. Iskratsch, E. Unger and R. E. Bittner (2009). "Aberrant development of neuromuscular junctions in glycosylation-defective Large(myd) mice." Neuromuscul Disord **19**(5): 366-378.

Hippenmeyer, S., R. M. Huber, D. R. Ladle, K. Murphy and S. Arber (2007). "ETS transcription factor Erm controls subsynaptic gene expression in skeletal muscles." Neuron **55**(5): 726-740.

Hornberger, T. A. (2011). "Mechanotransduction and the regulation of mTORC1 signaling in skeletal muscle." Int J Biochem Cell Biol **43**(9): 1267-1276.

Hughes, D. C., M. A. Wallace and K. Baar (2015). "Effects of aging, exercise, and disease on force transfer in skeletal muscle." Am J Physiol Endocrinol Metab **309**(1): E1-E10.

Ibraghimov-Beskrovnaya, O., J. M. Ervasti, C. J. Leveille, C. A. Slaughter, S. W. Sernett and K. P. Campbell (1992). "Primary structure of dystrophin-associated glycoproteins linking dystrophin to the extracellular matrix." Nature **355**(6362): 696-702.

Inoki, K. and K. L. Guan (2006). "Complexity of the TOR signaling network." Trends Cell Biol **16**(4): 206-212.

Inoki, K., Y. Li, T. Xu and K. L. Guan (2003). "Rheb GTPase is a direct target of TSC2 GAP activity and regulates mTOR signaling." Genes Dev **17**(15): 1829-1834.

Iyer, S. R., S. B. Shah, C. W. Ward, J. P. Stains, E. E. Spangenburg, E. S. Folker and R. M. Lovering (2019). "Differential YAP nuclear signaling in healthy and dystrophic skeletal muscle." Am J Physiol Cell Physiol **317**(1): C48-C57.

Jacinto, E., V. Facchinetti, D. Liu, N. Soto, S. Wei, S. Y. Jung, Q. Huang, J. Qin and B. Su (2006). "SIN1/MIP1 maintains rictor-mTOR complex integrity and regulates Akt phosphorylation and substrate specificity." Cell **127**(1): 125-137.

Jacinto, E., R. Loewith, A. Schmidt, S. Lin, M. A. Ruegg, A. Hall and M. N. Hall (2004). "Mammalian TOR complex 2 controls the actin cytoskeleton and is rapamycin insensitive." Nat Cell Biol **6**(11): 1122-1128.

Jackson, J. R., J. Mula, T. J. Kirby, C. S. Fry, J. D. Lee, M. F. Ubele, K. S. Campbell, J. J. McCarthy, C. A. Peterson and E. E. Dupont-Versteegden (2012). "Satellite cell depletion does not inhibit adult skeletal muscle regrowth following unloading-induced atrophy." Am J Physiol Cell Physiol **303**(8): C854-861.

Jacobs, B. L., C. A. Goodman and T. A. Hornberger (2014). "The mechanical activation of mTOR signaling: an emerging role for late endosome/lysosomal targeting." J Muscle Res Cell Motil **35**(1): 11-21.

Jaka, O., L. Casas-Fraile, A. Lopez de Munain and A. Saenz (2015). "Costamere proteins and their involvement in myopathic processes." Expert Rev Mol Med **17**: e12.

Jaworski, A., C. L. Smith and S. J. Burden (2007). "GA-binding protein is dispensable for neuromuscular synapse formation and synapse-specific gene expression." Mol Cell Biol **27**(13): 5040-5046.

Kaizuka, T., T. Hara, N. Oshiro, U. Kikkawa, K. Yonezawa, K. Takehana, S. Iemura, T. Natsume and N. Mizushima (2010). "Tti1 and Tel2 are critical factors in mammalian target of rapamycin complex assembly." J Biol Chem **285**(26): 20109-20116.

Kanzleiter, T., M. Rath, S. W. Gorgens, J. Jensen, D. S. Tangen, A. J. Kolnes, K. J. Kolnes, S. Lee, J. Eckel, A. Schurmann and K. Eckardt (2014). "The myokine decorin is regulated by contraction and involved in muscle hypertrophy." Biochem Biophys Res Commun **450**(2): 1089-1094.

Khanna, N., Y. Fang, M. S. Yoon and J. Chen (2013). "XPLN is an endogenous inhibitor of mTORC2." Proc Natl Acad Sci U S A **110**(40): 15979-15984.

Khurana, T. S., A. G. Rosmarin, J. Shang, T. O. Krag, S. Das and S. Gammeltoft (1999). "Activation of utrophin promoter by heregulin via the ets-related transcription factor complex GA-binding protein alpha/beta." Mol Biol Cell **10**(6): 2075-2086.

Kim, N., A. L. Stiegler, T. O. Cameron, P. T. Hallock, A. M. Gomez, J. H. Huang, S. R. Hubbard, M. L. Dustin and S. J. Burden (2008). "Lrp4 is a receptor for Agrin and forms a complex with MuSK." Cell **135**(2): 334-342.

Kirby, T. J., R. M. Patel, T. S. McClintock, E. E. Dupont-Versteegden, C. A. Peterson and J. J. McCarthy (2016). "Myonuclear transcription is responsive to mechanical load and DNA content but uncoupled from cell size during hypertrophy." Mol Biol Cell **27**(5): 788-798.

Kleinert, M., B. L. Parker, A. M. Fritzen, J. R. Knudsen, T. E. Jensen, R. Kjobsted, L. Sylow, M. Ruegg, D. E. James and E. A. Richter (2017). "Mammalian target of rapamycin complex 2 regulates muscle glucose uptake during exercise in mice." J Physiol **595**(14): 4845-4855.

Koike, S., L. Schaeffer and J. P. Changeux (1995). "Identification of a DNA element determining synaptic expression of the mouse acetylcholine receptor delta-subunit gene." Proc Natl Acad Sci U S A **92**(23): 10624-10628.

Kroger, S. (2018). "Proprioception 2.0: novel functions for muscle spindles." Curr Opin Neurol **31**(5): 592-598.

Kruger, M. and S. Kotter (2016). "Titin, a Central Mediator for Hypertrophic Signaling, Exercise-Induced Mechanosignaling and Skeletal Muscle Remodeling." Front Physiol **7**: 76.

Labeit, S., B. Kolmerer and W. A. Linke (1997). "The giant protein titin. Emerging roles in physiology and pathophysiology." Circ Res **80**(2): 290-294.

Lach-Trifilieff, E., G. C. Minetti, K. Sheppard, C. Ibebunjo, J. N. Feige, S. Hartmann, S. Brachat, H. Rivet, C. Koelbing, F. Morvan, S. Hatakeyama and D. J. Glass (2014). "An antibody blocking activin type II receptors induces strong skeletal muscle hypertrophy and protects from atrophy." Mol Cell Biol **34**(4): 606-618.

LaMarco, K., C. C. Thompson, B. P. Byers, E. M. Walton and S. L. McKnight (1991). "Identification of Ets- and notch-related subunits in GA binding protein." Science **253**(5021): 789-792.

Lange, S., F. Xiang, A. Yakovenko, A. Vihola, P. Hackman, E. Rostkova, J. Kristensen, B. Brandmeier, G. Franzen, B. Hedberg, L. G. Gunnarsson, S. M. Hughes, S. Marchand, T. Sejersen, I. Richard, L. Edstrom, E. Ehler, B. Udd and M. Gautel (2005). "The kinase domain of titin controls muscle gene expression and protein turnover." Science **308**(5728): 1599-1603.

Larsson, L., L. Edstrom, B. Lindegren, L. Gorza and S. Schiaffino (1991). "MHC composition and enzyme-histochemical and physiological properties of a novel fast-twitch motor unit type." Am J Physiol **261**(1 Pt 1): C93-101.

Lecker, S. H., A. Zavin, P. Cao, R. Arena, K. Allsup, K. M. Daniels, J. Joseph, P. C. Schulze and D. E. Forman (2012). "Expression of the irisin precursor FNDC5 in skeletal muscle correlates

with aerobic exercise performance in patients with heart failure." Circ Heart Fail **5**(6): 812-818.

Lee, D. F., H. P. Kuo, C. T. Chen, J. M. Hsu, C. K. Chou, Y. Wei, H. L. Sun, L. Y. Li, B. Ping, W. C. Huang, X. He, J. Y. Hung, C. C. Lai, Q. Ding, J. L. Su, J. Y. Yang, A. A. Sahin, G. N. Hortobagyi, F. J. Tsai, C. H. Tsai and M. C. Hung (2007). "IKK beta suppression of TSC1 links inflammation and tumor angiogenesis via the mTOR pathway." Cell **130**(3): 440-455.

Lee, K. Y., M. K. Singh, S. Ussar, P. Wetzel, M. F. Hirshman, L. J. Goodyear, A. Kispert and C. R. Kahn (2015). "Tbx15 controls skeletal muscle fibre-type determination and muscle metabolism." Nat Commun **6**: 8054.

Lee, S. J. and A. C. McPherron (2001). "Regulation of myostatin activity and muscle growth." Proc Natl Acad Sci U S A **98**(16): 9306-9311.

Li, L., W. C. Xiong and L. Mei (2018). "Neuromuscular Junction Formation, Aging, and Disorders." Annu Rev Physiol **80**: 159-188.

Li, X., D. C. McFarland and S. G. Velleman (2008). "Extracellular matrix proteoglycan decorin-mediated myogenic satellite cell responsiveness to transforming growth factor-beta1 during cell proliferation and differentiation Decorin and transforming growth factor-beta1 in satellite cells." Domest Anim Endocrinol **35**(3): 263-273.

Lin, W., R. W. Burgess, B. Dominguez, S. L. Pfaff, J. R. Sanes and K. F. Lee (2001). "Distinct roles of nerve and muscle in postsynaptic differentiation of the neuromuscular synapse." Nature **410**(6832): 1057-1064.

Linke, W. A., V. I. Popov and G. H. Pollack (1994). "Passive and active tension in single cardiac myofibrils." Biophys J **67**(2): 782-792.

Linnoila, J., Y. Wang, Y. Yao and Z. Z. Wang (2008). "A mammalian homolog of Drosophila tumorous imaginal discs, Tid1, mediates agrin signaling at the neuromuscular junction." Neuron **60**(4): 625-641.

Liu, M., D. W. Hammers, E. R. Barton and H. L. Sweeney (2016). "Activin Receptor Type IIB Inhibition Improves Muscle Phenotype and Function in a Mouse Model of Spinal Muscular Atrophy." PLoS One **11**(11): e0166803.

Liu, Y., S. L. Carroll, M. G. Klein and M. F. Schneider (1997). "Calcium transients and calcium homeostasis in adult mouse fast-twitch skeletal muscle fibers in culture." Am J Physiol **272**(6 Pt 1): C1919-1927.

Lu, Z., H. S. Je, P. Young, J. Gross, B. Lu and G. Feng (2007). "Regulation of synaptic growth and maturation by a synapse-associated E3 ubiquitin ligase at the neuromuscular junction." J Cell Biol **177**(6): 1077-1089.

Ma, X. M. and J. Blenis (2009). "Molecular mechanisms of mTOR-mediated translational control." Nat Rev Mol Cell Biol **10**(5): 307-318.

MacLennan, D. H., C. J. Brandl, S. Champaneria, P. C. Holland, V. E. Powers and H. F. Willard (1987). "Fast-twitch and slow-twitch/cardiac Ca2+ ATPase genes map to human chromosomes 16 and 12." Somat Cell Mol Genet **13**(4): 341-346.

Marcotte, G. R., D. W. West and K. Baar (2015). "The molecular basis for load-induced skeletal muscle hypertrophy." Calcif Tissue Int **96**(3): 196-210.

Margreth, A., E. Damiani and G. Tobaldin (1993). "Ratio of dihydropyridine to ryanodine receptors in mammalian and frog twitch muscles in relation to the mechanical hypothesis of excitation-contraction coupling." Biochem Biophys Res Commun **197**(3): 1303-1311.

Martin, P. T. and J. R. Sanes (1995). "Role for a synapse-specific carbohydrate in agrin-induced clustering of acetylcholine receptors." Neuron **14**(4): 743-754.

Martin, P. T., L. J. Scott, B. E. Porter and J. R. Sanes (1999). "Distinct structures and functions of related pre- and postsynaptic carbohydrates at the mammalian neuromuscular junction." Mol Cell Neurosci **13**(2): 105-118.

Maselli, R. A., J. Arredondo, O. Cagney, J. J. Ng, J. A. Anderson, C. Williams, B. J. Gerke, B. Soliven and R. L. Wollmann (2010). "Mutations in MUSK causing congenital myasthenic syndrome impair MuSK-Dok-7 interaction." Hum Mol Genet **19**(12): 2370-2379.

Maselli, R. A., V. Dunne, S. I. Pascual-Pascual, C. Bowe, M. Agius, R. Frank and R. L. Wollmann (2003). "Rapsyn mutations in myasthenic syndrome due to impaired receptor clustering." Muscle Nerve **28**(3): 293-301.

Matthews, V. B., M. B. Astrom, M. H. Chan, C. R. Bruce, K. S. Krabbe, O. Prelovsek, T. Akerstrom, C. Yfanti, C. Broholm, O. H. Mortensen, M. Penkowa, P. Hojman, A. Zankari, M. J. Watt, H. Bruunsgaard, B. K. Pedersen and M. A. Febbraio (2009). "Brain-derived neurotrophic factor is produced by skeletal muscle cells in response to contraction and enhances fat oxidation via activation of AMP-activated protein kinase." Diabetologia **52**(7): 1409-1418.

Mattson, M. P., K. Moehl, N. Ghena, M. Schmaedick and A. Cheng (2018). "Intermittent metabolic switching, neuroplasticity and brain health." Nat Rev Neurosci **19**(2): 63-80.

McPherron, A. C., A. M. Lawler and S. J. Lee (1997). "Regulation of skeletal muscle mass in mice by a new TGF-beta superfamily member." Nature **387**(6628): 83-90.

Meng, Z., Y. Qiu, K. C. Lin, A. Kumar, J. K. Placone, C. Fang, K. C. Wang, S. Lu, M. Pan, A. W. Hong, T. Moroishi, M. Luo, S. W. Plouffe, Y. Diao, Z. Ye, H. W. Park, X. Wang, F. X. Yu, S. Chien, C. Y. Wang, B. Ren, A. J. Engler and K. L. Guan (2018). "RAP2 mediates mechanoresponses of the Hippo pathway." Nature **560**(7720): 655-660.

Meng, Z. X., S. Li, L. Wang, H. J. Ko, Y. Lee, D. Y. Jung, M. Okutsu, Z. Yan, J. K. Kim and J. D. Lin (2013). "Baf60c drives glycolytic metabolism in the muscle and improves systemic glucose homeostasis through Deptor-mediated Akt activation." Nat Med **19**(5): 640-645.

Milan, G., V. Romanello, F. Pescatore, A. Armani, J. H. Paik, L. Frasson, A. Seydel, J. Zhao, R. Abraham, A. L. Goldberg, B. Blaauw, R. A. DePinho and M. Sandri (2015). "Regulation of autophagy and the ubiquitin-proteasome system by the FoxO transcriptional network during muscle atrophy." Nat Commun **6**: 6670.

Milone, M., X. M. Shen, D. Selcen, K. Ohno, J. Brengman, S. T. Iannaccone, C. M. Harper and A. G. Engel (2009). "Myasthenic syndrome due to defects in rapsyn: Clinical and molecular findings in 39 patients." Neurology **73**(3): 228-235.

Milton, R. L., M. T. Lupa and J. H. Caldwell (1992). "Fast and slow twitch skeletal muscle fibres differ in their distribution of Na channels near the endplate." Neurosci Lett **135**(1): 41-44.

Mobley, C. B., T. A. Hornberger, C. D. Fox, J. C. Healy, B. S. Ferguson, R. P. Lowery, R. M. McNally, C. M. Lockwood, J. R. Stout, A. N. Kavazis, J. M. Wilson and M. D. Roberts (2015). "Effects of oral phosphatidic acid feeding with or without whey protein on muscle protein synthesis and anabolic signaling in rodent skeletal muscle." J Int Soc Sports Nutr **12**: 32.

Moransard, M., L. S. Borges, R. Willmann, P. A. Marangi, H. R. Brenner, M. J. Ferns and C. Fuhrer (2003). "Agrin regulates rapsyn interaction with surface acetylcholine receptors, and this underlies cytoskeletal anchoring and clustering." J Biol Chem **278**(9): 7350-7359.

Morvan, F., J. M. Rondeau, C. Zou, G. Minetti, C. Scheufler, M. Scharenberg, C. Jacobi, P. Brebbia, V. Ritter, G. Toussaint, C. Koelbing, X. Leber, A. Schilb, F. Witte, S. Lehmann, E. Koch, S. Geisse, D. J. Glass and E. Lach-Trifilieff (2017). "Blockade of activin type II receptors with a dual anti-ActRIIA/IIB antibody is critical to promote maximal skeletal muscle hypertrophy." Proc Natl Acad Sci U S A **114**(47): 12448-12453.

Murach, K. A., C. S. Fry, T. J. Kirby, J. R. Jackson, J. D. Lee, S. H. White, E. E. Dupont-Versteegden, J. J. McCarthy and C. A. Peterson (2018). "Starring or Supporting Role? Satellite Cells and Skeletal Muscle Fiber Size Regulation." Physiology (Bethesda) **33**(1): 26-38.

Nam, T., J. H. Han, S. Devkota and H. W. Lee (2017). "Emerging Paradigm of Crosstalk between Autophagy and the Ubiquitin-Proteasome System." Mol Cells **40**(12): 897-905.

Neagoe, C., C. A. Opitz, I. Makarenko and W. A. Linke (2003). "Gigantic variety: expression patterns of titin isoforms in striated muscles and consequences for myofibrillar passive stiffness." J Muscle Res Cell Motil **24**(2-3): 175-189.

Neame, P. J., C. J. Kay, D. J. McQuillan, M. P. Beales and J. R. Hassell (2000). "Independent modulation of collagen fibrillogenesis by decorin and lumican." Cell Mol Life Sci **57**(5): 859-863.

Nichols, P., R. Croxen, A. Vincent, R. Rutter, M. Hutchinson, J. Newsom-Davis and D. Beeson (1999). "Mutation of the acetylcholine receptor epsilon-subunit promoter in congenital myasthenic syndrome." Ann Neurol **45**(4): 439-443.

O'Leary, D. A., P. G. Noakes, N. A. Lavidis, I. Kola, P. J. Hertzog and S. Ristevski (2007). "Targeting of the ETS factor GABPalpha disrupts neuromuscular junction synaptic function." Mol Cell Biol **27**(9): 3470-3480.

O'Neill, B. T., G. Bhardwaj, C. M. Penniman, M. T. Krumpoch, P. A. Suarez Beltran, K. Klaus, K. Poro, M. Li, H. Pan, J. M. Dreyfuss, K. S. Nair and C. R. Kahn (2019). "FoxO Transcription Factors Are Critical Regulators of Diabetes-Related Muscle Atrophy." Diabetes **68**(3): 556-570.

Ohno, K., B. Anlar and A. G. Engel (1999). "Congenital myasthenic syndrome caused by a mutation in the Ets-binding site of the promoter region of the acetylcholine receptor epsilon subunit gene." Neuromuscul Disord **9**(3): 131-135.

Okada, K., A. Inoue, M. Okada, Y. Murata, S. Kakuta, T. Jigami, S. Kubo, H. Shiraishi, K. Eguchi, M. Motomura, T. Akiyama, Y. Iwakura, O. Higuchi and Y. Yamanashi (2006). "The muscle protein Dok-7 is essential for neuromuscular synaptogenesis." Science **312**(5781): 1802-1805.

Ostrowski, K., T. Rohde, M. Zacho, S. Asp and B. K. Pedersen (1998). "Evidence that interleukin-6 is produced in human skeletal muscle during prolonged running." J Physiol **508 (Pt 3)**: 949-953.

Pankiv, S., T. H. Clausen, T. Lamark, A. Brech, J. A. Bruun, H. Outzen, A. Overvatn, G. Bjorkoy and T. Johansen (2007). "p62/SQSTM1 binds directly to Atg8/LC3 to facilitate degradation of ubiquitinated protein aggregates by autophagy." J Biol Chem **282**(33): 24131-24145.

Pardo, J. V., J. D. Siliciano and S. W. Craig (1983). "A vinculin-containing cortical lattice in skeletal muscle: transverse lattice elements ("costameres") mark sites of attachment between myofibrils and sarcolemma." Proc Natl Acad Sci U S A **80**(4): 1008-1012.

Parmar, N. and F. Tamanoi (2010). "Rheb G-Proteins and the Activation of mTORC1." Enzymes **27**: 39-56.

Patton, B. L., J. H. Miner, A. Y. Chiu and J. R. Sanes (1997). "Distribution and function of laminins in the neuromuscular system of developing, adult, and mutant mice." J Cell Biol **139**(6): 1507-1521.

Pearce, L. R., X. Huang, J. Boudeau, R. Pawlowski, S. Wullschleger, M. Deak, A. F. Ibrahim, R. Gourlay, M. A. Magnuson and D. R. Alessi (2007). "Identification of Protor as a novel Rictor-binding component of mTOR complex-2." Biochem J **405**(3): 513-522.

Pedersen, B. K. and M. A. Febbraio (2012). "Muscles, exercise and obesity: skeletal muscle as a secretory organ." Nat Rev Endocrinol **8**(8): 457-465.

Pereira, R. M. and J. Freire de Carvalho (2011). "Glucocorticoid-induced myopathy." Joint Bone Spine **78**(1): 41-44.

Peter, A. K., H. Cheng, R. S. Ross, K. U. Knowlton and J. Chen (2011). "The costamere bridges sarcomeres to the sarcolemma in striated muscle." Prog Pediatr Cardiol **31**(2): 83-88.

Peterson, T. R., M. Laplante, C. C. Thoreen, Y. Sancak, S. A. Kang, W. M. Kuehl, N. S. Gray and D. M. Sabatini (2009). "DEPTOR is an mTOR inhibitor frequently overexpressed in multiple myeloma cells and required for their survival." Cell **137**(5): 873-886.

Pette, D. (2002). "The adaptive potential of skeletal muscle fibers." Can J Appl Physiol **27**(4): 423-448.

Phillips, C., M. A. Baktir, M. Srivatsan and A. Salehi (2014). "Neuroprotective effects of physical activity on the brain: a closer look at trophic factor signaling." Front Cell Neurosci **8**: 170.

Polyzos, S. A., A. D. Anastasilakis, Z. A. Efstathiadou, P. Makras, N. Perakakis, J. Kountouras and C. S. Mantzoros (2018). "Irisin in metabolic diseases." Endocrine **59**(2): 260-274.

Prakash, Y. S., S. M. Miller, M. Huang and G. C. Sieck (1996). "Morphology of diaphragm neuromuscular junctions on different fibre types." J Neurocytol **25**(2): 88-100.

Pregelj, P., M. Trinkaus, D. Zupan, J. J. Trontelj and J. Sketelj (2007). "The role of muscle activation pattern and calcineurin in acetylcholinesterase regulation in rat skeletal muscles." J Neurosci **27**(5): 1106-1113.

Prives, J. and D. Bar-Sagi (1983). "Effect of tunicamycin, an inhibitor of protein glycosylation, on the biological properties of acetylcholine receptor in cultured muscle cells." J Biol Chem **258**(3): 1775-1780.

Puchner, E. M., A. Alexandrovich, A. L. Kho, U. Hensen, L. V. Schafer, B. Brandmeier, F. Grater, H. Grubmuller, H. E. Gaub and M. Gautel (2008). "Mechanoenzymatics of titin kinase." Proc Natl Acad Sci U S A **105**(36): 13385-13390.

Qaisar, R., G. Renaud, K. Morine, E. R. Barton, H. L. Sweeney and L. Larsson (2012). "Is functional hypertrophy and specific force coupled with the addition of myonuclei at the single muscle fiber level?" FASEB J **26**(3): 1077-1085.

Reid, B., C. R. Slater and G. S. Bewick (1999). "Synaptic vesicle dynamics in rat fast and slow motor nerve terminals." J Neurosci **19**(7): 2511-2521.

Reid, M. B. and Y. P. Li (2001). "Tumor necrosis factor-alpha and muscle wasting: a cellular perspective." Respir Res **2**(5): 269-272.

Reist, N. E., M. J. Werle and U. J. McMahan (1992). "Agrin released by motor neurons induces the aggregation of acetylcholine receptors at neuromuscular junctions." Neuron **8**(5): 865-868.

Richter, E. A., L. P. Garetto, M. N. Goodman and N. B. Ruderman (1982). "Muscle glucose metabolism following exercise in the rat: increased sensitivity to insulin." J Clin Invest **69**(4): 785-793.

Rios, E. and G. Brum (1987). "Involvement of dihydropyridine receptors in excitation-contraction coupling in skeletal muscle." Nature **325**(6106): 717-720.

Rodriguez Cruz, P. M., J. Palace and D. Beeson (2014). "Inherited disorders of the neuromuscular junction: an update." J Neurol **261**(11): 2234-2243.

Rooks, D., J. Praestgaard, S. Hariry, D. Laurent, O. Petricoul, R. G. Perry, E. Lach-Trifilieff and R. Roubenoff (2017). "Treatment of Sarcopenia with Bimagrumab: Results from a Phase II, Randomized, Controlled, Proof-of-Concept Study." J Am Geriatr Soc **65**(9): 1988-1995.

Rossi, S. G., A. E. Vazquez and R. L. Rotundo (2000). "Local control of acetylcholinesterase gene expression in multinucleated skeletal muscle fibers: individual nuclei respond to signals from the overlying plasma membrane." J Neurosci **20**(3): 919-928.

Ruegg, M. A. (2005). "Organization of synaptic myonuclei by Syne proteins and their role during the formation of the nerve-muscle synapse." Proc Natl Acad Sci U S A **102**(16): 5643-5644.

Ruegg, M. A., K. W. Tsim, S. E. Horton, S. Kroger, G. Escher, E. M. Gensch and U. J. McMahan (1992). "The agrin gene codes for a family of basal lamina proteins that differ in function and distribution." Neuron **8**(4): 691-699.

Ruff, R. L. and D. Whittlesey (1992). "Na+ current densities and voltage dependence in human intercostal muscle fibres." J Physiol **458**: 85-97.

Rybalka, E., C. A. Timpani, C. G. Stathis, A. Hayes and M. B. Cooke (2015). "Metabogenic and Nutriceutical Approaches to Address Energy Dysregulation and Skeletal Muscle Wasting in Duchenne Muscular Dystrophy." Nutrients **7**(12): 9734-9767.

Ryder, S., R. M. Leadley, N. Armstrong, M. Westwood, S. de Kock, T. Butt, M. Jain and J. Kleijnen (2017). "The burden, epidemiology, costs and treatment for Duchenne muscular dystrophy: an evidence review." Orphanet J Rare Dis **12**(1): 79.

Salviati, G., M. M. Sorenson and A. B. Eastwood (1982). "Calcium accumulation by the sarcoplasmic reticulum in two populations of chemically skinned human muscle fibers. Effects of calcium and cyclic AMP." J Gen Physiol **79**(4): 603-632.

Sancak, Y., T. R. Peterson, Y. D. Shaul, R. A. Lindquist, C. C. Thoreen, L. Bar-Peled and D. M. Sabatini (2008). "The Rag GTPases bind raptor and mediate amino acid signaling to mTORC1." Science **320**(5882): 1496-1501.

Sancak, Y., C. C. Thoreen, T. R. Peterson, R. A. Lindquist, S. A. Kang, E. Spooner, S. A. Carr and D. M. Sabatini (2007). "PRAS40 is an insulin-regulated inhibitor of the mTORC1 protein kinase." Mol Cell **25**(6): 903-915.

Sandri, M. (2013). "Protein breakdown in muscle wasting: role of autophagy-lysosome and ubiquitin-proteasome." Int J Biochem Cell Biol **45**(10): 2121-2129.

Sandri, M., C. Sandri, A. Gilbert, C. Skurk, E. Calabria, A. Picard, K. Walsh, S. Schiaffino, S. H. Lecker and A. L. Goldberg (2004). "Foxo transcription factors induce the atrophy-related ubiquitin ligase atrogin-1 and cause skeletal muscle atrophy." Cell **117**(3): 399-412.

Sartori, R., G. Milan, M. Patron, C. Mammucari, B. Blaauw, R. Abraham and M. Sandri (2009). "Smad2 and 3 transcription factors control muscle mass in adulthood." Am J Physiol Cell Physiol **296**(6): C1248-1257.

Savarese, M., J. Sarparanta, A. Vihola, B. Udd and P. Hackman (2016). "Increasing Role of Titin Mutations in Neuromuscular Disorders." J Neuromuscul Dis **3**(3): 293-308.

Sawa, C., M. Goto, F. Suzuki, H. Watanabe, J. Sawada and H. Handa (1996). "Functional domains of transcription factor hGABP beta1/E4TF1-53 required for nuclear localization and transcription activation." Nucleic Acids Res **24**(24): 4954-4961.

Schaeffer, L., A. de Kerchove d'Exaerde and J. P. Changeux (2001). "Targeting transcription to the neuromuscular synapse." Neuron **31**(1): 15-22.

Schaeffer, L., N. Duclert, M. Huchet-Dymanus and J. P. Changeux (1998). "Implication of a multisubunit Ets-related transcription factor in synaptic expression of the nicotinic acetylcholine receptor." EMBO J **17**(11): 3078-3090.

Schiaffino, S., L. Gorza, S. Sartore, L. Saggin, S. Ausoni, M. Vianello, K. Gundersen and T. Lomo (1989). "Three myosin heavy chain isoforms in type 2 skeletal muscle fibres." J Muscle Res Cell Motil **10**(3): 197-205.

Schiaffino, S., V. Hanzlikova and S. Pierobon (1970). "Relations between structure and function in rat skeletal muscle fibers." J Cell Biol **47**(1): 107-119.

Schiaffino, S. and C. Mammucari (2011). "Regulation of skeletal muscle growth by the IGF1-Akt/PKB pathway: insights from genetic models." Skelet Muscle **1**(1): 4.

Schiaffino, S. and C. Reggiani (2011). "Fiber types in mammalian skeletal muscles." Physiol Rev **91**(4): 1447-1531.

Schmidt, S. F., M. Rohm, S. Herzig and M. Berriel Diaz (2018). "Cancer Cachexia: More Than Skeletal Muscle Wasting." Trends Cancer **4**(12): 849-860.

Schnyder, S. and C. Handschin (2015). "Skeletal muscle as an endocrine organ: PGC-1alpha, myokines and exercise." Bone **80**: 115-125.

Schwaller, B., J. Dick, G. Dhoot, S. Carroll, G. Vrbova, P. Nicotera, D. Pette, A. Wyss, H. Bluethmann, W. Hunziker and M. R. Celio (1999). "Prolonged contraction-relaxation cycle of fast-twitch muscles in parvalbumin knockout mice." Am J Physiol **276**(2): C395-403.

Seaborne, R. A., D. C. Hughes, D. C. Turner, D. J. Owens, L. M. Baehr, P. Gorski, E. A. Semenova, O. V. Borisov, A. K. Larin, D. V. Popov, E. V. Generozov, H. Sutherland, Ahmetov, II, J. C. Jarvis, S. C. Bodine and A. P. Sharples (2019). "UBR5 is a novel E3 ubiquitin ligase involved in skeletal muscle hypertrophy and recovery from atrophy." J Physiol **597**(14): 3727-3749.

Seaborne, R. A., J. Strauss, M. Cocks, S. Shepherd, T. D. O'Brien, K. A. van Someren, P. G. Bell, C. Murgatroyd, J. P. Morton, C. E. Stewart and A. P. Sharples (2018). "Human Skeletal Muscle Possesses an Epigenetic Memory of Hypertrophy." Sci Rep **8**(1): 1898.

Seibenhener, M. L., T. Geetha and M. W. Wooten (2007). "Sequestosome 1/p62--more than just a scaffold." FEBS Lett **581**(2): 175-179.

Sengupta, S., T. R. Peterson and D. M. Sabatini (2010). "Regulation of the mTOR complex 1 pathway by nutrients, growth factors, and stress." Mol Cell **40**(2): 310-322.

Siciliano, G., C. Simoncini, S. Giannotti, V. Zampa, C. Angelini and G. Ricci (2015). "Muscle exercise in limb girdle muscular dystrophies: pitfall and advantages." Acta Myol **34**(1): 3-8.

Singhal, N. and P. T. Martin (2011). "Role of extracellular matrix proteins and their receptors in the development of the vertebrate neuromuscular junction." Dev Neurobiol **71**(11): 982-1005.

Souza, T. A., X. Chen, Y. Guo, P. Sava, J. Zhang, J. J. Hill, P. J. Yaworsky and Y. Qiu (2008). "Proteomic identification and functional validation of activins and bone morphogenetic protein 11 as candidate novel muscle mass regulators." Mol Endocrinol **22**(12): 2689-2702.

Spenst, L. F., A. D. Martin and D. T. Drinkwater (1993). "Muscle mass of competitive male athletes." J Sports Sci **11**(1): 3-8.

Street, S. F. (1983). "Lateral transmission of tension in frog myofibers: a myofibrillar network and transverse cytoskeletal connections are possible transmitters." J Cell Physiol **114**(3): 346-364.

Stump, C. S., E. J. Henriksen, Y. Wei and J. R. Sowers (2006). "The metabolic syndrome: role of skeletal muscle metabolism." Ann Med **38**(6): 389-402.

Sugiura, Y. and W. Lin (2011). "Neuron-glia interactions: the roles of Schwann cells in neuromuscular synapse formation and function." Biosci Rep **31**(5): 295-302.

Svard, J., T. H. Rost, C. E. N. Sommervoll, C. Haugen, O. A. Gudbrandsen, A. E. Mellgren, E. Rodahl, J. Ferno, S. N. Dankel, J. V. Sagen and G. Mellgren (2019). "Absence of the proteoglycan decorin reduces glucose tolerance in overfed male mice." Sci Rep **9**(1): 4614.

Taillandier, D. and C. Polge (2019). "Skeletal muscle atrogenes: from rodent models to human pathologies." Biochimie.

Takeshima, H., S. Nishimura, T. Matsumoto, H. Ishida, K. Kangawa, N. Minamino, H. Matsuo, M. Ueda, M. Hanaoka, T. Hirose and et al. (1989). "Primary structure and expression from complementary DNA of skeletal muscle ryanodine receptor." Nature **339**(6224): 439-445.

Talts, J. F., Z. Andac, W. Gohring, A. Brancaccio and R. Timpl (1999). "Binding of the G domains of laminin alpha1 and alpha2 chains and perlecan to heparin, sulfatides, alpha-dystroglycan and several extracellular matrix proteins." EMBO J **18**(4): 863-870.

Tang, W., S. Sencer and S. L. Hamilton (2002). "Calmodulin modulation of proteins involved in excitation-contraction coupling." Front Biosci **7**: d1583-1589.

Tintignac, L. A., H. R. Brenner and M. A. Ruegg (2015). "Mechanisms Regulating Neuromuscular Junction Development and Function and Causes of Muscle Wasting." Physiol Rev **95**(3): 809-852.

Tisdale, M. J. (1997). "Cancer cachexia: metabolic alterations and clinical manifestations." Nutrition **13**(1): 1-7.

Van der Meer, S. F., R. T. Jaspers and H. Degens (2011). "Is the myonuclear domain size fixed?" J Musculoskelet Neuronal Interact **11**(4): 286-297.

van der Meer, S. F., R. T. Jaspers, D. A. Jones and H. Degens (2011). "The time course of myonuclear accretion during hypertrophy in young adult and older rat plantaris muscle." Ann Anat **193**(1): 56-63.

Vogel, K. G. and J. A. Trotter (1987). "The effect of proteoglycans on the morphology of collagen fibrils formed in vitro." Coll Relat Res **7**(2): 105-114.

Wackerhage, H., B. J. Schoenfeld, D. L. Hamilton, M. Lehti and J. J. Hulmi (2019). "Stimuli and sensors that initiate skeletal muscle hypertrophy following resistance exercise." J Appl Physiol (1985) **126**(1): 30-43.

Wang, L., T. E. Harris, R. A. Roth and J. C. Lawrence, Jr. (2007). "PRAS40 regulates mTORC1 kinase activity by functioning as a direct inhibitor of substrate binding." J Biol Chem **282**(27): 20036-20044.

Warram, J. H., B. C. Martin, A. S. Krolewski, J. S. Soeldner and C. R. Kahn (1990). "Slow glucose removal rate and hyperinsulinemia precede the development of type II diabetes in the offspring of diabetic parents." Ann Intern Med **113**(12): 909-915.

Waters, S., K. Marchbank, E. Solomon, C. Whitehouse and M. Gautel (2009). "Interactions with LC3 and polyubiquitin chains link nbr1 to autophagic protein turnover." FEBS Lett **583**(12): 1846-1852.

Weatherbee, S. D., K. V. Anderson and L. A. Niswander (2006). "LDL-receptor-related protein 4 is crucial for formation of the neuromuscular junction." Development **133**(24): 4993-5000.

Whitham, M. and M. A. Febbraio (2016). "The ever-expanding myokinome: discovery challenges and therapeutic implications." Nat Rev Drug Discov **15**(10): 719-729.

Wojtaszewski, J. F., B. F. Hansen, Gade, B. Kiens, J. F. Markuns, L. J. Goodyear and E. A. Richter (2000). "Insulin signaling and insulin sensitivity after exercise in human skeletal muscle." Diabetes **49**(3): 325-331.

Wood, S. J. and C. R. Slater (2001). "Safety factor at the neuromuscular junction." Prog Neurobiol **64**(4): 393-429.

Wrann, C. D., J. P. White, J. Salogiannnis, D. Laznik-Bogoslavski, J. Wu, D. Ma, J. D. Lin, M. E. Greenberg and B. M. Spiegelman (2013). "Exercise induces hippocampal BDNF through a PGC-1alpha/FNDC5 pathway." Cell Metab **18**(5): 649-659.

Wu, H., W. C. Xiong and L. Mei (2010). "To build a synapse: signaling pathways in neuromuscular junction assembly." Development **137**(7): 1017-1033.

Yamada, S., S. Pokutta, F. Drees, W. I. Weis and W. J. Nelson (2005). "Deconstructing the cadherin-catenin-actin complex." Cell **123**(5): 889-901.

Yamaguchi, Y. (2002). "Glycobiology of the synapse: the role of glycans in the formation, maturation, and modulation of synapses." Biochim Biophys Acta **1573**(3): 369-376.

Yang, X., S. Arber, C. William, L. Li, Y. Tanabe, T. M. Jessell, C. Birchmeier and S. J. Burden (2001). "Patterning of muscle acetylcholine receptor gene expression in the absence of motor innervation." Neuron **30**(2): 399-410.

Yoon, M. S. (2017). "mTOR as a Key Regulator in Maintaining Skeletal Muscle Mass." Front Physiol **8**: 788.

You, J. S., H. C. Lincoln, C. R. Kim, J. W. Frey, C. A. Goodman, X. P. Zhong and T. A. Hornberger (2014). "The role of diacylglycerol kinase zeta and phosphatidic acid in the mechanical activation of mammalian target of rapamycin (mTOR) signaling and skeletal muscle hypertrophy." J Biol Chem **289**(3): 1551-1563.

Zhan, G., N. Huang, S. Li, D. Hua, J. Zhang, X. Fang, N. Yang, A. Luo and C. Yang (2018). "PGC-1alpha-FNDC5-BDNF signaling pathway in skeletal muscle confers resilience to stress in mice subjected to chronic social defeat." Psychopharmacology (Berl) **235**(11): 3351-3358.

Zhang, B., S. Luo, X. P. Dong, X. Zhang, C. Liu, Z. Luo, W. C. Xiong and L. Mei (2007). "Beta-catenin regulates acetylcholine receptor clustering in muscle cells through interaction with rapsyn." J Neurosci **27**(15): 3968-3973.

Zhang, W., L. Chang, C. Zhang, R. Zhang, Z. Li, B. Chai, J. Li, E. Chen and M. Mulholland (2015). "Irisin: A myokine with locomotor activity." Neurosci Lett **595**: 7-11.

Zhu, D., Z. Yang, Z. Luo, S. Luo, W. C. Xiong and L. Mei (2008). "Muscle-specific receptor tyrosine kinase endocytosis in acetylcholine receptor clustering in response to agrin." J Neurosci **28**(7): 1688-1696.

Ziegler, M. E., M. M. Hatch, N. Wu, S. A. Muawad and C. C. Hughes (2016). "mTORC2 mediates CXCL12-induced angiogenesis." Angiogenesis **19**(3): 359-371.

2 Aims of the Thesis

Part I / Manuscript I: Ladder climbing as a physiological resistance exercise model for skeletal muscle hypertrophy in mice

Physical exertion has been linked to increased muscular size, performance and health benefits. A sizable body of research has shed light on a plethora of complicated processes that control the adaptation of skeletal muscles to the physical demands placed on them. We now understand that regular resistance exercise (RE) triggers a transient increase in net muscle protein balance by inducing synthesis and concomitantly reducing breakdown of muscle protein, thus facilitating the accretion of muscle mass over time. A multitude of underlying pathways were discovered and thoroughly investigated, yet it remains unclear how exactly the mechanical stimulus of RE is converted into these biochemical signaling events required for muscular growth. The concept of a dedicated mechanoreceptor of muscle cells remains attractive, but no such protein was identified so far. A better understanding of how muscle growth is mechanically activated could lead to the development of pharmacological treatment strategies to counteract muscle wasting caused by disuse, disease and aging.

In the first part of this thesis, we aimed to investigate the effects of RE on the mouse skeletal muscle transcriptome to identify putative mechanosensing proteins involved in adaptive hypertrophy. In order to accomplish this goal, we aimed to establish a physiological RE model in mice that would avoid the confounding effects of the currently available methodologies.

Objective I: *Establish a physiological resistance exercise model for mice and investigate the effect of chronic resistance exercise on the skeletal muscle transcriptome.*

Part II / Manuscript II: Identification of Novel Synaptic Components by Transcriptome Profiling of the Murine Neuromuscular Junction

The neuromuscular junction (NMJ) has been studied as a prototypical synapse for over a century and ample research on it has contributed immensely to our understanding of the inner workings of synapses of the central nervous system. We now understand a lot about how the NMJ conducts signal transmission from motor neurons to the skeletal muscles and that it possesses an extensive safety margin to ensure reliable muscle contractions. Still, the NMJ can be subject to various conditions that perturb its function, causing potentially lifelong disability or even premature death. We hypothesized that the emergence of powerful next-generation sequencing technologies in recent years enables us to establish a more complete picture of the components making up the NMJ and thus provide novel target genes for consideration in the treatment of neuromuscular diseases affecting the NMJ.

In the second part of this thesis, we aimed to utilize laser-capture microdissection and next-generation RNA-sequencing to investigate the transcriptome of the fundamental myonuclei underlying the NMJ in two different skeletal muscles and identify novel NMJ components.

Objective II: *Identify novel components of the neuromuscular junction in the EDL and SOL muscles using next-generation RNA-sequencing.*

Part III / Sinergia Project: Effects of Aging on the Neuromuscular Junction Transcriptome

The third and final part of this thesis describes the findings of our contribution to the "Sinergia project for muscle wasting at high age", which was a joint effort of several research groups. In simple terms, sarcopenia is a multifaceted disease associated with the aging process, which leads to skeletal muscle mass wasting and functional impairments, severely impacting quality of life. The mechanisms underlying sarcopenia are still poorly understood, but evidence suggests that aging causes structural and functional perturbations of the NMJ in rodents. It is therefore conceivable that aging leads to gradual changes in the synaptic gene expression program, thus contributing to the observed disturbances. Within the framework

of the project, we received skeletal muscle samples (*tibialis anterior* muscle; TA) from 10-month-old and 30-month-old mice. Two different interventions, treatment with rapamycin and caloric restriction, were applied to the old groups starting from the age of 15 months. Our task was to generate RNA-sequencing datasets comparing the transcriptomes of young (10-month-old) and old (30-month-old) NMJs and to see how aging alters the NMJ transcriptome, as well as assess whether the different treatments ameliorated the putative aging-related adverse changes.

Objective III: *Determine whether aging leads to perturbations of the neuromuscular junction transcriptome.*

3 Manuscript I: Ladder climbing as a physiological resistance exercise model for skeletal muscle hypertrophy in mice

Martin Weihrauch[1], Regula Furrer[1, 2] and Christoph Handschin[1]

[1]Biozentrum, University of Basel, Klingelbergstrasse 50/70, CH-4056 Basel, Switzerland

[2]Regula Furrer conducted *ex vivo* contractile force measurements

3.1 Abstract

Despite numerous studies investigating the adaptive hypertrophic response of skeletal muscle to resistance exercise (RE) it remains unclear how exactly a mechanical stimulus translates into muscular growth. Therefore, we aimed to investigate the effects of RE on the mouse skeletal muscle transcriptome to identify putative mechanosensing-involved proteins in adaptive hypertrophy. We trained ten adult male C57BL/6JRj wild-type mice to climb a 60 cm high and near-vertical ladder device while carrying progressively heavier loads attached to their tails. Twelve weeks of 5-days-per-week RE enabled the mice to carry up to an additional 32 g, or roughly 110% of their own bodyweight for five sets of 5 min (15 to 20 complete ladder climbs per set). Although the mice vastly improved their ability of climbing the ladder device with heavier weights and increased training volume, we did not observe significant muscular hypertrophy or functional adaptations elicited by RE. Potential reasons for this are motivational issues of the animals and insufficient training stimulus intensity, as options of increasing attached weight to the animals were limited. Future approaches should aim to improve training stimulus intensity by increasing the amount of weight increments and absolute load, for example by utilizing denser weight materials.

3.2 Introduction

Skeletal muscle is a remarkably adaptive tissue that is capable of responding to metabolic as well as physical demands encountered in daily life. Skeletal muscle atrophies with disuse or malnourishment and hypertrophies upon increased contractile demands, for example in resistance exercise (RE) training **(Mikesky, Giddings et al. 1991)**. Increasing lean body mass via RE is a widely pursued task by weight-lifting individuals and professional athletes alike, as there is a strong correlation between muscle cross-sectional area and muscular strength **(Maughan, Watson et al. 1983)**. Additionally, maintenance of strength and muscle mass is directly associated with health and improved stress tolerance in the elderly, as well as throughout life **(Wolfe 2006)**.

Little is known about how the mechanical stimulus of skeletal muscle contractile overload translates into muscular growth and concomitant increases in strength. There is a variety of animal models developed to study overload-induced skeletal muscle hypertrophy. The ablation of different synergist muscles in the mouse hind limb (i.e. the *Gastrocnemius* (GAS) and *Soleus* (SOL) muscles) leads to a significant and chronic mechanical overload of the *Plantaris* (PLA) muscle. Significant increases in PLA muscle mass develop and are maintained two weeks (~87%), eight weeks (~120%) or even three months (~65%) after the intervention **(Baldwin, Valdez et al. 1982, Roy and Edgerton 1995, Perez-Schindler, Summermatter et al. 2013)**. Yet, the acute hypertrophic adaptations in the synergist ablation (SA) model are masked by inflammation caused by the surgical nature of the intervention **(Armstrong, Marum et al. 1979)**. This hampers the investigation and understanding of the early steps in overload-induced hypertrophic adaptations. Furthermore, the PLA muscle is chronically overloaded whenever the affected animal moves around in its cage. Unlike in human RE, there is no period of rest in order for the muscle to recover (i.e. supercompensation), which, paired with nutrition rich in amino acids, is crucial in human skeletal muscle growth. Indeed, overly short resting intervals between exercise bouts can lead to overtraining in humans, which may result in the deterioration of exercise performance **(Fry and Kraemer 1997)**.

Interestingly, while the PLA muscle can double in size in response to SA, its maximum specific force does not increase proportionally. These functional deficits may in part be explained by an initial inflammatory swelling causing interstitial space enlargement and decreased protein concentration, while later changes might be due to intracellular changes **(Kandarian and White 1989, Kandarian and White 1990)**. A time course of differential gene expression patterns in response to SA surgery is available **(Chaillou, Lee et al. 2013)**. Unfortunately, the majority of top hits in the microarray data, especially during the first few days of the time course, are intermixed with genes associated with inflammation and immune response. While it seems plausible for these pathways to play important roles in the hypertrophic response **(Koh and Pizza 2009, Tidball and Villalta 2010, Costamagna, Costelli et al. 2015)**, it cannot be ruled out that some if not most of these genes might be influenced by the surgery itself rather than by the mechanical overload. This makes it difficult to identify target genes and gene programs that may aid in understanding the complex transcriptional changes the hypertrophying muscle undergoes under mechanical load.

Therefore, it would be ideal to be able to study gene expression upon the physiological stimulus of resistance exercise, mimicking intermittent human RE, and to gain novel insights into the workings of the conversion of a mechanical stimulus into the adaptation of skeletal muscle to overload. To our knowledge, no established physiological resistance exercise methodology capable of inducing robust skeletal muscle hypertrophy in mice was available at the time of this study (2015). A plethora of models was developed for use with the rat, for it is much easier to handle, motivate, and train them to conduct a certain task **(Cholewa, Guimaraes-Ferreira et al. 2014)**. The rat animal model does not offer the same genetic tools that are available for mice, although the gap is closing **(Ellenbroek and Youn 2016)**. Mice are natural-born climbers and capable of holding their own body weight even on an inverted grid for an extended period. Accordingly, we found the ladder-climbing model to be a very promising mode of RE that might also be adapted for use with mice. Here, the animal has to climb a vertical ladder at a certain angle (70-90°) while also carrying sufficient load to produce the need of physiological adaptation (i.e. hypertrophy).

In our study, we adopted the rat ladder-climbing model for use with mice to mimic human RE parameters and aimed to establish a physiological RE model that allows the study of transcriptional changes in hypertrophying mouse muscles with fully functional strength adaptations. To assess the efficacy of our RE model, we measured body composition and hind limb muscle weight, as well as grip strength and gene expression levels of putatively hypertrophy-related genes.

3.3 Material and Methods

Animals. Fifteen-week-old male C57B/6JRj wild-type mice (JANVIER LABS, France) were randomly assigned to either a resistance exercise group (EX; N = 10) or sedentary control group (SED; N = 8). Animals were fed an ad libitum, regular chow diet (Provimi 3432) and kept under a 12-h/12-h light–dark cycle (light phase: 06:00 am to 18:00 pm) in a temperature-controlled room (21-22°C). The SED animals were kept in their home cages throughout the duration of the study. Body composition was determined after 0, 3, 8, 10, and 12 weeks with an EchoMRI-100 analyzer (EchoMRI Medical Systems). All experiments were performed in accordance with the principles of the Basel Declaration and with Federal and Cantonal Laws regulating the care and use of experimental animals in Switzerland, as well as institutional guidelines of the Biozentrum and the University of Basel. The protocol with all methods described here was approved by the cantonal veterinary office of the canton Basel-Stadt, under consideration of the well-being of the animals and the 3R principle.

Resistance exercise protocol. The EX animals were split into two training groups of five animals each for the duration of the study, as the ladder device only allowed for simultaneous training of five animals (**Figure 3-1 A**). The ladder was initially set to an inclination of about 70°, and ample cushioning material was placed at the bottom of the ladder for safety in case a mouse would fall off the ladder grid during climbs. Before beginning the RE protocol, the mice were acclimatized to climbing the ladder in two sessions without any attached weight. Mice were placed at the bottom of the ladder and quickly climbed to the top, requiring the occasional prod at the base of the tail for motivation. Leaden bullet weights for fishing poles

were modified to enable temporary attachment to the base of the tail of a mouse via adhesive tape. Available weights were 11, 19, and 32 g.

After the acclimatization sessions, the twelve-week RE protocol was started using 11 g weights for three sets of 5 min of continuous ladder climbing in session one. The rest period was 2 min between sets. A ladder climb counted as complete when a mouse climbed from the bottom of the ladder up to the top within 15 s. Upon reaching the top, mice were returned to the bottom immediately to perform another climb until a set was finished. Stopping and "coping behavior" (mice would jam the tips of their tails in between ladder steps, in order to rest the weight on the device itself) were initially quite common and required the occasional motivational prod to get them to climb again. Subsequent training sessions quickly lead to improved climbing speed and a reduction of falls and coping behavior. Set number and duration were continually increased until up to five sets of 5 min with 19 g of attached weight. Switching to 32 g of attached weight initially led to many falls and signs of exhaustion[1] at around the third set of a session. After a month of 5-days-per-week training, the mice were able to handle the 32 g weights and successfully completed five sets of 5 min of ladder climbing, with six to eleven complete ladder climbs per set. At his point, ladder inclination was increased to from 70° to 80°, thus further increasing training intensity. Climbing performance continued to improve as mice completed more complete ladder climbs per training set in the following weeks. We attempted to increase the attached weight to 43 g by adding an additional 11 g weight to the 32 g one. While some mice managed to climb successfully, others had trouble coping and would inevitably fall. This might be due to most of the tail being covered by the weights, substantially inhibiting its use for balance. As no consistent amount of complete ladder climbs was achievable with 43 g, the exercise protocol was continued with only 32 g of attached weight, but the number of complete ladder climbs continued to improve from session to session. After twelve weeks of RE, the mice completed between 15 to 20 complete ladder climbs per set with 32 g of attached weight.

[1] Mice would cling to the ladder steps without moving and even prodding would not get them to move up the ladder anymore. If this occurred, the set was stopped and the mice were set to rest.

Mice were sacrificed 48 h after their last training session by cervical dislocation to allow careful preparation of one EDL muscle per mouse for *ex vivo* contractile force measurements. The remaining hind limb muscles (*Quadriceps*, QUAD; *gastrocnemius*, GAS; *tibialis anterior*, TA; *plantaris*, PLA; *extensor digitorum longus*, EDL; *soleus*, SOL) were excised and weighed before snap-freezing in liquid nitrogen or embedding for cryosectioning (only GAS, SOL, and PLA) in 10% Tragacanth (Sigma-Aldrich, catalog no. G1128) using liquid nitrogen-cooled 2-methylbutane.

Grip strength test. Maximal grip strength of all four limbs was measured after 0, 3, 8, 10, and 12 weeks of training by using a grip strength meter (Chatillon). Briefly, mice were lifted gently by their tail and allowed to grip with all four limbs on a grid, which was attached to the grip strength meter. The mice were then pulled horizontally backwards and away from the grip strength meter, until they released their grip and let go of the grid. Peak force in grams force (gf) was measured. The mean of the highest three out of five measurements was used for the analysis. Measurements were taken with 1-min intervals of recovery in-between. Care was taken to always conduct the experiment in the same room and at the same time of day, which was on a Monday following a weekend, during which no RE sessions had taken place and the mice were properly recovered.

Weight-bearing four-limbs hanging time test. Four-limbs hanging time while bearing an additional weight of 19 g was measured once at the end of the last week of the exercise protocol. 19 g weights were attached to SED and EX animals and they were put on an inverted grid on top of a tall box. Time until they dropped onto the cushioning below was measured. Five such measurements were taken with at least 5 min of rest between measurements. The single best value was used for the analysis.

***Ex vivo* contractile force measurements.** One EDL muscle per mouse was subject to *ex vivo* contractile force measurements. After careful dissection, EDL muscles were maintained in a Sylgard-covered (Sigma-Aldrich, catalog no. 761036) petri dish containing Krebs-Ringer solution with continuous oxygen supply. Krebs-Ringer solution contained 137 mM NaCl, 24 mM $NaHCO_3$ 11 mM Glucose, 5 mM KCl, 2 mM $CaCl_2$-$2H_2O$, 1 mM $MgSO_4$-$7H_2O$, and 1 mM

NaH_2PO_4-H_2O (Chemicals were purchased from Fluka). Knotting loops of surgical silk around an EDL muscles' distal and proximal tendons allowed its attachment to a force transducer (1200A Isolated Muscle System; Aurora Scientific) on one end and to a fixed pin on the other. The muscle was gradually adjusted to its optimal length (L_o), which is achieved at peak twitch force (P_t), by lengthening in 5 mN increments. Peak tetanic force (P_o) was recorded with 500-ms stimulation at 120 and 150 Hz. Specific peak and twitch forces were calculated by normalization to the cross-sectional area (CSA) according to the formula: CSA (mm^2) = muscle wet weight (mg)/[fiber length (l_f, mm) x 1.06 mg/mm^3], with $l_f = l_o \times 0.44$ for EDL **(Brooks and Faulkner 1988)**. DMAv5.010 software was used for analyzing the data.

Muscle cross-sectional area. Cryosections of GAS, PLA, and SOL muscles were cut with a cryostat at 12 µm thickness (Leica, CM1950). Sections were air-dried for 2 h at RT and incubated overnight with a Wheat Germ Agglutinin, Alexa Fluor™ 488 conjugate (Invitrogen, catalog no. W11261) diluted 1:500 in 0.1% Triton-X/PBS at 4°C. The next day, sections were washed twice with PBS for 5 min, followed by EtOH-dehydration for 2 min each in 70% and 100% EtOH respectively. Sections were mounted with CitiFluor™-AF1 (VWR, catalog no. 100496-532) and pictures taken for cross-sectional area analysis using a ZEISS Axio Scan.Z1 slide scanner system. Cross-sectional area was measured by quantifying the minimum distance of parallel tangents at opposing particle borders (minimal "Feret's diameter") of whole muscle sections using the ImageJ and cell^p software packages (Olympus Soft Imaging Solutions).

Isolation of RNA and synthesis of cDNA. Total RNA was extracted from muscle tissue by phase-separation using TRI Reagent (Sigma Aldrich, catalog no. T9424) as per the manufacturers' protocol. RNA concentration and purity were measured with a NanoDrop 1000 spectrophotometer (Thermo Scientific). One µg of isolated RNA was used for cDNA synthesis with the SuperScript II reverse transcriptase (Invitrogen, catalog no. 18064-014).

Semiquantitative real-time PCR. Relative mRNA levels were measured by semiquantitative real-time PCR (qPCR) on a StepOnePlus™ Real-Time PCR System (Applied Biosystems, catalog no. 4376600) using Fast SYBR™ Green Master Mix (Applied Biosystems, catalog no. 4385612). The expression values of the reference genes *Tbp* and *Hprt* were averaged and used for normalization. Gene expression fold changes relative to the SED group were calculated with the comparative $\Delta\Delta C_T$ method for relative quantification as per the manufacturers' instructions (Applied Biosystems). Primer pairs were checked for similar PCR efficiency. Melting curve analysis was performed to control for the formation of multiple, unspecific PCR products or primer-dimers. Two technical replicates were done for each PCR reaction, and negative control reactions were added (i.e., no template and no reverse transcription controls). Primer sequences used are shown in **Table 3-1**.

Table 3-1. Primer sequences used for gene expression analyses with qPCR.

Gene name	Forward	Reverse
Ccnd1	TCAAGTGTGACCCGGACTG	ATGTCCACATCTCGCACGTC
Ckmt2	CCACACCAGGGTGATCTCAAT	TCGAGGGGCAAGTCAAAATGT
Hprt	TCAGTCAACGGGGGACATAAA	GGGGCTGTACTGCTTAACCAG
Igf-1	ATAGAGCCTGCGCAATGGAATA	ATTGGTGGGCAGGGATAATGA
Igf-2	AGCTGACCTCATTTCCCGAT	GAATGTGCGACGGGACAGAA
Mmp2	AACGGTCGGGAATACAGCAG	GTAAACAAGGCTTCATGGGGG
Mstn	GCTGGCCCAGTGGATCTAAA	GCCCCTCTTTTTCCACATTTT
Ppargc1a	AGCCGTGACCACTGACAACGAG	GCTGCATGGTTCTGAGTGCTAAG
Tbp	ATATAATCCCAAGCGATTTGC	GTCCGTGGCTCTCTTATTCTC
Ubtf	GGATGCCACTACGAAGGAGG	GATGTTCAGCTCAGGGTGCT

Primers are listed in 5'-3' direction.

Statistical analyses. All statistical analyses were performed using GraphPad Prism 8 (GraphPad Software) unless indicated otherwise. Differences in body composition, hind limb muscle weights, and four limb grip strength between SED and EX groups were compared using multiple t-tests with correction for multiple comparisons using the Holm-Sidak method without assuming equal standard deviations. Differences in weight-bearing inverted grid hanging test time were compared using an unpaired, nonparametric Mann-Whitney rank comparison test. Differences in gene expression were compared with multiple t-tests with

correction for multiple comparisons using the Holm-Sidak method on the ΔCT values. Differences in *ex vivo* contractile force measurements between the SED and EX groups were compared with parametric t-tests. In general, p-values lower than 0.05 were considered to indicate statistical significance.

3.4 Results

Body composition, muscle weight and myofiber size

We determined body composition at week 0 (prior to the exercise intervention), as well as after 3, 5, 8, and 12 weeks (immediately before sacrifice) of the study. Body composition before and after the exercise intervention, final muscle weights and myofiber size are shown in **Figure 3-1 B-D** and summarized in **Table 3-2**.

Table 3-2. Body composition before (week 0) and at the end (week 12) of the twelve-week resistance exercise intervention, as well as final muscle weights.

Group		SED	EX
Body weight (g)	Week 0	27.66 ± 1.13	28.31 ± 1.31
	Week 12	29.72 ± 1.90	28.97 ± 1.48
Fat mass (g)	Week 0	2.46 ± 0.49	2.33 ± 0.35
	Week 12	3.31 ± 1.11	2.39 ± 0.30
Lean mass (g)	Week 0	22.67 ± 0.69	23.19 ± 1.22
	Week 12	23.14 ± 1.18	23.50 ± 1.38
Muscle weight (mg)	*Soleus*	9.91 ± 1.35	10.94* ± 1.02
	Extensor digitorum longus	12.06 ± 0.75	12.14 ± 1.11
	Plantaris	18.89 ± 1.17	19.20 ± 1.37
	Tibialis anterior	55.39 ± 3.95	58.99 ± 3.50
	Gastrocnemius	135.56 ± 6.61	145.97* ± 6.70
	Quadriceps	225.65 ± 8.45	229.84 ± 8.18
Myofiber size (min. ferets' diameter in µm; N = 4)	*Gastrocnemius*	23.06 ± 1.24	22.82 ± 1.41
	Plantaris	20.00 ± 1.15	19.87 ± 1.72
	Soleus	16.90 ± 1.51	17.14 ± 0.65

Groups: **SED** = sedentary control group; **EX** = resistance exercise group. Data shown as mean ± SD; * $p \leq 0.05$; N = 8-10.

Grip strength

We assessed grip strength at week 0 (prior to the exercise intervention), as well as after 3, 5, 8, and 12 weeks (the day before sacrifice) of the study via four-limb grip strength tests. Additionally, in the last week of the study, we performed a weight-bearing inverted grid hanging time test, to which the animals were not acclimatized beforehand. The EX group held on to the grid significantly longer compared with the SED group. Overall, four-limb grip strength increased in both, SED and EX animals over the course of the study, without a significant difference between groups at any time point. In the weight-bearing inverted grid hanging time test at week twelve, EX animals performed significantly better compared to SED animals ($p < 0.003$; **Table 3-3** and **Figure 3-2**).

Table 3-3. Four-limb grip strength measurements before (Week 0) and at the end (Week 12) of the 12-week resistance exercise intervention, as well as weight-bearing inverted grid hanging time test results.

Group		SED	EX
Grip strength (grams force, gf)	Week 0	251.63 ± 25.75	249.34 ± 16.35
	Week 12	298.00 ± 25.36	319.6 ± 19.73
Weight-bearing inverted grid hanging test time (s)	Week 12	27.63 ± 24.65	142.80** ± 107.81

The weight-bearing inverted grid hanging time test was only performed during the last week of the resistance exercise intervention (Week 12). Groups: **SED** = sedentary control group; **EX** = resistance exercise group. Data shown as mean ± SD; ** $p < 0.01$; N = 8-10.

Ex vivo contractile force

We measured *ex vivo* muscle force of the EDL muscle to compare contractility between the SED and EX groups after the exercise intervention (**Figure 3-3**). There were no significant differences in any of the measurements, which are summarized in **Table 3-4**.

Table 3-4. *Ex vivo* muscle contractility of the EDL muscle after 12 weeks of resistance exercise.

Group	Frequency	SED	EX
Peak twitch force (mN)		49.82 ± 5.72	50.62 ± 5.03
Specific peak twitch force (mN/mm²)		49.30 ± 7.26	53.57 ± 5.84
Peak tetanic force (mN)	120 Hz	301.51 ± 42.75	320.21 ± 37.74
	150 Hz	332.88 ± 29.50	357.35 ± 32.38
Specific peak tetanic force (mN/mm²)	120 Hz	313.14 ± 53.23	339.51 ± 47.03
	150 Hz	345.54 ± 44.44	378.86 ± 45.00

Groups: **SED** = sedentary control group; **EX** = resistance exercise group. Data shown as mean ± SD; N = 7-10.

Gene expression

To investigate whether twelve weeks of RE influence the gene expression levels of several putatively hypertrophy-related genes (selected based on literature), we determined their relative expression levels with qPCR in the GAS and QUAD muscles (**Figure 3-4 A-B**). None of the measured genes were differentially expressed between the SED and EX groups at the end of the study.

3.5 Discussion

The physiological resistance exercise model of weight-bearing ladder climbing described here lead to task-specific performance improvements, but did not induce significant muscular hypertrophy.

The twelve-week RE intervention did not influence overall body composition (**Figure 3-1 D-F**), which is in line with the observations of hind limb muscle weight and cross-sectional area (**Figure 3-1 B-C**). The resistance exercise group (EX) tended to having a slightly reduced fat mass relative to body weight($p > 0.08$ at weeks 3, 5, 8 and 12), which might have been due to the RE training and/or increased stress levels caused by the intervention itself. This observation might in turn explain the trend towards a slightly increased lean mass relative to body weight at week 12 ($p > 0.057$) in the EX group. We detected a slight increase in muscle mass relative to body weight in the SOL (~ 10%) and GAS muscles (~ 6%), but the magnitude of these increases is marginal compared to ladder climbing exercise study results in the rat (23% absolute increase in FHL muscle weight, **(Hornberger and Farrar 2004)**; 20% increase in QUAD cross-sectional area, **(Jung, Ahn et al. 2015)**).

The EX animals displayed a larger capacity to resist gravity in a weight-bearing inverted grid hanging test when compared to the sedentary control group (SED) (**Figure 3-2 B**). This experiment was confounded by the fact that the SED animals were not acclimatized to carrying weights attached to their tails. Other measurements of strength, such as longitudinal four-limb grip strength tests (**Figure 3-2 A**) and *ex vivo* contractility measurements of the EDL muscle (**Figure 3-2 C**) did not indicate general performance improvements. These observations might indicate that adaptations of the EX animals to the model were mostly specific to the task, and that the measurements of strength taken were not suitable to accurately determine performance. Although the *ex vivo* contractility measurements of the EDL muscle (**Figure 3-2 C**) avoided issues with balance and behavior, they displayed no difference in strength between SED and EX animals. It is possible that the EDL muscle is not strongly involved in the ladder-climbing task and therefore displayed no

increases in its contractility. It would therefore have been interesting to see contractility measures of other, potentially more involved muscles as well. Nevertheless, the EX animals greatly improved their capacity of weight-bearing ladder climbing over the duration of the RE training.

The physiological resistance exercise model of weight-bearing ladder climbing described here lead to task-specific performance improvements, but did not induce significant muscular hypertrophy. The described RE model therefore does not facilitate studies of transcriptional changes related to skeletal muscle hypertrophy. Involuntary RE models, such as the ladder climbing described here, are unlikely to produce sufficient hypertrophy with mice. Compared to rats, mice are more difficult to motivate, which hampers exercise compliance, and options to provide sufficiently stimulating progressive overload are limited **(Spangenberg and Wichman 2018)**. Future efforts should focus on establishing a voluntary RE protocol with sufficient intensity to induce hypertrophy and include analysis of the forelimb muscles. Ideally, the chosen RE modality excludes or reduces aerobic components as much as possible.

3.6 Figures

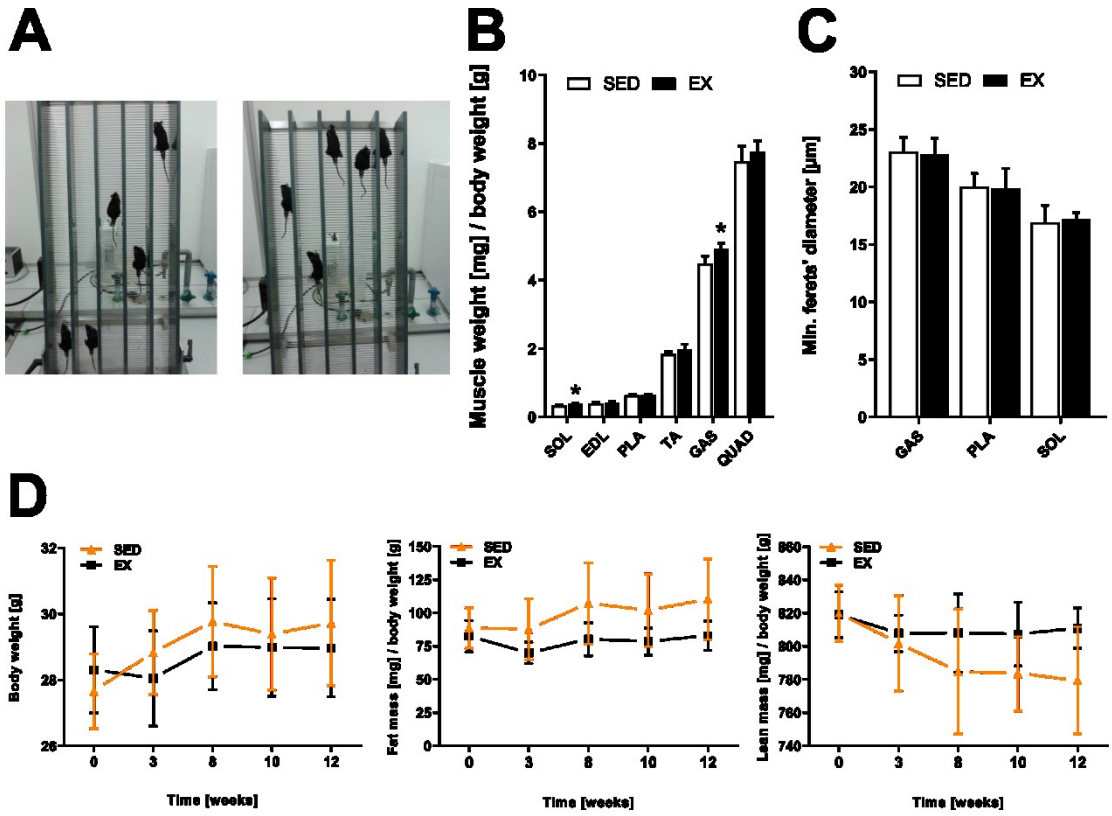

Figure 3-1. Muscle mass and size, as well as body composition after twelve weeks of ladder-climbing resistance exercise. A) Photo of the weight-bearing ladder climbing resistance exercise. Weights were attached to the base of the tail and mice had to repeatedly climb a near-vertical ladder device. **B)** Muscle weight normalized to body weight of six different hind limb muscles. N = 7-10. **C)** Muscle cross-sectional area determined by measuring the minimal ferets' diameter. N = 4. **D)** Body weight, fat- and lean-mass as determined by EchoMRI. Fat- and lean-mass were normalized to body weight. N = 8-10. Groups: **SED** = sedentary control group; **EX** = resistance exercise group. Data shown as mean ± SD; * $p \leq 0.05$.

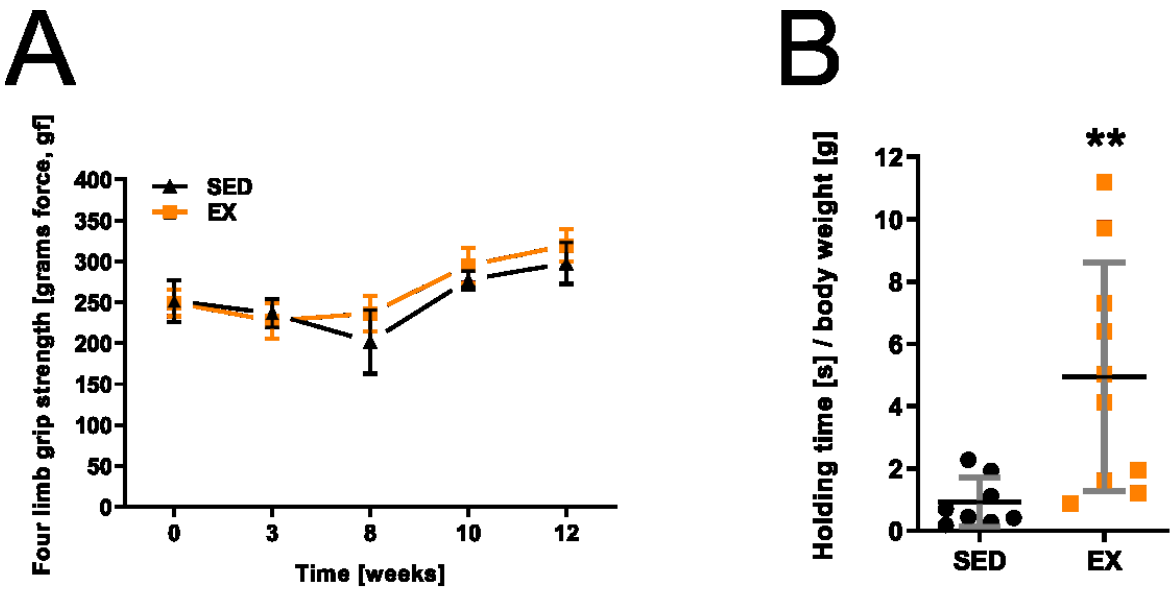

Figure 3-2. Grip strength measurements. A) Longitudinal four-limb grip strength tests of sedentary control group (SED) and resistance exercise group (EX) mice. Grip strength measurements took place in week 0, 3, 5, 8, and 12. **B)** Weight-bearing inverted grid hanging time test of SED and EX mice after twelve weeks of resistance exercise. Hanging time in seconds was normalized to body weight. Groups: **SED** = sedentary control group; **EX** = resistance exercise group. Data shown as mean ± SD; ** $p \leq 0.01$; N = 8-10.

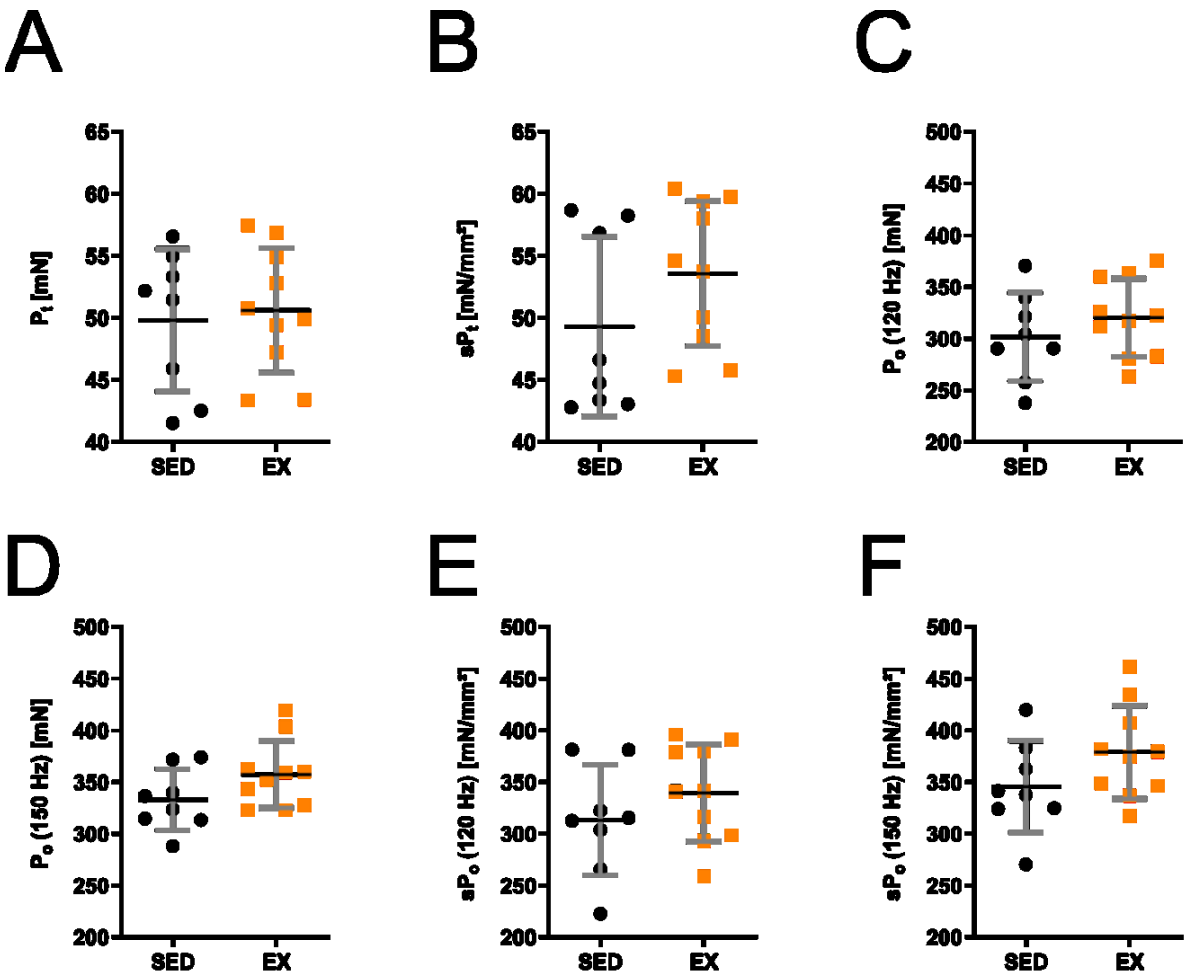

Figure 3-3. ***Ex vivo*** **muscle force measurements of the EDL muscle after twelve weeks of resistance exercise. A)** Peak twitch force. **B)** Peak tetanic force (120 Hz). **C)** Peak tetanic force (150 Hz). **D)** Specific peak twitch force. **E)** Specific peak tetanic force (120 Hz). **F)** Specific peak tetanic force (150 Hz). Groups: **SED** = sedentary control group; **EX** = resistance exercise group. Data shown as mean ± SD; N = 8-10.

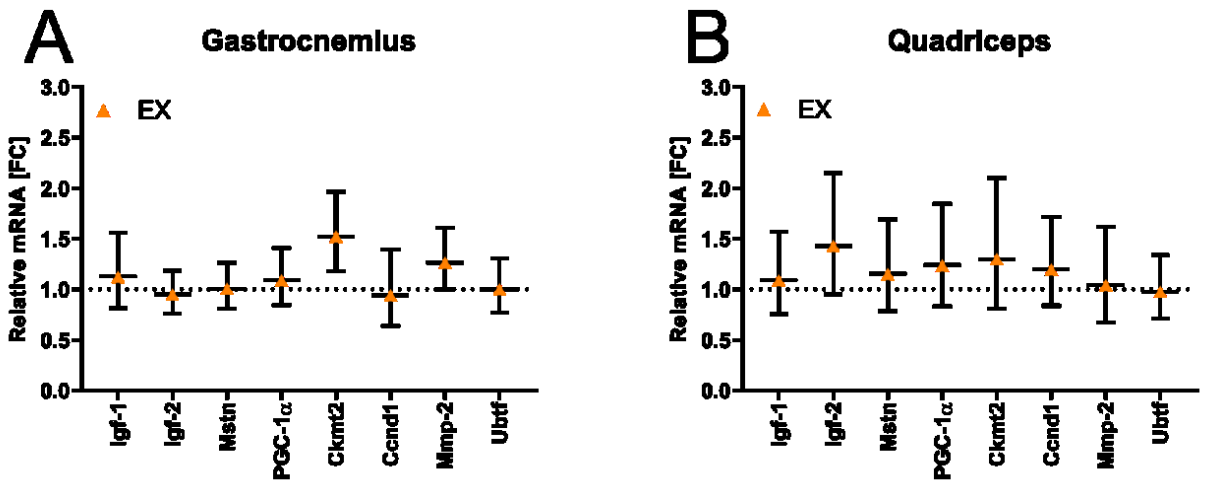

Figure 3-4. Twelve weeks of resistance exercise did not induce gene expression of putative hypertrophy-related genes. Expression of putative hypertrophy-related genes in EX relative to SED (dotted lines) animals in the **A)** *Gastrocnemius* and **B)** *Quadriceps* muscles was measured with semiquantitative qPCR. Groups: **SED** = sedentary control group; **EX** = resistance exercise group. Values are fold change of EX relative to SED ± fold-change range; N = 8-10.

3.7 References

Armstrong, R. B., P. Marum, P. Tullson and C. W. t. Saubert (1979). "Acute hypertrophic response of skeletal muscle to removal of synergists." J Appl Physiol Respir Environ Exerc Physiol **46**(4): 835-842.

Baldwin, K. M., V. Valdez, R. E. Herrick, A. M. MacIntosh and R. R. Roy (1982). "Biochemical properties of overloaded fast-twitch skeletal muscle." J Appl Physiol Respir Environ Exerc Physiol **52**(2): 467-472.

Brooks, S. V. and J. A. Faulkner (1988). "Contractile properties of skeletal muscles from young, adult and aged mice." J Physiol **404**: 71-82.

Chaillou, T., J. D. Lee, J. H. England, K. A. Esser and J. J. McCarthy (2013). "Time course of gene expression during mouse skeletal muscle hypertrophy." J Appl Physiol (1985) **115**(7): 1065-1074.

Cholewa, J., L. Guimaraes-Ferreira, T. da Silva Teixeira, M. A. Naimo, X. Zhi, R. B. de Sa, A. Lodetti, M. Q. Cardozo and N. E. Zanchi (2014). "Basic models modeling resistance training: an update for basic scientists interested in study skeletal muscle hypertrophy." J Cell Physiol **229**(9): 1148-1156.

Costamagna, D., P. Costelli, M. Sampaolesi and F. Penna (2015). "Role of Inflammation in Muscle Homeostasis and Myogenesis." Mediators Inflamm **2015**: 805172.

Ellenbroek, B. and J. Youn (2016). "Rodent models in neuroscience research: is it a rat race?" Dis Model Mech **9**(10): 1079-1087.

Fry, A. C. and W. J. Kraemer (1997). "Resistance exercise overtraining and overreaching. Neuroendocrine responses." Sports Med **23**(2): 106-129.

Hornberger, T. A., Jr. and R. P. Farrar (2004). "Physiological hypertrophy of the FHL muscle following 8 weeks of progressive resistance exercise in the rat." Can J Appl Physiol **29**(1): 16-31.

Jung, S., N. Ahn, S. Kim, J. Byun, Y. Joo, S. Kim, Y. Jung, S. Park, I. Hwang and K. Kim (2015). "The effect of ladder-climbing exercise on atrophy/hypertrophy-related myokine expression in middle-aged male Wistar rats." J Physiol Sci **65**(6): 515-521.

Kandarian, S. C. and T. P. White (1989). "Force deficit during the onset of muscle hypertrophy." J Appl Physiol (1985) **67**(6): 2600-2607.

Kandarian, S. C. and T. P. White (1990). "Mechanical deficit persists during long-term muscle hypertrophy." J Appl Physiol (1985) **69**(3): 861-867.

Koh, T. J. and F. X. Pizza (2009). "Do inflammatory cells influence skeletal muscle hypertrophy?" Front Biosci (Elite Ed) **1**: 60-71.

Maughan, R. J., J. S. Watson and J. Weir (1983). "Strength and cross-sectional area of human skeletal muscle." J Physiol **338**: 37-49.

Mikesky, A. E., C. J. Giddings, W. Matthews and W. J. Gonyea (1991). "Changes in muscle fiber size and composition in response to heavy-resistance exercise." Med Sci Sports Exerc **23**(9): 1042-1049.

Perez-Schindler, J., S. Summermatter, G. Santos, F. Zorzato and C. Handschin (2013). "The transcriptional coactivator PGC-1alpha is dispensable for chronic overload-induced skeletal muscle hypertrophy and metabolic remodeling." Proc Natl Acad Sci U S A **110**(50): 20314-20319.

Roy, R. R. and V. R. Edgerton (1995). "Response of mouse plantaris muscle to functional overload: comparison with rat and cat." Comp Biochem Physiol A Physiol **111**(4): 569-575.

Spangenberg, E. M. F. and A. Wichman (2018). "Methods for Investigating the Motivation of Mice to Explore and Access Food Rewards." J Am Assoc Lab Anim Sci **57**(3): 244-252.

Tidball, J. G. and S. A. Villalta (2010). "Regulatory interactions between muscle and the immune system during muscle regeneration." Am J Physiol Regul Integr Comp Physiol **298**(5): R1173-1187.

Wolfe, R. R. (2006). "The underappreciated role of muscle in health and disease." Am J Clin Nutr **84**(3): 475-482.

4 Manuscript II: Identification of Novel Synaptic Components by Transcriptome Profiling of the Murine Neuromuscular Junction

Martin Weihrauch[1] and Christoph Handschin[1]

[1]Biozentrum, University of Basel, Klingelbergstrasse 50/70, CH-4056 Basel, Switzerland

4.1 Abstract

The neuromuscular junction (NMJ) has been studied for over a century, yet we still do not have a complete picture of all its structural and functional components, knowledge of which is paramount in devising treatment strategies for certain neuromuscular diseases. We hypothesized that we could identify novel NMJ components by performing next-generation RNA-sequencing on fundamental myonuclei underlying the NMJ of fast-twitch *extensor digitorum longus* (EDL) and slow-twitch *soleus* (SOL) muscles. We successfully generated EDL and SOL NMJ gene expression profiles and validated several known and novel NMJ genes with semiquantitative qPCR. We found the expression levels of canonical NMJ genes to be nearly identical between the EDL and SOL, which suggests that the core NMJ gene program might be well conserved between different skeletal muscle types. We overexpressed one of our potential novel NMJ components, the transcription factor T-box 21 (TBX21), in the *tibialis anterior* (TA) muscle and observed an increased density of postsynaptic acetylcholine receptors. TBX21 may thus represent a novel transcription factor contributing to the regulation of the NMJ gene program, with a role in postsynaptic sensitivity. Our NMJ gene expression profiles provide novel target genes that may support and inform future studies into neuromuscular diseases.

4.2 Introduction

The neuromuscular junction (NMJ) has been studied for over a century and ample research has revealed many insights into its molecular structure and function as a prototypical synapse **(Hughes, Kusner et al. 2006)**. Skeletal myofibers are multinucleated syncytia and typically contain far in excess of a hundred myonuclei. Only a small subset of these aggregate directly underneath the NMJ and express a distinct gene program **(Ruegg 2005)**. These so-called fundamental myonuclei presumably express most of the components necessary for the postsynaptic specializations of the myofiber membrane at the NMJ and expression of these components becomes silenced in the extrajunctional myonuclei concomitant with innervation **(Schaeffer, de Kerchove d'Exaerde et al. 2001)**. Several previous studies have attempted to unravel the NMJ transcriptome, identifying novel genes that potentially code for functional and structural NMJ components **(Kishi, Kummer et al. 2005, McGeachie, Koishi et al. 2005, Nazarian, Bouri et al. 2005, Sieburth, Ch'ng et al. 2005, Jevsek, Jaworski et al. 2006, Ketterer, Zeiger et al. 2010)**. However, it is likely that we are still missing the complete picture of all the different proteins involved in NMJ development, maintenance and stabilization, owing to the limitations of previously available sequencing technologies and the inherent difficulties of isolating the fundamental myonuclei that underlie the NMJ. We hypothesized that the emergence of powerful next-generation sequencing technologies in recent years may enable us to establish a more complete picture of the components making up the NMJ. This would allow us to potentially provide novel target genes for therapeutic approaches aimed at treating neuromuscular diseases such as congenital myasthenic syndromes. Congenital myasthenic syndromes are a class of diseases caused by gene mutations of various components of the NMJ. To date over 30 different such myasthenic syndromes are known, yet a large number of causative genetic mutations are still undiscovered. Furthermore, fast-twitch muscles and consequently fast-type NMJs are more frequently affected by perturbations caused by neuromuscular diseases compared to slow-twitch muscles and slow-type NMJs **(Wang and Pessin 2013, Nijssen, Comley et al. 2017)**. This might be due to the fact that fast- and slow-type NMJs structurally and functionally differ **(Fahim, Holley et al. 1984, Waerhaug and Lomo 1994, Sieck and Prakash 1997)**. It is

therefore conceivable that there are underlying transcriptomic differences between the fundamental myonuclei of these two NMJ types.

In order to provide a more complete picture of the NMJ transcriptome and to identify new NMJ components and potential differences between slow- and fast-type NMJs, we combined laser-capture microdissection with highly sensitive next-generation RNA-sequencing to interrogate the NMJ transcriptomes of the predominantly fast-twitch *extensor digitorum longus* (EDL) and the predominantly slow-twitch *soleus* (SOL) muscles. Here, we report the successful expression profiling of NMJs of the EDL and SOL muscles and provide a large number of genes potentially encoding for novel NMJ components. We also compared the EDL and SOL NMJ transcriptomes and report on commonalities and differences. Furthermore, we overexpressed one such potential novel NMJ gene, the transcription factor T-box 21 (TBX21), in the *tibialis anterior* (TA) muscle and describe how overexpression of TBX21 influences NMJ morphology and thus may represent a novel regulator of the NMJ gene program.

4.3 Material and Methods

Animals. Adult male C57B/6JRj wild type mice were purchased from JANVIER LABS, France. Animals were fed an ad libitum, regular chow diet (Provimi 3432) and kept under a 12-h/12-h light–dark cycle (light phase: 06:00 am to 18:00 pm) in a temperature-controlled room (21-22°C) in the animal facility of the Biozentrum (University of Basel). All experiments were performed in accordance with the principles of the Basel Declaration and with Federal and Cantonal Laws regulating the care and use of experimental animals in Switzerland, as well as institutional guidelines of the Biozentrum and the University of Basel. The protocol with all methods described here was approved by the cantonal veterinary office of the canton Basel-Stadt, under consideration of the well-being of the animals and the 3R principle.

Tissue preparation for laser capture microdissection. The EDL and SOL muscles of six 15-week-old adult male C57B/6JRj wild type mice were rapidly dissected and immediately immersed in Krebs-Ringer solution (137 mmol/L NaCl, 24 mmol/L $NaHCO_3$, 11 mmol/L

Glucose, 5 mmol/L KCl, 2 mmol/L $CaCl_2$-$2H_2O$, 1 mmol/L $MgSO_4$-$7H_2O$, and 1 mmol/L NaH_2PO_4-H_2O; chemicals were purchased from Fluka) containing α-Bungarotoxin, Alexa Fluor™ 488 conjugate (diluted 1:500; Thermo Fisher Scientific, catalog no. B13422) for 45 min to allow visualization of NMJs. After incubation, muscles were washed two times 2 min in Krebs-Ringer solution, partially embedded in 10% Tragacanth (Sigma-Aldrich, catalog no. G1128), frozen in liquid nitrogen-cooled 2-Methylbutane (-150°C; Sigma-Aldrich, catalog no. M32631), and stored at -80°C until further processing. Serial cross-sections of 20 µm thickness containing NMJ areas were cut at -20°C with a cryostat (Leica Biosystems). Up to 30 serial sections were mounted per RNase AWAY®-treated (Sigma-Aldrich, catalog no. 83931-250ML) regular glass slide (Menzel). To inactivate endogenous RNases, sections were dehydrated inside the cryostat chamber for 10 min and then stored at -80°C in 50 ml conical tubes containing several grams of desiccant (ROTH, silica Gel Orange, catalog no. P077.4) to prevent tissue rehydration. Slides were processed within 72 h.

Laser-capture microdissection of NMJ and non-NMJ areas. Laser capture microdissection (LCM) was performed using a PALM MicroBeam system (Zeiss) consisting of an inverted microscope with a motorized stage, an ultraviolet laser and an X-Cite fluorescence illuminator. The microdissection process was visualized with an AxioCam ICc camera (Zeiss) coupled to a computer and controlled by the PALM RoboSoftware (Zeiss). Specifically, synaptic regions were visualized under fluorescence microscopy with an x20 objective. Synaptic ("NMJ") and extrasynaptic ("XNMJ") tissue areas of roughly 0.5 mm^2 (the equivalent of about 200 NMJ areas) were selected, cut and catapulted by laser pulses, utilizing automated laser-pressure catapulting (autoLPC) mode, into the caps of opaque AdhesiveCap 500 PCR tubes (Zeiss, catalog no. 415190-9211-001). For every sample, the AdhesiveCap PCR tube cap was checked for presence of catapulted tissue, indicating laser capture success. We captured roughly 180 NMJ areas per biological replicate (six animals, both EDL and SOL muscles), thus totaling about 2200 captured NMJ areas. The LCM procedure is depicted in **Figure 4-1 A**. The sample collection for RNA-sequencing culminated in the addition of 10 µl of Single-cell lysis buffer (Clontech, catalog no. 635013) and incubation at RT for 5 min. Afterwards, samples were frozen on dry ice for transport and stored at -80°C until further processing. Sequencing libraries were prepared from the total lysates without isolation of

RNA. The sample collection for qPCR analyses was conducted separately and is described below. We thus generated synaptically-enriched RNA-sequencing data of two different types of skeletal muscle. Two synaptically enriched "NMJ" biological replicates of the SOL muscle and one "XNMJ" control sample of the EDL muscle failed the RNA-sequencing process, leaving four "NMJ" samples for the SOL and five "XNMJ" samples for the EDL muscle. All other samples were sequenced successfully.

RNA extraction and cDNA synthesis from laser-captured tissue. Total RNA extraction was performed by spin-column-based and phenol-free separation suitable for LCM frozen tissue samples with the RNAqueous™-Micro Total RNA Isolation Kit (Thermo Fisher Scientific, catalog no. AM1931). The manufacturers' protocol was adapted for use with AdhesiveCap 500 PCR tubes from Zeiss, as efficient tissue lysis is crucial for successful RNA extraction from LCM tissue. To lyse laser-captured material, 10 µl lysis buffer (from the Kit) was added into the top of an AdhesiveCap PCR tube and pipetted up and down at least ten times before dispensing the lysate into the bottom of the tube. This step was repeated a second time, resulting in a total volume of 20 µl lysis buffer. The tubes were then frozen on dry ice for transport and storage in a -80°C freezer. The AdhesiveCap lid was checked under the microscope after each pipetting step and the absence of captured material indicated successful suspension of tissue in the lysis buffer. Prior to RNA-extraction, additional lysis buffer was added to a final volume of 100 µl. Samples were then mixed by gentle pipetting, and subjected to 30 min incubation at 42°C in a water bath. The remaining steps were then performed as per the manufacturers' protocol. The optional DNAse treatment step was performed utilizing the RNase-Free DNase Set (Qiagen, catalog no. 79254). Finally, the RNA was eluted in two times 10 µl of preheated elution solution and stored at -80°C until further processing.

Low-input RNA-Sequencing. The laser-captured whole tissue lysates were used for RNA-sequencing library generation as per the SMART-Seq2 methodology **(Picelli, Faridani et al. 2014)**. The protocol used was the SMART-Seq2 NexteraXT Standard Protocol. Quality control of the cDNA-sequencing-libraries was conducted with the Agilent Bioanalyzer (Agilent) and the average fragment size of the libraries was determined. The libraries were sequenced

(Single-end reads, 76 sequencing cycles) using a NextSeq 500 system (Illumina) at the Quantitative Genomics Facility of the Department of Biosystems Science and Engineering (D-BSSE) of the ETH Zürich in Basel. The entire process from sequencing library preparation to RNA-sequencing was conducted by D-BSSE personnel.

RNA-sequencing data preprocessing, read mapping and analysis. The raw sequencing reads (FASTQ-files) were quality filtered and sequencing adapters were trimmed using BBDuk from BBTools (Version 38.57) with the following non-standard parameters: ktrim = r, k = 21, mink = 11, hdist = 2, qtrim = rl, trimq = 12, ftm = 5. The following annotation files were used for read mapping: Gencode Release M22 (GRCm38.p6) of the transcript sequences, which includes the nucleotide sequences of all transcripts on the reference chromosomes. GTF file: comprehensive gene annotation (regions: CHR), which contains the comprehensive gene annotation on the reference chromosomes only. Salmon (Version 0.14.1) was used to generate an index with the following non-standard parameters: --k 29, --type quasi, --gencode (as Gencode annotation files are used). Salmon quasi-mapping was run with these parameters: --libType U, --validateMappings, --fldMean 454, --fldSD 66, --seqBias (the average fragment length of the sequencing libraries was 454 with a standard deviation of 66) **(Patro, Duggal et al. 2017)**.

RNA-sequencing data analysis was conducted with R (Version 3.6.0) and R-Studio (Version 1.1.463) running on CentOS Linux 7 (sciCORE R-Studio server service). The edgeR package (Version 3.26.7) from Bioconductor (Version 3.9.0) was used for differential gene expression analysis. Other packages used for data handling and plotting were tidyverse (1.2.1), pheatmap (1.0.12), biomaRt (2.40.3), RColorBrewer (1.1.2), tximport (1.12.3) and GenomicFeatures (1.36.0).

We defined a gene to be differentially expressed, or synaptically enriched at the NMJ, if it had at least a 2-fold change in expression and a false discovery rate (FDR) adjusted p-value of < 0.05. After sequencing library normalization and pre-filtering to remove low-count genes, 14981 genes were found to be expressed in our dataset.

Calculations were performed at sciCORE (http://scicore.unibas.ch/) scientific computing core facility at University of Basel.

Semiquantitative real-time PCR. Relative mRNA levels were determined by semiquantitative real-time PCR (qPCR) on a StepOnePlus system (Applied Biosystems, catalog no. 4376600) using Fast SYBR green PCR master mix (Applied Biosystems, catalog no. 4385612). Expression of the reference gene *Hprt* was used for the normalization of the ΔCT method for relative quantification. qPCR data was analyzed with unpaired, two-tailed student's t-test on the ΔCT-values. Primer pairs were checked for similar PCR efficiency, and melting curve analysis was performed to control for the formation of multiple, unspecific PCR products or primer-dimers. Two technical replicates were done for each PCR reaction, and negative control reactions were added (i.e., no template and no reverse transcription controls). Primer sequences used are shown in **Table 4-1**.

Table 4-1. Primer sequences used for gene expression analyses with semiquantitative qPCR.

Gene name	Forward	Reverse
Aplp2	CTCTCCAAGGGAAAGTGCGT	TCGGGGGAATCATCGCTTTA
B4galnt3	CCCTGAACCACAGGTATGGC	ATCAACGGCTGGGATGTTCC
Chpf	AGGCCGTCAGAACTCGGTAT	GGTGTCCCAGAGTTCGGTTT
Chrne	CTCTGCCAGAACCTGGGTG	GACAGTTCCTCTCCAGTGGC
Crym	CCACAAAGCTGTTGAAGCCC	GCGGTTCCACATTCTCACCT
Dlk1	AAGTGTGTAACTGCCCCTGG	TGCAAGCCCGAACGTCTATT
Dmd	TAATGTCAGGTTCTCCGCGTATAG	GATATCCATGGGCTGGTCATTTTG
Hprt	TCAGTCAACGGGGGACATAAA	GGGGCTGTACTGCTTAACCAG
Hs6st2	CAGGCGGATGCACGACC	ATCCATGTTCCCGACGCTGG
Nell2	CACTACCCATCTCCTTCGGT	GGAAAAGGAACCCAGCCAAAG
Scn3b	AGCTCAGGAAAATGCGTCTGA	CACCCACATCCACCTTACCC
Tbx21	ACTAAGCAAGGACGGCGAAT	TAATGGCTTGTGGGCTCCAG
Utrn	GAGGCTCGCTTCTACATGCT	TGATGACACCATCGCCAGAC

Primers are listed in 5'-3' direction.

***In vivo* muscle electroporation.** MYC-DDK-tagged *Tbx21* (Origene, catalog no. MR227202) and pCAG-eGFP (Sonidel) expression plasmids were prepared with the EndoFree® Plasmid Maxi Kit (Qiagen, catalog no. 12362) according to the manufacturers' protocol. The working plasmid concentration for the intramuscular injections was adjusted to 1 µg/µl with Opti-

MEM (Thermo Fisher Scientific, catalog no. 31985062). Three twelve-week-old adult male C57B/6JRj wild type mice (JANVIER LABS, France) were anesthetized via isoflurane inhalation and analgetically treated with Meloxicam (Metacam® injectable (5mg/ml)) at 5 mg/kg by s.c. injection. After both legs were shaved, the *tibialis anterior* (TA) muscle was bilaterally injected transcutaneous with 25 µl of 80 IU/ml hyaluronidase solution (Irvine Scientific, catalog no. 90101), at two separate sites each (50 µl total injection volume) to ensure optimal distribution of the solution within the muscles. Hyaluronidase solution was used to improve transfection efficiency. During the ensuing 1-hour incubation time the mouse was returned into its home cage and allowed to recover from the anesthesia. Electroporations were carried out with the NEPA21 Super Electroporator (NEPAGENE) equipped with a CUY650P10 (NEPAGENE, catalog no. CUY650P10) tweezer-type electrode and according to manufacturers' recommendations if not stated otherwise. After the 1-hour incubation with the hyaluronidase solution, the mouse was re-anesthetized and two times 25 µl of the diluted MYC-DDK-tagged *Tbx21* plasmid preparation were injected at two opposite sites of one TA muscle. Electroporation was conducted immediately after the injections, with three trains of three poration pulses each (poration pulse voltage: 80 V; number of poration pulses: 3; pulse length: 30 ms; pulse interval: 50 ms; decay rate : 10%; polarity: bipolar; current limit: ON (*in vivo*)). The procedure was then repeated on the other TA muscle with the pCAG-eGFP control plasmid. The mice were returned to their home cage after the procedure. Another dose of Meloxicam was administered the following day. The mice were sacrificed after six weeks and their TA muscles dissected and fixed for 30 min with 4% paraformaldehyde (PFA) for subsequent immunostainings and NMJ-morphology analysis.

Immunohistochemistry. The electroporated and PFA-fixed TA muscles were carefully pried apart with sharp forceps under a dissection microscope into small myofiber bundles of a few and up to several dozen myofibers each. These small myofiber bundles (around 60 per TA muscle) were washed with PBS, neutralized with 0.1M Glycin in PBS for 15 min at RT, and then permeabilized and simultaneously blocked with 3% BSA and 1% Triton-X in PBS for 2h at RT. Afterwards, the bundles were incubated with the primary antibody solution o/n (~ 16 h) at 4°C on a rocking platform. The primary antibody solution consisted of antibodies

targeting Neurofilament "2H3" (used at 0.05 µg/ml; from Developmental Studies Hybridoma Bank (DSHB)), Synaptic vesicle glycoprotein 2A "SV2" (used at 0.2 µg/ml; from DSHB), and Anti-DDK (used at 1 µg/ml; from Origene, catalog no. TA50011-100). Both, 2H3 and SV2 antibodies have the isotype IgG1. The small myofiber bundles were then washed with PBS and incubated for 2h at RT with the secondary antibody solution, which consisted of α-Bungarotoxin, Alexa Fluor™ 647 conjugate (used at 1 µg/ml; Thermo Fisher Scientific, catalog no. B35450), Goat anti-Mouse IgG2a Cross-Adsorbed Secondary Antibody, Alexa Fluor™ 488 (used at 2 µg/ml; Thermo Fisher Scientific, catalog no. A-21131) and Goat anti-Mouse IgG1 Cross-Adsorbed Secondary Antibody, Alexa Fluor™ 568 (used at 2 µg/ml; Thermo Fisher Scientific, catalog no. A-21124). The muscle bundles were then washed with PBS and about 20 such bundles were arranged per Superfrost Plus™ glass slide (VWR, catalog no. 630-0951), mounted with several drops of VECTASHIELD® Antifade Mounting Medium with DAPI (Vector Laboratories, catalog no. H-1200-10), and finally a glass coverslip (#1.5; VWR, catalog no. 631-0147) was used with very little pressure to enclose the arranged muscle bundles. The slides were allowed to cure over night, sealed with nail polish the next day, and stored at 4°C in the dark until use.

2H3 was deposited to the DSHB by Jessell, T.M. / Dodd, J. (DSHB Hybridoma Product 2H3). SV2 was deposited to the DSHB by Buckley, K.M. (DSHB Hybridoma Product SV2).

Confocal imaging and NMJ-morphology analysis. The small myofiber bundles were imaged at the Biozentrum Imaging Core Facility with a SP8 confocal microscope (Leica Microsystems) with a x63 1.4 NA oil-immersion objective and x2 zoom at a resolution of 512x512 pixels and a frame size of 92.44x92.44 µm. The pinhole aperture was set to 1 Airy unit. Confocal Z-stacks with system-optimized step size were acquired at a scanning speed of 200 Hz and with two-times line averaging. Correctly oriented ("face up") NMJs were checked for the expression of TBX21 by confirming the presence of MYC-DDK-signal in their fundamental nuclei (for a high-resolution example see **Figure 4-8 B**). The NMJs of eGFP-transfected myofibers were imaged in the same fashion to serve as controls (**Figure 4-8 A**). Several NMJ morphological parameters were measured with Fiji as described by others **(Schindelin, Arganda-Carreras et al. 2012, Jones, Reich et al. 2016)**. Briefly, thresholding

was applied to maximum intensity Z-stack projections of the imaged postsynaptic endplate and the presynaptic nerve terminal, respectively. After manual optimizations and cleaning of excess noise, this resulted in binary representations of the postsynaptic endplate and the presynaptic nerve terminal. The innervating axon diameter was measured and the axon then manually erased from the presynaptic image in order to measure nerve terminal area and perimeter with standard Fiji functions. Area and perimeter of the AChR of the postsynaptic endplate was measured in analogue fashion. Then, after subtraction of the background and another binarization, a representation of the entire endplate was generated. Diameter, perimeter and area of this was measured. We also calculated postsynaptic "compactness", which is a derived variable defined as AChR area divided by the endplate area multiplied by 100. A total of 33 NMJs (~ 11 NMJs / animal; N = 3) against 28 NMJs (~ 10 NMJs / animal; N = 3) were evaluated from TBX21- (right leg) and eGFP- (left leg, same animal) transfected TA muscles, respectively.

4.4 Results

Expression profiling of fast-twitch EDL and slow-twitch SOL neuromuscular junctions

We used laser-capture microdissection (LCM) to isolate neuromuscular junction areas ("NMJ" or "synaptically enriched tissue") and equal amounts of adjacent, extrasynaptic tissue as control ("XNMJ" or "extrasynaptic control tissue") from serial cryosections of the fast-twitch EDL and the slow-twitch SOL muscles of six 15-week-old male C57B/6JRj wild type mice (JANVIER LABS, France) (**Figure 4-1**). The isolated tissues were lysed and used for RNA-sequencing. Principal coordinate analysis (PCoA) showed four distinct clusters of samples (**Figure 4-2**), each belonging to one of the four expected conditions: Synaptically enriched EDL ("EDL_NMJ"), extrasynaptic EDL control ("EDL_XNMJ"), synaptically enriched SOL ("SOL_NMJ"), and extrasynaptic SOL control ("SOL_XNMJ").

We then assessed differentially expressed genes and summarized the results of the different comparisons in **Table 4-2**. We found 652 genes to be synaptically enriched with a positive fold change > 2 in the EDL muscle (**Figure 4-3 A**; comparison: EDL_NMJ vs. EDL_XNMJ), and 159 such genes for the SOL muscle (**Figure 4-4 A**; comparison: SOL_NMJ vs.

SOL_XNMJ). Among the top 50 synaptically enriched genes in the EDL according to both fold change and FDR p-value (fold change > 32, FDR p-value < 0.001) were well-known NMJ genes such as *Musk*, *Chrna1, Chrnd, Colq,* and *Nes* (**Figure 4-3 B**). Among the top 50 synaptically enriched genes in the SOL (fold change > 16, FDR p-value < 0.01) were the well-known NMJ genes *Ache*, *Dusp6*, *Dok7*, and *Etv5* (**Figure 4-4 B**). These results indicated that we had successfully captured synaptically enriched genes of the NMJ for both muscles. Additionally, we directly compared the synaptically enriched EDL with the synaptically enriched SOL samples (EDL_NMJ vs. SOL_NMJ) to identify genes that are differentially expressed between the NMJs of the two muscles. This comparison yielded a list of 36 genes that were more abundant in the synaptic EDL and 141 genes that were more abundant in the synaptic SOL (**Figure 4-5 A**). The top three genes that were more expressed in the synaptic EDL according to their fold change were *H2-Aa*, *Ifitm10*, and *Dlk1*, while for the synaptic SOL these were *Serpinb1a*, *Nell2*, and *Igfbp2* (**Figure 4-5 B**). We also created a list of 77 genes that were synaptically enriched in both muscles. This "core NMJ" list contains many well-known NMJ genes, but also ones that have not previously been shown to be enriched at the NMJ, according to literature queries (**Figure 4-6**).

Table 4-2. Differentially expressed genes of the different comparisons.

Comparison	Genes with positive fold change	Genes with negative fold change
EDL_NMJ vs. EDL_XNMJ	652	217
SOL_NMJ vs. SOL_XNMJ	159	12
EDL_NMJ vs. SOL_NMJ	36 (EDL)[1]	141 (SOL)[1]

Groups: **EDL_XNMJ**, extrasynaptic EDL; **EDL_NMJ**, synaptic EDL; **SOL_XNMJ**, extrasynaptic SOL; **SOL_NMJ**, synaptic SOL. [1], 36 genes were higher in the EDL, while 141 genes were higher in the SOL in this direct synaptic vs. synaptic sample comparison.

Gene ontology enrichment analysis

We performed functional annotation analysis using PANTHER Gene Ontology Enrichment (GO) Analysis, focusing on genes with a positive fold change **(Ashburner, Ball et al. 2000, Huang da, Sherman et al. 2009, Huang da, Sherman et al. 2009, The Gene Ontology 2019)**. Before submitting our different comparison lists, we removed predicted and non-coding genes (e.g. *4933427D14Rik*, *Gm49015*, *Gm2115*…), resulting in a list of 525

differentially expressed genes with a positive fold change for the EDL (EDL_NMJ vs. EDL_XNMJ) and a list of 142 such genes for the SOL (SOL_NMJ vs. SOL_XNMJ). We determined the five most enriched GO terms according to FDR-adjusted p-value for the biological process (BP), molecular function (MF), and cellular component (CC) categories of our different comparison lists. For the synaptic EDL vs. extrasynaptic EDL comparison, *postsynaptic membrane organization*, *extracellular matrix structural constituent*, and *neuromuscular junction* were the top hits for BP, MF, and CC, respectively (**Figure 4-3 C-E**). For the synaptic SOL vs. extrasynaptic SOL comparison, *positive regulation of postsynaptic membrane organization*, *protein binding*, and *neuromuscular junction* were the top hits for BP, MF, and CC, respectively (**Figure 4-4 C-E**). For the synaptic EDL vs. synaptic SOL comparison, *transition between fast and slow* fiber, *striated muscle thin* filament, and *actin* binding were the top hits for BP, MF, and CC, respectively (**Figure 4-5 C-E**). Our gene ontology enrichment analysis indicated that we successfully generated NMJ gene expression profiles for the EDL and SOL muscles, as all of the most significant GO terms were involved with the NMJ. The GO terms enriched in the comparison of synaptic EDL with synaptic SOL samples indicated a large influence of general myofiber type differences.

Validation of RNA-sequencing data with semiquantitative qPCR

We verified our RNA-sequencing results using semiquantitative qPCR with biologically independent samples (**Figure 4-7**). As expected, known NMJ genes such as *Chrne, Utrn,* and *Dcn* were synaptically enriched in the EDL and SOL muscles, while the gene coding for Dystrophin (*Dmd*), which is known to be more expressed extrasynaptically, was not. We verified the synaptic enrichment of the potentially novel NMJ genes *Crym, Hs6st2, Tbx21*, *B4galnt3* and *Chpf*. *Dlk1* was synaptically enriched in the EDL muscle, but not in the SOL, while *Nell2* and *Scn3b* were synaptically enriched in the SOL but not the EDL. *Aplp2* was synaptically enriched in both muscles, but showed stronger expression in the EDL compared to the SOL. Several of the investigated genes were barely or not at all detectable in the extrasynaptic tissue samples. We also compared the fold changes in our RNA-sequencing data vs. our qPCR measurements. For example, synaptic enrichment of *Chrne* was comparable between the different methods. The comparisons are summarized in **Table 4-3**.

Table 4-3. Comparison of synaptic enrichment fold changes between RNA-sequencing and semiquantitative qPCR.

Gene	Method	EDL_NMJ vs. EDL_XNMJ fold change	SOL_NMJ vs. SOL_XNMJ fold change	EDL_NMJ vs. SOL_NMJ fold change
Chrne	RNA-seq	40.97 (*)	53.57 (*)	None
	qPCR	56.43 (***)	57.91 (**)	0.97 (n.s.)
Utrn	RNA-seq	5.92 (*)	5.35 (n.s.)	0.65 (n.s.)
	qPCR	14.23 (**)	10.66 (***)	1.33 (*)
Dcn	RNA-seq	3.63 (***)	4.05 (***)	None
	qPCR	2.41 (*)	7.22 (***)	0.33 (n.s.)
Dmd	RNA-seq	0.279 (**)	1.28 (n.s.)	0.41 (n.s.)
	qPCR	0.68 (n.s.)	0.81 (n.s.)	0.84 (n.s.)
Scn3b	RNA-seq	23.76 (*)	50.04 (**)	0.07 (n.s.)
	qPCR	N.D.	*synaptic*	None
Aplp2	RNA-seq	10.46 (***)	3.44 (**)	4.43 (***)
	qPCR	5.93 (**)	3.81 (**)	1.55 (**)
[1]Crym	RNA-seq	12.43 (n.s.)	246.42 (***)	2.31 (n.s.)
	qPCR	*synaptic*	*synaptic*	None
[1]Hs6st2	RNA-seq	9524 (***)	8.33 (n.s.)	3.43 (n.s.)
	qPCR	13.04 (**)	12.29 (**)	1.06 (n.s.)
[1]Tbx21	RNA-seq	918 (***)	9.35 (n.s.)	3.75 (n.s.)
	qPCR	*synaptic*	*synaptic*	None
[1]B4galnt3	RNA-seq	323.34 (***)	506.7 (***)	None
	qPCR	*synaptic*	*synaptic*	None
[1]Chpf	RNA-seq	203.48 (***)	22.47 (**)	None
	qPCR	*synaptic*	6.32 (*)	None
[1]Dlk1	RNA-seq	423.5 (***)	0.22 (n.s.)	423.5 (**)
	qPCR	*synaptic*	N.D.	None
[1]Nell2	RNA-seq	None	141.28 (**)	0.001 (***)
	qPCR	None	*synaptic*	None

Synaptic: Indicates that a gene was detected only in the synaptic samples and was undetectable in the extrasynaptic samples and therefore a fold change could not be determined. N.D. indicates that a gene was undetected in all samples of the respective comparison. Groups: **EDL_XNMJ**, extrasynaptic EDL; **EDL_NMJ**, synaptic EDL; **SOL_XNMJ**, extrasynaptic SOL; **SOL_NMJ**, synaptic SOL. Data shown as fold change; * $p \leq 0.05$, ** $p \leq 0.01$, ***, $p \leq 0.001$; n.s., not significant; None, no data available. [1], potential novel NMJ genes.

Effects of *in vivo* muscle electroporation of TBX21 on NMJ morphology

We queried the animal transcription factor data base 3.0 **(Hu, Miao et al. 2019)** with the list of our synaptically enriched genes in the EDL and SOL to potentially identify transcription factors which might be involved in regulating the NMJ gene program. Our query revealed the transcription factor T-box 21 (TBX21) among our most highly synaptically enriched genes. T-box 21 is perhaps best known for its role in T-helper cell lineage commitment **(Miller and Weinmann 2010, Kanhere, Hertweck et al. 2012)**. Since the transcription factor ETV5, which partially controls subsynaptic gene expression at the NMJ **(Hippenmeyer, Huber et al. 2007)**, plays a role in T-helper cell development as well **(Koh, Hufford et al. 2016)**, we hypothesized that TBX21 may thus be involved in the regulation of NMJ structure and function by acting as a novel NMJ transcription factor. We overexpressed TBX21 in the TA muscle via *in vivo* muscle electroporation of a *Tbx21* expression plasmid with a MYC-DDK tag. NMJs transfected with TBX21 displayed reduced presynaptic nerve terminal area and increased postsynaptic AChR "compactness" (which indicates a larger quantity of AChRs within the endplate area.) when compared to eGFP-transfected controls. Other measured morphological parameters of the NMJ, such as axon diameter, nerve terminal perimeter, or endplate diameter, remained unchanged (**Figure 4-8 C-K**). These findings indicate a role of the transcription factor TBX21 in regulating NMJ morphology.

4.5 Discussion

We utilized laser-capture microdissection (LCM) and next-generation RNA-sequencing to investigate the transcriptome of fundamental myonuclei that underlie the NMJ, and which express a distinct gene program compared to extrajunctional myonuclei. We successfully generated transcriptomic datasets of the NMJ for the predominantly fast-twitch EDL (**Figure 4-3**) and the predominantly slow-twitch SOL (**Figure 4-4**) muscles as evidenced by the large enrichment of canonical NMJ genes in our synaptic samples, which in turn enriched gene ontology terms clearly associated with the NMJ. We validated several known and potentially novel NMJ genes by semiquantitative qPCR (**Figure 4-7**).

Our LCM- and RNA-sequencing-based approach lead to strong synaptic enrichment, as we detected over 300 genes with fold changes above 50-fold in the EDL and over 60 such genes in the SOL muscle. A study performed over a decade ago utilized a similar approach of LCM coupled with microarray technology to conduct transcriptomic profiling of NMJs of the TA muscle and reported average mRNA fold changes of 8.9, 5.5, and 4 for the known NMJ-associated genes *Chrne, Chrna1* and *Nes*, while we now report fold changes of 41, 38 and 33, respectively **(Nazarian, Bouri et al. 2005)**. Another such study comparing synaptic with extrasynaptic TA using LCM and microarray-based NMJ expression profiling reported larger fold changes of 300 for *Chrna1*, 117 for *Chrne* and 79 for *Nes* **(Ketterer, Zeiger et al. 2010)**. However, Ketterer et al. (2010) reported less than 20 genes with fold changes larger than 50 in their synaptic vs. extrasynaptic TA comparison. Compared to these literature results, our RNA-sequencing-based approach lead to improved synaptic enrichment. Granted, we have to be careful when drawing conclusions from dataset comparisons involving different muscles and technologies, as the EDL, SOL and TA are all different muscles and it is known that significant transcriptomic diversity among skeletal muscles exist **(Terry, Zhang et al. 2018)**. Furthermore, a large fold change value does not necessarily imply strong expression of a gene, which is important to consider for genes with little or no expression in the samples a comparison is made with. Nevertheless, our EDL and SOL NMJ expression profiles contain many known and previously described NMJ genes, including various acetylcholine receptor (AChR) subunits and other examples such as *Nes, Musk, Prka1a, Cd24a, Etv5, Dusp6, Phldb2*

and *Scn3b* **(Beam, Caldwell et al. 1985, Kishi, Kummer et al. 2005, McGeachie, Koishi et al. 2005, Nazarian, Bouri et al. 2005, Jevsek, Jaworski et al. 2006, Hippenmeyer, Huber et al. 2007, Ketterer, Zeiger et al. 2010)**. We also provide a large number of potentially novel NMJ genes, many of which show far larger synaptic enrichment than known NMJ genes, perhaps owing to their exceptionally low expression in extrasynaptic regions of the myofiber.

Among the most highly enriched genes at the EDL NMJ was *Tbx21*, with a fold change of over 900. We confirmed the synaptic enrichment of *Tbx21* with semiquantitative qPCR and found that it was equally expressed at the SOL NMJ (**Figure 4-7 G**). Furthermore, *Tbx21* was indicated to be expressed in the synaptic endplate band of the mouse diaphragm, underlining its potential importance at the NMJ **(Hippenmeyer, Huber et al. 2007)**. *Tbx21* encodes for the T-box transcription factor T-box 21 (TBX21), which is also known as T-Bet and so far has no established role at the NMJ. T-box proteins are involved in a broad range of pathways and often function as transcriptional activators or repressors. We hypothesized that TBX21 might be involved in the regulation of the NMJ gene program in the fundamental NMJ-associated myonuclei. Indeed, TBX21 has the ability to alter the state of chromatin towards transcriptional activation by associating with histone-modifying complexes and recruiting methyltransferase activity to target promotors **(Lewis, Miller et al. 2007, Miller, Huang et al. 2008)**. Overexpression of TBX21 in the TA muscle lead to reduced presynaptic nerve terminal area and increased postsynaptic AChR density six weeks after the muscle electroporation (**Figure 4-8**). This increase in postsynaptic AChR density might indicate a role of TBX21 in AChR turnover and/or clustering, and may thus have a positive impact on postsynaptic sensitivity. However, we have to take into account that our results are based on a relatively small number of images (~ 10 images per biological replicate, N = 3) due to the rarity of correctly positioned ("face up") NMJs with *Tbx21*-transfected myonuclei. Thus, further research is needed to confirm and expand our observed effects of TBX21 on the NMJ. Specifically, an inducible, muscle-specific transgenic mouse model for TBX21 with an expression tag would allow circumventing the restrictions of *in vivo* muscle electroporation described above and allow confirmation of our described morphologic effects of TBX21 overexpression on the NMJ. Furthermore, electrophysiological measurements would shed light in the potential effect on neurotransmission strength, and LCM together with RNA-

sequencing could reveal the potential influence of TBX21 on the NMJ gene program. These studies could be complemented with an additional TBX21 loss-of-function approach, e.g. via intramuscular injection of adeno-associated viruses (AAV) to express shRNAs against TBX21. Finally, ChIP-Seq experiments utilizing the expression tag would reveal TBX21 DNA binding sites, although it has to be established first whether whole-muscle tissue could be used or whether LCM would be required for these experiments.

To investigate whether there are fundamental differences between the NMJ transcriptomes of fast- and slow-type NMJs that would help explain their structural and functional differences, we compared our NMJ gene expression profiles of the predominantly fast-twitch EDL and the predominantly slow-twitch SOL muscles. Principal coordinate analysis revealed two major differences between the samples of our study (**Figure 4-2**). One major difference was due to LCM region, being either synaptic or extrasynaptic, and the other due to muscle type, being either EDL or SOL. While the synaptic EDL and SOL samples cluster together based on their muscle type, the distance between the two synaptic clusters on the first principal coordinate is relatively short in comparison to the large difference due to muscle type that separates the two muscles on the second principal coordinate, indicating that the two synaptic clusters might be relatively similar. Indeed, the direct synaptic EDL vs. synaptic SOL comparison was dominated by large expression differences of myofiber type-specific genes, such as various myosin heavy chains (e.g. *Myh2*, *Myh6*, *Myh7*,), troponins (e.g. *Tnni1, Tnnt1*) and calcium-buffering proteins (*Pvalb*), indicating a possible contamination of our synaptic samples with extrasynaptic myonuclei. This observation was further supported by the top gene ontology terms (e.g. *transition between fast and slow fiber*) that were enriched by the synaptic EDL vs. synaptic SOL comparison (**Figure 4-5 C-E**). Consequently, the direct comparison of the synaptic EDL with the synaptic SOL samples revealed a relatively small set of genes differing between the two muscles when these general muscle differences were accounted for via filtering out genes that were not synaptically enriched in the respective synaptic vs. extrasynaptic comparisons of the EDL and SOL (**Figure 4-5 B**). Furthermore, the expression level of canonical NMJ genes, such as *Chrne, Chrnd, Chrna1, Chrnb1, MuSK, Etv5,* and *Utrn*, was nearly identical between the synaptic EDL and SOL samples, which indicates that the different muscles share great similarity of their NMJ gene programs (**Figure 4-9 A-**

G). One of the genes with the largest expression differences between the synaptic samples of the muscles was delta like non-canonical Notch ligand 1 (*Dlk1*); its expression was over 400-fold higher in the synaptic EDL vs. synaptic SOL. Furthermore, *Dlk1* mRNA was undetectable in all but the synaptic EDL samples in our semiquantitative qPCR validation experiments, suggesting its exclusive synaptic expression in the fast-twitch EDL (**Figure 4-7 K**). Despite the large fold change of *Dlk1*, its expression strength in the synaptic EDL samples was still at a relatively low ~ 2 counts per million (CPM) in our sequencing dataset (**Figure 4-9 J**). Interestingly, DLK1 alone is sufficient to drive the fast motor neuron biophysical signature by suppressing Notch signaling **(Muller, Cherukuri et al. 2014)**, which raises the question whether fast motor neuron-derived *Dlk1* mRNA is transported to and locally translated at the nerve terminal to exert similar functions, since Notch signaling was found the be required for activity-dependent synaptic plasticity at the Drosophila NMJ **(de Bivort, Guo et al. 2009)**.

Regardless of muscle type, contamination with other cell types present at the NMJ reveal certain limitations of the LCM technique in isolating fundamental NMJ myonuclei, as genes expressed in e.g. Schwann cells were highly enriched in the synaptic tissue samples (e.g. *Sox10* with a 1193-fold change in the synaptic vs. extrasynaptic EDL comparison). We are therefore unable to distinguish whether a synaptically enriched gene in our NMJ expression profile actually originated from muscle itself or was expressed by another cell type present at the NMJ that was co-isolated with LCM. This highlights the importance of further experiments that confirm the origin of a potential novel NMJ gene, especially when considering the concept of motor neuron-derived mRNAs at the NMJ. *In situ* hybridization approaches could be used to confirm the origin of candidate genes such as *Dlk1*. The limitations discussed above may have hindered our ability to assess the full extent of transcriptomic differences between EDL and SOL muscle NMJs. However, the idea of a powerful determinant of NMJ type such as a DLK1 appears attractive and future research will evaluate the potential role of DLK1 in determining NMJ type.

4.6 Figures

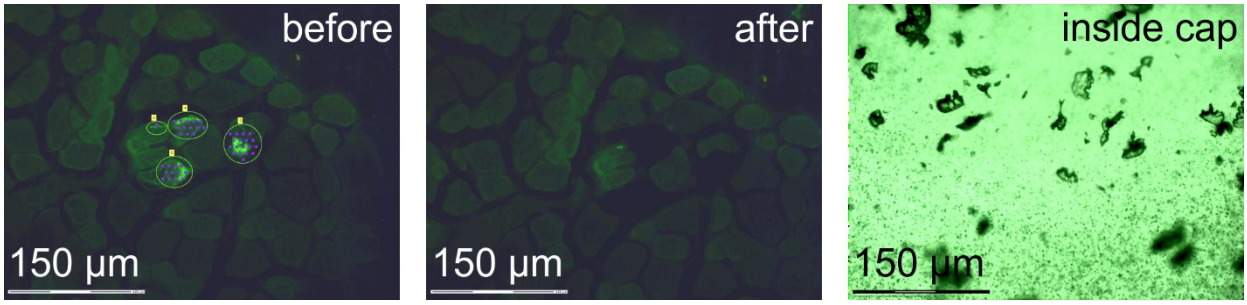

Figure 4-1. Laser-capture microdissection (LCM) procedure for the isolation of neuromuscular junction areas. The "before" image shows several synaptic areas (green fluorescence signal) marked for LCM. A defocused UV-laser impulse was fired at each individual purple dot in the marked areas to isolate the desired tissue by lifting it up into a specialized adhesive PCR tube cap. The "after" image confirms the successful microdissection of the desired tissue areas. The "inside cap" picture shows the bits of isolated tissue that were captured by the LCM procedure. Scale bar, 150 µm.

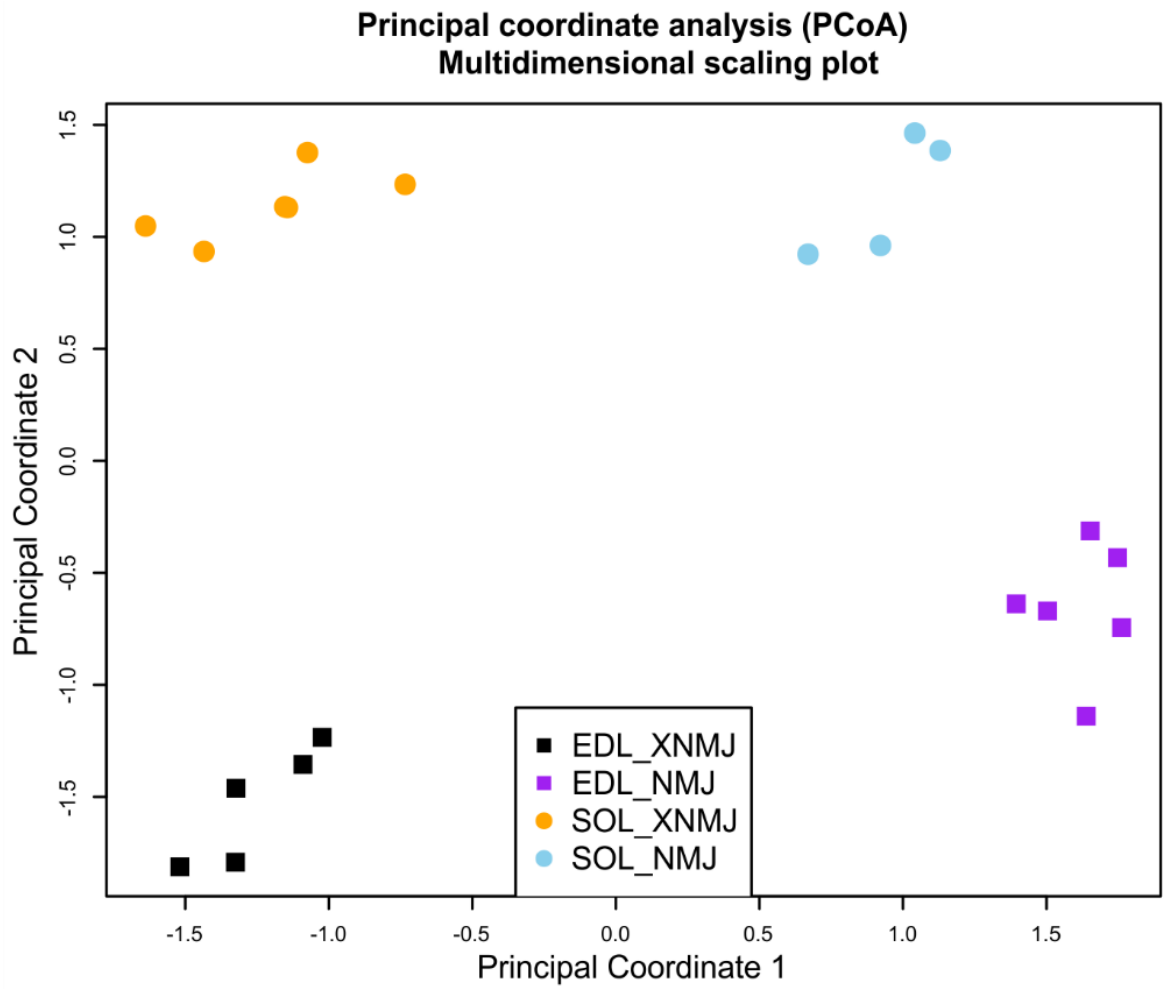

Figure 4-2. Principal coordinate analysis (PCoA) reveals sample clusters according to synaptic or extrasynaptic origin, as well as according to muscle type. Each plot symbol represents a sample. Distance between samples can be interpreted as the typical log2 fold change of the top 500 genes that distinguish them. Groups: **EDL_XNMJ**, extrasynaptic EDL; **EDL_NMJ**, synaptic EDL; **SOL_XNMJ**, extrasynaptic SOL; **SOL_NMJ**, synaptic SOL.

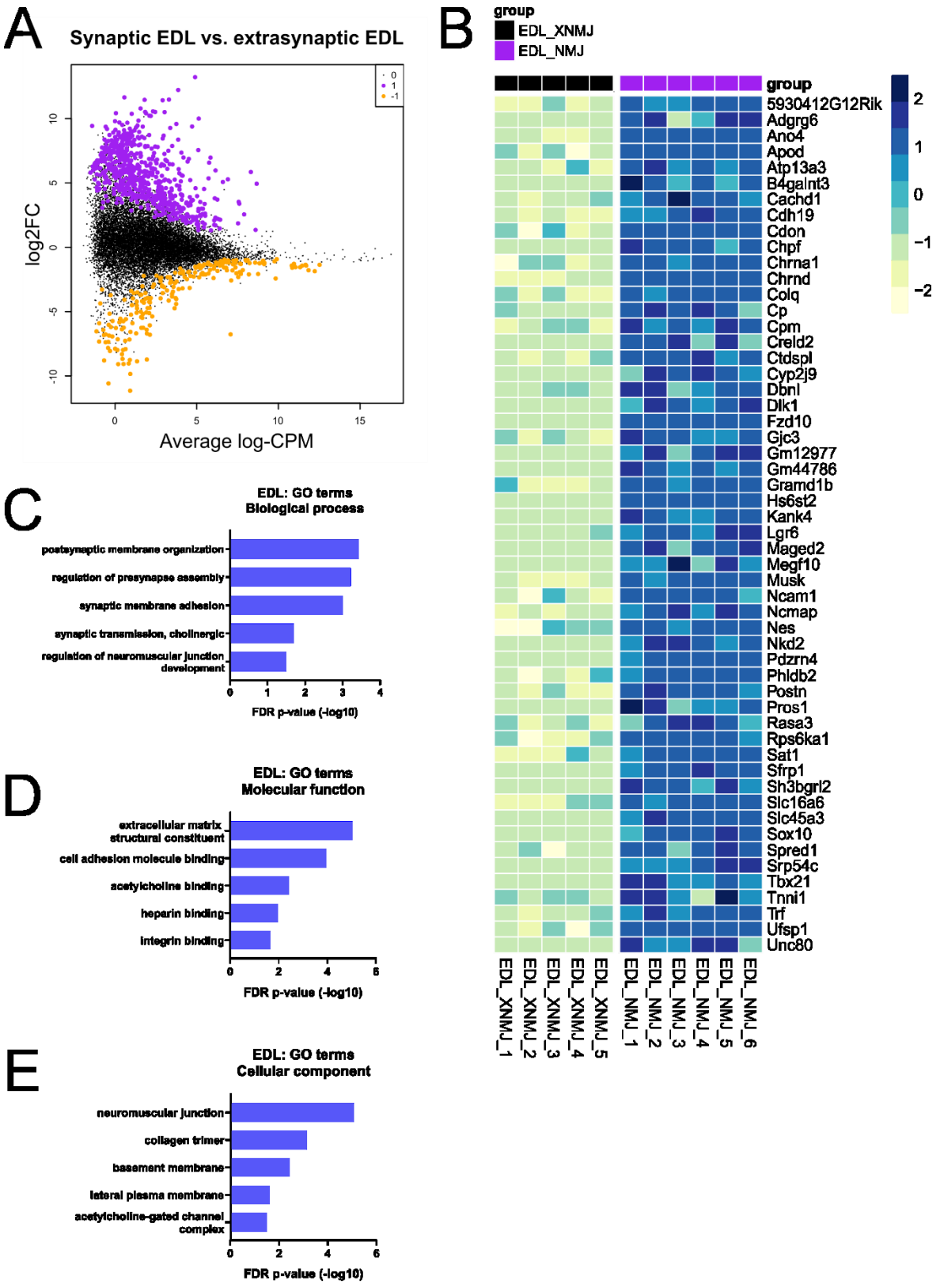
A
Synaptic EDL vs. extrasynaptic EDL
log2FC
Average log-CPM
B
group
EDL_XNMJ
EDL_NMJ
group
5930412G12Rik
Adgrg6
Ano4
Apod
Atp13a3
B4galnt3
Cachd1
Cdh19
Cdon
Chpf
Chrna1
Chrnd
Colq
Cp
Cpm
Creld2
Ctdspl
Cyp2j9
Dbnl
Dlk1
Fzd10
Gjc3
Gm12977
Gm44786
Gramd1b
Hs6st2
Kank4
Lgr6
Maged2
Megf10
Musk
Ncam1
Ncmap
Nes
Nkd2
Pdzrn4
Phldb2
Postn
Pros1
Rasa3
Rps6ka1
Sat1
Sfrp1
Sh3bgrl2
Slc16a6
Slc45a3
Sox10
Spred1
Srp54c
Tbx21
Tnni1
Trf
Ufsp1
Unc80
EDL_XNMJ_1
EDL_XNMJ_2
EDL_XNMJ_3
EDL_XNMJ_4
EDL_XNMJ_5
EDL_NMJ_1
EDL_NMJ_2
EDL_NMJ_3
EDL_NMJ_4
EDL_NMJ_5
EDL_NMJ_6
C
EDL: GO terms
Biological process
postsynaptic membrane organization
regulation of presynapse assembly
synaptic membrane adhesion
synaptic transmission, cholinergic
regulation of neuromuscular junction development
FDR p-value (-log10)
D
EDL: GO terms
Molecular function
extracellular matrix structural constituent
cell adhesion molecule binding
acetylcholine binding
heparin binding
integrin binding
FDR p-value (-log10)
E
EDL: GO terms
Cellular component
neuromuscular junction
collagen trimer
basement membrane
lateral plasma membrane
acetylcholine-gated channel complex
FDR p-value (-log10)

Figure 4-3. Neuromuscular junction gene expression profile of the EDL muscle. A) Mean-difference plot of synaptic vs. extrasynaptic EDL muscle showing log2 fold changes (log2FC) of genes on the Y-axis plotted against the average gene expression strength in log2 counts per million (log-CPM) on the X-axis. Each black dot represents an expressed gene in the study (legend "0"). Differentially expressed genes (FDR p-value < 0.05) with a positive fold change are marked in purple (legend "1"), while genes with a negative fold change are marked in orange (legend "-1"). **B)** Unclustered heatmap visualization of the top 50 synaptically enriched genes in the synaptic EDL samples according to both fold change as well as FDR p-value (fold change > 32, FDR p-value < 0.001). Shown are scaled CPM expression values of all synaptic and extrasynaptic EDL samples. Darker hues of blue represent stronger expression in these samples. Groups: **EDL_XNMJ**, extrasynaptic EDL; **EDL_NMJ**, synaptic EDL. **C-E)** PANTHER gene ontology enrichment analysis of the biological process, molecular function, and cellular component categories. Shown are the top five terms in each category according to FDR p-value.

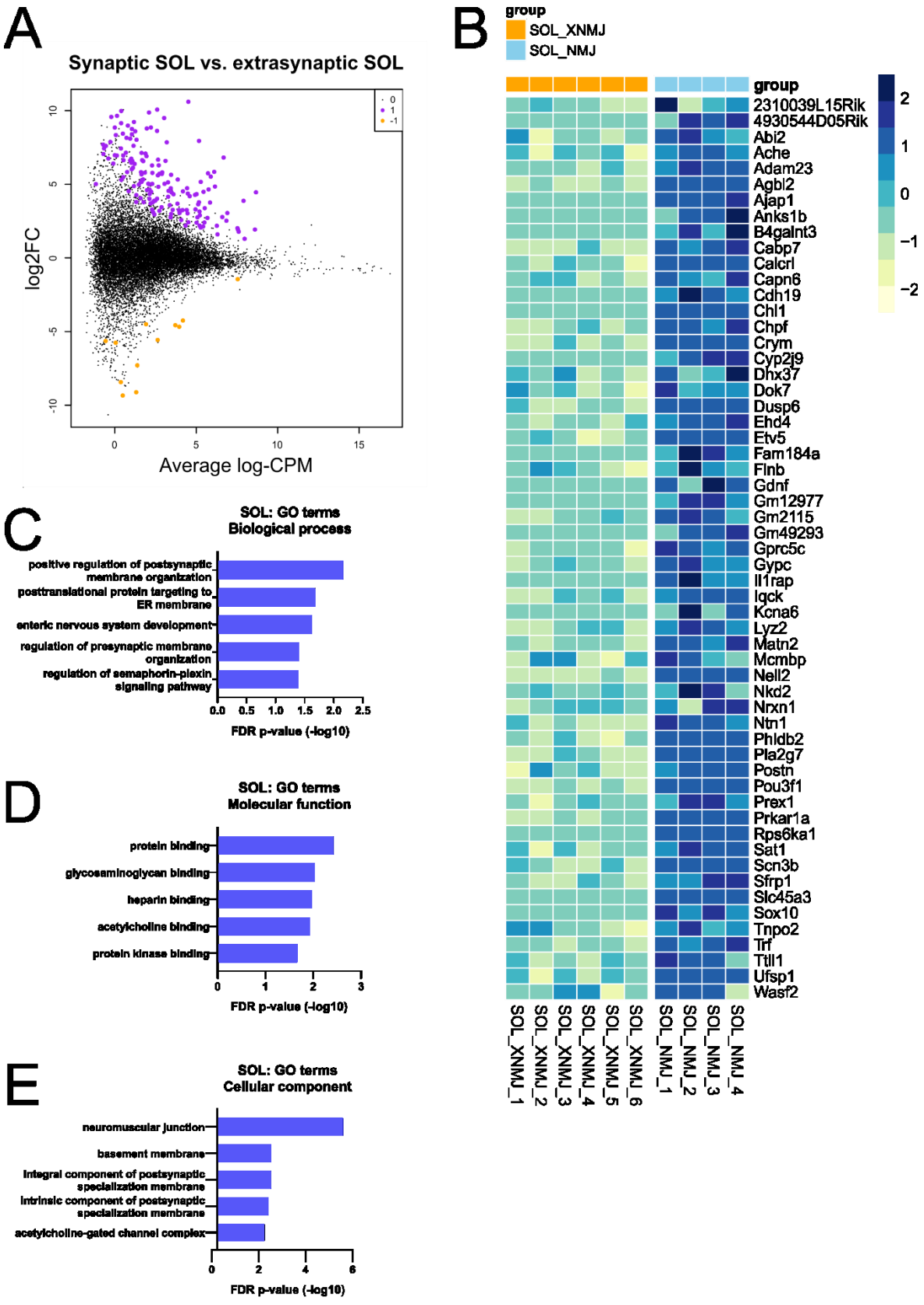
A
Synaptic SOL vs. extrasynaptic SOL
log2FC
Average log-CPM
B
group
SOL_XNMJ
SOL_NMJ
2310039L15Rik
4930544D05Rik
Abi2
Ache
Adam23
Agbl2
Ajap1
Anks1b
B4galnt3
Cabp7
Calcrl
Capn6
Cdh19
Chl1
Chpf
Crym
Cyp2j9
Dhx37
Dok7
Dusp6
Ehd4
Etv5
Fam184a
Flnb
Gdnf
Gm12977
Gm2115
Gm49293
Gprc5c
Gypc
Il1rap
Iqck
Kcna6
Lyz2
Matn2
Mcmbp
Nell2
Nkd2
Nrxn1
Ntn1
Phldb2
Pla2g7
Postn
Pou3f1
Prex1
Prkar1a
Rps6ka1
Sat1
Scn3b
Sfrp1
Slc45a3
Sox10
Tnpo2
Trf
Ttll1
Ufsp1
Wasf2
SOL_XNMJ_1
SOL_XNMJ_2
SOL_XNMJ_3
SOL_XNMJ_4
SOL_XNMJ_5
SOL_XNMJ_6
SOL_NMJ_1
SOL_NMJ_2
SOL_NMJ_3
SOL_NMJ_4
C
SOL: GO terms
Biological process
positive regulation of postsynaptic membrane organization
posttranslational protein targeting to ER membrane
enteric nervous system development
regulation of presynaptic membrane organization
regulation of semaphorin-plexin signaling pathway
FDR p-value (-log10)
D
SOL: GO terms
Molecular function
protein binding
glycosaminoglycan binding
heparin binding
acetylcholine binding
protein kinase binding
FDR p-value (-log10)
E
SOL: GO terms
Cellular component
neuromuscular junction
basement membrane
integral component of postsynaptic specialization membrane
intrinsic component of postsynaptic specialization membrane
acetylcholine-gated channel complex
FDR p-value (-log10)

Figure 4-4. Neuromuscular junction gene expression profile of the SOL muscle. A) Mean-difference plot of synaptic vs. extrasynaptic SOL muscle showing log2 fold changes (log2FC) of genes on the Y-axis plotted against the average gene expression strength in log counts per million (log-CPM) on the X-axis. Each black dot represents an expressed gene in the study (legend "0"). Differentially expressed genes (FDR p-value < 0.05) with a positive fold change are marked in purple (legend "1"), while genes with a negative fold change are marked in orange (legend "-1"). **B)** Unclustered heatmap visualization of the top 50 synaptically enriched genes in the synaptic SOL samples according to both fold change as well as FDR p-value (fold change > 16, FDR p-value < 0.01). Shown are scaled CPM expression values of all synaptic and extrasynaptic SOL samples. Darker hues of blue represent stronger expression in these samples. Groups: **SOL_XNMJ**, extrasynaptic SOL; **SOL_NMJ**, synaptic SOL. **C-E)** PANTHER gene ontology enrichment analysis of the biological process, molecular function, and cellular component categories. Shown are the top five terms in each category according to FDR p-value.

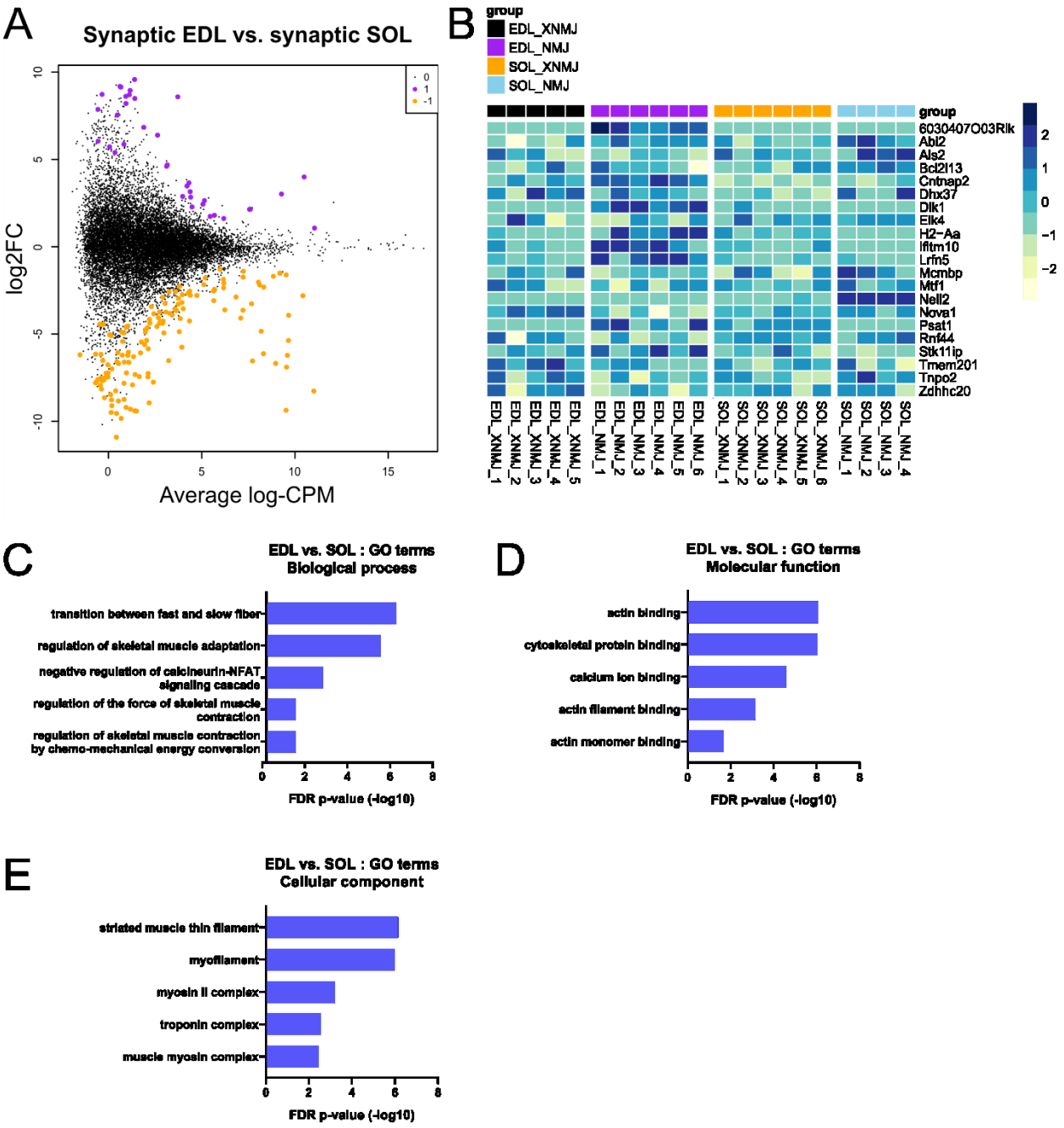
A
Synaptic EDL vs. synaptic SOL
log2FC
Average log-CPM
B
group
EDL_XNMJ
EDL_NMJ
SOL_XNMJ
SOL_NMJ
6030407O03Rik
Abl2
Als2
Bcl2l13
Cntnap2
Dhx37
Dlk1
Elk4
H2-Aa
Ifitm10
Lrfn5
Mcmbp
Mtf1
Nell2
Nova1
Psat1
Rnf44
Stk11ip
Tmem201
Tnpo2
Zdhhc20
C
EDL vs. SOL : GO terms
Biological process
transition between fast and slow fiber
regulation of skeletal muscle adaptation
negative regulation of calcineurin-NFAT signaling cascade
regulation of the force of skeletal muscle contraction
regulation of skeletal muscle contraction by chemo-mechanical energy conversion
FDR p-value (-log10)
D
EDL vs. SOL : GO terms
Molecular function
actin binding
cytoskeletal protein binding
calcium ion binding
actin filament binding
actin monomer binding
FDR p-value (-log10)
E
EDL vs. SOL : GO terms
Cellular component
striated muscle thin filament
myofilament
myosin II complex
troponin complex
muscle myosin complex
FDR p-value (-log10)

Figure 4-5. Neuromuscular junction gene expression differences between the EDL and SOL muscles. A) Mean-difference plot of synaptic EDL vs. synaptic SOL showing log2 fold changes (log2FC) of genes on the Y-axis plotted against the average gene expression strength in log-counts-per-million (log-CPM) on the X-axis. Each black dot represents an expressed gene in the study (legend "0"). Differentially expressed genes (FDR p-value < 0.05) which are more strongly expressed in the synaptic EDL are marked in purple (legend "1"), while genes more strongly expressed in the synaptic SOL are marked in orange (legend "-1"). **B)** Unclustered heatmap visualization of strongly differentially expressed genes according to both fold change as well as FDR p-value (fold change > 8, FDR p-value < 0.05) between synaptic EDL and synaptic SOL. In order to filter out the general muscle difference effect, only genes that were also synaptically enriched in the respective synaptic vs. extrasynaptic comparisons of the EDL and SOL were included. Shown are scaled CPM expression values of all synaptic EDL and SOL samples. Darker hues of blue represent stronger expression in these samples. **C-E)** PANTHER gene ontology enrichment analysis of the biological process, molecular function, and cellular component categories. Shown are the top five terms in each category according to FDR p-value. Groups: **EDL_XNMJ**, extrasynaptic EDL; **EDL_NMJ**, synaptic EDL; **SOL_XNMJ**, extrasynaptic SOL; **SOL_NMJ**, synaptic SOL.

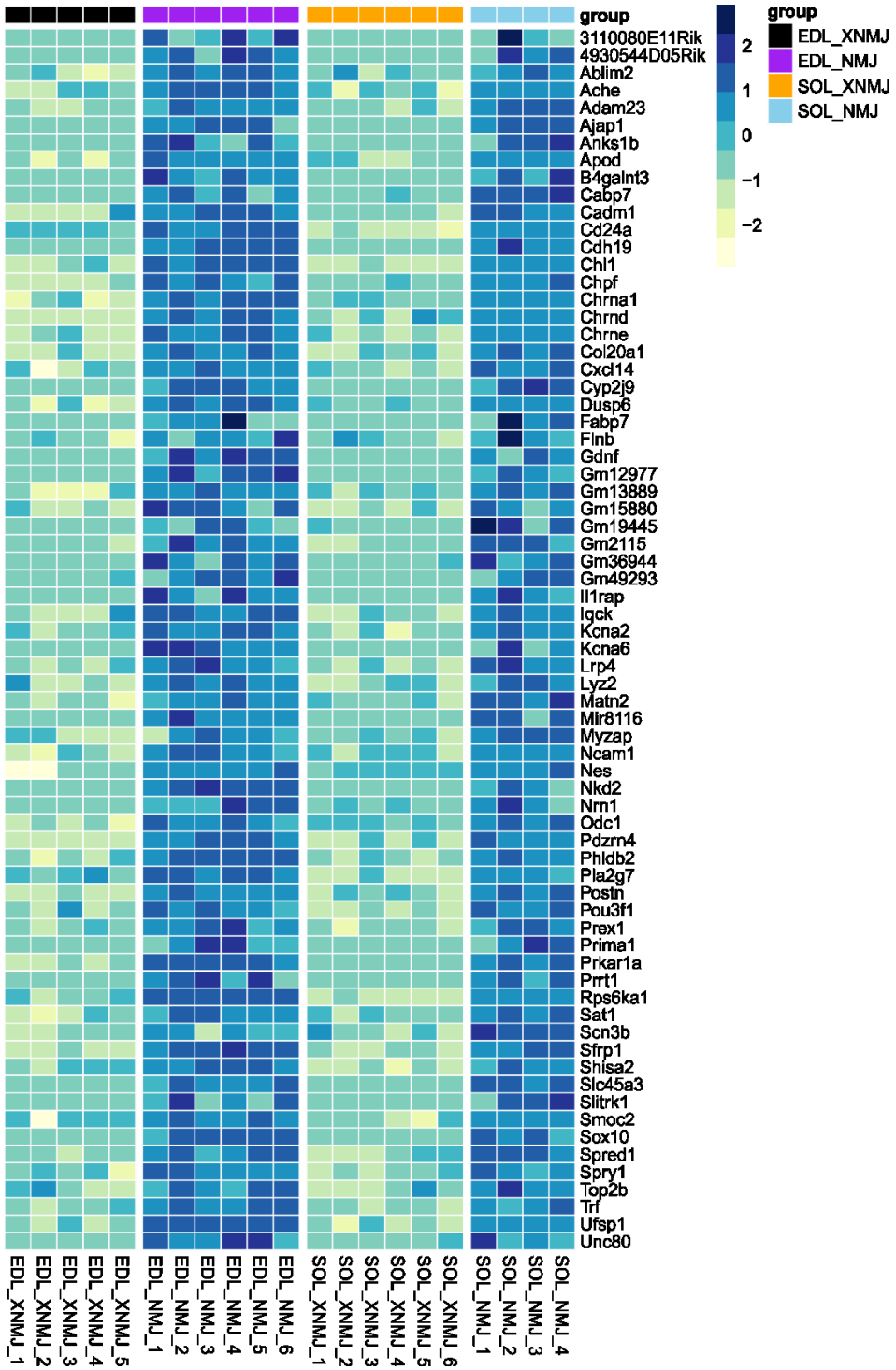

Figure 4-6. Unclustered heatmap visualization of all genes that were synaptically enriched in both the EDL as well as the SOL. Shown are scaled CPM expression values of all synaptic and extrasynaptic EDL and SOL samples. Darker hues of blue represent stronger expression in these samples. Groups: **EDL_XNMJ**, extrasynaptic EDL; **EDL_NMJ**, synaptic EDL; **SOL_XNMJ**, extrasynaptic SOL; **SOL_NMJ**, synaptic SOL.

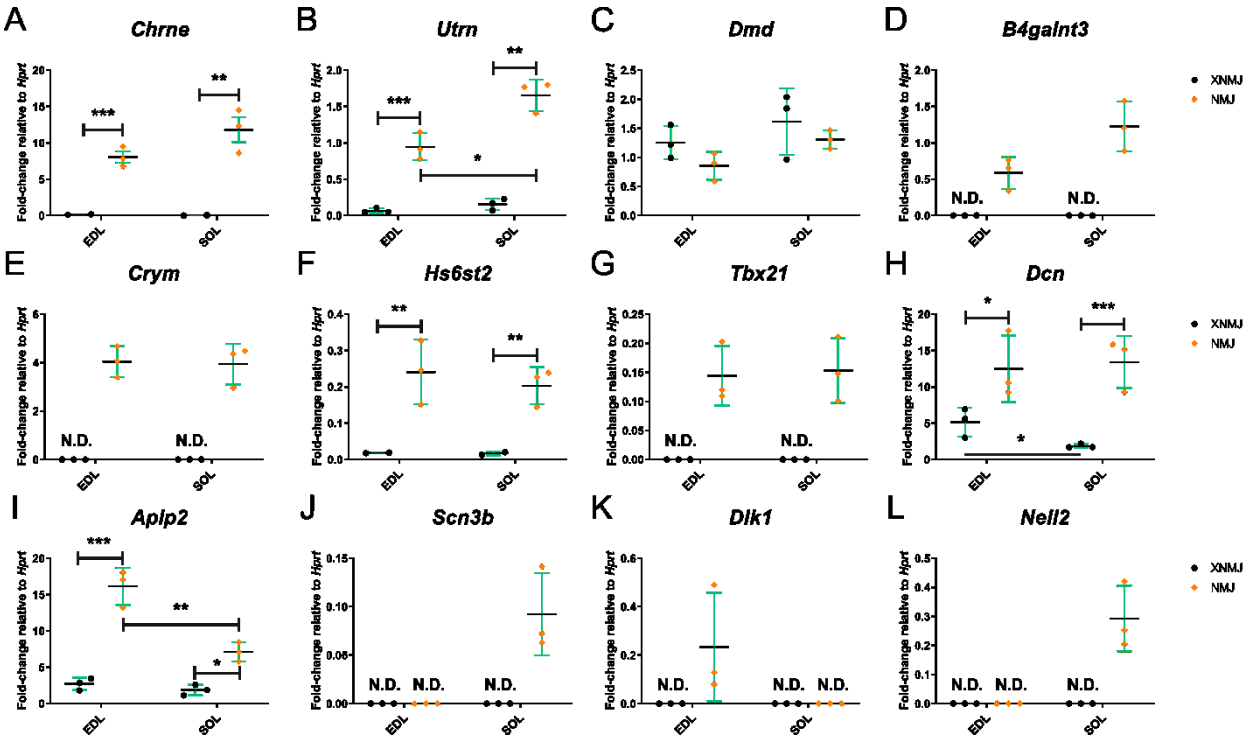

Figure 4-7. RNA-sequencing data validation with semiquantitative qPCR of laser-captured synaptic and extrasynaptic tissue of the EDL and SOL muscle. All expression values are fold changes relative to the reference gene *Hprt.* Black dots indicate extrasynaptic (XNMJ) biological replicates, while orange diamonds indicate synaptic (NMJ) ones. Data shown as mean ± SD of triplicate samples, * $p < 0.05$, ** $p < 0.01$, *** $p < 0.001$; N.D., undetected.

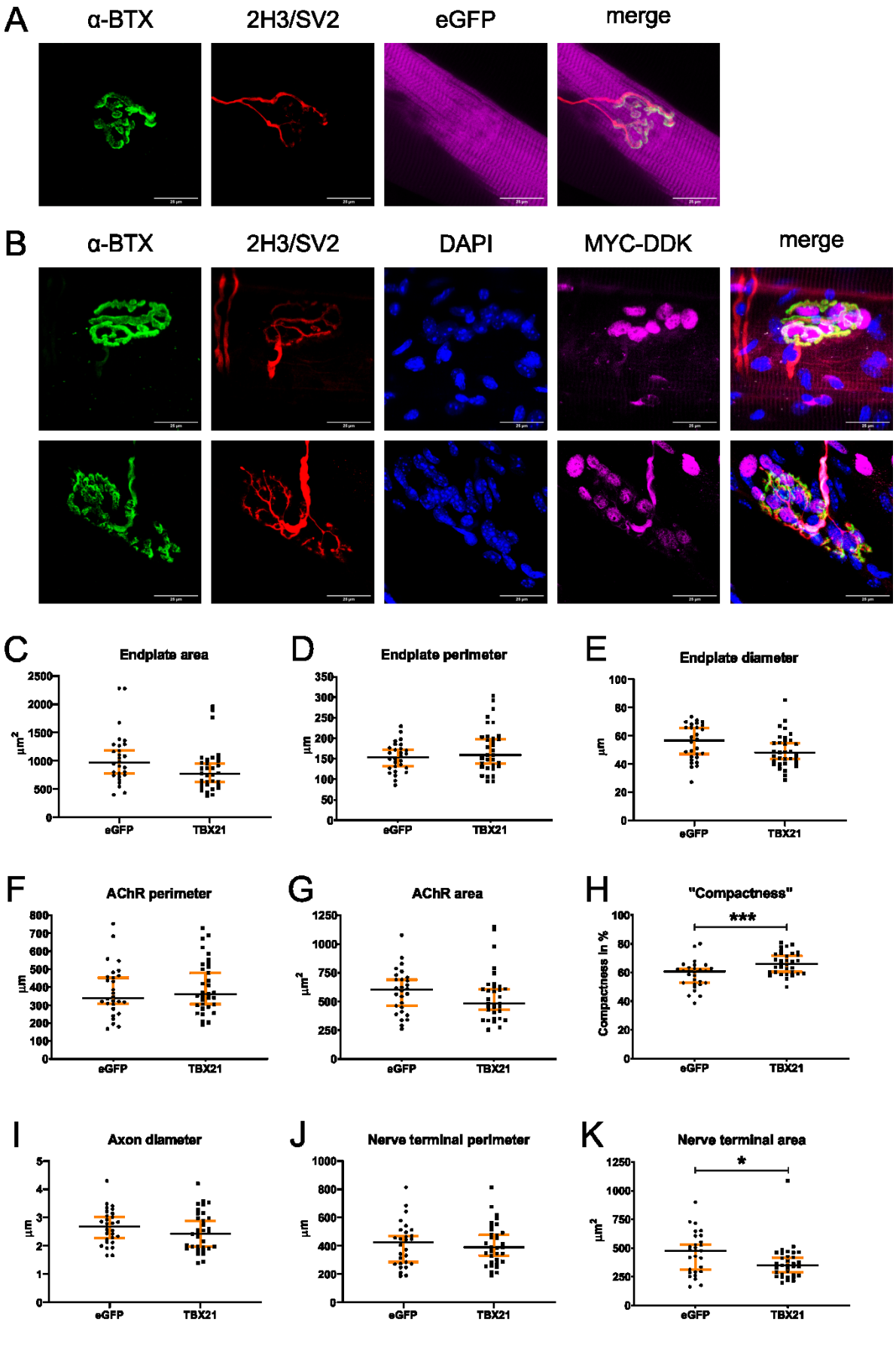
A
α-BTX
2H3/SV2
eGFP
merge
B
α-BTX
2H3/SV2
DAPI
MYC-DDK
merge
C
Endplate area
µm²
eGFP
TBX21
D
Endplate perimeter
µm
eGFP
TBX21
E
Endplate diameter
µm
eGFP
TBX21
F
AChR perimeter
µm
eGFP
TBX21
G
AChR area
µm²
eGFP
TBX21
H
"Compactness"
***
Compactness in %
eGFP
TBX21
I
Axon diameter
µm
eGFP
TBX21
J
Nerve terminal perimeter
µm
eGFP
TBX21
K
Nerve terminal area
*
µm²
eGFP
TBX21

Figure 4-8. Overexpression of TBX21 in the *tibialis anterior* (TA) muscle leads to increased acetylcholine receptor (AChR) density in the synaptic endplate. Confocal microscopy images of NMJs in TA myofiber bundles electroporated with **A)** an eGFP expression plasmid, or **B)** electroporated with a MYC-DDK-tagged *Tbx21* expression plasmid. **C-K)** NMJ morphology parameters determined six weeks after electroporation with either eGFP or *Tbx21*. **C)** Total postsynaptic endplate area. **D)** Postsynaptic endplate perimeter. **E)** Postsynaptic endplate diameter. **F)** Perimeter of the postsynaptic AChRs. **G)** Total area of the postsynaptic AChRs. **H)** "Compactness" (AChR density at the synaptic endplate). **I)** Axon diameter. **J)** Perimeter of the presynaptic nerve terminal. **K)** Total area of the presynaptic nerve terminal. **α-BTX**: α-Bungarotoxin; **2H3/SV2**: Two different antibodies staining Neurofilament (2H3) and synaptic vesicle glycoprotein 2A (SV2). **eGFP**: Enhanced green fluorescent protein. **MYC-DDK**: Antibody targeting the MYC-DDK tag; merge: Compound image of all respective channels. Data shown as median ± 95% confidence intervals; * $p \leq 0.05$, ** $p \leq 0.01$, *** $p \leq 0.001$. Images of three biological replicates per condition were combined for the analysis. Scale bar: 25 µm.

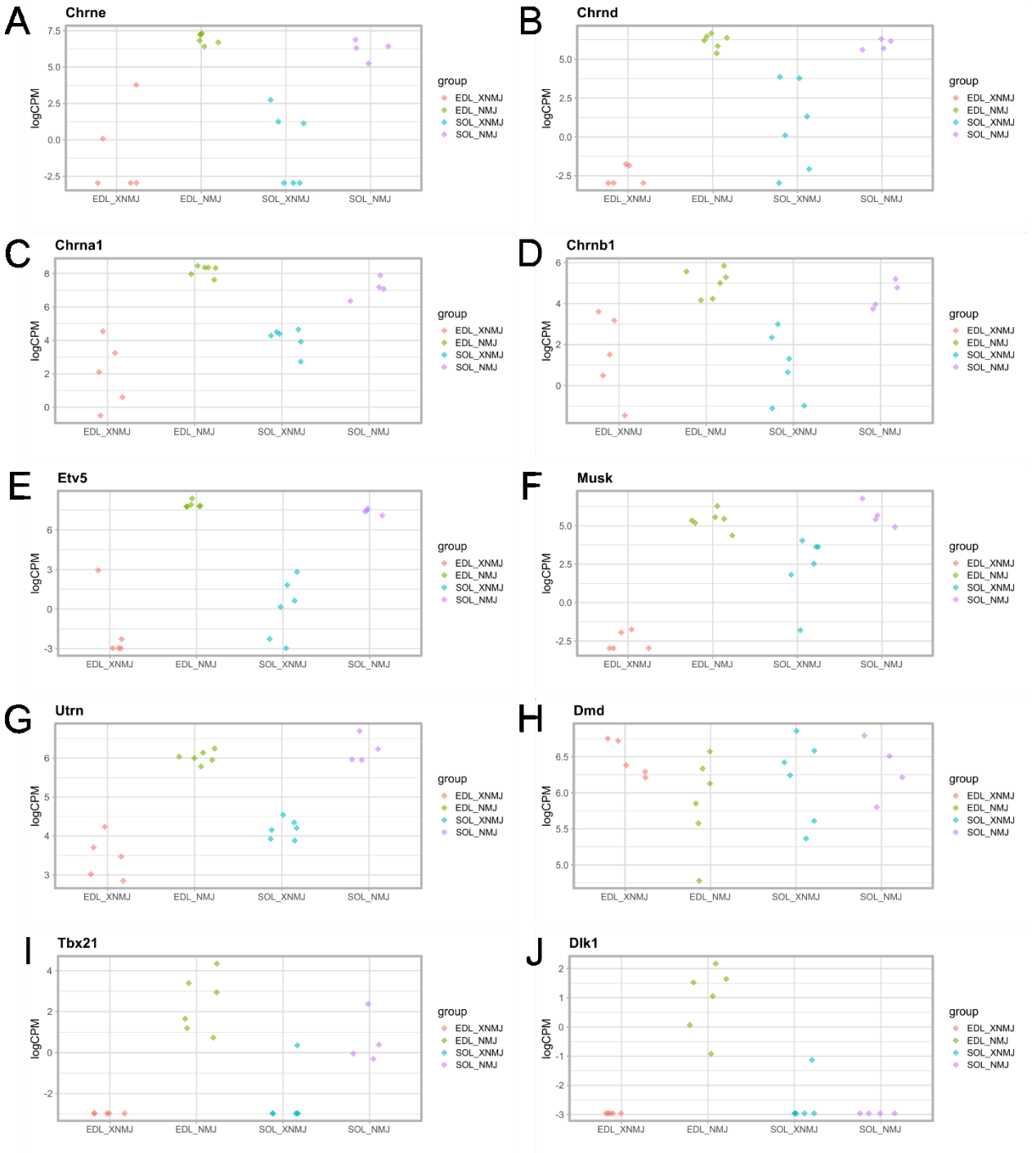

Figure 4-9. Gene expression plots of known and potential novel NMJ genes. Gene expression in log2 counts per million (logCPM) of the RNA-sequencing count data of the indicated individual genes across all experimental groups is shown. Each diamond represents a sample. Groups: **EDL_XNMJ**, extrasynaptic EDL; **EDL_NMJ**, synaptic EDL; **SOL_XNMJ**, extrasynaptic SOL; **SOL_NMJ**, synaptic SOL.

4.7 References

Ashburner, M., C. A. Ball, J. A. Blake, D. Botstein, H. Butler, J. M. Cherry, A. P. Davis, K. Dolinski, S. S. Dwight, J. T. Eppig, M. A. Harris, D. P. Hill, L. Issel-Tarver, A. Kasarskis, S. Lewis, J. C. Matese, J. E. Richardson, M. Ringwald, G. M. Rubin and G. Sherlock (2000). "Gene ontology: tool for the unification of biology. The Gene Ontology Consortium." Nat Genet **25**(1): 25-29.

Beam, K. G., J. H. Caldwell and D. T. Campbell (1985). "Na channels in skeletal muscle concentrated near the neuromuscular junction." Nature **313**(6003): 588-590.

de Bivort, B. L., H. F. Guo and Y. Zhong (2009). "Notch signaling is required for activity-dependent synaptic plasticity at the Drosophila neuromuscular junction." J Neurogenet **23**(4): 395-404.

Fahim, M. A., J. A. Holley and N. Robbins (1984). "Topographic comparison of neuromuscular junctions in mouse slow and fast twitch muscles." Neuroscience **13**(1): 227-235.

Hippenmeyer, S., R. M. Huber, D. R. Ladle, K. Murphy and S. Arber (2007). "ETS transcription factor Erm controls subsynaptic gene expression in skeletal muscles." Neuron **55**(5): 726-740.

Hu, H., Y. R. Miao, L. H. Jia, Q. Y. Yu, Q. Zhang and A. Y. Guo (2019). "AnimalTFDB 3.0: a comprehensive resource for annotation and prediction of animal transcription factors." Nucleic Acids Res **47**(D1): D33-D38.

Huang da, W., B. T. Sherman and R. A. Lempicki (2009). "Bioinformatics enrichment tools: paths toward the comprehensive functional analysis of large gene lists." Nucleic Acids Res **37**(1): 1-13.

Huang da, W., B. T. Sherman and R. A. Lempicki (2009). "Systematic and integrative analysis of large gene lists using DAVID bioinformatics resources." Nat Protoc **4**(1): 44-57.

Hughes, B. W., L. L. Kusner and H. J. Kaminski (2006). "Molecular architecture of the neuromuscular junction." Muscle Nerve **33**(4): 445-461.

Jevsek, M., A. Jaworski, L. Polo-Parada, N. Kim, J. Fan, L. T. Landmesser and S. J. Burden (2006). "CD24 is expressed by myofiber synaptic nuclei and regulates synaptic transmission." Proc Natl Acad Sci U S A **103**(16): 6374-6379.

Jones, R. A., C. D. Reich, K. N. Dissanayake, F. Kristmundsdottir, G. S. Findlater, R. R. Ribchester, M. W. Simmen and T. H. Gillingwater (2016). "NMJ-morph reveals principal components of synaptic morphology influencing structure-function relationships at the neuromuscular junction." Open Biol **6**(12).

Kanhere, A., A. Hertweck, U. Bhatia, M. R. Gokmen, E. Perucha, I. Jackson, G. M. Lord and R. G. Jenner (2012). "T-bet and GATA3 orchestrate Th1 and Th2 differentiation through lineage-specific targeting of distal regulatory elements." Nat Commun **3**: 1268.

Ketterer, C., U. Zeiger, M. T. Budak, N. A. Rubinstein and T. S. Khurana (2010). "Identification of the neuromuscular junction transcriptome of extraocular muscle by laser capture microdissection." Invest Ophthalmol Vis Sci **51**(9): 4589-4599.

Kishi, M., T. T. Kummer, S. J. Eglen and J. R. Sanes (2005). "LL5beta: a regulator of postsynaptic differentiation identified in a screen for synaptically enriched transcripts at the neuromuscular junction." J Cell Biol **169**(2): 355-366.

Koh, B., M. M. Hufford, D. Pham, M. R. Olson, T. Wu, R. Jabeen, X. Sun and M. H. Kaplan (2016). "The ETS Family Transcription Factors Etv5 and PU.1 Function in Parallel To Promote Th9 Cell Development." J Immunol **197**(6): 2465-2472.

Lewis, M. D., S. A. Miller, M. M. Miazgowicz, K. M. Beima and A. S. Weinmann (2007). "T-bet's ability to regulate individual target genes requires the conserved T-box domain to recruit histone methyltransferase activity and a separate family member-specific transactivation domain." Mol Cell Biol **27**(24): 8510-8521.

McGeachie, A. B., K. Koishi, Z. B. Andrews and I. S. McLennan (2005). "Analysis of mRNAs that are enriched in the post-synaptic domain of the neuromuscular junction." Mol Cell Neurosci **30**(2): 173-185.

Miller, S. A., A. C. Huang, M. M. Miazgowicz, M. M. Brassil and A. S. Weinmann (2008). "Coordinated but physically separable interaction with H3K27-demethylase and H3K4-methyltransferase activities are required for T-box protein-mediated activation of developmental gene expression." Genes Dev **22**(21): 2980-2993.

Miller, S. A. and A. S. Weinmann (2010). "Molecular mechanisms by which T-bet regulates T-helper cell commitment." Immunol Rev **238**(1): 233-246.

Muller, D., P. Cherukuri, K. Henningfeld, C. H. Poh, L. Wittler, P. Grote, O. Schluter, J. Schmidt, J. Laborda, S. R. Bauer, R. M. Brownstone and T. Marquardt (2014). "Dlk1 promotes a fast motor neuron biophysical signature required for peak force execution." Science **343**(6176): 1264-1266.

Nazarian, J., K. Bouri and E. P. Hoffman (2005). "Intracellular expression profiling by laser capture microdissection: three novel components of the neuromuscular junction." Physiol Genomics **21**(1): 70-80.

Nijssen, J., L. H. Comley and E. Hedlund (2017). "Motor neuron vulnerability and resistance in amyotrophic lateral sclerosis." Acta Neuropathol **133**(6): 863-885.

Patro, R., G. Duggal, M. I. Love, R. A. Irizarry and C. Kingsford (2017). "Salmon provides fast and bias-aware quantification of transcript expression." Nat Methods **14**(4): 417-419.

Picelli, S., O. R. Faridani, A. K. Bjorklund, G. Winberg, S. Sagasser and R. Sandberg (2014). "Full-length RNA-seq from single cells using Smart-seq2." Nat Protoc **9**(1): 171-181.

Ruegg, M. A. (2005). "Organization of synaptic myonuclei by Syne proteins and their role during the formation of the nerve-muscle synapse." Proc Natl Acad Sci U S A **102**(16): 5643-5644.

Schaeffer, L., A. de Kerchove d'Exaerde and J. P. Changeux (2001). "Targeting transcription to the neuromuscular synapse." Neuron **31**(1): 15-22.

Schindelin, J., I. Arganda-Carreras, E. Frise, V. Kaynig, M. Longair, T. Pietzsch, S. Preibisch, C. Rueden, S. Saalfeld, B. Schmid, J. Y. Tinevez, D. J. White, V. Hartenstein, K. Eliceiri, P. Tomancak

and A. Cardona (2012). "Fiji: an open-source platform for biological-image analysis." Nat Methods **9**(7): 676-682.

Sieburth, D., Q. Ch'ng, M. Dybbs, M. Tavazoie, S. Kennedy, D. Wang, D. Dupuy, J. F. Rual, D. E. Hill, M. Vidal, G. Ruvkun and J. M. Kaplan (2005). "Systematic analysis of genes required for synapse structure and function." Nature **436**(7050): 510-517.

Sieck, G. C. and Y. S. Prakash (1997). "Morphological adaptations of neuromuscular junctions depend on fiber type." Can J Appl Physiol **22**(3): 197-230.

Terry, E. E., X. Zhang, C. Hoffmann, L. D. Hughes, S. A. Lewis, J. Li, M. J. Wallace, L. A. Riley, C. M. Douglas, M. A. Gutierrez-Monreal, N. F. Lahens, M. C. Gong, F. Andrade, K. A. Esser and M. E. Hughes (2018). "Transcriptional profiling reveals extraordinary diversity among skeletal muscle tissues." Elife **7**.

The Gene Ontology, C. (2019). "The Gene Ontology Resource: 20 years and still GOing strong." Nucleic Acids Res **47**(D1): D330-D338.

Waerhaug, O. and T. Lomo (1994). "Factors causing different properties at neuromuscular junctions in fast and slow rat skeletal muscles." Anat Embryol (Berl) **190**(2): 113-125.

Wang, Y. and J. E. Pessin (2013). "Mechanisms for fiber-type specificity of skeletal muscle atrophy." Curr Opin Clin Nutr Metab Care **16**(3): 243-250.

5 Sinergia Project: Effects of Aging on the Neuromuscular Junction Transcriptome

Contributions to this project: Martin Weihrauch received *tibialis anterior* muscles from young and old mice from Dr. Daniel J. Ham. Martin Weihrauch conducted all of the experiments and analyses pertaining to this project report.

Contributions to future manuscript:
The sequencing dataset of laser-capture microdissected NMJs described here will be included in a joint Sinergia project publication with several other authors. Martin Weihrauch also contributed to the initial analysis of the dataset.

5.1 Abstract

The hallmarks of aging include progressive loss of muscle mass and strength, alongside neurophysiological perturbations. The neuromuscular junction (NMJ) is critically involved in age-related musculoskeletal impairments, but it remains unclear whether detrimental alterations of the NMJ precede or follow the functional decline of muscle. We hypothesized that aging might lead to dysregulation of the NMJ gene program and thus contribute to the structural and functional decline of the NMJ. We used laser-capture microdissection to isolate fundamental myonuclei underlying the NMJ and generated NMJ gene expression profiles of the *tibialis anterior* (TA) muscle of 10-month-old and 30-month-old mice with next-generation RNA-sequencing to investigate whether aging leads to perturbations of the NMJ gene program. Our results revealed the NMJ gene program to be remarkably stable, with identical gene expression levels of canonical NMJ genes. Our findings argue against the hypothesis that aging leads to a broad deterioration of the NMJ gene program that would contribute to perturbations of NMJ structure and function.

5.2 Introduction

Aging causes progressive loss of muscle mass and function, also known as sarcopenia, which gravely impacts quality of life in the elderly, predisposing them to an increased risk of all-cause mortality **(Janssen, Shepard et al. 2004, Narici and Maffulli 2010)**. One neurophysiological consequence of aging is the remodeling of the neuromuscular junction (NMJ), which leads to reduced size, fragmentation and functional impairments of the postsynaptic apparatus **(Valdez, Tapia et al. 2010, Jang and Van Remmen 2011)**. Aging myofibers undergo denervation and re-innervation cycles that lead to remodeling of motor units. Fast-twitch fibers are more susceptible to such denervation events and may become re-innervated through axonal sprouting of slow motor neurons, resulting in a conversion of fast-twitch type II to slow-twitch type I myofibers. Importantly, age-related remodeling events at the NMJ may precede myofiber alterations **(Deschenes, Roby et al. 2010)**. It has been suggested that aging changes neuromuscular junctions mainly through the accumulation of myofiber segment damage at the NMJ. While the myofiber segment first degenerates and then quickly regenerates, this leaves the affected NMJ permanently perturbed **(Li, Lee et al. 2011)**. However, it is also conceivable that aging leads to perturbations of the NMJ gene program, the dysregulation of which might lead to prolonged acetylcholine receptor turnover and disruption of pre- and post-synaptic apposition. If aging perturbs the NMJ gene program this may predispose them to damage.

Caloric restriction (CR), the reduction of daily caloric intake by about 30 to 40%, ameliorates detrimental effects of aging and increases lifespan **(Golbidi, Daiber et al. 2017)**. Importantly, CR attenuates age-related changes in mouse NMJs by significantly reducing the occurrence of fragmented, faint, and denervated postsynaptic sites **(Valdez, Tapia et al. 2010)**. Various CR mimetics exist and can slow the aging of NMJs and myofibers **(Stockinger, Maxwell et al. 2017)**. One such CR mimetic is rapamycin (RM), which provides health benefits and extends lifespan in rodents **(Ehninger, Neff et al. 2014, Zhang, Bokov et al. 2014)**. Since both, CR and RM may exert beneficial effects on the NMJ gene program and counteract its putative age-related perturbation, we set out to investigate the effect of aging on the NMJ transcriptome and included experimental groups with CR and RM treatment.

In this study, we combined laser-capture microdissection of the NMJ with next-generation RNA-sequencing to generate NMJ gene expression profiles of the *tibialis anterior* (TA) muscle of 10-month-old and 30-month-old mice to investigate whether aging leads to perturbations of the NMJ gene program. Furthermore, we examined the effect of treatment with CR and RM on the aging NMJ transcriptome.

5.3 Material and Methods

Animals, tissue harvest and sample preparation. There were four different groups of male C57BL/6 mice, 10-month-old (only control (CT)) and 30-month-old mice (from control (CT), rapamycin-treated (RM), and caloric restriction-treated (CR) groups). The 30-month-old mice were treated with either RM (~ 4 mg/kg per day) or CR starting from the age of 15-month. The mice were raised and treated by Dr. Daniel J. Ham. *Tibialis anterior* (TA) muscles of 10-month-old (only control (CT)) and 30-month-old mice (from control (CT), rapamycin-treated (RM), and caloric restriction-treated (CR) groups) were rapidly dissected and immediately immersed in 1 ml of preservative Krebs-Ringer solution containing α-Bungarotoxin (Alexa Fluor™ 488 conjugate; 3 µl/ml) for 1 hour. After incubation the muscles were partially embedded in 10% gum tragacanth (Sigma-Aldrich, catalog no. G1128), frozen in liquid nitrogen-cooled 2-Methylbutane (-150°C; Sigma-Aldrich, catalog no. M32631), and stored at -80°C until further processing.

Serial frozen cross-sections of 20 µm thickness containing NMJ areas were cut at -20°C using a cryostat (Leica). Up to 30 serial sections were mounted per RNase AWAY®-treated (Sigma-Aldrich) regular glass slide (Menzel). In order to deactivate endogenous RNases, sections were dehydrated in 100% EtOH inside the cryostat chamber for 5 min and then stored at -80°C in 50-ml conical tubes containing several grams of desiccant (ROTH, silica Gel Orange, catalog no. P077.4) to prevent tissue rehydration. The TA muscles of eight animals per condition were used for the laser-capture experiments.

Laser-capture microdissection Laser-capture microdissection (LCM) was performed using a PALM MicroBeam system (Zeiss) consisting of an inverted microscope with a motorized

stage, an ultraviolet laser and an X-Cite fluorescence illuminator. The microdissection process was visualized with an AxioCam ICc camera coupled to a computer and controlled by the PALM RoboSoftware. Synaptic regions were visualized utilizing fluorescence (α-Bungarotoxin - Alexa Fluor™ 488 conjugate) microscopy with an x20 objective. A yellow fluorescent protein (YFP)-filter was used to reduce background noise and improve visualization. About 300 synaptic regions ("NMJ") and an equivalent amount of extrasynaptic ("XNMJ") tissue areas equaling roughly 0.65 mm^2 were collected per sample, resulting in a total number of about 9600 collected NMJ areas. Selected areas were cut and catapulted by laser pulses, utilizing automated laser-pressure catapulting (autoLPC) mode, into opaque AdhesiveCap 500 PCR tubes (Zeiss). For every sample, the lid of the AdhesiveCap PCR tube was checked for presence of successfully catapulted tissue, indicating laser-capture success.

In order to lyse laser-captured material, 10 µl Single-Cell Lysis Buffer (Clontech, catalog no. 635013) supplemented with freshly-added Protector RNase Inhibitor (Roche) was added into the top of an AdhesiveCap PCR tube and pipetted up and down about ten times before dispensing the lysate into the bottom of a 1.5 ml reaction tube (Eppendorf). Afterwards the AdhesiveCap lid was checked under the microscope and the absence of captured material indicated successful suspension of tissue in the lysis buffer. Samples were lysed for 5 min at RT and then stored immediately at -80°C until further processing. The whole process from thawing a slide until completed tissue lysis was kept under an hour to avoid RNA degradation by endogenous RNAses present in the tissue.

Low-input RNA-Sequencing. The laser-captured whole tissue lysates were used for RNA-sequencing library generation with the SMART-Seq v4 Ultra Low Input RNA Kit for Sequencing (Clontech, catalog no. 634894) and according to the SMART-Seq v4 Half Volume NexteraXT Standard Protocol. Usage of this kit and protocol supposedly improves upon the SMART-Seq2 method that was employed in the preceding NMJ-sequencing project detailed in Manuscript II of this thesis. Quality control of the cDNA-sequencing-libraries was conducted with the Agilent Bioanalyzer (Agilent) and the average fragment size of the libraries was determined. The libraries were sequenced (Single-end reads, 76 sequencing cycles) using a NextSeq 500 system (Illumina) at the Quantitative Genomics Facility of the

Department of Biosystems Science and Engineering (D-BSSE) of the ETH Zürich in Basel. The entire process from sequencing library preparation to RNA-sequencing was conducted by D-BSSE personnel.

RNA-sequencing data preprocessing, read mapping and analysis. The raw sequencing reads (FASTQ-files) were quality-filtered and sequencing-adapter-trimmed using BBDuk from BBTools (Version 38.57) with the following non-standard parameters: ktrim = r, k = 23, mink = 11, hdist = 1, qtrim = rl, trimq = 10, ftm = 5, minlen = 35. The following annotation files were used for read mapping: Gencode Release M22 (GRCm38.p6) of the transcript sequences, which includes the nucleotide sequences of all transcripts on the reference chromosomes. GTF file: comprehensive gene annotation (regions: CHR), which contains the comprehensive gene annotation on the reference chromosomes only). Salmon (Version 0.14.1) was used to generate an index with the following non-standard parameters: --k 29, --type quasi, --gencode (as Gencode annotation files are used). Salmon quasi-mapping was run with these parameters: --libType U, --validateMappings, --fldMean 102, --fldSD 62, --seqBias (the average fragment length of the sequencing libraries was 102 with a standard deviation of 62) **(Patro, Duggal et al. 2017)**.

RNA-sequencing data analysis was conducted with R (Version 3.6.0) and R-Studio (Version 1.1.463) running on CentOS Linux 7 (sciCORE R-Studio server service). The edgeR package (Version 3.26.7) from Bioconductor (Version 3.9.0) was used for differential gene expression analysis. Other packages used for data handling and plotting were tidyverse (1.2.1), pheatmap (1.0.12), biomaRt (2.40.3), RColorBrewer (1.1.2), tximport (1.12.3) and GenomicFeatures (1.36.0).

Differential gene expression was determined via genewise statistical tests relative to a fold change threshold of log2(1.5) with the glmTreat() methodology of the edgeR package, which improves upon the false discovery rate of existing methods and potentially identifies more biologically relevant genes **(McCarthy and Smyth 2009)**. Genes that passed this fold change threshold and had a FDR p-value < 0.05 were called differentially expressed in this study.

After sequencing library normalization and pre-filtering to remove low-count genes, 18621 genes were found to be expressed in our dataset.

Functional annotation analyses with the Database for Annotation, Visualization and Integrated Discovery (DAVID) Bioinformatics Resources 6.8 and term enrichment were based on FDR p-values.

Calculations were performed at sciCORE (http://scicore.unibas.ch/) scientific computing core facility at University of Basel.

5.4 Results

Expression profiling of young and old neuromuscular junctions of the *tibialis anterior* muscle

We used laser-capture microdissection (LCM) to isolate neuromuscular junction areas ("NMJ" or "synaptically enriched tissue") and equal amounts of adjacent, extrasynaptic tissue as control ("XNMJ" or "extrasynaptic control tissue") from serial cryosections of the *tibialis anterior* (TA) muscle of 10-month-old ("young") sedentary control mice, as well as of 30-month-old ("old") sedentary control mice, 30-month-old RM-treated mice, and of 30-month-old CR-treated mice. The LCM-isolated tissues were lysed and the total lysate used for RNA-sequencing. We used principal coordinate analysis (PCoA) to investigate whether there are any distinct patterns of gene expression among the samples. The first principal coordinate clearly separates the samples into either extrasynaptic or synaptic origin, while the second principal coordinate does not clearly subdivide the samples into additional clusters (**Figure 5-1 A**). Further analysis of the second and third principal coordinates did not reveal further sample clusters (**Figure 5-1 B**).

We then investigated differential gene expression between the various experimental conditions and summarized the results in **Table 5-1**. We found 1079 genes to be synaptically enriched in the 10-month-old synaptic control samples compared to the respective

extrasynaptic control samples (10M.NMJ.CT vs. 10M.XNMJ.CT). The same comparison with the 30-month-old control samples yielded 744 genes (30M.NMJ.CT vs. 30M.XNMJ.CT). We did not detect any differentially expressed genes between the young and old synaptic samples (30M.NMJ.CT vs. 10M.NMJ.CT). The different comparisons of the young and old control groups are shown in **Figure 5-2**.

Table 5-1. Differentially expressed genes between the different comparisons.

Comparison	Genes with positive fold change	Genes with negative fold change
10M.NMJ.CT vs. 10M.XNMJ.CT	1079	464
30M.NMJ.CT vs. 30M.XNMJ.CT	744	289
30M.NMJ.CT vs. 10M.NMJ.CT	0	0
30M.XNMJ.CT vs. 10M.XNMJ.CT	38	23
30M.NMJ.RM vs. 30M.XNMJ.RM	710	103
30M.NMJ.CR vs. 30M.XNMJ.CR	867	173
30M.NMJ.CR vs. 30M.NMJ.CT	1	4
30M.NMJ.RM vs. 30M.NMJ.CT	0	0

Differential gene expression was determined via gene-wise statistical tests relative to a fold change threshold of log2(1.5); FDR p-value < 0.05. Groups: **10M.NMJ.CT**, 10-month control, synaptic; **10M.XNMJ.CT**, 10-month control, extrasynaptic; **30M.NMJ.CT**, 30-month control, synaptic; **30M.XNMJ.CT**, 30-month control, extrasynaptic. **30M.NMJ.RM**, 30-month rapamycin-treated, synaptic; **30M.XNMJ.RM**, 30-month rapamycin-treated, extrasynaptic; **30M.NMJ.CT**, 30-month control, synaptic; **30M.NMJ.CR**, 30-month caloric restriction-treated, synaptic; **30M.XNMJ.CR**, 30-month caloric restriction-treated, extrasynaptic.

To confirm whether we successfully enriched synaptic tissue we looked at the genes with the strongest fold changes and lowest p-values in the 10-month control group (**Figure 5-3 A**) and the 30-month control group (**Figure 5-3 B**). Among the top 50 synaptically enriched genes of the 10-month control were *Ache, Chrne, Chrna1, Chrnd, Gdnf, Erbb3, Etv5, Dusp6* and many others, all of which represent well-known NMJ genes **(Nazarian, Bouri et al. 2005, Hippenmeyer, Huber et al. 2007, Wu, Xiong et al. 2010)**. The top synaptically enriched genes in the 30-month control group were very similar. These findings confirmed the successful enrichment of synaptic tissue with LCM.

Gene expression of canonical neuromuscular junction components is not different between young and old mice

Since we did not detect any differentially expressed genes between the 10-month-old and 30-month-old groups, we decided to look directly at log2-transformed counts per million (logCPM) of canonical neuromuscular junction components, as it is conceivable that there are slight expression differences that did not pass our cutoffs for differential gene expression. The genes *Chrne* (**Figure 5-6 A**) and *Etv5* (**Figure 5-6 B**) are well known to be enriched at the neuromuscular junction. Both genes showed equally strong and stable expression values across the experimental conditions, although *Etv5* appeared to be expressed slightly stronger in the extrasynaptic samples. The median difference in synaptic versus extrasynaptic expression of *Chrne* was over 1000 counts per million, irrespective of age and conditions, highlighting its immense synaptic enrichment. As expected, *Utrn* (**Figure 5-6 C**) was synaptically enriched, while *Dmd* (**Figure 5-6 D**), which is known to be more expressed extrasynaptically, was not. Expectedly, both *Utrn* and *Dmd* showed stronger extrasynaptic expression than *Chrne* or *Etv5*, further strengthening the validity of our RNA-sequencing dataset. While *Aplp2* (**Figure 5-6 E**) was moderately expressed in the extrasynaptic samples, it was nevertheless strongly enriched at the NMJ. *Dusp6* (**Figure 5-6 F**) showed synaptic expression values comparable to *Chrne*. While *Musk* (**Figure 5-6 G**) was certainly enriched at the NMJ, it was less so than *Chrne*.

As there were no differentially expressed genes between the synaptic samples of the 30-month and 10-month control groups (**Figure 5-2 C**), we looked at their respective extrasynaptic samples, which yielded 38 genes with stronger expression in the old samples (**Figure 5-4 B**) and 23 genes with stronger expression in the young samples (**Figure 5-4 A**) (Comparison: 30M.XNMJ.CT vs. 10M.XNMJ.CT). Functional annotation analysis of these genes with DAVID Bioinformatics Resources 6.8 did not reveal any enriched terms, most likely owing to the small number of genes detected.

Treatment with rapamycin or caloric restriction had no pronounced effects on the neuromuscular junction transcriptome

While we detected a large amount of synaptically enriched genes in the RM-treated and CR-treated samples compared to their respective controls, the comparison of the synaptic RM and CR against the synaptic 30-month-old control samples yielded few or even no differentially expressed genes (**Table 5-1** and **Figure 5-5**).

5.5 Discussion

The goal of this study was to investigate whether aging perturbs the NMJ gene program, a dysregulation of which could contribute to the observed age-related structural and functional alterations of the NMJ. We also examined the effect of treatment with caloric restriction (CR) and rapamycin (RM) on the aging NMJ transcriptome. Our results revealed the NMJ gene program to be remarkably stable, with nearly identical gene expression levels of canonical NMJ genes, regardless of age or treatment.

Although the results of this study did not reveal overt effects of aging on the NMJ transcriptome, it is possible that aging leads to subtle gene expression changes in a large number of genes, which could have a cumulative affect resulting in profound biological effects. As the skeletal muscle transcriptome undergoes significant changes with age **(Shafiee, Asgari et al. 2018)**, we investigated whether we detected such general aging differences between our young and old extrasynaptic samples. However, we detected only a very small number of genes to be differentially expressed. Given the ultra-low input and lack of precise control of input amount in this RNA-sequencing dataset, it seems reasonable that smaller fold changes between genes, especially of ones with lower expression strength, may go undetected when using conventional cutoff detection values (i.e. fold change > 2, adjusted p-value < 0.05). Additionally, the effects of noise are generally more pronounced for genes with relatively small expression strengths in a given sample or experimental condition. In this case, gene set enrichment analyses and comparison with whole-muscle aging time course data may reveal common patterns of gene expression perturbation induced by aging.

A recent transcriptomic study of the effects of sarcopenia on skeletal muscle reported gene expression changes associated with the neuromuscular junction **(Lin, Chang et al. 2018)**. Specifically, Lin et al. (2018) reported decreased gene expression of apolipoprotein E (*ApoE*), docking protein 7 (*Dok7*), syntrophin alpha 1 (*Snta1*), and aquaporin 4 (*Aqp4*), as well as genes encoding several serpins in the aging muscle. They also report increased gene expression of cholinergic receptor nicotinic alpha 1 subunit (*Chrna1*), cholinergic receptor nicotinic beta 1 subunit (*Chrnb1*), and of low density lipoprotein receptor-related protein 4 (*Lrp4*). According to Lin et al. (2018), the observed increase of *Chrna1*, *Chrnb1*, and *Lrp4* expressions reflects the change of myofiber types during aging, as slow-twitch myofibers have wider NMJs and larger nerve terminal areas than the fast-twitch myofibers. They conclude that their observed changes of neuromuscular junction-associated genes suggest a potential compensatory mechanism during NMJ decline by up-regulating acetylcholine receptors **(Lin, Chang et al. 2018)**. Our NMJ-specific results did not reflect the described age-related changes in NMJ-associated genes, as none of the above genes were differentially expressed between our young and old synaptic samples. Furthermore, there also was no striking increase or decrease in the respective fold changes of these genes in the young synaptic vs. extrasynaptic and the old synaptic vs. extrasynaptic comparison of these genes. For example, *Chrnb1* had a 5-fold change in the young and only a slightly lower 3.5-fold change in the old mice, which might indicate a somewhat lower synaptic enrichment in the old. However, as shown in **Figure 5-6**, gene expression of all canonical NMJ genes we looked at was nearly identical between young and old NMJs. We have to take into account that Li et al. (2018) compared 3-month-old with 24-month-old mice, while we compared 10-month-old to 30-month-old mice.

We conclude that our findings argue against the hypothesis that aging leads to a broad deterioration of the NMJ gene program that would contribute to perturbations of NMJ structure and function.

5.6 Figures

A

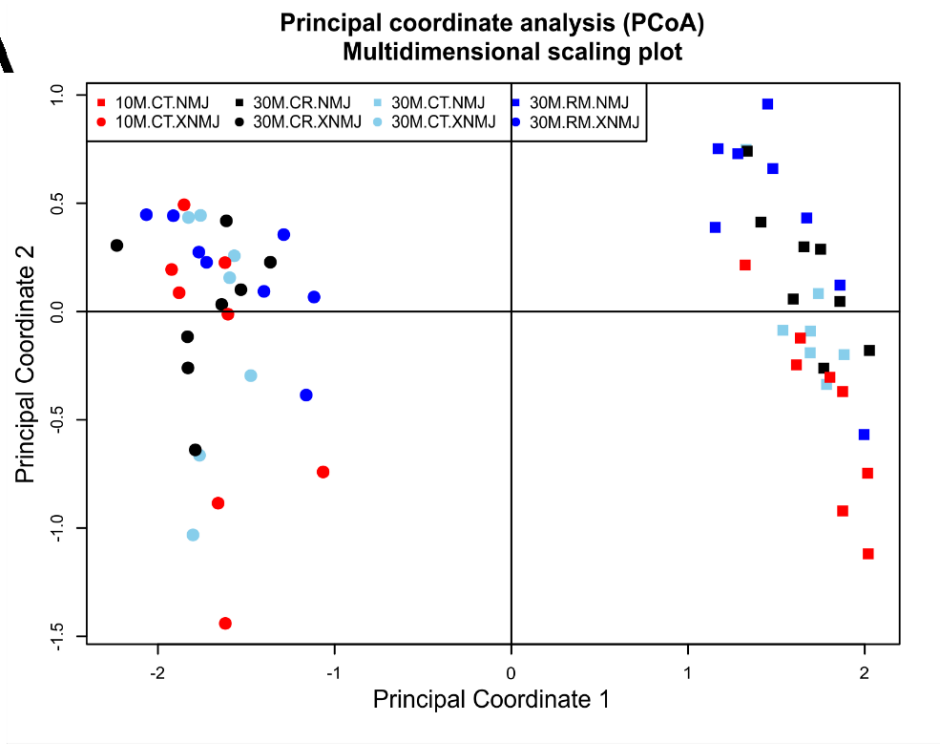

B

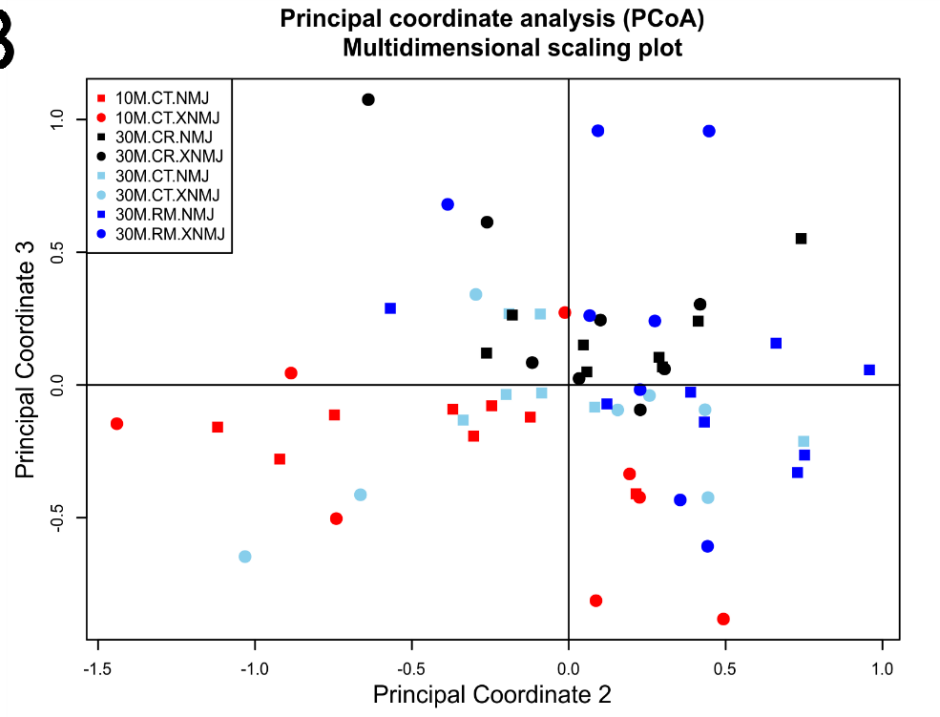

Figure 5-1. Principal coordinate analysis (PCoA) reveals sample clusters according to synaptic or extrasynaptic origin, but does not clearly separate samples by age. Principal coordinate analysis of the **A)** First and second, and of the **B)** second and third principal coordinates. Each plot symbol represents a sample. Distance between samples can be interpreted as the typical log2 fold change of the top 500 genes that distinguish them. Legend symbols: 10M, 10-month-old; 30M, 30-month-old; CT, untreated control group; CR, caloric restriction group; RM, rapamycin group; NMJ, synaptic samples; XNMJ, extrasynaptic samples.

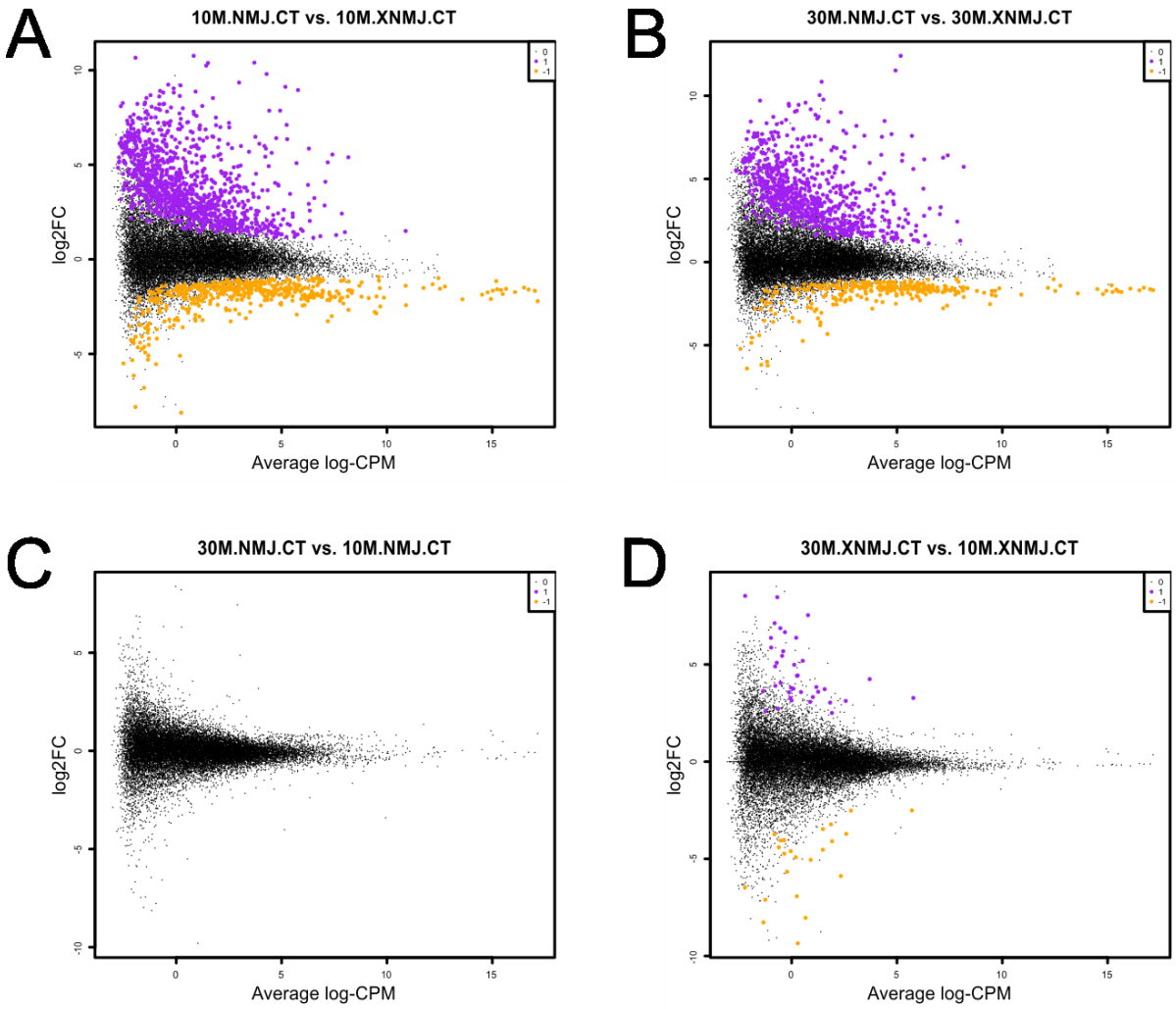

Figure 5-2. Aging does not lead to pronounced changes in gene expression at the neuromuscular junction. Mean-difference plots showing log2 fold changes (log2FC) of genes on the Y-axis plotted against the average gene expression strength in log2 counts per million (log-CPM) on the X-axis. Each black dot represents an expressed gene in the study (legend "0"). Differentially expressed genes (FDR p-value < 0.05) with a positive fold change are marked in purple (legend "1"), while genes with a negative fold change are marked in orange (legend "-1"). **A)** Synaptic vs. extrasynaptic 10-month-old control. This comparison yielded a large number of differentially expressed genes. **B)** Synaptic vs. extrasynaptic 30-month-old control. **C)** Synaptic 30-month-old control vs. synaptic 10-month-old control. The direct comparison of old vs. young synaptic samples did not yield any differentially expressed genes. **D)** Extrasynaptic 30-month-old control vs. extrasynaptic 10-month-old control. The direct comparison of old vs. young extrasynaptic samples yielded a low number of differentially expressed genes. Groups: **10M.NMJ.CT**, 10-month control, synaptic; **10M.XNMJ.CT**, 10-month control, extrasynaptic; **30M.NMJ.CT**, 30-month control, synaptic; **30M.XNMJ.CT**, 30-month control, extrasynaptic.

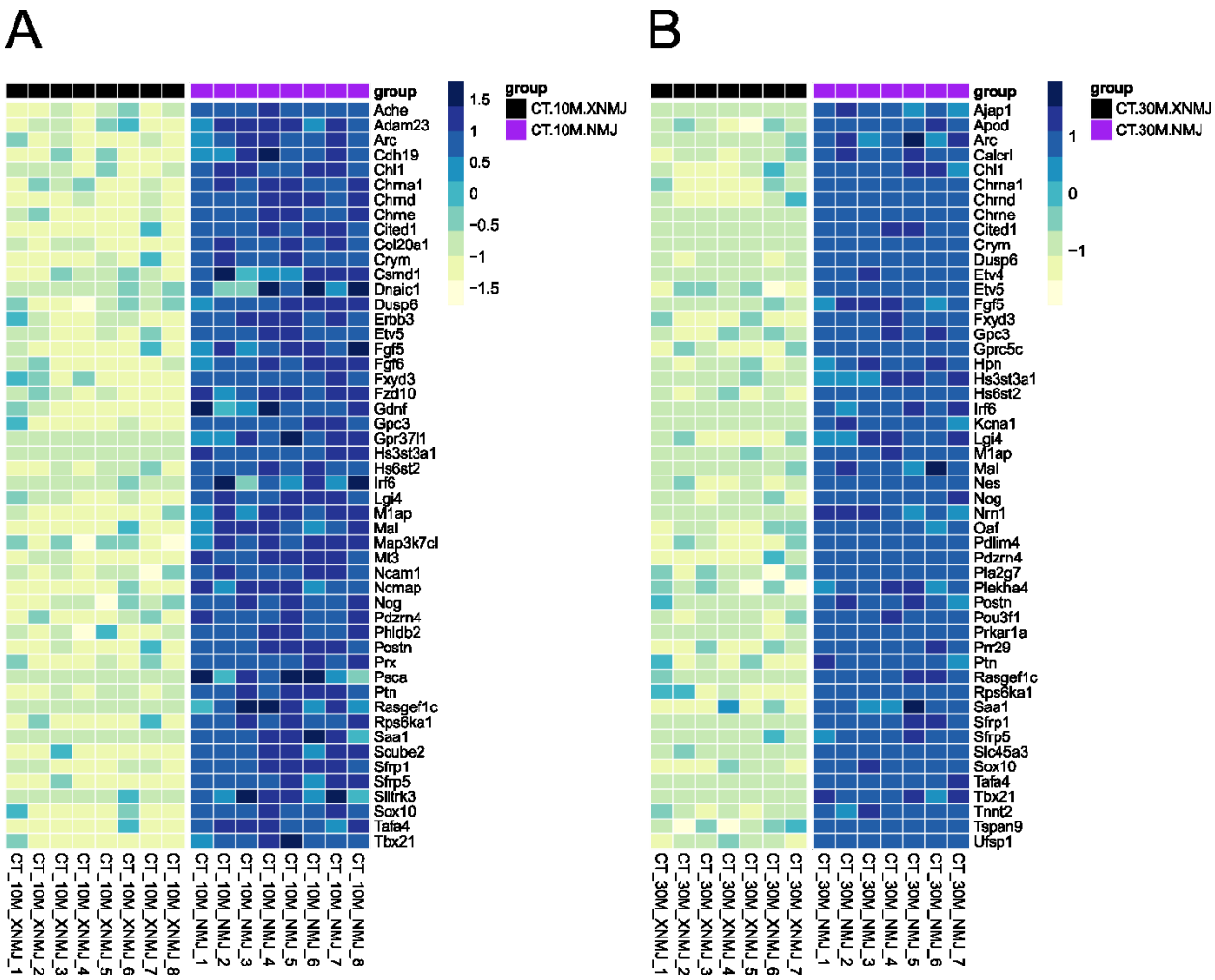

Figure 5-3. Top 50 synaptically enriched genes of 10-month and 30-month-old animals. Unclustered heatmap visualization of the top 50 enriched genes by fold change (FDR p-value < $1*10^{-8}$) in the synaptic samples of the **A)** 10-month control and **B)** 30-month control animals. Shown are scaled CPM expression values of all respective synaptic and extrasynaptic samples. Darker hues of blue represent stronger expression in these samples. Groups: **CT.10M.XNMJ**, 10-month control, extrasynaptic; **CT.10M.NMJ**, 10-month control, synaptic; **CT.30M.XNMJ**, 30-month control, extrasynaptic; **CT.30M.NMJ**, 30-month control, synaptic.

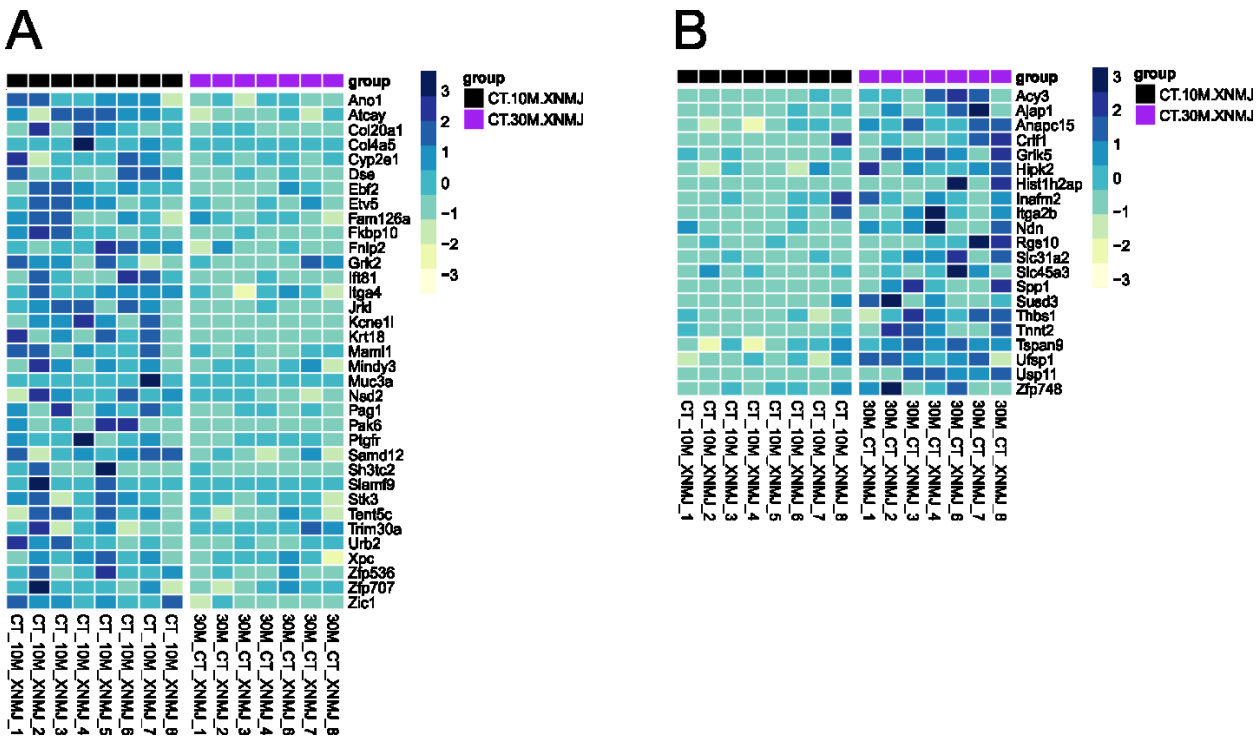

Figure 5-4. Unclustered heatmap visualization of all differentially expressed genes between young and old extrasynaptic controls. A) Genes with stronger expression in the 10-month-old extrasynaptic control samples. **B)** Genes with stronger expression in the 30-month-old extrasynaptic control samples. Shown are scaled CPM expression values of all respective extrasynaptic samples. FDR p-value cutoff for differential expression was set to < 0.05. Darker hues of blue represent stronger expression in these samples. Groups: **CT.10M.XNMJ**, 10-month control, extrasynaptic; **CT.30M.NMJ**, 30-month control, extrasynaptic.

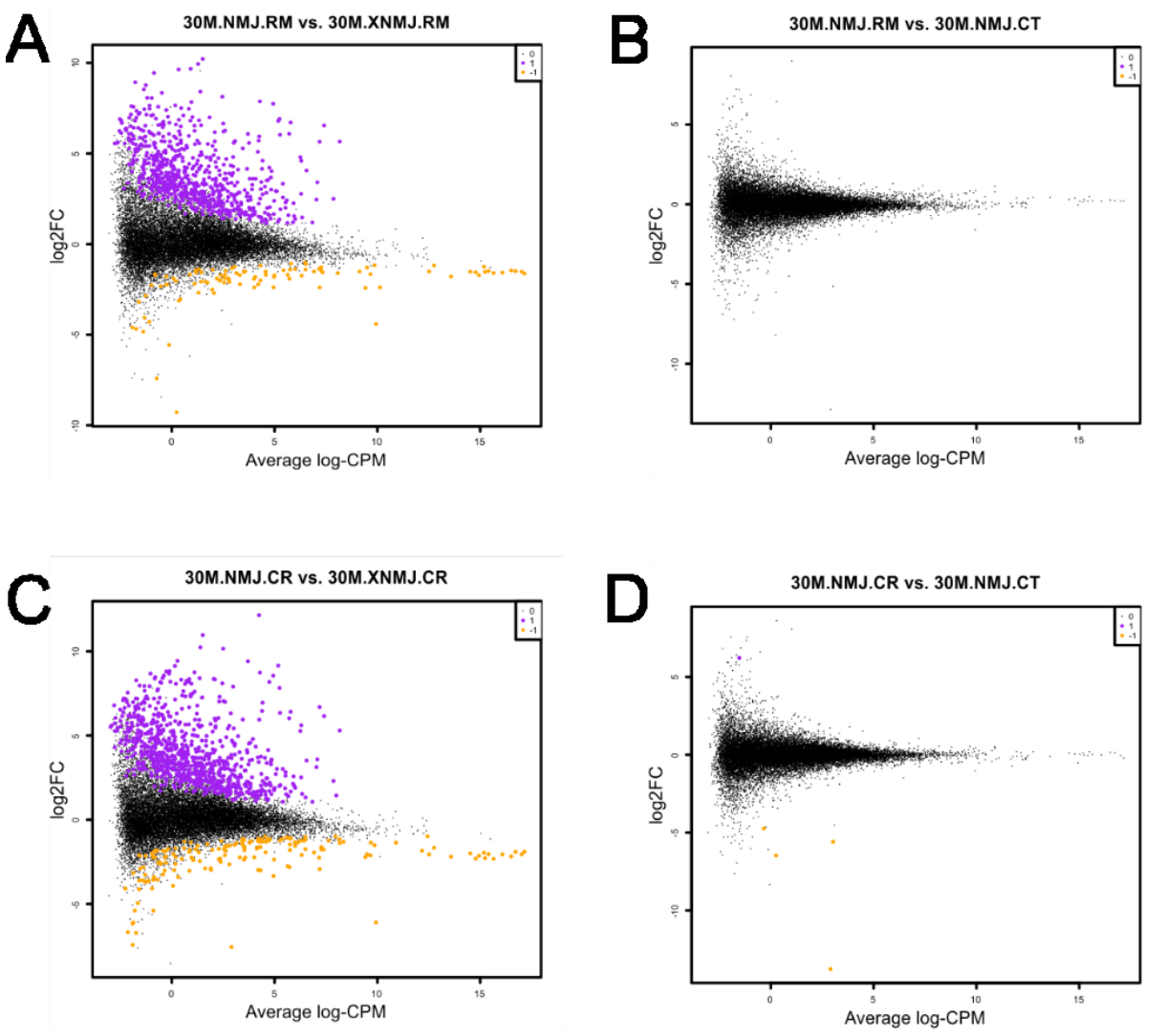

Figure 5-5. Treatment with rapamycin (RM) or caloric restriction (CR) had no pronounced effects on the neuromuscular junction transcriptome when compared to the aging control. Mean-difference plots showing log2 fold changes (log2FC) of genes on the Y-axis plotted against the average gene expression strength in log2 counts per million (log-CPM) on the X-axis. Each black dot represents an expressed gene in the study (legend "0"). Differentially expressed genes (FDR p-value < 0.05) with a positive fold change are marked in purple (legend "1"), while genes with a negative fold change are marked in orange (legend "-1"). **A)** Synaptic vs. extrasynaptic 30-month RM. **B)** Synaptic RM vs. synaptic 30-month control. **C)** Synaptic CR vs. extrasynaptic CR. **D)** Synaptic CR vs. synaptic 30-month control. Groups: **30M.NMJ.RM**, 30-month rapamycin-treated, synaptic; **30M.XNMJ.RM**, 30-month rapamycin-treated, extrasynaptic; **30M.NMJ.CT**, 30-month control, synaptic; **30M.NMJ.CR**, 30-month caloric restriction-treated, synaptic; **30M.XNMJ.CR**, 30-month caloric restriction-treated, extrasynaptic.

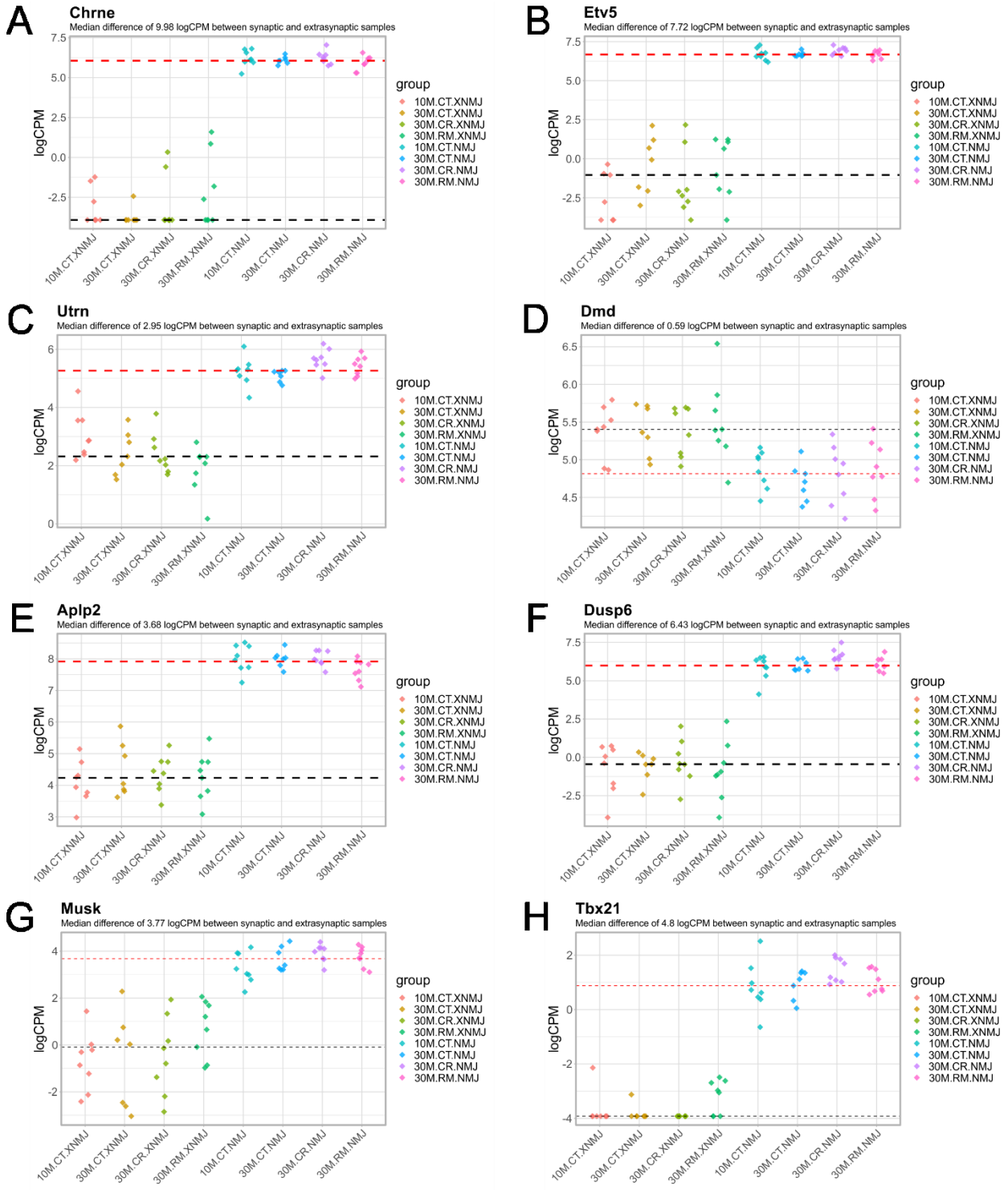

Figure 5-6. Gene expression of canonical neuromuscular junction components is remarkably stable between young and old mice. Gene expression in log2 counts per million (logCPM) of individual genes across all experimental groups is shown. The two dashed lines show the median expression value either of all synaptic samples (red) or of all extrasynaptic samples (black), irrespective of age and condition. The median difference in logCPM is given in the plot subtitles.

5.7 References

Deschenes, M. R., M. A. Roby, M. K. Eason and M. B. Harris (2010). "Remodeling of the neuromuscular junction precedes sarcopenia related alterations in myofibers." Exp Gerontol **45**(5): 389-393.

Ehninger, D., F. Neff and K. Xie (2014). "Longevity, aging and rapamycin." Cell Mol Life Sci **71**(22): 4325-4346.

Golbidi, S., A. Daiber, B. Korac, H. Li, M. F. Essop and I. Laher (2017). "Health Benefits of Fasting and Caloric Restriction." Curr Diab Rep **17**(12): 123.

Hippenmeyer, S., R. M. Huber, D. R. Ladle, K. Murphy and S. Arber (2007). "ETS transcription factor Erm controls subsynaptic gene expression in skeletal muscles." Neuron **55**(5): 726-740.

Jang, Y. C. and H. Van Remmen (2011). "Age-associated alterations of the neuromuscular junction." Exp Gerontol **46**(2-3): 193-198.

Janssen, I., D. S. Shepard, P. T. Katzmarzyk and R. Roubenoff (2004). "The healthcare costs of sarcopenia in the United States." J Am Geriatr Soc **52**(1): 80-85.

Li, Y., Y. Lee and W. J. Thompson (2011). "Changes in aging mouse neuromuscular junctions are explained by degeneration and regeneration of muscle fiber segments at the synapse." J Neurosci **31**(42): 14910-14919.

Lin, I. H., J. L. Chang, K. Hua, W. C. Huang, M. T. Hsu and Y. F. Chen (2018). "Skeletal muscle in aged mice reveals extensive transformation of muscle gene expression." BMC Genet **19**(1): 55.

McCarthy, D. J. and G. K. Smyth (2009). "Testing significance relative to a fold-change threshold is a TREAT." Bioinformatics **25**(6): 765-771.

Narici, M. V. and N. Maffulli (2010). "Sarcopenia: characteristics, mechanisms and functional significance." Br Med Bull **95**: 139-159.

Nazarian, J., K. Bouri and E. P. Hoffman (2005). "Intracellular expression profiling by laser capture microdissection: three novel components of the neuromuscular junction." Physiol Genomics **21**(1): 70-80.

Patro, R., G. Duggal, M. I. Love, R. A. Irizarry and C. Kingsford (2017). "Salmon provides fast and bias-aware quantification of transcript expression." Nat Methods **14**(4): 417-419.

Shafiee, G., Y. Asgari, A. Soltani, B. Larijani and R. Heshmat (2018). "Identification of candidate genes and proteins in aging skeletal muscle (sarcopenia) using gene expression and structural analysis." PeerJ **6**: e5239.

Stockinger, J., N. Maxwell, D. Shapiro, R. deCabo and G. Valdez (2017). "Caloric Restriction Mimetics Slow Aging of Neuromuscular Synapses and Muscle Fibers." J Gerontol A Biol Sci Med Sci **73**(1): 21-28.

Valdez, G., J. C. Tapia, H. Kang, G. D. Clemenson, Jr., F. H. Gage, J. W. Lichtman and J. R. Sanes (2010). "Attenuation of age-related changes in mouse neuromuscular synapses by caloric restriction and exercise." Proc Natl Acad Sci U S A **107**(33): 14863-14868.

Wu, H., W. C. Xiong and L. Mei (2010). "To build a synapse: signaling pathways in neuromuscular junction assembly." Development **137**(7): 1017-1033.

Zhang, Y., A. Bokov, J. Gelfond, V. Soto, Y. Ikeno, G. Hubbard, V. Diaz, L. Sloane, K. Maslin, S. Treaster, S. Rendon, H. van Remmen, W. Ward, M. Javors, A. Richardson, S. N. Austad and K. Fischer (2014). "Rapamycin extends life and health in C57BL/6 mice." J Gerontol A Biol Sci Med Sci **69**(2): 119-130.

6 General discussion

6.1 Ladder climbing as a physiological resistance exercise model for skeletal muscle hypertrophy in mice

Discussion and future perspectives

Objective I: *Establish a physiological resistance exercise model for mice and investigate the effect of chronic resistance exercise on the skeletal muscle transcriptome.*

Progressive resistance exercise training is the most effective strategy to physiologically increase muscle mass and strength in humans. Interestingly, low muscle strength in the elderly is independently associated with elevated risk of all-cause mortality irrespective of muscle mass **(Newman, Kupelian et al. 2006, Li, Xia et al. 2018)**. Many pharmacological approaches have aimed at increasing muscle mass, however the resulting larger muscle mass was often not entirely functional and displayed reductions in specific muscular strength **(Lach-Trifilieff, Minetti et al. 2014, Liu, Hammers et al. 2016, Morvan, Rondeau et al. 2017)**. Despite numerous studies in recent decades, we still understand relatively little about the exact mechanisms by which skeletal muscle hypertrophy occurs in response to mechanical stimulation during muscle contraction **(Burkholder 2007, Schoenfeld 2012)**.

The three primary mechanisms presumably driving skeletal muscle hypertrophy are mechanical tension, metabolic stress, and muscle damage. It is clear that mechanical tension such as during resistance exercise (RE) leads to transient increases in muscle protein synthesis, which subsequently causes protein accumulation within myofibers, but the exact role of muscle damage and metabolic stress remains unclear **(Tang, Perco et al. 2008, Damas, Phillips et al. 2016)**. Long-term increases in muscle size due to RE were linked to activation of mTOR and its downstream target RPS6KB1, which results in increased protein synthesis rates **(Baar and Esser 1999, Terzis, Georgiadis et al. 2008)**. However, changes in the balance of muscle protein synthesis alone cannot explain the complex orchestration of

myofiber growth. There must be some way for myofibers to detect mechanical tension and turn this stimulus into signals that mediate hypertrophy. Specialized mechanoreceptors were hypothesized to facilitate this task, some of which are discussed in the introduction to this thesis, but so far they have eluded efforts to detect them **(Goodman, Hornberger et al. 2015, Bamman, Roberts et al. 2018)**.

The absolute mechanical load does not seem to govern the degree of muscular hypertrophy as long as the RE is carried out to muscular failure **(Schoenfeld, Grgic et al. 2017)**. Yet, larger RE training volume enhances hypertrophy without additional strength gains **(Schoenfeld, Contreras et al. 2019)**. Indeed, it has been shown that high-load versus low-load RE training confers different adaptations in terms of muscular strength, despite equal ensuing hypertrophy, reflecting most likely neuromuscular adaptations (task specificity). In addition, the influence of metabolic stress on skeletal muscle hypertrophy has been investigated by combining low-load RE with blood flow restriction of the exercised muscle groups. Similar degrees of hypertrophy were found in this modality compared with traditional high-load RE **(Lixandrao, Ugrinowitsch et al. 2018)**. However, the exact mechanisms behind the apparent effects of metabolic stress and muscle damage on hypertrophy and strength are difficult to study, as neither occur in an entirely independent way from mechanical tension.

Recently, the changes that occur in the muscle transcriptome upon RE have received increasing attention. Synergist ablation (SA) surgery has been used as an animal model of skeletal muscle hypertrophy and a robust increase of myonuclear transcriptional activity was reported during the early stages of myofiber hypertrophy **(Kirby, Patel et al. 2016)**. Yet, the acute hypertrophic adaptations in the SA model are masked by inflammation caused by the surgical nature of the intervention **(Armstrong, Marum et al. 1979)**. Transcriptomic studies in human subjects are extremely challenging due to large differences between different classes of non-, modest-, and extreme-responders to RE, large differences between myofiber types, and large differences between young and old subjects **(Raue, Trappe et al. 2012, Thalacker-Mercer, Stec et al. 2013)**. However, pronounced differences in myonuclear transcriptional ability were detected between young and old humans, as well as in aged mice

(Kirby, Lee et al. 2015, Brook, Wilkinson et al. 2016). It is clear from these various studies of the muscle transcriptome in response to RE that increased ribosomal biogenesis, in part mediated by mTORC1 and its downstream target p70S6K, is a central hallmark of skeletal muscle hypertrophy **(Bamman, Roberts et al. 2018)**. Yet, the exact transcriptional mechanisms governing muscle transcriptomic changes in response to RE warrant further investigation.

Therefore, it would be ideal to be able to study changes in gene expression patterns upon the physiological stimulus of RE mimicking human RE, but at the same time avoiding many of the confounding issues discussed above. This would allow us to gain novel insights into the workings of the conversion of a mechanical stimulus into the adaptation of skeletal muscle to overload. To this end, we aimed at establishing ladder climbing as a physiological resistance exercise model for skeletal muscle hypertrophy in mice. However, our devised training model had several shortcomings that prevented it from robustly inducing hypertrophy, which we will address in the following paragraphs. The training protocol employed in our study might have been insufficient to induce larger adaptations in muscle mass. For example, available weights (originally leaden bullet weights for fishing) were limited to 11, 19, or 32 g, which probably did not allow for sufficiently fine-grained progressive overload in terms of weight. Instead, we eventually had to increase exercise volume by conducting more ladder climbs at the same maximal intensity (32 g) per training session. Additionally, it was evident that the resistance exercise group (EX) could have handled larger absolute weights if only the weights had not impaired their balance by covering too much of their tails (i.e. adding a 11 g weight in addition to a 32 g weight). It would most likely be beneficial to use weights of smaller dimensions (i.e. using denser materials, for example Wolfram (density of 19.25 g/cm^2) compared to Lead (density 11.342 g/cm^2) and more fine-grained incremental steps for RE training (weights in proper steps of 5 g, from 5 to 100 g). This might enable sufficiently stimulating progressive overload to induce hypertrophy.

In a similar ladder training model with rats **(Hornberger and Farrar 2004)**, the rats were eventually able to carry up to 287% of their own body weight, a much greater intensity

compared to what we achieved in our model (~110% of body weight). However, unlike with rats, for which a load-carrying device can be attached to their relatively sturdy tails, this kind of setup is not feasible with mice. In another study with rats, the authors employed a weighted harness to apply the progressive overloading, mimicking weight-bearing human exercise. Increased GAS muscle mass and hind limb grip strength was reported **(Strickland, Abel et al. 2016)**. We considered a similar approach using weighted vests with mice, but discarded the idea as compliance in mice would be a big issue. Compared to rats, which can be coerced into ladder climbing with a behavior-reinforcing food reward, mice are much more difficult to motivate. If task intensity grows too difficult, it is likely that mice would rather stop or simply drop from the ladder, hampering training protocol compliance.

In terms of RE volume, the typical rat ladder-climbing study conducted about four to nine complete ladder climbs per training session, three to six times per week, albeit with increasing intensity within or between sessions **(Hornberger and Farrar 2004, Strickland, Abel et al. 2016)**. Resistance exercise training volume may be beneficial in terms of muscular hypertrophy **(Schoenfeld, Contreras et al. 2019)**. In our study, the mice eventually carried 32 g, or approximately 110% of their own body weight for 5 sets per session, each lasting 5 min. During each individual training set, a mouse would complete between 15 and 20 ladder climbs before it could no longer be motivated to continue the task and required a resting period. We conducted the training sessions 5 days a week, Monday through Friday. Thus, total weekly RE volume (up to 500 complete ladder climbs) was larger compared with the rat studies, yet exercise intensity was markedly lower due to loading constraints, possibly resulting in a more aerobic exercise component. We did not assess aerobic performance, as a maximum running capacity test would have confounded our results. Despite the relatively large RE volume when compared to the above-mentioned rat studies, no overt hypertrophy of the assessed muscles ensued.

Resistance exercise model approaches other than weight-bearing ladder climbing were developed recently. One such RE modality that is feasible with mice is so-called resistance running, a type of loaded treadmill or voluntary wheel running. In one study, 10 weeks of voluntary resistance-wheel exercise (RWE) elicited muscle mass increases of the

SOL (~ 52%), GAS (~ 26.5%) and QUAD (~ 16.5%) muscles **(Soffe, Radley-Crabb et al. 2016)**. In several studies of RWE, the SOL muscle usually shows the largest hypertrophic response, whereas the TA and EDL muscles were reported to be exempt from hypertrophy **(Konhilas, Widegren et al. 2005, Legerlotz, Elliott et al. 2008, Soffe, Radley-Crabb et al. 2016)**. Interestingly, no additional benefits in terms of SOL muscle hypertrophy between a "low resistance" (resistance capped at 5 g) and "high resistance" (resistance capped at 12 g) wheel-running protocol was reported **(Konhilas, Widegren et al. 2005)**. Perhaps unexpectedly, RWE did not induce hypertrophy in the *triceps brachii* muscle of the forelimb, yet grip strength was improved **(Soffe, Radley-Crabb et al. 2016)**, except in one study of a mdx mouse model, which is a popular model for studying Duchenne muscular dystrophy **(Bulfield, Siller et al. 1984, Call, McKeehen et al. 2010)**. Although RWE has certain benefits, it does bring a substantial aerobic component and thus presents more of a mixed type of exercise, not necessarily reflecting pure muscular adaptations in terms of hypertrophy, as discussed by Roemers et al. **(Roemers, Mazzola et al. 2018)**. The authors argue that a RWE group should always be tested together with a non-resistance wheel-running group to discern resistance from endurance exercise adaptations. Furthermore, unloaded voluntary tower climbing in the home cage was recently investigated as a potential RE model, but no functional or muscular changes were reported **(Roemers, Mazzola et al. 2018)**. This stands in contrast to the findings of a comparable study in which just 3x3 min of unloaded isometric strength training (simply holding on to a vertical grid) induced sizable gains in muscle mass and cross-sectional diameter **(Kruger, Gessner et al. 2013)**. We also tried this isometric RE modality, but even adding weights to the exercise paradigm (the mice carried 32 g for three times 5 min of vertical grid holding in week eight of the pilot study) did not lead to gains in muscle mass in our hands (**Figure 6-1**).

There is significant interest and need of a physiological resistance exercise model capable of inducing robust functional skeletal muscle hypertrophy in mice. Hypothetically, if the ladder climbing model described here can be improved by the measures discussed above and indeed induces robust hypertrophy of several mouse muscles, the model can then be used to study early, as well as late adaptations to physiological RE. By conducting a time course of RE training, we could analyze the muscle transcriptome, proteome, and secretome response to acute and chronic RE. Sampling should take place before and after the first exercise bout, after one week of RE, and then after two, four, eight, and 16 weeks in order to capture the entire range of the adaptive process. Blood samples would aid in the discovery of potential secreted myokines and improve our understanding of the secretion of already established myokines in response to contractile activity. While certainly labor-intensive, conducting the study as a time course would allow to trace temporal changes in gene expression, protein abundance, myokine levels and perhaps even epigenetic changes in response to RE. We could investigate epigenetic changes by conducting reduced representation bisulfite sequencing to analyze genome-wide methylation profiles, as it has recently been shown that transient DNA hypomethylation of gene-specific promotor regions precedes increases in mRNA expression in response to acute exercise **(Meissner, Gnirke et al. 2005, Barres, Yan et al. 2012)**. It would also be interesting to conduct ATAC-seq (Assay for Transposase-Accessible Chromatin using sequencing) in order to gain a better understanding of how chromatin accessibility changes throughout the adaptive process to RE **(Buenrostro, Giresi et al. 2013)**. The obtained gene expression and proteomic data could then be analyzed in combination to narrow down key changes that occur in response to RE and during skeletal muscle hypertrophy both on a transcriptional and translational level. The identified, highly upregulated (or repressed) candidate genes could help to find novel mechanosensitive participants and pathways, thus aiding our understanding of mechanotransduction. To this end, investigating the phosphoproteome might yield additional information about potential protein activity modifications upon acute and chronic contractile activity, possibly revealing novel kinases or activity of kinase domains of already known proteins involved in these signaling events.

The established model, as well as results obtained from the hypothetical time course study above, could then also be used to investigate various disease models. Perhaps certain genes/proteins/myokines identified to play important roles in skeletal muscle hypertrophy in our hypothetical time course study may ameliorate insulin sensitivity in mouse models of obesity and type 2 diabetes mellitus. We could use the resistance exercise intervention itself to find potential factors that may ameliorate symptoms of metabolic syndrome and diabetes, as RE may perhaps be particularly effective in these cases. To this end we could use our RE model to train e.g. high-fat diet mice (if feasible) or a genetic diabetes model to study in detail how, on a molecular level, physiological RE improves glycemic control, insulin sensitivity, lean muscle mass, and bone mineral density **(Miller, Sherman et al. 1984, Nelson, Fiatarone et al. 1994, Baribault 2016)**. Furthermore, the RE model could be used to investigate the effect of pharmacological compounds on the development of grip strength and muscle contractility. For this, *in situ* muscle force measurements could be used to evaluate beneficial effects of compounds on muscle force-producing capabilities.

Systemic and muscular diseases, such as cancer cachexia, metabolic syndrome, diabetes and sarcopenia cause muscle wasting, insulin resistance, weakness, frailty and metabolic perturbations, leading to increased all-cause mortality. Associated healthcare costs are immense and there is an urgent need for treatment and novel therapeutic interventions. A sparsity of pharmaceutical and physiological interventions for the amelioration of muscle mass and functional losses in disease, disuse and aging puts emphasis on the importance of a better understanding of the transcriptional and posttranscriptional control of muscular size. Pharmacological treatment options should focus first on ameliorating muscular weakness and second on increasing muscle mass. A physiological RE model and the various study approaches proposed in this thesis could help us in better understanding fundamental processes in hypertrophy and strength gains and therefore provide means to find therapeutic options and potentially design more effective resistance exercise programs to better promote skeletal muscle growth.

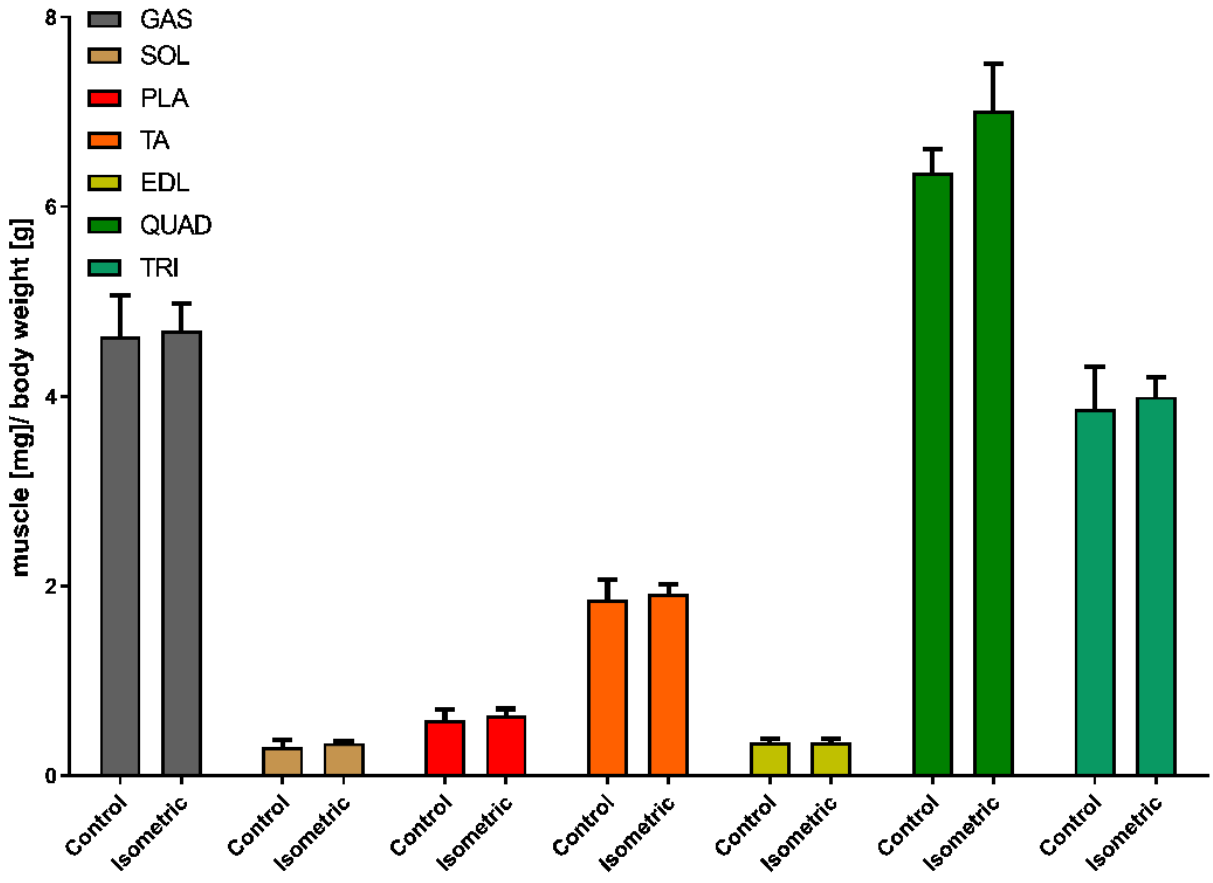

Figure 6-1. Muscle weight after eight weeks of isometric strength training. Mice were trained to hold on to a vertical grid with progressively heavier weights attached to the base of their tails ("Isometric" group). At the end of the study, the mice performed three times 5 min of vertical grid holding while carrying 32 g, three times per week. Control animals were sedentary. Shown is muscle weight normalized to body weight. Data shown as mean ± SD; N = 5.

6.2 Identification of Novel Synaptic Components by Transcriptome Profiling of the Murine Neuromuscular Junction

Discussion and future perspectives

Objective II: *Identify novel components of the neuromuscular junction in the EDL and SOL muscles using next-generation RNA-sequencing.*

In this project, we set out to develop a methodology that combines laser-capture microdissection (LCM) with next-generation RNA-sequencing technology to identify novel components of the neuromuscular junction (NMJ). We achieved our primary goal and successfully identified a large number of potential novel NMJ genes in the EDL and SOL muscles, thus improving upon previous approaches from literature. However, our attempts to validate the localization of several novel NMJ genes, namely *Tbx21, Crym, Hs6st2, Dlk1* and *Nell2,* to the NMJ via immunostaining with commercially available antibodies were unsuccessful. None of our attempts yielded a specific signal, either due to problems with antibody penetration into our muscle whole-mount and even single-fiber preparations, or due to inherent problems of the antibodies themselves (unsuitable for staining muscle tissue, or generally unspecific binding). It might be worthwhile to generate at least two different custom affinity-purified polyclonal antibodies against synthetic peptides of each candidate, which might lead to less unspecific staining. Alternatively, *in situ* hybridization approaches such as RNAscope® could be used to validate localization of the candidate mRNA to the NMJ.

In order to compile a more concrete set of candidates for future investigations, we conducted some additional pathway analysis. We used DAVID Bioinformatics Resources 6.8 to conduct further functional annotation analysis of our EDL and SOL muscle NMJ expression profiles and focused on the overlap of both muscles (**Huang da, Sherman et al. 2009, Huang da, Sherman et al. 2009).** DAVID **"**SEQ_FEATURE" and "KEYWORD" are functional annotation categories similar to GO / KEGG. The analysis revealed the DAVID SEQ_FEATUREs *signal peptide* and *glycosylation site: N-linked (GlcNAc…)* along with the KEYWORDs *glycoprotein* and *signal* as highly enriched terms in both muscles (**Figure 6-2 F-G**). The

number of genes associated with an enriched DAVID term was lower for the SOL, relative to the lower number of differentially expressed genes in that list (see **Table 4-2**). The functional annotation analysis of our EDL and SOL NMJ expression profiles clearly hints at the importance of signaling events involving glycosylation, as well as the organization of the extracellular matrix. This finding is perhaps not overly surprising, since it is known that specific glycans are concentrated at the NMJ and exert important regulatory functions **(Yamaguchi 2002)**. One example would be the extensive glycosylation of α-dystroglycan, which loses its ability to properly anchor various canonical NMJ components at the basal lamina if it becomes hypoglycosylated, for example due to mutations in its glycosylating enzymes in congenital myasthenia **(Ervasti and Campbell 1993, Talts, Andac et al. 1999, Endo 2005)**. Deficiencies in post-translational modifications of α-dystroglycan are thought to involve O-glycosylation pathways **(Grewal and Hewitt 2003)**. Our gene expression profiles included the gene encoding for glutamine-fructose-6-phosphate transaminase 1 (*Gfpt1*; fold change of 10 in the EDL NMJ). Deficiency of GFPT1 in muscle is known to cause congenital myasthenic syndrome with glycosylation defects, and was reported to result in reduced cell-surface expression of muscle AChRs **(Zoltowska, Webster et al. 2013, Issop, Hathazi et al. 2018)**. Modified glycosaminoglycans such as chondroitin, dermatan and heparan sulfate proteoglycans are ubiquitous components of the cell surface, extracellular matrix and of basement membranes, where they exert important structural and regulatory functions. For example, acetylcholinsterase is anchored to the synaptic basal lamina by its collagenic tail ColQ, which contains two heparin-binding domains that interact with surface heparan sulfate proteoglycans **(Aldunate, Casar et al. 2004)**. Also, agrin is perhaps the most prominent heparan sulfate proteoglycan within the NMJ basal lamina, where it is bound by laminin and plays fundamental roles in NMJ formation, function and maintenance **(Denzer, Brandenberger et al. 1997, Li, Xiong et al. 2018)**. The immense enrichment of genes in DAVID functional annotation (**Figure 6-2**) and PANTHER gene ontology terms (**Figure 4-3 C-E**) such as *postsynaptic membrane organization*, *synaptic membrane adhesion*, *basement membrane*, *heparin binding, glycoprotein, signal peptide* and many more prompted us to curate a selection of highly synaptically enriched enzymes that are putatively involved in the modulation of basal lamina components at the NMJ and thus potentially contributing to the regulation of a multitude of NMJ components via post-translational modifications (**Figure**

6-3). Interestingly, a targeted glycan-related screen revealed the functional pair of *Sulf1* and *Hs6st* in the regulation of WNT and BMP trans-synaptic signaling at the Drosophila NMJ **(Dani, Nahm et al. 2012)**. Our curated list contains *Hs6st1, Hs6st2,* as well as *Sulf2*, as highly enriched prospective NMJ components of the EDL muscle, and the findings at the Drosophila NMJ suggest a potentially similar role of these enzymes at the vertebrate NMJ, warranting further research.

To provide further support for the importance of these potentially basal lamina-modifying enzymes with structural and functional implications for the NMJ, we looked at the overlap of our EDL NMJ expression profile from Manuscript II and our young TA NMJ expression profile (10M.NMJ.CT vs. 10M.XNMJ.CT) from the Sinergia project dataset (**Figure 6-4**). The overlap included and thus further validated the importance of the genes *Hs6st2, Chpf, Chst15, Galnt15, Galnt18,* and *B4galnt3*. Unique to the TA were further potentially important genes encoding for enzymes such as *Hs3st3a1, Hs3st3b1, Gal3st1* and many more examples. Congenital myasthenic syndromes with glycosylation defects often involve mutations in enzymes that control central processes in glycoprotein modifications. For example, GFPT1 is the rate-limiting enzyme of the hexosamine pathway and regulates the availability of precursors for N- and O-linked glycosylation of proteins. Mutations of GFPT1 thus have broad implications for the glycosylation of a potentially large number of NMJ components **(Senderek, Muller et al. 2011)**. Importantly, mutations in other genes further downstream of GFPT1 may cause myasthenias as well, with critical roles in the impairment of neutransmission **(Issop, Hathazi et al. 2018)**. Another example is dolichyl-phosphate (UDP-N-acetylglucosamine) N-acetylglucosaminephosphotransferase 1 (DPAGT1), which is an essential enzyme catalyzing the first committed step of N-linked protein glycosylation, and mutations of which cause congenital myasthenic syndrome with tubular aggregates **(Belaya, Finlayson et al. 2012)**. It is therefore highly likely that mutations of other enzymes further downstream of the N- and O-linked glycosylation pathways, but also of other posttranslational modifications, such as heparan sulfate proteoglycan sulfation, play an important role in neuromuscular disease. We strongly suggest further investigation of our provided candidate list in **Figure 6-3**, as there is a high likelihood that there are at least some candidates with highly important roles at the NMJ among them. Another interesting, albeit

unrelated candidate gene would be *Pdzrn4*, which is the fourth most highly enriched gene in the synaptic EDL, with a fold change of 2853. Since MuSK internalization can lead to its proteasomal degradation mediated in part by the E3 ubiquitin ligase PDZ domain-containing RING finger protein 3 (PDZRN3), which constitutes an important regulator of MuSK signaling contributing to precise and dynamic control of synaptic development **(Lu, Je et al. 2007)**, investigating the potential role of the PDZRN3-paralog PDZ domain-containing RING finger protein 4 (PDZRN4) in MuSK-signaling would be interesting. Functional investigation of the suggested candidates could be achieved with inducible, muscle-specific mouse models assessing NMJ morphology, ultrastructure and neurotransmission strength. These studies could be complemented with loss-of-function experiments utilizing intramuscular AAV-shRNA injections. Alternatively, a CRISPR approach to generate muscle-specific knockout of our suggested candidates may be used as well. Functional evaluation of our suggested candidates could provide novel targets for treatment strategies of neuromuscular diseases such as congenital myasthenic syndromes.

We compared the fold changes obtained in our different studies and comparisons and included the TA NMJ dataset from Ketterer et al., 2010 (**Table 6-1**). From this comparison, it is clear that no single dataset is perfect on its own. Perhaps our TA dataset from the Sinergia project is the most comprehensive NMJ transcriptome available yet, but nevertheless most likely still does not contain every existing NMJ component. We definitely achieved a better quality dataset in the Sinergia project compared to the preceding EDL and SOL project. This was due to several improvements we made to the methodology. For one, we collected a slightly larger amount of NMJs per sample (300 vs. < 200) and worked with a larger number of biological replicates (N = 8 vs. N = 6). Perhaps the best improvements came from different sequencing library preparation kits used by the D-BSSE, which led to more robust data with much less noise overall for the Sinergia TA dataset. However, both studies worked with whole tissue lysates without RNA-isolation, which comes with the caveat of a lack of control over the exact input amounts of RNA. We controlled input amount solely by capturing equal numbers of NMJ areas and equal amounts of extrajunctional control tissue (based on area in mm^2). In order to judge the RNA quality of our LCM tissue, we once collected a large representative sample of several times the amount of NMJ areas we would collect for a

regular sample in the study, isolated RNA and measured RNA integrity with an Agilent BioAnalyzer RNA 6000 Pico Kit. Our LCM tissue had a RNA integrity number (RIN) of 8, indicating good-quality RNA. It might be worth trying to collect a larger amount of NMJs (> 600; with a lower number of biological replicates to reduce workload) and to conduct RNA-isolation, thus gaining control over the exact input amounts for RNA-sequencing. It would be worth evaluating whether we could conduct NMJ proteomics to evaluate and support our transcriptomic findings with protein data.

In conclusion, we were able to identify a large number of potential novel NMJ genes with our approach, and our NMJ gene profile analyses of the EDL and SOL muscles revealed a set of highly interesting candidates to follow up on in future research. We most likely still have not identified all components that make up the NMJ, but transcriptomic studies such as this allow us to appreciate the incredible biological complexity of the neuromuscular synapse, a better understanding of which provides the basis for discovering novel treatment approaches in neuromuscular disease.

Table 6-1. Gene expression fold change comparison of known and potentially novel NMJ components of the EDL and SOL (from Manuscript II study) and of the TA (from Sinergia project), as well as of the available TA dataset from Ketterer et al., 2010.

Gene Name	EDL	SOL	TA (Sinergia project)	TA (Ketterer et al., 2010)
Aplp2	10.4	3.4	17.1	-
B4galnt3	323.3	506.7	18	-
Chpf	203.4	22.4	10.8	-
Chst15	23.2	-	5.7	-
Chrna1	38.8	8.2	57.9	300.7
Chrnb1	7	n.s.	5.1	2.5
Chrnd	1020.9	12.4	652.2	13
Chrne	40.9	53.5	556.7	117.5
Crym	n.s.	246.4	232.6	20.3
Dusp6	24	19.4	81.6	60/80/100
Erbb3	n.s.	n.s.	58.24	-
Dlk1	423.5	n.s.	78.3	-
Etv5	n.s.	112.6	494.4	164
Galnt15	27.2	-	3.6	-
Galnt18	46.8	-	11.14	-
Hs6st2	9524	n.s.	232.4	-
Musk	668.8	n.s.	14.9	-
Nell2	n.s.	141.2	21.9	-
Pdzrn4	2853.3	23.4	126.1	7.3
Sox10	1193	938.4	58.6	2.6
Tbx21	918.6	n.s.	129.1	-

Fold changes are from the respective synaptic vs. extrasynaptic comparisons of our datasets. The TA dataset from Ketter et al., 2010 was taken from their supplemental table S2 TAsin vs TAfib (set 2) **(Ketterer, Zeiger et al. 2010)**. If a gene was not detected to be differentially expressed due to a cutoff FDR p-value > 0.05, this was indicated with n.s., not significant.

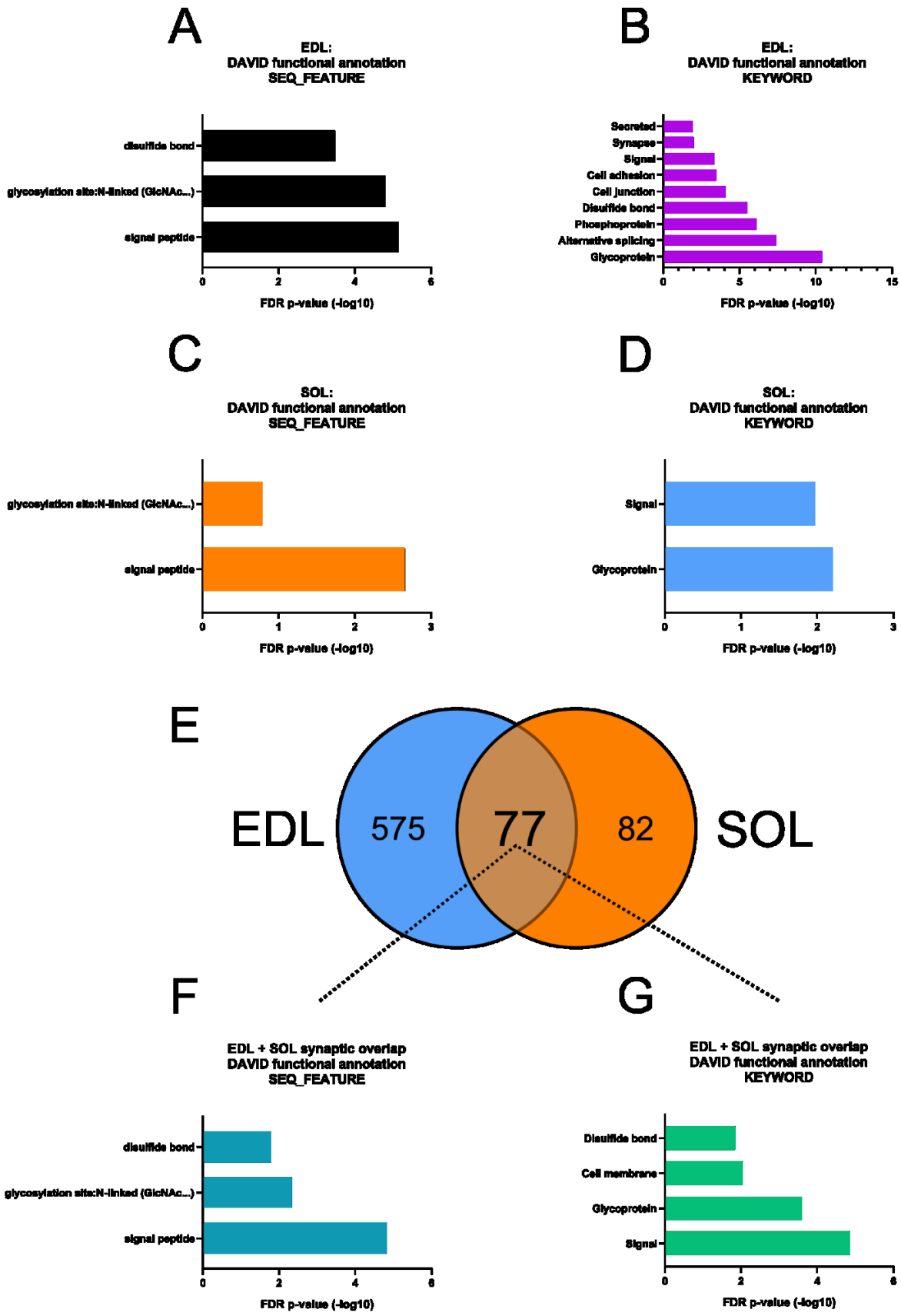
A
EDL:
DAVID functional annotation
SEQ_FEATURE
disulfide bond
glycosylation site:N-linked (GlcNAc...)
signal peptide
0
2
4
6
FDR p-value (-log10)
B
EDL:
DAVID functional annotation
KEYWORD
Secreted
Synapse
Signal
Cell adhesion
Cell junction
Disulfide bond
Phosphoprotein
Alternative splicing
Glycoprotein
0
5
10
15
FDR p-value (-log10)
C
SOL:
DAVID functional annotation
SEQ_FEATURE
glycosylation site:N-linked (GlcNAc...)
signal peptide
0
1
2
3
FDR p-value (-log10)
D
SOL:
DAVID functional annotation
KEYWORD
Signal
Glycoprotein
0
1
2
3
FDR p-value (-log10)
E
EDL
575
77
82
SOL
F
EDL + SOL synaptic overlap
DAVID functional annotation
SEQ_FEATURE
disulfide bond
glycosylation site:N-linked (GlcNAc...)
signal peptide
0
2
4
6
FDR p-value (-log10)
G
EDL + SOL synaptic overlap
DAVID functional annotation
KEYWORD
Disulfide bond
Cell membrane
Glycoprotein
Signal
0
2
4
6
FDR p-value (-log10)

Figure 6-2. DAVID functional annotation analysis of the EDL and SOL muscles individually, as well as of their overlap. A) Significant DAVID SEQ_FEATURE and **B)** KEYWORD terms resulting from functional annotation analysis of all synaptically enriched genes of the EDL muscle. **C)** Significant DAVID SEQ_FEATURE and **D)** KEYWORD terms resulting from functional annotation analysis of all synaptically enriched genes of the SOL muscle. **E)** Venn-diagram depicting overlap and difference of synaptically enriched genes in the EDL and SOL muscles. **F)** Significant DAVID SEQ_FEATURE and **G)** KEYWORD terms of the EDL and SOL overlap (77 genes) indicated by the black dotted line.

Gene	Protein	Processes involved in	Fold change	Functions
Hs6st2	Heparan sulfate 6-O-sulfotransferase 2	Glycosaminoglycan metabolism, heparan sulfate biosynthesis	9525.4	6-O-sulfation enzyme which catalyzes the transfer of sulfate from 3'-phosphoadenosine 5'-phosphosulfate (PAPS) to position 6 of the N-sulfoglucosamine residue (GlcNS) of heparan sulfate.
St6gal1	**Beta galactoside alpha 2,6 sialyltransferase 1**	**O-linked glycosylation**	**815.4**	**Transfers sialic acid from CMP-sialic acid to galactose-containing acceptor substrates.**
Chpf2	Chondroitin polymerizing factor 2	Glycosaminoglycan metabolism, Chondroitin sulfate/dermatan sulfate metabolism	546.1	Transfers glucuronic acid (GlcUA) from UDP-GlcUA to N-acetylgalactosamine residues on the non-reducing end of the elongating chondroitin polymer. Has no N-acetylgalactosaminyltransferase activity.
B4galnt3	**Beta-1,4-N-acetyl-galactosaminyl transferase 3**	**Metabolism, N-glycan acetylgalactosamine transfer**	**323.4**	**Transfers N-acetylgalactosamine (GalNAc) from UDP-GalNAc to N-acetylglucosamine-beta-benzyl with a beta-1,4-linkage to form N,N'-diacetyllactosediamine, GalNAc-beta-1,4-GlcNAc structures in N-linked glycans and probably O-linked glycans.**
St3gal4	ST3 beta-galactoside alpha-2,3-sialyltransferase 4	O-linked glycosylation	242.9	Catalyzes the formation of the NeuAc-alpha-2,3-Gal-beta-1,4-GlcNAc-, and NeuAc-alpha-2,3-Gal-beta-1,3-GlcNAc- sequences found in terminal carbohydrate groups of glycoproteins and glycolipids.
Chpf1	**Chondroitin polymerizing factor 1**	**Glycosaminoglycan metabolism, Chondroitin sulfate/dermatan sulfate metabolism**	**203.4**	**Has both beta-1,3-glucuronic acid and beta-1,4-N-acetylgalactosamine transferase activity. Transfers glucuronic acid (GlcUA) from UDP-GlcUA and N-acetylgalactosamine (GalNAc) from UDP-GalNAc to the non-reducing end of the elongating chondroitin polymer.**
Galnt18	Polypeptide N-acetylgalactosaminyltransferase 18	O-linked glycosylation	46.8	Catalyzes the initial reaction in O-linked oligosaccharide biosynthesis, the transfer of an N-acetyl-D-galactosamine residue to a serine or threonine residue on the protein receptor.
Galnt15	**Polypeptide N-acetylgalactosaminyltransferase 15**	**O-linked glycosylation**	**27.3**	**Catalyzes the initial reaction in O-linked oligosaccharide biosynthesis, the transfer of an N-acetyl-D-galactosamine residue to a serine or threonine residue on the protein receptor.**
Chst15	Carbohydrate sulfotransferase 15	Glycosaminoglycan metabolism, Chondroitin sulfate/dermatan sulfate metabolism	23.2	Sulfotransferase that transfers sulfate from 3'-phosphoadenosine 5'-phosphosulfate (PAPS) to the C-6 hydroxyl group of the GalNAc 4-sulfate residue of chondroitin sulfate A and forms chondroitin sulfate E containing GlcA-GalNAc(4,6-SO(4)) repeating units.
Sulf2	**Sulfatase 2 / Heparan sulfate 6-O-endosulfatase**	**Heparan sulfate activity modulation**	**21.7**	**Exhibits arylsulfatase activity and highly specific endoglucosamine-6-sulfatase activity. It can remove sulfate from the C-6 position of glucosamine within specific subregions of intact heparin.**
Hs6st1	Heparan sulfate 6-O-sulfotransferase 1	Glycosaminoglycan metabolism, heparan sulfate biosynthesis	16.6	6-O-sulfation enzyme which catalyzes the transfer of sulfate from 3'-phosphoadenosine 5'-phosphosulfate (PAPS) to position 6 of the N-sulfoglucosamine residue (GlcNS) of heparan sulfate.
Gfpt1	**Glutamine fructose-6-phosphate transaminase 1**	**Synthesis of substrates in N-glycan biosynthesis**	**10.7**	**Involved in congenital myasthenic syndromes with glycosylation defects. Controls the flux of glucose into the hexosamine pathway. Most likely involved in regulating the availability of precursors for N- and O-linked glycosylation of proteins.**

Figure 6-3. Curated list of synaptically enriched enzymes putatively involved in the structural and functional modulation of the NMJ basal lamina. The information for involved processes and function of the genes was adapted from the NCBI gene databank at ncbi.nlm.nih.gov and the UniProt knowledgebase (UniProtKB) at uniprot.org. Fold changes are from the synaptic against extrasynaptic EDL RNA-sequencing comparison.

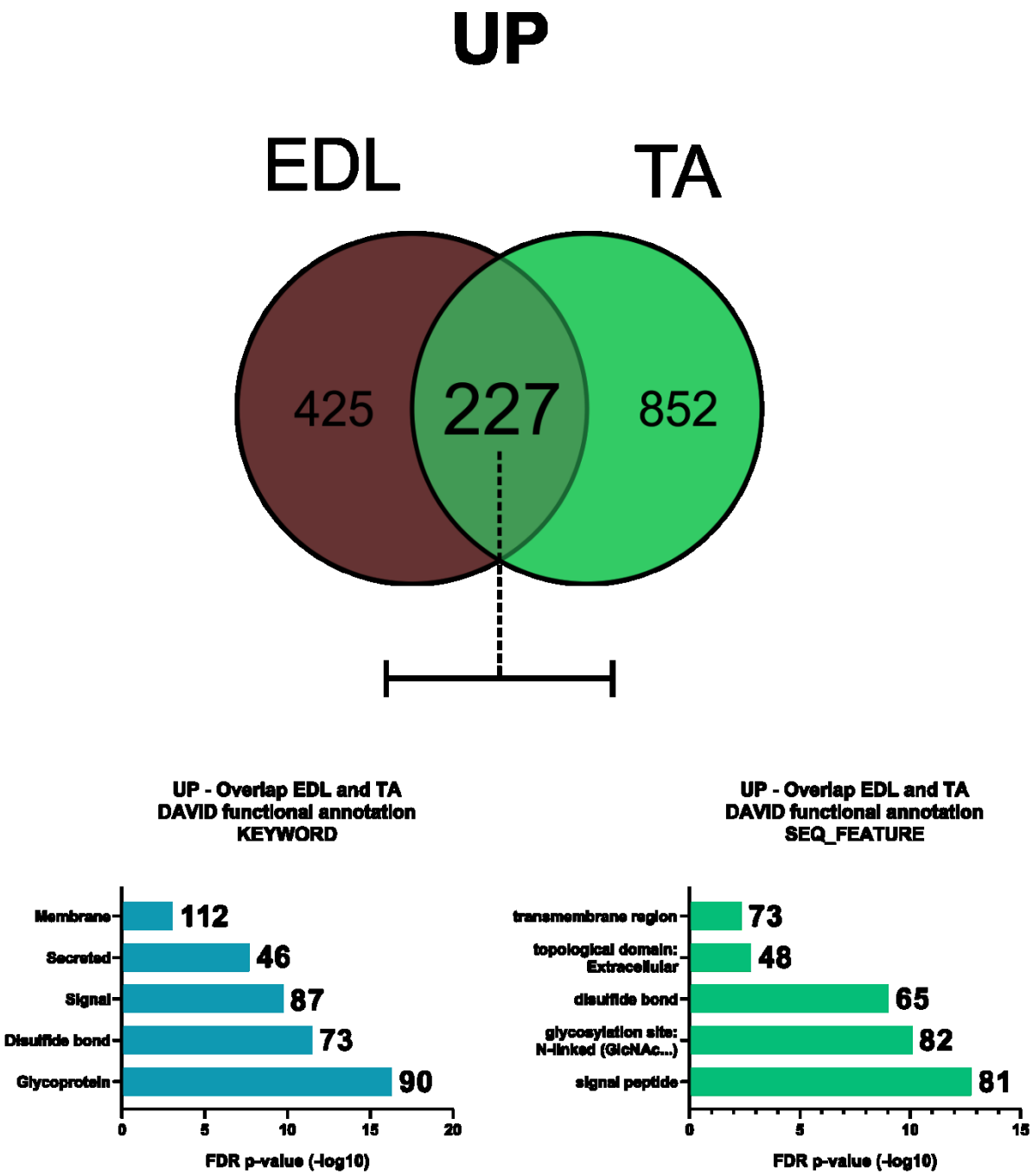

Figure 6-4. DAVID functional annotation analysis of the overlap of the EDL (Manuscript II) and TA (Sinergia project) muscle NMJ expression profiles. The Venn-diagram shows the overlap and difference of differentially expressed genes with a positive fold change (**UP**: synaptically enriched genes). The five most significant DAVID KEYWORDs and SEQ_FEATUREs resulting from querying DAVID Bioinformatics Resources with the overlap (227 genes) are shown. Numbers next to the barplots indicate the number of genes enriching the respective terms.

6.3 Effects of Aging on the Neuromuscular Junction Transcriptome

Discussion and future perspectives

Objective III: *Determine whether aging leads to perturbations of the neuromuscular junction transcriptome.*

The neuromuscular junction (NMJ) is critically involved in age-related musculoskeletal impairments. We hypothesized that aging might lead to dysregulation of the NMJ gene program and thus contribute to the structural and functional decline of the NMJ that is observed with age. It has been suggested that aging changes NMJs mainly through the accumulation of myofiber segment damage at the NMJ. While the myofiber segment first degenerates and then quickly regenerates, this leaves the affected NMJ permanently perturbed **(Li, Lee et al. 2011)**. However, it is also conceivable that aging leads to perturbations of the NMJ gene program, the dysregulation of which might lead to prolonged acetylcholine receptor turnover and disruption of pre- and post-synaptic apposition. If aging perturbs the NMJ gene program this may predispose them to damage. We used laser-capture microdissection to isolate fundamental myonuclei underlying the NMJ and generated NMJ gene expression profiles of the *tibialis anterior* (TA) muscle of young (10-month-old) and very old (30-month-old) mice with next-generation RNA-sequencing to investigate whether aging leads to perturbations of the NMJ gene program. Our results revealed the NMJ gene program to be remarkably stable, with identical gene expression levels of canonical NMJ genes. Our findings argue against the hypothesis that aging leads to a broad deterioration of the NMJ gene program that would contribute to perturbations of NMJ structure and function. We have thus achieved the primary goal of the project.

The direct comparison of 10-month-old against 30-month-old synaptic control samples did not yield any differentially expressed genes. However, there was a difference in the total number of synaptically enriched and decreased genes (**Table 5-1**). We grouped all of the young and old synaptically enriched genes, as well as all of the young and old synaptically decreased genes of the respective comparisons into two separate Venn-

diagrams. This allowed us to see which genes were synaptically enriched or decreased in both groups, and which genes were particular to just young or old NMJs (**Figure 6-5**). We found an overlap of 423 genes that were synaptically enriched in both age groups, while 656 genes were unique to the young group and 321 genes were unique to the old (**Figure 6-5 A**). Furthermore, 130 genes were synaptically decreased in both groups, while 167 were unique to the young group and 54 were unique to the old (**Figure 6-5 B**). Before submitting the different lists of overlapping and differing genes to DAVID Bioinformatics Resources for functional annotation analysis, we removed predicted and non-coding genes, as those are not available in the respective annotation databanks. The synaptically enriched overlap of both groups (423 genes) was thus reduced to 378 genes for the submission. DAVID **"**SEQ_FEATURE" and "KEYWORD" are functional annotation categories similar to GO / KEGG. The most enriched DAVID KEYWORDs of this overlap were *glycoprotein, disulfide bond, secreted* and *signal*, together with the DAVID SEQ_FEATUREs *signal peptide, glycosylation site: N-linked (GlcNAc…)* and *disulfide bond*. The most enriched DAVID KEYWORDs in the subset of 527 synaptically enriched genes unique to the 10-month control were *glycoprotein, disulfide bond, phosphoprotein, collagen, immunity* and *signal*, as well as the DAVID SEQ_FEATUREs *signal peptide* and *glycosylation site: N-linked (GlcNAc…)*. The most enriched DAVID KEYWORDs in the subset of 266 synaptically enriched genes unique to the 30-month control were *disulfide bond, glycoprotein, phosphoprotein, cell adhesion* and *secreted*, as well as the DAVID SEQ_FEATUREs *disulfide bond, signal peptide* and *glycosylation site: N-linked (GlcNAc…)*. All of the synaptically enriched terms we found here are in agreement with our findings in the discussion to Manuscript II (**Figure 6-2**) and our comparison of the two different NMJ transcriptome datasets (**Figure 6-4**), lending further support to our proposed list of interesting candidate genes to investigate in future research (**Figure 6-3**).

The subset of 130 genes that were synaptically decreased in both the young and old groups (Venn-diagram overlap in **Figure 6-5 B**) could not be used for DAVID functional annotation analyses, as this list contained many entries that were not available in the DAVID annotation databank. The list contained a large amount of mitochondrially encoded components of the electron transport chain (e.g. *mt-Atp6*, *mt-Atp8*, *mt-Co1 to mt-Co3*, *mt-Cytb*, *mt-Nd1 to mt-Nd6*, *mt-Rnr1*, *mt-Rnr2*, and 22 different mitochondrial transfer RNAs).

Fittingly, the subset of 167 genes unique to the 10-month-old control group enriched the DAVID KEYWORDs *transit peptide, mitochondrion,* and *mitochondrion: Inner membrane*, as well as the DAVID SEQ_FEATURE *transit peptide: Mitochondrion*. Among the genes enriching most of these terms were Ubiquinol cytochrome c reductase core protein 2 (*Uqcrc2*), Creatine kinase, mitochondrial 2 (*Ckmt2*), Oxoglutarate dehydrogenase (*Ogdh*) and ATP synthase subunit delta, mitochondrial (*Atp5d*). The subset of 54 synaptically decreased genes unique to the 30-month-old control did not enrich any DAVID terms, probably due to the relatively low number of entries in the list. Taken together, our analysis of synaptically decreased genes suggests a reduction of mitochondrial bioenergetic complexes in mitochondria at the NMJ, mostly irrespective of age as we found most mitochondrially encoded genes in the Venn-diagram overlap (**Figure 6-5 B)**. Importantly, most of the mitochondrially encoded genes mentioned above have some of the strongest gene expression values in the entire dataset, and in some cases exhibit expression strength in excess of 200000 counts per million (**Figure 6-6 A-B**). To visualize this we representatively plotted *mt-Atp6, mt-Cytb, mt-Co3,* and *mt-Nd3* (**Figure 6-6 C-F**).

The overall reduction in mitochondrially encoded genes seems surprising, as synapses generally possess a large amount of mitochondria and we would assume that we isolated comparatively more mitochondria with LCM in the synaptic samples compared to the extrasynaptic ones **(Ly and Verstreken 2006, Vos, Lauwers et al. 2010)**. If anything, we would have expected a larger reduction of these genes in the old group. Perhaps age-related mitochondrial perturbations led to an increased amount of dysfunctional mitochondria at the NMJ and we simply measured the result of that. Alternatively, age-related perturbations in the extrajunctional muscle tissue, which we used as a control, had greater variability and led to the observed outcome in our old synaptic versus extrasynaptic comparison. Another possibility is the fact that mitochondria cluster within the presynaptic nerve terminal and release calcium to modulate synaptic potentiation at the NMJ and therefore might be specialized for calcium buffering at the NMJ, especially for synaptic vesicle handling on the presynaptic side **(Yang, He et al. 2003, Lee and Peng 2006, Vos, Lauwers et al. 2010)**. Mitochondrial calcium uptake is essential for neuromuscular transmission **(David and Barrett 2003)**. Synaptic and extrasynaptic mitochondria have been successfully

isolated and characterized from the rat brain and variations in mitochondrial enzymatic activities dependent upon the subcellular localization of the organelle were reported **(Lai, Walsh et al. 1977)**. Proteomic profiling of neuronal mitochondria revealed an upregulation of mitochondrial inner membrane bioenergetics complexes, which suggests that distinct synaptic and non-synaptic mitochondrial protein expression may reflect altered local requirements for energetic expenditure. Additionally, synaptic mitochondria in the brain differed morphologically compared to non-synaptic mitochondria and are more susceptible to calcium overload **(Brown, Sullivan et al. 2006, Graham, Eaton et al. 2017)**.

Our results are in disagreement with the above observations of synaptic mitochondria in central nervous system. The Krebs cycle generates the master metabolite α-ketoglutarate, transamination of which yields the neurotransmitter glutamate. Glutamate can further be decarboxylated to yield GABA, another neurotransmitter **(Bak, Schousboe et al. 2006)**. Since the vertebrate NMJ uses the neurotransmitter acetylcholine exclusively, one possible hypothesis is that mitochondria at the NMJ might be specialized for calcium handling and therefore downregulate their expression of electron transport chain and Krebs cycle proteins as opposed to synaptic mitochondria in the brain. Indeed, in addition to our observed downregulation of a large amount of mitochondrially encoded components of the electron transport chain, we observed decreased expression of the gene encoding for α-ketoglutarate dehydrogenase (*Ogdh)* (**Figure 6-6 G**), a rate-limiting enzyme in the Krebs cycle. Furthermore, the gene encoding for mitochondrial isocitrate dehydrogenase 2 (*Idh2*) (**Figure 6-6 H**), an enzyme that produces α-ketoglutarate from isocitrate, was synaptically decreased as well. It would thus be interesting to investigate respiration and calcium buffering capabilities of NMJ mitochondria and compare the results with non-synaptic mitochondria of the muscle and brain, although this might be challenging to do experimentally. We could perform mitochondrial calcium uptake assays on NMJ mitochondria isolated via LCM. However, cryopreservation of functionally intact mitochondria, as would be required for LCM of serial muscle cryosections, might be a limiting factor. Skeletal muscle mitochondria are difficult to cryopreserve, and simple freeze-thawing of muscle tissue is associated with severe damage of mitochondria. One study found that cryopreservation of functionally intact muscle mitochondria might be possible by using fine-tuned amounts of glycerol and DMSO

(Kuznetsov, Kunz et al. 2003). Perhaps this method could also be applied to our LCM workflow and allow the isolation of functionally intact NMJ mitochondria. Furthermore, collecting adequate amounts of tissue in order to analyze mitochondrial respiration and calcium buffering might not be feasible via LCM. Dysregulation of calcium handling is a common underlying event in the pathophysiology of muscular dystrophies **(Vallejo-Illarramendi, Toral-Ojeda et al. 2014)**. Understanding whether (pre-) synaptic mitochondria possess specializations in calcium handling might have implications for neuromuscular diseases where perturbations of calcium handling plays a role and have not been taken into consideration previously.

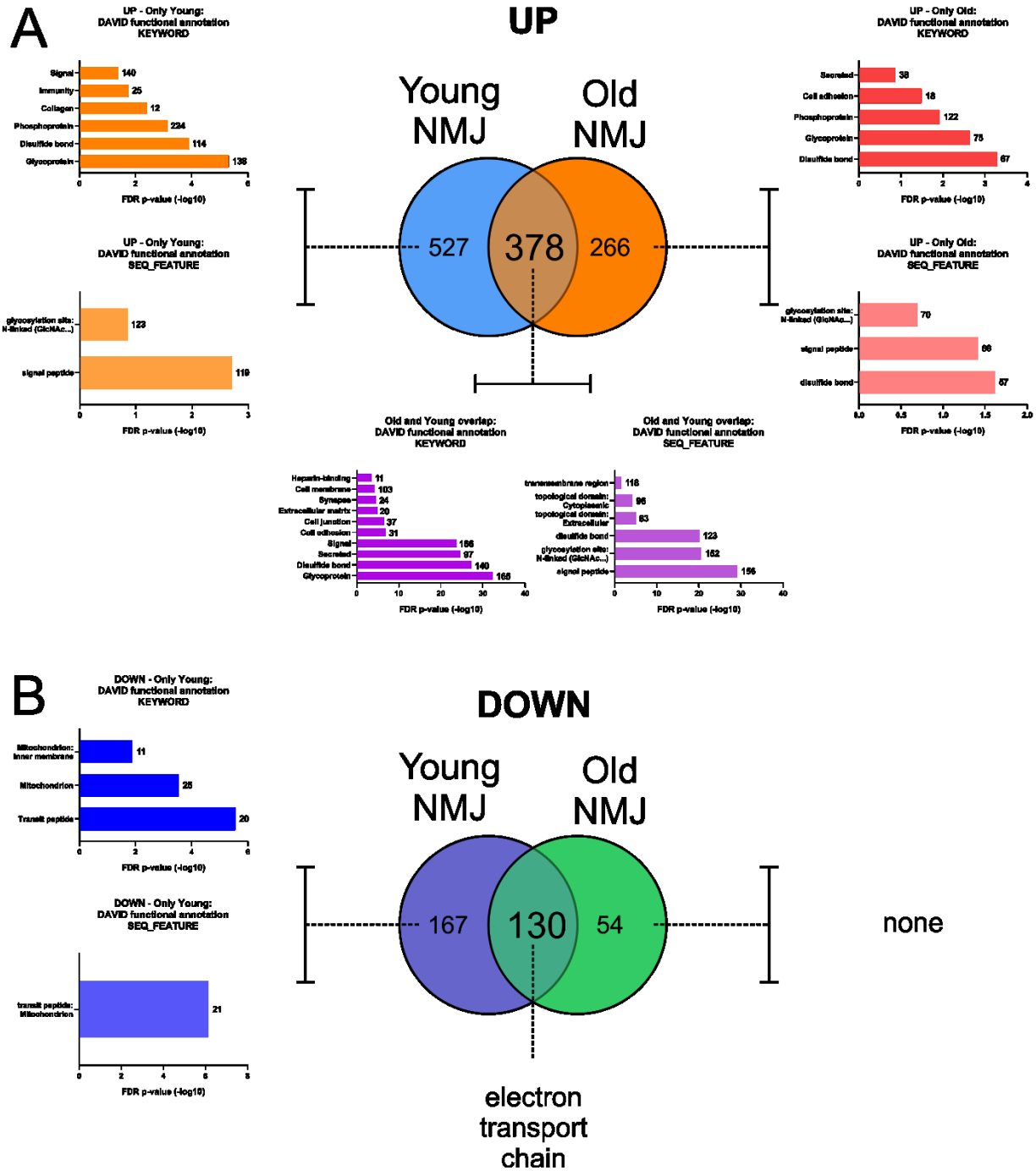
A
UP
Young NMJ
Old NMJ
527
378
266
UP - Only Young: DAVID functional annotation KEYWORD
Signal 140
Immunity 25
Collagen 12
Phosphoprotein 224
Disulfide bond 114
Glycoprotein 138
FDR p-value (-log10)
UP - Only Young: DAVID functional annotation SEQ_FEATURE
glycosylation site: N-linked (GlcNAc...) 123
signal peptide 119
FDR p-value (-log10)
UP - Only Old: DAVID functional annotation KEYWORD
Secreted 38
Cell adhesion 18
Phosphoprotein 122
Glycoprotein 75
Disulfide bond 67
FDR p-value (-log10)
UP - Only Old: DAVID functional annotation SEQ_FEATURE
glycosylation site: N-linked (GlcNAc...) 70
signal peptide 66
disulfide bond 57
FDR p-value (-log10)
Old and Young overlap: DAVID functional annotation KEYWORD
Heparin-binding 11
Cell membrane 103
Synapse 24
Extracellular matrix 20
Cell junction 37
Cell adhesion 31
Signal 186
Secreted 97
Disulfide bond 140
Glycoprotein 165
FDR p-value (-log10)
Old and Young overlap: DAVID functional annotation SEQ_FEATURE
transmembrane region 116
topological domain: Cytoplasmic 96
topological domain: Extracellular 83
disulfide bond 123
glycosylation site: N-linked (GlcNAc...) 152
signal peptide 156
FDR p-value (-log10)
B
DOWN
Young NMJ
Old NMJ
167
130
54
none
electron transport chain
DOWN - Only Young: DAVID functional annotation KEYWORD
Mitochondrion: Inner membrane 11
Mitochondrion 25
Transit peptide 20
FDR p-value (-log10)
DOWN - Only Young: DAVID functional annotation SEQ_FEATURE
transit peptide: Mitochondrion 21
FDR p-value (-log10)

Figure 6-5. DAVID functional annotation analysis of young and old neuromuscular junction gene expression patterns. Venn-diagrams showing overlap and difference of differentially expressed genes with a **A)** positive fold change (**UP**: synaptically enriched genes) or **B)** negative fold change (**DOWN**: synaptically decreased genes) between the respective young and old synaptic against extrasynaptic control group comparisons. Dotted lines indicate the respective subset of genes used for DAVID functional annotation analysis. For each subset, significant (FDR p-value < 0.25) DAVID KEYWORDs and SEQ_FEATUREs are shown. Numbers next to the barplots indicate the number of genes enriching the respective terms. **Young NMJ**: Differentially expressed genes of the synaptic vs. extrasynaptic 10-month control group; **Old NMJ**: Differentially expressed genes of the synaptic vs. extrasynaptic 30-month control group.

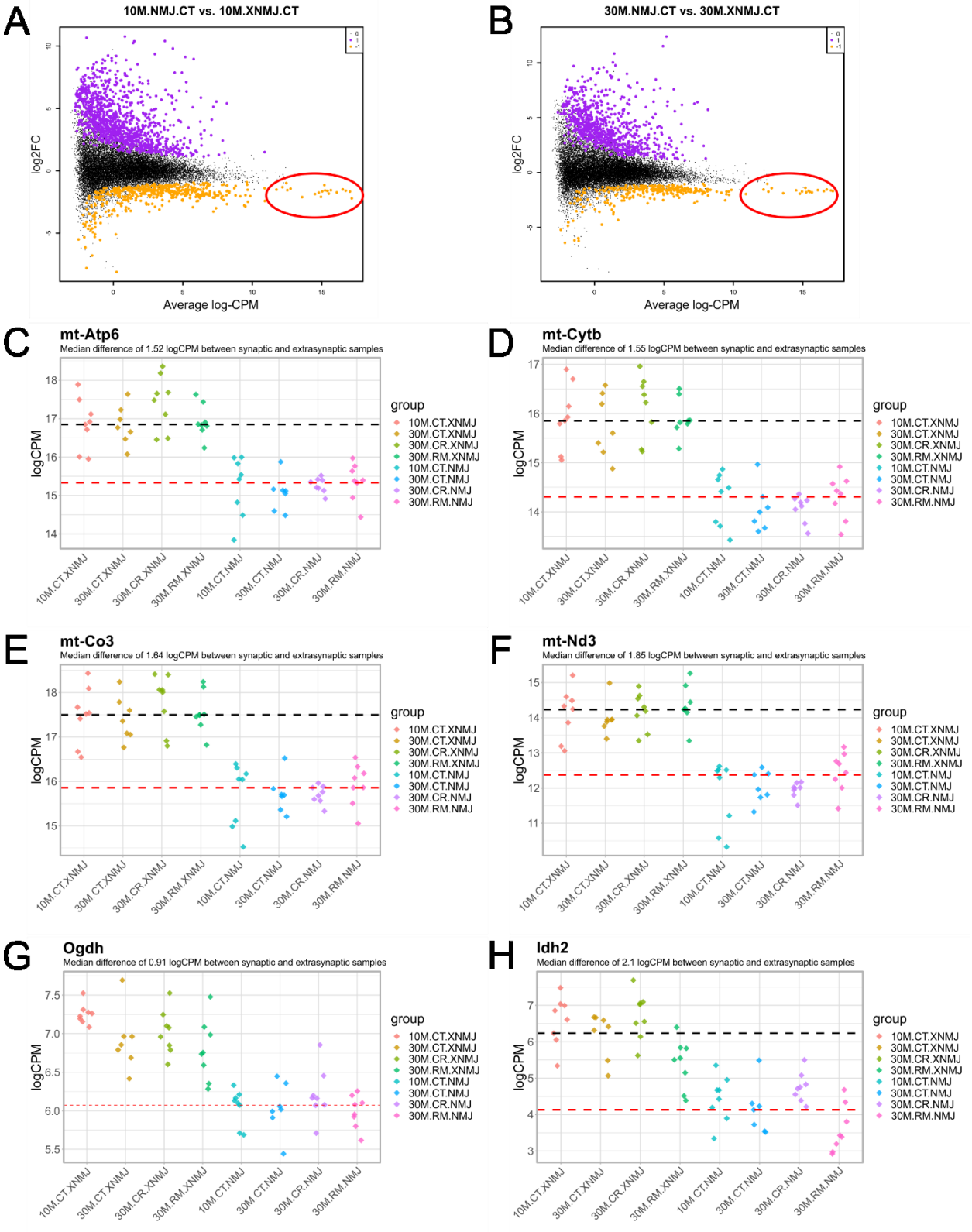
A
10M.NMJ.CT vs. 10M.XNMJ.CT
log2FC
Average log-CPM
B
30M.NMJ.CT vs. 30M.XNMJ.CT
log2FC
Average log-CPM
C
mt-Atp6
Median difference of 1.52 logCPM between synaptic and extrasynaptic samples
logCPM
D
mt-Cytb
Median difference of 1.55 logCPM between synaptic and extrasynaptic samples
logCPM
E
mt-Co3
Median difference of 1.64 logCPM between synaptic and extrasynaptic samples
logCPM
F
mt-Nd3
Median difference of 1.85 logCPM between synaptic and extrasynaptic samples
logCPM
G
Ogdh
Median difference of 0.91 logCPM between synaptic and extrasynaptic samples
logCPM
H
Idh2
Median difference of 2.1 logCPM between synaptic and extrasynaptic samples
logCPM
group
10M.CT.XNMJ
30M.CT.XNMJ
30M.CR.XNMJ
30M.RM.XNMJ
10M.CT.NMJ
30M.CT.NMJ
30M.CR.NMJ
30M.RM.NMJ

Figure 6-6. Reduced expression of mitochondrially encoded electron transport chain and Krebs cycle components at the NMJ. A, B) Mean-difference plots showing log2 fold changes (log2FC) of genes on the Y-axis plotted against the average gene expression strength in log2 counts per million (log-CPM) on the X-axis. Each black dot represents an expressed gene in the study (legend "0"). Differentially expressed genes (FDR p-value < 0.05) with a positive fold change are marked in purple (legend "1"), while genes with a negative fold change are marked in orange (legend "-1"). The red circles mark mitochondrially encoded genes, which are synaptically decreased in both young and old samples, but are among the genes with the strongest expression in the dataset. **A)** Synaptic vs. extrasynaptic 10-month-old control. **B)** Synaptic vs. extrasynaptic 30-month-old control. **C-H)** Gene expression in log2 counts per million (logCPM) of individual genes across all experimental groups is shown. The two dashed lines show the median expression value either of all synaptic samples (red) or of all extrasynaptic samples (black), irrespective of age and condition. The median difference in logCPM is given in the plot subtitles. Groups: **10M.NMJ.CT**, 10-month control, synaptic; **10M.XNMJ.CT**, 10-month control, extrasynaptic; **30M.NMJ.CT**, 30-month control, synaptic; **30M.XNMJ.CT**, 30-month control, extrasynaptic. **30M.NMJ.RM**, 30-month rapamycin-treated, synaptic; **30M.XNMJ.RM**, 30-month rapamycin-treated, extrasynaptic; **30M.NMJ.CT**, 30-month control, synaptic; **30M.NMJ.CR**, 30-month caloric restriction-treated, synaptic; **30M.XNMJ.CR**, 30-month caloric restriction-treated, extrasynaptic.

6.4 References

Aldunate, R., J. C. Casar, E. Brandan and N. C. Inestrosa (2004). "Structural and functional organization of synaptic acetylcholinesterase." Brain Res Brain Res Rev **47**(1-3): 96-104.

Armstrong, R. B., P. Marum, P. Tullson and C. W. t. Saubert (1979). "Acute hypertrophic response of skeletal muscle to removal of synergists." J Appl Physiol Respir Environ Exerc Physiol **46**(4): 835-842.

Baar, K. and K. Esser (1999). "Phosphorylation of p70(S6k) correlates with increased skeletal muscle mass following resistance exercise." Am J Physiol **276**(1): C120-127.

Bak, L. K., A. Schousboe and H. S. Waagepetersen (2006). "The glutamate/GABA-glutamine cycle: aspects of transport, neurotransmitter homeostasis and ammonia transfer." J Neurochem **98**(3): 641-653.

Bamman, M. M., B. M. Roberts and G. R. Adams (2018). "Molecular Regulation of Exercise-Induced Muscle Fiber Hypertrophy." Cold Spring Harb Perspect Med **8**(6).

Baribault, H. (2016). "Mouse Models of Type 2 Diabetes Mellitus in Drug Discovery." Methods Mol Biol **1438**: 153-175.

Barres, R., J. Yan, B. Egan, J. T. Treebak, M. Rasmussen, T. Fritz, K. Caidahl, A. Krook, D. J. O'Gorman and J. R. Zierath (2012). "Acute exercise remodels promoter methylation in human skeletal muscle." Cell Metab **15**(3): 405-411.

Belaya, K., S. Finlayson, C. R. Slater, J. Cossins, W. W. Liu, S. Maxwell, S. J. McGowan, S. Maslau, S. R. Twigg, T. J. Walls, S. I. Pascual Pascual, J. Palace and D. Beeson (2012). "Mutations in DPAGT1 cause a limb-girdle congenital myasthenic syndrome with tubular aggregates." Am J Hum Genet **91**(1): 193-201.

Brook, M. S., D. J. Wilkinson, W. K. Mitchell, J. N. Lund, B. E. Phillips, N. J. Szewczyk, P. L. Greenhaff, K. Smith and P. J. Atherton (2016). "Synchronous deficits in cumulative muscle

protein synthesis and ribosomal biogenesis underlie age-related anabolic resistance to exercise in humans." J Physiol **594**(24): 7399-7417.

Brown, M. R., P. G. Sullivan and J. W. Geddes (2006). "Synaptic mitochondria are more susceptible to Ca2+overload than nonsynaptic mitochondria." J Biol Chem **281**(17): 11658-11668.

Buenrostro, J. D., P. G. Giresi, L. C. Zaba, H. Y. Chang and W. J. Greenleaf (2013). "Transposition of native chromatin for fast and sensitive epigenomic profiling of open chromatin, DNA-binding proteins and nucleosome position." Nat Methods **10**(12): 1213-1218.

Bulfield, G., W. G. Siller, P. A. Wight and K. J. Moore (1984). "X chromosome-linked muscular dystrophy (mdx) in the mouse." Proc Natl Acad Sci U S A **81**(4): 1189-1192.

Burkholder, T. J. (2007). "Mechanotransduction in skeletal muscle." Front Biosci **12**: 174-191.

Call, J. A., J. N. McKeehen, S. A. Novotny and D. A. Lowe (2010). "Progressive resistance voluntary wheel running in the mdx mouse." Muscle Nerve **42**(6): 871-880.

Damas, F., S. M. Phillips, C. A. Libardi, F. C. Vechin, M. E. Lixandrao, P. R. Jannig, L. A. Costa, A. V. Bacurau, T. Snijders, G. Parise, V. Tricoli, H. Roschel and C. Ugrinowitsch (2016). "Resistance training-induced changes in integrated myofibrillar protein synthesis are related to hypertrophy only after attenuation of muscle damage." J Physiol **594**(18): 5209-5222.

Dani, N., M. Nahm, S. Lee and K. Broadie (2012). "A targeted glycan-related gene screen reveals heparan sulfate proteoglycan sulfation regulates WNT and BMP trans-synaptic signaling." PLoS Genet **8**(11): e1003031.

David, G. and E. F. Barrett (2003). "Mitochondrial Ca2+ uptake prevents desynchronization of quantal release and minimizes depletion during repetitive stimulation of mouse motor nerve terminals." J Physiol **548**(Pt 2): 425-438.

Denzer, A. J., R. Brandenberger, M. Gesemann, M. Chiquet and M. A. Ruegg (1997). "Agrin binds to the nerve-muscle basal lamina via laminin." J Cell Biol **137**(3): 671-683.

Endo, T. (2005). "Aberrant glycosylation of alpha-dystroglycan and congenital muscular dystrophies." Acta Myol **24**(2): 64-69.

Ervasti, J. M. and K. P. Campbell (1993). "A role for the dystrophin-glycoprotein complex as a transmembrane linker between laminin and actin." J Cell Biol **122**(4): 809-823.

Goodman, C. A., T. A. Hornberger and A. G. Robling (2015). "Bone and skeletal muscle: Key players in mechanotransduction and potential overlapping mechanisms." Bone **80**: 24-36.

Graham, L. C., S. L. Eaton, P. J. Brunton, A. Atrih, C. Smith, D. J. Lamont, T. H. Gillingwater, G. Pennetta, P. Skehel and T. M. Wishart (2017). "Proteomic profiling of neuronal mitochondria reveals modulators of synaptic architecture." Mol Neurodegener **12**(1): 77.

Grewal, P. K. and J. E. Hewitt (2003). "Glycosylation defects: a new mechanism for muscular dystrophy?" Hum Mol Genet **12 Spec No 2**: R259-264.

Hornberger, T. A., Jr. and R. P. Farrar (2004). "Physiological hypertrophy of the FHL muscle following 8 weeks of progressive resistance exercise in the rat." Can J Appl Physiol **29**(1): 16-31.

Issop, Y., D. Hathazi, M. M. Khan, R. Rudolf, J. Weis, S. Spendiff, C. R. Slater, A. Roos and H. Lochmuller (2018). "GFPT1 deficiency in muscle leads to myasthenia and myopathy in mice." Hum Mol Genet **27**(18): 3218-3232.

Ketterer, C., U. Zeiger, M. T. Budak, N. A. Rubinstein and T. S. Khurana (2010). "Identification of the neuromuscular junction transcriptome of extraocular muscle by laser capture microdissection." Invest Ophthalmol Vis Sci **51**(9): 4589-4599.

Kirby, T. J., J. D. Lee, J. H. England, T. Chaillou, K. A. Esser and J. J. McCarthy (2015). "Blunted hypertrophic response in aged skeletal muscle is associated with decreased ribosome biogenesis." J Appl Physiol (1985) **119**(4): 321-327.

Kirby, T. J., R. M. Patel, T. S. McClintock, E. E. Dupont-Versteegden, C. A. Peterson and J. J. McCarthy (2016). "Myonuclear transcription is responsive to mechanical load and DNA content but uncoupled from cell size during hypertrophy." Mol Biol Cell **27**(5): 788-798.

Konhilas, J. P., U. Widegren, D. L. Allen, A. C. Paul, A. Cleary and L. A. Leinwand (2005). "Loaded wheel running and muscle adaptation in the mouse." Am J Physiol Heart Circ Physiol **289**(1): H455-465.

Kruger, K., D. K. Gessner, M. Seimetz, J. Banisch, R. Ringseis, K. Eder, N. Weissmann and F. C. Mooren (2013). "Functional and muscular adaptations in an experimental model for isometric strength training in mice." PLoS One **8**(11): e79069.

Kuznetsov, A. V., W. S. Kunz, V. Saks, Y. Usson, J. P. Mazat, T. Letellier, F. N. Gellerich and R. Margreiter (2003). "Cryopreservation of mitochondria and mitochondrial function in cardiac and skeletal muscle fibers." Anal Biochem **319**(2): 296-303.

Lach-Trifilieff, E., G. C. Minetti, K. Sheppard, C. Ibebunjo, J. N. Feige, S. Hartmann, S. Brachat, H. Rivet, C. Koelbing, F. Morvan, S. Hatakeyama and D. J. Glass (2014). "An antibody blocking activin type II receptors induces strong skeletal muscle hypertrophy and protects from atrophy." Mol Cell Biol **34**(4): 606-618.

Lai, J. C., J. M. Walsh, S. C. Dennis and J. B. Clark (1977). "Synaptic and non-synaptic mitochondria from rat brain: isolation and characterization." J Neurochem **28**(3): 625-631.

Lee, C. W. and H. B. Peng (2006). "Mitochondrial clustering at the vertebrate neuromuscular junction during presynaptic differentiation." J Neurobiol **66**(6): 522-536.

Legerlotz, K., B. Elliott, B. Guillemin and H. K. Smith (2008). "Voluntary resistance running wheel activity pattern and skeletal muscle growth in rats." Exp Physiol **93**(6): 754-762.

Li, L., W. C. Xiong and L. Mei (2018). "Neuromuscular Junction Formation, Aging, and Disorders." Annu Rev Physiol **80**: 159-188.

Li, R., J. Xia, X. I. Zhang, W. G. Gathirua-Mwangi, J. Guo, Y. Li, S. McKenzie and Y. Song (2018). "Associations of Muscle Mass and Strength with All-Cause Mortality among US Older Adults." Med Sci Sports Exerc **50**(3): 458-467.

Li, Y., Y. Lee and W. J. Thompson (2011). "Changes in aging mouse neuromuscular junctions are explained by degeneration and regeneration of muscle fiber segments at the synapse." J Neurosci **31**(42): 14910-14919.

Liu, M., D. W. Hammers, E. R. Barton and H. L. Sweeney (2016). "Activin Receptor Type IIB Inhibition Improves Muscle Phenotype and Function in a Mouse Model of Spinal Muscular Atrophy." PLoS One **11**(11): e0166803.

Lixandrao, M. E., C. Ugrinowitsch, R. Berton, F. C. Vechin, M. S. Conceicao, F. Damas, C. A. Libardi and H. Roschel (2018). "Magnitude of Muscle Strength and Mass Adaptations Between High-Load Resistance Training Versus Low-Load Resistance Training Associated with Blood-Flow Restriction: A Systematic Review and Meta-Analysis." Sports Med **48**(2): 361-378.

Lu, Z., H. S. Je, P. Young, J. Gross, B. Lu and G. Feng (2007). "Regulation of synaptic growth and maturation by a synapse-associated E3 ubiquitin ligase at the neuromuscular junction." J Cell Biol **177**(6): 1077-1089.

Ly, C. V. and P. Verstreken (2006). "Mitochondria at the synapse." Neuroscientist **12**(4): 291-299.

Meissner, A., A. Gnirke, G. W. Bell, B. Ramsahoye, E. S. Lander and R. Jaenisch (2005). "Reduced representation bisulfite sequencing for comparative high-resolution DNA methylation analysis." Nucleic Acids Res **33**(18): 5868-5877.

Miller, W. J., W. M. Sherman and J. L. Ivy (1984). "Effect of strength training on glucose tolerance and post-glucose insulin response." Med Sci Sports Exerc **16**(6): 539-543.

Morvan, F., J. M. Rondeau, C. Zou, G. Minetti, C. Scheufler, M. Scharenberg, C. Jacobi, P. Brebbia, V. Ritter, G. Toussaint, C. Koelbing, X. Leber, A. Schilb, F. Witte, S. Lehmann, E. Koch, S. Geisse, D. J. Glass and E. Lach-Trifilieff (2017). "Blockade of activin type II receptors with a dual anti-ActRIIA/IIB antibody is critical to promote maximal skeletal muscle hypertrophy." Proc Natl Acad Sci U S A **114**(47): 12448-12453.

Nelson, M. E., M. A. Fiatarone, C. M. Morganti, I. Trice, R. A. Greenberg and W. J. Evans (1994). "Effects of high-intensity strength training on multiple risk factors for osteoporotic fractures. A randomized controlled trial." JAMA **272**(24): 1909-1914.

Newman, A. B., V. Kupelian, M. Visser, E. M. Simonsick, B. H. Goodpaster, S. B. Kritchevsky, F. A. Tylavsky, S. M. Rubin and T. B. Harris (2006). "Strength, but not muscle mass, is associated with mortality in the health, aging and body composition study cohort." J Gerontol A Biol Sci Med Sci **61**(1): 72-77.

Raue, U., T. A. Trappe, S. T. Estrem, H. R. Qian, L. M. Helvering, R. C. Smith and S. Trappe (2012). "Transcriptome signature of resistance exercise adaptations: mixed muscle and fiber type specific profiles in young and old adults." J Appl Physiol (1985) **112**(10): 1625-1636.

Roemers, P., P. N. Mazzola, P. P. De Deyn, W. J. Bossers, M. J. G. van Heuvelen and E. A. van der Zee (2018). "Burrowing as a novel voluntary strength training method for mice: A comparison of various voluntary strength or resistance exercise methods." J Neurosci Methods **300**: 112-126.

Schoenfeld, B. J. (2012). "Does exercise-induced muscle damage play a role in skeletal muscle hypertrophy?" J Strength Cond Res **26**(5): 1441-1453.

Schoenfeld, B. J., B. Contreras, J. Krieger, J. Grgic, K. Delcastillo, R. Belliard and A. Alto (2019). "Resistance Training Volume Enhances Muscle Hypertrophy but Not Strength in Trained Men." Med Sci Sports Exerc **51**(1): 94-103.

Schoenfeld, B. J., J. Grgic, D. Ogborn and J. W. Krieger (2017). "Strength and Hypertrophy Adaptations Between Low- vs. High-Load Resistance Training: A Systematic Review and Meta-analysis." J Strength Cond Res **31**(12): 3508-3523.

Senderek, J., J. S. Muller, M. Dusl, T. M. Strom, V. Guergueltcheva, I. Diepolder, S. H. Laval, S. Maxwell, J. Cossins, S. Krause, N. Muelas, J. J. Vilchez, J. Colomer, C. J. Mallebrera, A. Nascimento, S. Nafissi, A. Kariminejad, Y. Nilipour, B. Bozorgmehr, H. Najmabadi, C. Rodolico, J. P. Sieb, O. K. Steinlein, B. Schlotter, B. Schoser, J. Kirschner, R. Herrmann, T. Voit, A. Oldfors, C. Lindbergh, A. Urtizberea, M. von der Hagen, A. Hubner, J. Palace, K. Bushby, V. Straub, D.

Beeson, A. Abicht and H. Lochmuller (2011). "Hexosamine biosynthetic pathway mutations cause neuromuscular transmission defect." Am J Hum Genet **88**(2): 162-172.

Soffe, Z., H. G. Radley-Crabb, C. McMahon, M. D. Grounds and T. Shavlakadze (2016). "Effects of loaded voluntary wheel exercise on performance and muscle hypertrophy in young and old male C57Bl/6J mice." Scand J Med Sci Sports **26**(2): 172-188.

Strickland, J. C., J. M. Abel, R. T. Lacy, J. S. Beckmann, M. A. Witte, W. J. Lynch and M. A. Smith (2016). "The effects of resistance exercise on cocaine self-administration, muscle hypertrophy, and BDNF expression in the nucleus accumbens." Drug Alcohol Depend **163**: 186-194.

Talts, J. F., Z. Andac, W. Gohring, A. Brancaccio and R. Timpl (1999). "Binding of the G domains of laminin alpha1 and alpha2 chains and perlecan to heparin, sulfatides, alpha-dystroglycan and several extracellular matrix proteins." EMBO J **18**(4): 863-870.

Tang, J. E., J. G. Perco, D. R. Moore, S. B. Wilkinson and S. M. Phillips (2008). "Resistance training alters the response of fed state mixed muscle protein synthesis in young men." Am J Physiol Regul Integr Comp Physiol **294**(1): R172-178.

Terzis, G., G. Georgiadis, G. Stratakos, I. Vogiatzis, S. Kavouras, P. Manta, H. Mascher and E. Blomstrand (2008). "Resistance exercise-induced increase in muscle mass correlates with p70S6 kinase phosphorylation in human subjects." Eur J Appl Physiol **102**(2): 145-152.

Thalacker-Mercer, A., M. Stec, X. Cui, J. Cross, S. Windham and M. Bamman (2013). "Cluster analysis reveals differential transcript profiles associated with resistance training-induced human skeletal muscle hypertrophy." Physiol Genomics **45**(12): 499-507.

Vallejo-Illarramendi, A., I. Toral-Ojeda, G. Aldanondo and A. Lopez de Munain (2014). "Dysregulation of calcium homeostasis in muscular dystrophies." Expert Rev Mol Med **16**: e16.

Vos, M., E. Lauwers and P. Verstreken (2010). "Synaptic mitochondria in synaptic transmission and organization of vesicle pools in health and disease." Front Synaptic Neurosci **2**: 139.

Yamaguchi, Y. (2002). "Glycobiology of the synapse: the role of glycans in the formation, maturation, and modulation of synapses." Biochim Biophys Acta **1573**(3): 369-376.

Yang, F., X. P. He, J. Russell and B. Lu (2003). "Ca2+ influx-independent synaptic potentiation mediated by mitochondrial Na(+)-Ca2+ exchanger and protein kinase C." J Cell Biol **163**(3): 511-523.

Zoltowska, K., R. Webster, S. Finlayson, S. Maxwell, J. Cossins, J. Muller, H. Lochmuller and D. Beeson (2013). "Mutations in GFPT1 that underlie limb-girdle congenital myasthenic syndrome result in reduced cell-surface expression of muscle AChR." Hum Mol Genet **22**(14): 2905-2913.

7 Appendices

7.1 Appendix A: Pharmacological targeting of exercise adaptations in skeletal muscle: Benefits and pitfalls

Biochemical Pharmacology 147 (2018) 211–220

Contents lists available at ScienceDirect

Biochemical Pharmacology

journal homepage: www.elsevier.com/locate/biochempharm

Commentary

Pharmacological targeting of exercise adaptations in skeletal muscle: Benefits and pitfalls

Martin Weihrauch, Christoph Handschin *

Biozentrum, University of Basel, Basel, Switzerland

ARTICLE INFO

Article history:
Received 15 September 2017
Accepted 18 October 2017
Available online 20 October 2017

Chemical compounds:
AICAR (PubChem CID 266934)
Metformin (PubChem CID 4091)
MK-8722 (PubChem CID not available)
PF-739 (PubChem CID not available)
R419 (PubChem CID not available)
Cpd14 (PubChem CID not available)
GW501516 (PubChem CID 9803963)
Rapamycin (PubChem CID 5284616)
SR-18292 (PubChem CID not available)
β-Hydroxy β-methylbutyric acid (HMB) (PubChem CID 69362)
Creatine (PubChem CID 586)
Citrulline malate (PubChem CID 162762)
L-citrulline (PubChem CID 9750)
Scriptaid (PubChem CID 5186)

Keywords:
Exercise
Skeletal muscle
AMPK
mTOR
PPARβ/δ
PGC-1α
Dietary supplements
Exercise mimetics

ABSTRACT

Exercise exerts significant effects on the prevention and treatment of many diseases. However, even though some of the key regulators of training adaptation in skeletal muscle have been identified, this biological program is still poorly understood. Accordingly, exercise-based pharmacological interventions for many muscle wasting diseases and also for pathologies that are triggered by a sedentary lifestyle remain scarce. The most efficacious compounds that induce muscle hypertrophy or endurance are hampered by severe side effects and are classified as doping. In contrast, dietary supplements with a higher safety margin exert milder outcomes. In recent years, the design of pharmacological agents that activate the training program, so-called "exercise mimetics", has been proposed, although the feasibility of such an approach is highly debated. In this review, the most recent insights into key regulatory factors and therapeutic approaches aimed at leveraging exercise adaptations are discussed.

Contents

Abbreviations: 1 RM, one repetition maximum; CM, citrulline malate; Cr, creatine; EE, endurance exercise; HIT, high intensity training; HMB, β-hydroxy-β-methylbutyric acid; MELAS, maternally inherited mitochondrial encephalomyopathy, lactic acidosis, and stroke-like episodes syndrome; PCr, phosphocreatine; RE, resistance exercise; T2DM, type 2 diabetes mellitus.

* Corresponding author.
E-mail address: christoph.handschin@unibas.ch (C. Handschin).

https://doi.org/10.1016/j.bcp.2017.10.006
0006-2952/

1. Introduction

Physical activity is one of the most efficient, (cost-)effective and accessible treatments for obesity and other diseases [1]. Endurance exercise (EE) and resistance exercise (RE) significantly ameliorate the symptoms of various chronic pathologies, e.g. by reducing inflammation and insulin resistance, bolstering mood and general well-being, lowering stress levels and even positively influencing cognitive function [1]. Many of these systemic effects are mediated by signaling molecules that are produced and secreted by skeletal muscle in response to exercise [2]. Skeletal muscle is a remarkably malleable tissue capable of responding to physical and metabolic demands, which makes skeletal muscle an attractive target for pharmacological interventions to mimic exercise in order to enhance performance and ameliorate diseases. Generally speaking, EE training leads to increased mitochondrial content and thus oxidative capacity, while RE training elicits changes in size and contractile properties of muscle fibers [3]. Some studies indicate that a combination of both modes of exercise may confer synergistic benefits [4] while others suggest that concurrent EE and RE may interfere with each other. Depending on the amount and modality of concurrent EE with RE, EE could hamper the hypertrophic response of the body to RE via the so-called "exercise interference" effect [5].

Increased mitochondrial content, fatty acid oxidation and capillary density facilitating oxygen exchange and nutrient uptake of EE-trained muscle fibers collectively provide adequate oxygen and substrate supply as well as the enzymatic capacity needed for aerobic energy production in times of elevated demand. Traditionally, prolonged sessions of EE have mostly been used to induce beneficial adaptations, while alternative training modalities have emerged in recent years [6]. In high intensity training (HIT) featuring exercise bouts of higher intensity but significantly shorter duration, similar or even better adaptations in mitochondrial content and capillary density compared to moderate-intensity continuous training (MICT) were achieved [7], presumably by inducing a stronger stimulus to recruit more muscle fibers. In contrast to the potent effect on exercise adaptations, some evidence suggests that HIT may be less effective than prolonged training in a disease-context [8], while other data indicate an enhanced effectiveness in pathological situations [9].

RE leads to an increased myofiber size and elicits changes in the abundance of contractile and metabolic proteins of the exercised muscles [10]. RE triggers the accretion of protein in the growing myofiber, a process thought to be largely governed by the mammalian target of rapamycin (mTOR) [3]. RE may also increase proliferation of muscle stem cells, called satellite cells, which fuse with and thus donate their myonuclei to the growing myofibers to maintain equal myonuclear domains.

1.1. Mechanistic aspects of exercise-induced skeletal muscle adaptation

Even though the mechanisms underlying the plastic changes of skeletal muscle after exercise are far from being fully understood, several important regulators were identified. In this section, some key aspects of these regulators are summarized, including their potential for pharmacological modulation in diseases (Fig. 1).

1.2. Peroxisome proliferator-activated receptor-γ (PPARγ) coactivator 1α (PGC-1α)

PGC-1α was originally identified in brown adipose tissue (BAT) as a coactivator of PPARγ [11]. However, PGC-1α is expressed in all tissues that are rich in mitochondria and show high oxidative capacity, including the heart, brain, kidney and skeletal muscle [11]. In all of these tissues, PGC-1α is pivotal in regulating a plethora of biological responses related to glucose and fatty acid metabolism, most of which are functionally linked to the potent effect on mitochondrial biogenesis [11]. In addition, PGC-1α controls tissue-specific programs, e.g. a fiber-type switching in skeletal muscle, thermogenesis in BAT or gluconeogenesis in the liver. Thus, for almost two decades since its discovery, PGC-1α has been recognized as a powerful regulator of cellular energy metabolism and mitochondrial capacity in health and disease [12].

In skeletal muscle, PGC-1α is highly inducible by acute and chronic EE training in rodents [13] and humans [14], where it orchestrates many of the adaptations to exercise like increased oxidative metabolism or vascularization [15]. PGC-1α interacts with and activates a number of transcription factor partners and therefore serves as a pleiotropic modulator of a multitude of pathways, ultimately leading to an endurance-trained phenotype [15,16]. Due to this effect, PGC-1α constitutes an attractive drug target [17], however with several hurdles and pitfalls that have to be overcome. In most tissues, the physiological regulation of PGC-1α results in transient bursts of expression, while constitutive elevation, in particular at supraphysiological levels, might lead to a detrimental outcome. For example, constitutive, postnatal cardiac overexpression of PGC-1α leads to exacerbated mitochondrial biogenesis in cardiomyocytes and consequently to heart failure [18]. In a different study using an inducible mouse model where PGC-1α expression was elevated for several weeks in the heart, the development of reversible cardiomyopathy with abnormal mitochondrial ultrastructure was observed [19]. Moreover, skeletal muscle-specific transgenic animals with supraphysiological PGC-1α expression exhibited a myopathic phenotype [20,21]. In contrast, sustained elevation of PGC-1α at physiological levels in skeletal muscle leads to a variety of beneficial effects resembling the adaptation of EE [20]. Such transgenic overexpression

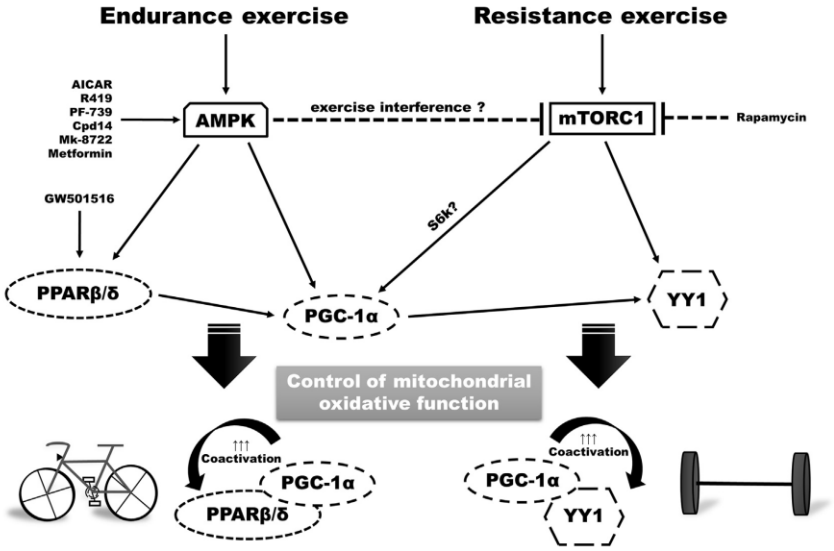

Fig. 1. Different exercise modalities and pharmacological compounds modulate mitochondrial function. Endurance exercise leads to the activation of AMPK and consequently to increased coactivation of PPARβ/δ by PGC-1α, resulting in improved mitochondrial oxidative function. Different pharmacological compounds may activate this pathway even in absence of endurance exercise and at least partially confer endurance performance benefits. Resistance exercise activates mTORC1 and increases coactivation of YY1 by PGC-1α, presumably via phosphorylation of S6K (ribosomal protein S6 kinase). This also affects mitochondrial function. Rapamycin and other pharmacologic inhibitors of mTORC1, but also exercise interference can blunt this response. Exercise interference is a controversially discussed mechanism by which concurrent endurance exercise may negatively impact adaptations to resistance exercise by decreasing mTORC1 activity. AICAR, R419, Cpd14, Mk-8722, PF-739 and Metformin are (potential) pharmacologic AMPK activators. GW501516 is a known pharmacologic PPARβ/δ activator. Arrows indicate activation, dashed lines indicate inhibition.

of PGC-1α in muscle entails a switch towards oxidative type IIa, and to a lesser extent, type I muscle fibers with elevated expression of mitochondrial markers, boosted mitochondrial number and size as well as improved fatigue resistance [20]. In addition, in several muscle wasting conditions such as denervation, hind limb unloading and even in Duchenne Muscular Dystrophy (DMD), elevation of muscle PGC-1α reduces muscle atrophy and improves muscle function [22]. However, this mouse line also exhibits signs of pathology in specific contexts, e.g. when exposed to a high fat diet [23] and curiously, a reduced number of satellite cells, even though this reduction is not linked to an impaired regenerative capacity [17]. Tissue selectivity in pharmacological modulation of PGC-1α might have to be aimed for, e.g. in the treatment of type 2 diabetes mellitus (T2DM). T2DM is a chronic metabolic disorder characterized by insulin resistance, hyperglycemia and insulin deficiency. Behavioral, environmental, as well as genetic factors play a role in the development of the disease. A combination of physical activity, dietary interventions and medication has been the weapon of choice in combatting T2DM [24]. In T2DM, PGC-1α levels are heterogeneously dysregulated in various tissues, for example constitutively elevated in the liver [25] and pancreas [26], but at the same time decreased in skeletal muscle [27]. The increased activity of PGC-1α in the liver stimulates gluconeogenesis [25] contributing to insulin resistance, while in the pancreas, this coactivator suppresses insulin secretion [26] and thus promotes insulin deficiency. The decreased levels of PGC-1α in diabetic skeletal muscle lead to reduced oxidative phosphorylation, diminished glucose transporter 4 (GLUT4) expression and ultimately to glucose intolerance [28] as skeletal muscle normally accounts for the majority of insulin-stimulated glucose uptake, storage and utilization [29]. A therapeutic approach aimed at normalizing PGC-1α levels would thus increase skeletal muscle PGC-1α activity, while concomitantly inhibiting PGC-1α in liver and pancreas. While the tissue-specific regulation and effects of PGC-1α are still poorly understood, the selective coactivation of transcription factor binding partners in different cell types could potentially be leveraged for this purpose. For example, PGC-1α coactivates the hepatic nuclear factor-4α (HNF-4α) in the control of hepatic gluconeogenesis [25]. Since this interaction is preferentially observed in the liver and not skeletal muscle or other tissues that lack substantial HNF-4α expression, selective inhibitors of the PGC-1α-HNF-4α interaction could constitute a feasible strategy to counteract excessive glucose production in T2DM [25]. Unfortunately, compounds that block or enhance the coactivation of specific transcription factors by PGC-1α are still rare. Proof-of-concept for a therapeutical approach to reduce PGC-1α activity in the liver of T2DM mice was demonstrated in a recent screening study, in which a compound, SR-18292, was identified to increase acetylation of PGC-1α, thereby reducing the coactivation of HNF-4α and ultimately the expression of the gluconeogenic genes phosphoenolpyruvate carboxykinase 1 (*PCK1*) and glucose-6-phosphatase catalytic (*G6PC*) in the liver (Fig. 2) [30]. Treatment with SR-18292 resulted in diminished hepatic glucose production and thereby ameliorated the diabetic phenotype of these animals. However, since acetylation as a mechanism of regulation of PGC-1α activity is observed in different tissues including skeletal muscle [31], treatment with a non-tissue selective deacetylation inhibitor could potentially lead to unwanted side effects. Thus, pharmacological modulation of PGC-1α would optimally have to be achieved in a temporally and spatially controlled manner within a therapeutic window to avoid detrimental outcomes of insufficient and exacerbated PGC-1α levels [22] (Fig. 3).

Muscle PGC-1α is a target of the myocyte enhancer factor-2/histone deacetylase (MEF2/HDAC) regulatory pathway, which is

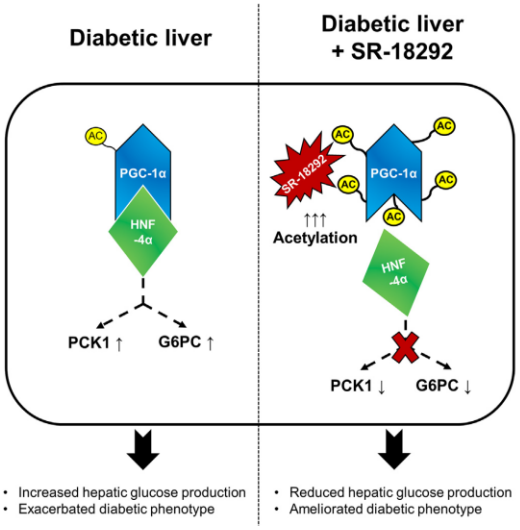

Fig. 2. Pharmacological modulation of PGC-1α acetylation affects the interaction with transcription factor binding partners. PGC-1α expression is increased in the diabetic liver, where it interacts with and coactivates HNF-4α to boost expression levels of the gluconeogenic genes PCK1 and G6PC. The result is increased hepatic glucose production that negatively affects the diabetic phenotype. The compound SR-18292 reduces the interaction between PGC-1α and HNF-4α by increasing PGC-1α acetylation, resulting in lower PCK1 and G6PC levels, reduced hepatic glucose production, and thus amelioration of the diabetic phenotype. SR-18292, as well as similar compounds modifying hepatic PGC-1α-HNF-4α interactions, could therefore prove to be effective treatment options in T2DM.

largely in control of mitochondrial function [32,33]. Class I-specific HDAC inhibitors accordingly increase PGC-1α expression in cultured myotubes, leading to augmented mitochondrial biogenesis and oxygen consumption [34]. Class IIa HDACs can repress gene expression in skeletal muscle via interaction with MEF2 transcription factors, forming a corepressor complex [35]. In a recent study, Gaur et al. (2016) identified a class IIa HDAC inhibitor, called Scriptaid, which, when chronically administered to mice, induced exercise-like systemic and skeletal muscle-specific metabolic adaptations [36]. Furthermore, Scriptaid invoked positive cardiac effects and enhanced muscle insulin action in diet-induced obese mice [37].

Finally, even though overexpression of PGC-1α seems sufficient to induce most plastic changes related to endurance training, muscle-specific loss-of-function of PGC-1α animal models still exhibit some exercise adaptations, indicating potential redundancies in the regulation of these extremely physiologically relevant pathways. Thus, the involvement of PGC-1α in the control of this complex biological program most likely is highly specific in terms of spatial and temporal control of a complicated transcriptional network [15].

1.3. Peroxisome proliferator-activated receptor β/δ (PPARβ/δ)

PPARβ/δ is a nuclear receptor encoded by the *PPARD* gene and is the PPAR isoform with the highest expression in skeletal muscle [38]. Upon binding of fatty acids and other ligands, PPARs become transcriptionally active, heterodimerize with retinoid X receptors (RXR), and recruit coactivators and histone acetyltransferase (HAT) complexes to stimulate the expression of target genes. Inversely, PPARs can also inhibit gene expression by assembling corepressors and histone deacetylases (HDAC) [39]. PPARβ/δ activity plays a key role in the regulation of a wide variety of metabolic processes, but has also been implicated in the development of chronic diseases such as obesity, atherosclerosis, diabetes and cancer [40]. The switch towards oxidative muscle fibers triggered by PPARβ/δ and the concomitant switch of fuel source from glucose to fatty acids [41] can at least in part be explained by the epistasis with PGC-1α. PPARβ/δ not only is an upstream regulator of PGC-1α,

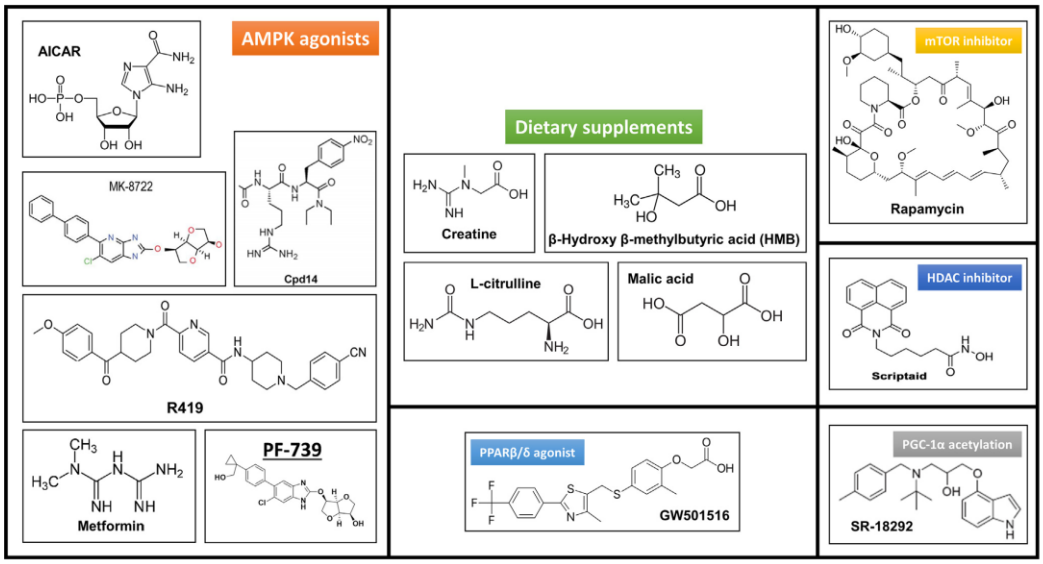

Fig. 3. Chemical structures of the compounds discussed in this review.

but also a transcription factor binding partner [42], even though PGC-1α function is not dependent on PPARβ/δ [43].

Based on its effect on skeletal muscle and the presence of a well-characterized ligand-binding domain, PPARβ/δ is an interesting pharmacological target for muscular and metabolic diseases. GW501516, better known as Cardarine[1] or Endurobol[2] amongst performance-seeking athletes,[3] is a well-characterized PPARβ/δ agonist with promising effects on skeletal muscle, yet it is an example of a failed "exercise mimetic". In mice, GW501516, either when combined with exercise or at higher doses by itself, induces some hallmarks of EE adaptation such as mitochondrial biogenesis, fatty acid oxidation, an oxidative fiber-type switch and improved insulin sensitivity via AMP-activated protein kinase (AMPK) [41]. GW501516 has also been proposed as a treatment for DMD by stimulating the expression of utrophin A and restoring sarcolemmal integrity in mature *mdx* mice (an X chromosome-linked mouse mutant that exhibits histological lesions characteristic of muscular dystrophy) [44]. To its detriment however, tumorigenic effects of GW501516 have been reported and development was discontinued by Glaxo in Phase II clinical trials [45]. Despite these important issues, GW501516/Cardarine/Endurobol is openly available on the black market and its side effects are deceptively downplayed.[1,2,3] Accordingly, the World Anti-Doping Agency (WADA) has issued an unusual warning about its toxicity to athletes looking for potential performance enhancements.[4]

1.4. AMP-activated protein kinase (AMPK)

AMPK is a known upstream regulator of skeletal muscle PGC-1α and is involved in the initiation of mitochondrial biogenesis [46]. AMPK serves as a sensor of cellular energy levels as it is activated by a low ATP to AMP ratio, low glucose or glycogen [47]. Once activated, AMPK promotes processes to rectify this dysbalance, e.g. by enhancing glucose transport and fatty acid oxidation through GLUT4 transport to the sarcolemma [48] and inhibition of acetyl-CoA carboxylase [49], respectively. Importantly, AMPK was shown to be indispensable for the activation of PGC-1α and calcium/calmodulin-dependent protein kinase type IV (CaMKIV) in response to chronic energy deprivation [46]. Accordingly, pharmacological activation of AMPK by 5-aminoimidazole-4-carboxamide ribonucleotide (AICAR) improved endurance capacity in mice by over 40% [50]. However, as part of the catabolic program controlled by AMPK, AICAR also increases the expression of E3 ligases and thereby promotes protein degradation [51]. Therefore, it is unclear whether a beneficial outcome can be achieved in humans with acceptable side effects caused by a signaling pathway that primarily activates catabolic processes [52]. Like GW501516, AICAR has been banned by WADA and added to the list of prohibited substances in sports[5]. In addition to AICAR, several other AMPK-activating compounds have recently been discovered e.g. R419, Cpd14, MK-8722, and PF-739. The pan-AMPK activator MK-8722 has recently been tested in different animal models and even though an improvement in glucose homeostasis was observed, the concomitant cardiac hypertrophy would be highly troubling, particularly for athletes [53]. PF-739, a close analog of MK-8722, was concurrently discovered in an independent fashion. PF-739, a closely related analog of MK-8722, activates skeletal muscle AMPK and lowers blood glucose levels in preclinical studies independent of hepatic AMPK activation [54]. R419 is a compound that was found to inhibit mitochondrial complex I and to acutely activate AMPK [55]. Thereby, R419 improves exercise capacity and skeletal muscle insulin sensitivity, at least in obese mice [56]. Cpd14 is capable of blocking *de novo* purine biosynthesis by inhibiting the enzyme aminoimidazole carboxamide ribonucleotide transformylase/inosine monophosphate cyclohydrolase (ATIC). This leads to increased levels of endogenous AICAR (also known as ZMP), which then activates AMPK. Treatment with Cpd14 may thus serve as another therapeutic strategy against metabolic disorders [57].

1.5. Mammalian target of rapamycin (mTOR)

The mTOR signaling pathway plays a central regulatory role in many cellular processes and is implicated in a large number of pathological conditions and diseases [58]. mTOR is a highly conserved serine/threonine protein kinase that forms two structurally and functionally distinct complexes: mTOR Complex 1 (mTORC1), which governs anabolic processes such as protein synthesis in response to nutrients or RE, and mTOR Complex 2 (mTORC2), which controls many other cellular processes and has recently been shown to regulate muscle glucose uptake during EE [59]. Not surprising based on the activation by RE, mTORC1 signaling plays a fundamental role in the hypertrophic response of skeletal muscle [3]. mTORC1 also influences mitochondrial function by regulating mitochondrial oxygen consumption and oxidative capacity through the cooperative modulation of the activity of the transcription factor yin-yang 1 (YY1) together with PGC-1α [60]. At the moment, rapamycin and rapalogs are the only clinically approved pharmacological mTOR modulators used for immunosuppressive and cancer treatment [61]. Experimentally, rapamycin-induced inhibition of mTORC1 enhances longevity in mice [62]. Interestingly, inhibition of the rapamycin-sensitive mTOR component only partially blunted the activation of muscle protein synthesis and the hypertrophic response following chronic RE [63], suggesting additional rapamycin-insensitive mechanisms to contribute to this exercise response. In genetic models for sustained, skeletal muscle-specific inhibition or activation of mTORC1, pathological consequences were reported [64,65]. It thus is unclear if and how therapeutic effects could be achieved with a pharmacological activator of mTOR.

2. Dietary supplementation in health and disease

As outlined above, pharmacological targeting of known regulators of exercise adaptation in skeletal muscle is still in its infancy. Other compounds with a known effect on muscle size and function include many drugs that are banned as doping and in most cases exhibit inacceptable side effects in non-substitution therapy, such as anabolic steroids or β2-adrenergic receptor agonists. Dietary supplements constitute a third category of substances that are used to boost muscle performance, even though the true efficacy of dietary supplements to improve exercise performance is often highly disputed. Since these types of compounds are not regulated by the FDA, purity and dose often are difficult to estimate in over-the-counter formulations. Nevertheless, we will discuss some of the most sought-after dietary supplements that are prescribed to patients and used by athletes to increase strength, skeletal muscle mass, or overall well-being. The effects of macronutrients, micronutrients (such as vitamins and antioxidants), and nutraceuticals on skeletal muscle mass, metabolism and exercise adaptations are not a focus of this review and will therefore not be covered in detail (see [66] for more details on these aspects).

[1] https://www.evolutionary.org/cardarine-gw-501516-explained (Accessed 07.07.2017).
[2] https://runswimthrowcheat.blogspot.ch/2014/02/gw501516-endurobol-and-doping-whats-all.html (Accessed 14.08.2017).
[3] https://www.steroid.com/Cardarine.php (Accessed 07.07.2017).
[4] https://www.wada-ama.org/en/media/news/2013-03/wada-issues-alert-on-gw501516 (Accessed 07.07.2017).
[5] https://www.wada-ama.org/ (Accessed 07.07.2017).

2.1. Creatine (Cr)

With hundreds of studies over the last decades, Cr is one of the most studied dietary supplements that is readily available on the market, inexpensive and routinely used by recreational and professional athletes. Cr is a naturally occurring amine that is synthesized endogenously by the liver, pancreas and kidney from the amino acids glycine, methionine and arginine at a rate of roughly 2 g per day [67], or taken up in the diet, mostly found in meat and wild fish (Cr uptake of <5 g/day). Cr enters muscle cells against a concentration gradient via the Cr transporter (CreaT) [68]. The majority of Cr content in the body is found in skeletal muscle (>90%) and lower amounts are found in the testicles, brain and bones [67].

Oral Cr supplementation can increase muscular Cr levels by up to 20%, which correspondingly leads to an increase in the mean phosphocreatine (PCr)/inorganic phosphate ratio in the skeletal muscle [69,70]. PCr anaerobically donates a phosphate group to ADP to form ATP during the first 10 s of an intense muscular effort. ATP can be resynthesized a dozen times faster from PCr compared to oxidative phosphorylation and almost a hundred times faster compared to *de novo* pathways [71]. Increased muscular PCr levels upon oral Cr supplementation thus may increase exercise performance. Cr supplementation could also improve recovery by reducing muscle cell damage and inflammation following exhaustive exercise, as shown in finishers of a 30 km race [72].

Oral Cr supplementation also improved heavy RE performance in various studies, presumably by enabling higher quality training sessions (enhanced average lifting volume per session) [73]. Overall increases in fat-free mass and measures of strength, such as squat and bench press performance, were observed [73]. The observed boost in fat-free mass and strength was linked to an elevated intracellular water content and cell swelling, which in itself could serve as an anabolic stimulus [74,75]. Short-term Cr supplementation modulated transcript and protein levels of genes and kinases involved in osmosensing, protein and glycogen synthesis, satellite cell proliferation and other signal transduction pathways [74]. Accordingly, it is thought that at least some of the weight gain associated with Cr supplementation is due to increased total body water retention and not necessarily muscle mass [75]. The average boost in muscle strength when combining RE with Cr ingestion compared to a placebo was reported to be around 8% [76]. However, the response to Cr supplementation is highly variable in different individuals [76], which may explain the contradictory results found in some studies where Cr supplementation showed no effect on RE performance or the anabolic response [77]. Importantly, at a rate of 2–3 g/day of oral Cr supplementation, it may take up to one month before muscle tissue is fully saturated and Cr levels reach a plateau (roughly 20% over normal Cr levels). Studies should therefore consider employing a "loading phase", where 20 g/day of Cr is supplemented for 6 days to ensure saturation. Increased muscular Cr levels can then be maintained via continued Cr ingestion of 2 g/day after reaching this plateau [70].

2.1.1. Creatine in duchenne muscular dystrophy

DMD is a genetic disorder characterized by progressive muscle degeneration and weakness caused by the absence of *Dystrophin*, a structural protein that contributes to protection from mechanical stress [78]. Oral Cr supplementation of 5 g/day for 8 weeks significantly increased the mean PCr/inorganic phosphate ratio in young boys suffering from DMD [69]. Patients reported a subjective improvement by Cr supplementation compared to placebo and their muscle strength was preserved, at least in the short term. However, the study provided no evidence for a long-term effect of the treatment [69]. In another study, four months of Cr supplementation led to an increase in fat-free mass and grip strength, as well as to a reduction in a marker of bone breakdown in boys affected by DMD [79]. Several other studies provide further evidence for a positive effect of Cr supplementation on bone mineral density, especially when combined with exercise or increased locomotion [80–82]. Furthermore, it has been reported that Cr improves mitochondrial function and prevents calcium buildup in a mouse model for DMD (*mdx* mice) [83]. As oral Cr is generally well-tolerated, supplementation strategies may provide symptomatic relief for patients affected by muscular dystrophies such as Duchenne and Becker Muscular Dystrophy, a milder form of DMD.

2.1.2. Creatine in type 2 diabetes mellitus

When combined with an exercise program, Cr supplementation (5 g/day) improves glycemic control in T2DM patients, most likely due to an increase in recruitment of GLUT4 to the sarcolemma [84]. Notably, Cr supplementation in combination with exercise also enhanced glucose metabolism by the same GLUT4-dependent mechanism in an immobilization/rehabilitation study [85]. It is important to stress that participants of studies that failed to combine Cr supplementation with exercise showed no improvements in insulin sensitivity and glucose tolerance, despite an elevated muscle Cr content [86]. Interestingly, increased muscle glycogen storage was observed, yet GLUT4 mRNA and protein content remained unchanged [86]. Collectively, the current research suggests that Cr supplementation, normally well-tolerated, could be a tool for ameliorating T2DM, but only when combined with exercise. This poses a limitation on its use for the treatment of obese and elderly individuals, where sufficient levels of physical exertion might not be achieved, thus rendering Cr supplementation potentially ineffective.

2.2. Citrulline malate and L-citrulline

The amino acid ornithine merges with carbamoyl phosphate, forming the amino acid citrulline in the urea cycle [87]. Citrulline, in particular when supplemented orally, accelerates ammonia clearance, which accumulates in working muscles during exercise, and thereby ameliorates fatigue [88]. Malate is an organic salt often used as a food preservative and as a supplement, the effect of malate aims at improving the stability of citrulline by a direct interaction. Citrulline malate (CM) mitigates the build-up of excess lactate, acidosis and hyperammonemia in the blood [89]. Even though accumulation of lactate and the acidosis resulting from the associated protons might not be involved in causing muscle fatigue as previously proposed [90], accumulation of ammonia is a less ambiguous fatigue factor due to the inhibitory effect on cellular energy processes. A single dose of CM (8 g) has been shown to increase levels of arginine and ornithine in the body, improve exercise performance and reduce muscle soreness 24–48 h post RE [91], indicating that CM could elicit ergogenic effects. Moreover, CM allowed for significantly more repetitions in the later sets (4 or more sets) of intense RE, where muscular fatigue, and not strength itself becomes the limiting factor. This increase in total repetitions leads to an enhanced effective training volume and may thus contribute to a better training stimulus. In a recent study, however, acute CM supplementation (12 g) did not improve the repeated high-intensity cycling performance or time-to-exhaustion of well-trained males [92]. Interestingly, oral L-citrulline supplementation reduced completion time of a cycling trial by 1.5% in healthy trained men compared to placebo controls and increased plasma L-arginine levels [93]. L-citrulline significantly improved the subjective perception of concentration and muscle fatigue immediately after exercise [93]. Therefore, whether acute CM (or L-citrulline alone) supplementation increases work capacity in high-intensity anaerobic exercise with short rest times

remains debatable. Chronic CM supplementation over 15 days (6 g/day) enhanced skeletal muscle power output and lead to a lower pH-to-power ratio, eliciting improved oxidative energy turnover [94]. Unfortunately, only a few long-term studies investigating the ergogenic effects of continuous CM supplementation on exercise adaptations have been conducted so far and further research in this area is required. However, despite research literature being inconclusive and sparse, CM supplementation enjoys a huge popularity amongst strength and endurance athletes and has been coined the "Fatigue Fighter" in popular online media[6].

2.2.1. Citrulline and mitochondrial diseases

Citrulline and the amino acid arginine are nitric oxide (NO) precursors. Of note, oral L-citrulline supplementation leads to a greater boost in arginine levels than arginine supplementation itself [95]. A deficiency in NO plays a major role in the maternally inherited mitochondrial encephalomyopathy, lactic acidosis, and stroke-like episodes syndrome (MELAS) [96]. This mitochondrial disorder is believed to result from several interacting mechanisms, including microvasculature angiopathy and impaired mitochondrial energy production [96]. Children with MELAS have lower arginine and citrulline flux, plasma arginine, and NO production [97]. L-Citrulline supplementation increases all of these parameters [97]. Thus, long-term studies investigating the role of NO precursors like L-citrulline in the treatment of mitochondrial diseases should be conducted to explore their therapeutic potential.

2.3. β-Hydroxy-β-methylbutyric acid (HMB)

HMB is a metabolite derived from leucine and its ketoacid α-ketoisocaproate. Much like Cr, HMB is naturally biosynthesized in humans and is a popular dietary supplement with the potential to increase lean body mass, muscular strength and size, reduce skeletal muscle damage, and enhance speed of recovery post-exercise [98]. A daily dose of 3 g of HMB helps to maintain or even gain muscle mass and was deemed relatively safe in the long-term, even though safety in a disease context has been questioned [99]. HMB (3 g/day over 6 weeks of daily training and supplementation) has been used successfully to reduce muscular damage in young endurance athletes measured by a reduction in circulating creatine kinase (CK) and lactate dehydrogenase (LDH) after a 20 km run [100]. Furthermore, acute pre-exercise HMB free acid-supplementation (3 g) improved markers of exercise-induced damage in RE-trained men [98]. In RE, acute HMB supplementation also improved the perceived recovery status of participants, implying that pre-exercise HMB supplementation might be a good strategy to improve training frequency due to quicker recovery from exercise bouts. However, 9 weeks of 3 g/day HMB coupled with RE training had a negligible effect on overall body composition of RE-trained men, but substantially increased lower-body strength measures (9.1% leg extension 1 RM increase) [101]. Thus, despite results suggesting small benefits, the overall effect of HMB on RE is inconclusive.

2.3.1. HMB in fiber atrophy pathologies

In the context of disease, HMB most prominently ameliorates proteolysis and leads to increased lean body mass in patients, e.g. in cancer/AIDS-related cachexia, immobilization, sepsis and steroid medication (reviewed in [102]). Furthermore, 12 weeks [103] or even 1 year [104] of daily HMB supplementation (1.5–5 g per day) counteracted sarcopenia in elderly people by increasing muscle mass, at least in combination with Arginine (Arg) and/or Lysine (Lys). However, strength increases were only observed when the HMB/Arg/Lys-cocktail was supplemented with Vitamin D, indicating a synergistic effect [104].

In conclusion, HMB supplementation shows beneficial effects in healthy, exercising subjects, in certain diseases where proteolysis occurs, and in the elderly, especially when combined with other nutrients such as Arg, Lys, and Vitamin D.

3. Exercise mimetics as a novel approach

Since the efficacy of existing drugs, supplements and nutraceuticals in muscle diseases remains small, novel therapeutic avenues are considered to remedy the situation of skeletal muscle to constitute one of the most undermedicated organs. In recent years, the concept of designing "exercise mimetics", pharmacological compounds that recapitulate the many beneficial effects of EE and/or RE, has been proposed [50]. However, this concept is highly controversial and the "exercise mimetics" that have been tested so far predominantly remain in the experimental stage in rodents, with little evidence of feasibility and efficacy in humans [52]. Indeed, the pleiotropic effects of exercise in muscle and other organs are difficult to reconcile with the consequences that can be elicited by a single compound, thoroughly discussed in an excellent review by Booth and Laye [105]. Importantly, in contrast to the high safety of *bona fide* exercise, even drugs with limited beneficial effects on physical performance entail considerable adverse effects, such as in the case of erythropoietin [106]. The use and abuse of anabolic steroids in an effort to increase muscle mass, aesthetics, and muscular strength, while being extremely effective [107], triggers serious side effects, which in the worst case can be lethal [108]. Furthermore, many of the effects of "exercise mimetics" observed in rodents could not be recapitulated in humans, at least to the same extent. For example, the polyphenol resveratrol induces an endurance-trained state with the corresponding metabolic adaptations in mice, but has little or no effect in humans (summarized in [52]). It is currently unclear whether inherent differences between mice and men are responsible for these discrepancies e.g. in absorption, biotransformation and elimination of xenobiotics, the significantly higher metabolic rate of mice, or the extreme difference in life span and hence the aging process. Alternatively, as outlined by Laye and Booth [105], the experimental setting used to test these compounds in rodents might also confound the findings vis-à-vis translation into the human context. In most home cages, mice are in a state of sedentariness, and training interventions might not reflect true exercise, but merely reconstitute the normal activity levels of these rodents in the wild. In other words, the "control" group in rodent studies may be inadequate to capture the normal, basal state of human physiology and therefore result in a divergent outcome in regard to so-called "exercise mimetics".

However, even the concept of a hypothetical "exercise mimetic" for human use could be questioned for many reasons [105]. For example, the human body has evolved to handle periods of strenuous physical activity, yet inadvertently has to compensate with rest and regeneration. This poses a huge challenge, as accurate pharmacological activation of exercise pathways to an adequate amplitude and time is difficult to achieve. Initiating and maintaining a metabolic overdrive for prolonged periods of time could potentially result in dangerous consequences as constant activation of exercise pathways likely induces a chronic catabolic state due to the inhibition of protein synthesis and activation of autophagy, e.g. by activation of AMPK and the ensuing inhibition of mTOR. In the liver, chronic mTORC1 activation could furthermore promote carcinogenesis [109]. Experimentally, skeletal muscle-specific long-term activation of mTORC1 in a transgenic mouse model leads to the development of a severe late-onset myopathy related to impaired autophagy [64]. Inversely, chronic inhibition of mTORC1 activity likewise triggers a myopathic phenotype

[6] https://www.bodybuilding.com/fun/citrulline-malate-the-fatigue-fighter.html (Accessed 07.07.2017).

[65], underlining the importance of adequate exercise and rest/recovery cycles.

One approach to mitigate these side-effects of chronic exercise pathway activation could be personalized, intermittent treatment, replicating the undulating nature of human exercise training. By administering "exercise mimetics" in an on-and-off fashion and thus allowing for sufficient recovery time between interventions, one could potentially reap the benefits in terms of positive adaptations without having to deal with the detrimental effects.

4. Future directions

For the time being, changes in life style that entail physical activity and a balanced diet remain the most effective, affordable, and accessible form of treatment and prevention of chronic diseases [1], however with the caveat of compliance and exercise intolerance in some patients. "Exercise mimetics" remain an intriguing concept, even though a more limited scope might have to be aimed for. Thus, a partial and/or intermittent activation of specific exercise pathways could be a promising approach to prevent and treat individual diseases, in particular in patient populations with a compromised exercise tolerance or a reduced ability to train. Optimally, these types of interventions, either by drugs or dietary supplements, should however be combined with *bona fide* physical activity whenever possible. For example, the paradoxical acceleration of the development of insulin resistance in high fat diet-fed PGC-1α skeletal muscle-specific transgenic animals [23] was reversed by concomitant training [110]. Whatever pharmacological strategy intended for disease treatment will emerge, the potential of misuse as performance-enhancing aids by athletes (or even non-athletes!) exists, paving the road for difficult-to-control doping strategies under the veil of treatment. Nevertheless, these considerations should not negatively influence the development of novel treatment strategies that are needed in muscular dystrophies, sarcopenia, cachexia and other severe pathological contexts for which no therapy exists at the moment.

Acknowledgments

We thank Regula Furrer and Joaquín Pérez-Schindler for comments and suggestions for this manuscript. The work in our laboratory is supported by the Swiss National Science Foundation, the European Research Council (ERC) Consolidator grant 616830-MUSCLE_NET, Swiss Cancer Research grant KFS-3733-08-2015, the Swiss Society for Research on Muscle Diseases (SSEM), SystemsX.ch, the "Novartis Stiftung für Medizinisch-Biologische Forschung" and the University of Basel.

Conflict of interest

The authors have no conflict of interest related to this manuscript.

References

[1] C. Handschin, B.M. Spiegelman, The role of exercise and PGC1alpha in inflammation and chronic disease, Nature 454 (7203) (2008) 463–469.
[2] S. Schnyder, C. Handschin, Skeletal muscle as an endocrine organ: PGC-1alpha, myokines and exercise, Bone 80 (2015) 115–125.
[3] B. Egan, J.R. Zierath, Exercise metabolism and the molecular regulation of skeletal muscle adaptation, Cell Metab. 17 (2) (2013) 162–184.
[4] L. Wang, H. Mascher, N. Psilander, E. Blomstrand, K. Sahlin, Resistance exercise enhances the molecular signaling of mitochondrial biogenesis induced by endurance exercise in human skeletal muscle, J. Appl. Physiol. 111 (5) (1985) 1335–1344 (2011).
[5] V.G. Coffey, J.A. Hawley, Concurrent exercise training: do opposites distract? J. Physiol. 595 (9) (2017) 2883–2896.
[6] G.A. Dudley, W.M. Abraham, R.L. Terjung, Influence of exercise intensity and duration on biochemical adaptations in skeletal muscle, J. Appl. Physiol. Respir. Environ. Exercise Physiol. 53 (4) (1982) 844–850.
[7] M.J. MacInnis, M.J. Gibala, Physiological adaptations to interval training and the role of exercise intensity, J. Physiol. 595 (9) (2017) 2915–2930.
[8] L. Nybo, E. Sundstrup, M.D. Jakobsen, M. Mohr, T. Hornstrup, L. Simonsen, et al., High-intensity training versus traditional exercise interventions for promoting health, Med. Sci. Sports Exerc. 42 (10) (2010) 1951–1958.
[9] Z. Milanovic, G. Sporis, M. Weston, Effectiveness of high-intensity interval training (HIT) and continuous endurance training for VO2max improvements: a systematic review and meta-analysis of controlled trials, Sports Med. 45 (10) (2015) 1469–1481.
[10] F.W. Booth, K.M. Baldwin, Muscle plasticity: energy demand and supply processes, Compr. Physiol. (2011) 1075–1123.
[11] P. Puigserver, Z. Wu, C.W. Park, R. Graves, M. Wright, B.M. Spiegelman, A cold-inducible coactivator of nuclear receptors linked to adaptive thermogenesis, Cell 92 (6) (1998) 829–839.
[12] B.N. Finck, D.P. Kelly, PGC-1 coactivators: inducible regulators of energy metabolism in health and disease, J. Clin. Invest. 116 (3) (2006) 615–622.
[13] K. Baar, A.R. Wende, T.E. Jones, M. Marison, L.A. Nolte, M. Chen, et al., Adaptations of skeletal muscle to exercise: rapid increase in the transcriptional coactivator PGC-1, FASEB J. 16 (14) (2002) 1879–1886.
[14] H. Pilegaard, B. Saltin, P.D. Neufer, Exercise induces transient transcriptional activation of the PGC-1alpha gene in human skeletal muscle, J. Physiol. 546 (Pt 3) (2003) 851–858.
[15] B. Kupr, C. Handschin, Complex Coordination of Cell Plasticity by a PGC-1alpha-controlled Transcriptional Network in Skeletal Muscle, Front. Physiol. 6 (2015) 325.
[16] S. Schnyder, B. Kupr, C. Handschin, Coregulator-mediated control of skeletal muscle plasticity – a mini-review, Biochimie 136 (2017) 49–54.
[17] I. Dinulovic, R. Furrer, M. Beer, A. Ferry, B. Cardel, C. Handschin, Muscle PGC-1alpha modulates satellite cell number and proliferation by remodeling the stem cell niche, Skelet. Muscle 6 (1) (2016) 39.
[18] J.J. Lehman, P.M. Barger, A. Kovacs, J.E. Saffitz, D.M. Medeiros, D.P. Kelly, Peroxisome proliferator-activated receptor gamma coactivator-1 promotes cardiac mitochondrial biogenesis, J. Clin. Invest. 106 (7) (2000) 847–856.
[19] L.K. Russell, C.M. Mansfield, J.J. Lehman, A. Kovacs, M. Courtois, J.E. Saffitz, et al., Cardiac-specific induction of the transcriptional coactivator peroxisome proliferator-activated receptor gamma coactivator-1alpha promotes mitochondrial biogenesis and reversible cardiomyopathy in a developmental stage-dependent manner, Circ. Res. 94 (4) (2004) 525–533.
[20] J. Lin, H. Wu, P.T. Tarr, C.Y. Zhang, Z. Wu, O. Boss, et al., Transcriptional co-activator PGC-1 alpha drives the formation of slow-twitch muscle fibres, Nature 418 (6899) (2002) 797–801.
[21] S. Miura, E. Tomitsuka, Y. Kamei, T. Yamazaki, Y. Kai, M. Tamura, et al., Overexpression of peroxisome proliferator-activated receptor gamma co-activator-1alpha leads to muscle atrophy with depletion of ATP, Am. J. Pathol. 169 (4) (2006) 1129–1139.
[22] C. Handschin, The biology of PGC-1alpha and its therapeutic potential, Trends Pharmacol. Sci. 30 (6) (2009) 322–329.
[23] C.S. Choi, D.E. Befroy, R. Codella, S. Kim, R.M. Reznick, Y.J. Hwang, et al., Paradoxical effects of increased expression of PGC-1alpha on muscle mitochondrial function and insulin-stimulated muscle glucose metabolism, Proc. Natl. Acad. Sci. U.S.A. 105 (50) (2008) 19926–19931.
[24] L. Chen, D.J. Magliano, P.Z. Zimmet, The worldwide epidemiology of type 2 diabetes mellitus–present and future perspectives, Nat. Rev. Endocrinol. 8 (4) (2011) 228–236.
[25] J.C. Yoon, P. Puigserver, G. Chen, J. Donovan, Z. Wu, J. Rhee, et al., Control of hepatic gluconeogenesis through the transcriptional coactivator PGC-1, Nature 413 (6852) (2001) 131–138.
[26] J.C. Yoon, G. Xu, J.T. Deeney, S.N. Yang, J. Rhee, P. Puigserver, et al., Suppression of beta cell energy metabolism and insulin release by PGC-1alpha, Dev. Cell 5 (1) (2003) 73–83.
[27] V.K. Mootha, C.M. Lindgren, K.F. Eriksson, A. Subramanian, S. Sihag, J. Lehar, et al., PGC-1alpha-responsive genes involved in oxidative phosphorylation are coordinately downregulated in human diabetes, Nat. Genet. 34 (3) (2003) 267–273.
[28] M.E. Patti, A.J. Butte, S. Crunkhorn, K. Cusi, R. Berria, S. Kashyap, et al., Coordinated reduction of genes of oxidative metabolism in humans with insulin resistance and diabetes: Potential role of PGC1 and NRF1, Proc. Natl. Acad. Sci. U.S.A. 100 (14) (2003) 8466–8471.
[29] G.I. Shulman, D.L. Rothman, T. Jue, P. Stein, R.A. DeFronzo, R.G. Shulman, Quantitation of muscle glycogen synthesis in normal subjects and subjects with non-insulin-dependent diabetes by 13C nuclear magnetic resonance spectroscopy, N. Engl. J. Med. 322 (4) (1990) 223–228.
[30] K. Sharabi, H. Lin, C.D. Tavares, J.E. Dominy, J.P. Camporez, R.J. Perry, et al., Selective chemical inhibition of PGC-1alpha gluconeogenic activity ameliorates type 2 diabetes, Cell 169 (1) (2017) 148–160. e15.
[31] Z. Gerhart-Hines, J.T. Rodgers, O. Bare, C. Lerin, S.H. Kim, R. Mostoslavsky, et al., Metabolic control of muscle mitochondrial function and fatty acid oxidation through SIRT1/PGC-1alpha, EMBO J. 26 (7) (2007) 1913–1923.
[32] M.P. Czubryt, J. McAnally, G.I. Fishman, E.N. Olson, Regulation of peroxisome proliferator-activated receptor gamma coactivator 1 alpha (PGC-1 alpha) and mitochondrial function by MEF2 and HDAC5, Proc. Natl. Acad. Sci. U.S.A. 100 (4) (2003) 1711–1716.
[33] C. Handschin, J. Rhee, J. Lin, P.T. Tarr, B.M. Spiegelman, An autoregulatory loop controls peroxisome proliferator-activated receptor gamma coactivator 1alpha expression in muscle, Proc. Natl. Acad. Sci. U.S.A. 100 (12) (2003) 7111–7116.

[34] A. Galmozzi, N. Mitro, A. Ferrari, E. Gers, F. Gilardi, C. Godio, et al., Inhibition of class I histone deacetylases unveils a mitochondrial signature and enhances oxidative metabolism in skeletal muscle and adipose tissue, Diabetes 62 (3) (2013) 732–742.
[35] T.A. McKinsey, C.L. Zhang, E.N. Olson, Control of muscle development by dueling HATs and HDACs, Curr. Opin. Genet. Dev. 11 (5) (2001) 497–504.
[36] V. Gaur, T. Connor, A. Sanigorski, S.D. Martin, C.R. Bruce, D.C. Henstridge, et al., Disruption of the class IIa HDAC corepressor complex increases energy expenditure and lipid oxidation, Cell Rep. 16 (11) (2016) 2802–2810.
[37] V. Gaur, T. Connor, K. Venardos, D.C. Henstridge, S.D. Martin, C. Swinton, et al., Scriptaid enhances skeletal muscle insulin action and cardiac function in obese mice, Diabetes Obes. Metab. 19 (7) (2017) 936–943.
[38] X. Yang, M. Downes, R.T. Yu, A.L. Bookout, W. He, M. Straume, et al., Nuclear receptor expression links the circadian clock to metabolism, Cell 126 (4) (2006) 801–810.
[39] Y. Shi, M. Hon, R.M. Evans, The peroxisome proliferator-activated receptor delta, an integrator of transcriptional repression and nuclear receptor signaling, Proc. Natl. Acad. Sci. U.S.A. 99 (5) (2002) 2613–2618.
[40] J.N. Feige, L. Gelman, L. Michalik, B. Desvergne, W. Wahli, From molecular action to physiological outputs: peroxisome proliferator-activated receptors are nuclear receptors at the crossroads of key cellular functions, Prog. Lipid Res. 45 (2) (2006) 120–159.
[41] W. Fan, W. Waizenegger, C.S. Lin, V. Sorrentino, M.X. He, C.E. Wall, et al., PPARdelta promotes running endurance by preserving glucose, Cell Metab. 25 (5) (2017) 1186–1193. e4.
[42] M. Schuler, F. Ali, C. Chambon, D. Duteil, J.M. Bornert, A. Tardivel, et al., PGC1alpha expression is controlled in skeletal muscles by PPARbeta, whose ablation results in fiber-type switching, obesity, and type 2 diabetes, Cell Metab. 4 (5) (2006) 407–414.
[43] J. Perez-Schindler, K. Svensson, E. Vargas-Fernandez, G. Santos, W. Wahli, C. Handschin, The coactivator PGC-1alpha regulates skeletal muscle oxidative metabolism independently of the nuclear receptor PPARbeta/delta in sedentary mice fed a regular chow diet, Diabetologia 57 (11) (2014) 2405–2412.
[44] P. Miura, J.V. Chakkalakal, L. Boudreault, G. Belanger, R.L. Hebert, J.M. Renaud, et al., Pharmacological activation of PPARbeta/delta stimulates utrophin A expression in skeletal muscle fibers and restores sarcolemmal integrity in mature mdx mice, Hum. Mol. Genet. 18 (23) (2009) 4640–4649.
[45] A. Sahebkar, G.T. Chew, G.F. Watts, New peroxisome proliferator-activated receptor agonists: potential treatments for atherogenic dyslipidemia and non-alcoholic fatty liver disease, Expert Opin. Pharmacother. 15 (4) (2014) 493–503.
[46] H. Zong, J.M. Ren, L.H. Young, M. Pypaert, J. Mu, M.J. Birnbaum, et al., AMP kinase is required for mitochondrial biogenesis in skeletal muscle in response to chronic energy deprivation, Proc. Natl. Acad. Sci. U.S.A. 99 (25) (2002) 15983–15987.
[47] D.G. Hardie, D. Carling, The AMP-activated protein kinase–fuel gauge of the mammalian cell? Eur. J. Biochem. 246 (2) (1997) 259–273.
[48] T. Hayashi, M.F. Hirshman, N. Fujii, S.A. Habinowski, L.A. Witters, L.J. Goodyear, Metabolic stress and altered glucose transport: activation of AMP-activated protein kinase as a unifying coupling mechanism, Diabetes 49 (4) (2000) 527–531.
[49] N. Kudo, A.J. Barr, R.L. Barr, S. Desai, G.D. Lopaschuk, High rates of fatty acid oxidation during reperfusion of ischemic hearts are associated with a decrease in malonyl-CoA levels due to an increase in 5'-AMP-activated protein kinase inhibition of acetyl-CoA carboxylase, J. Biol. Chem. 270 (29) (1995) 17513–17520.
[50] V.A. Narkar, M. Downes, R.T. Yu, E. Embler, Y.X. Wang, E. Banayo, et al., AMPK and PPARdelta agonists are exercise mimetics, Cell 134 (3) (2008) 405–415.
[51] K. Nakashima, Y. Yakabe, AMPK activation stimulates myofibrillar protein degradation and expression of atrophy-related ubiquitin ligases by increasing FOXO transcription factors in C2C12 myotubes, Biosci. Biotechnol. Biochem. 71 (7) (2007) 1650–1656.
[52] C. Handschin, Caloric restriction and exercise "mimetics": ready for prime time? Pharmacol. Res. 103 (2016) 158–166.
[53] R.W. Myers, H.P. Guan, J. Ehrhart, A. Petrov, S. Prahalada, E. Tozzo, et al., Systemic pan-AMPK activator MK-8722 improves glucose homeostasis but induces cardiac hypertrophy, Science 357 (6350) (2017) 507–511.
[54] E.C. Cokorinos, J. Delmore, A.R. Reyes, B. Albuquerque, R. Kjobsted, N.O. Jorgensen, et al., Activation of skeletal muscle AMPK promotes glucose disposal and glucose lowering in non-human primates and mice, Cell Metab. 25 (5) (2017) 1147–1159. e10.
[55] Y. Jenkins, T.Q. Sun, V. Markovtsov, M. Foretz, W. Li, H. Nguyen, et al., AMPK activation through mitochondrial regulation results in increased substrate oxidation and improved metabolic parameters in models of diabetes, PLoS One 8 (12) (2013) e81870.
[56] K. Marcinko, A.L. Bujak, J.S. Lally, R.J. Ford, T.H. Wong, B.K. Smith, et al., The AMPK activator R419 improves exercise capacity and skeletal muscle insulin sensitivity in obese mice, Mol. Metab. 4 (9) (2015) 643–651.
[57] D.J. Asby, F. Cuda, M. Beyaert, F.D. Houghton, F.R. Cagampang, A. Tavassoli, AMPK Activation via Modulation of De Novo Purine Biosynthesis with an Inhibitor of ATIC Homodimerization, Chem. Biol. 22 (7) (2015) 838–848.
[58] M. Laplante, D.M. Sabatini, mTOR signaling in growth control and disease, Cell 149 (2) (2012) 274–293.
[59] M. Kleinert, B.L. Parker, A.M. Fritzen, J.R. Knudsen, T.E. Jensen, R. Kjobsted, et al., Mammalian target of rapamycin complex 2 regulates muscle glucose uptake during exercise in mice, J. Physiol. 595 (14) (2017) 4845–4855.
[60] J.T. Cunningham, J.T. Rodgers, D.H. Arlow, F. Vazquez, V.K. Mootha, P. Puigserver, mTOR controls mitochondrial oxidative function through a YY1-PGC-1alpha transcriptional complex, Nature 450 (7170) (2007) 736–740.
[61] J. Li, S.G. Kim, J. Blenis, Rapamycin: one drug, many effects, Cell Metab. 19 (3) (2014) 373–379.
[62] W.R. Swindell, Rapamycin in mice, Aging (Albany NY) 9 (9) (2017) 1941–1942.
[63] R. Ogasawara, S. Fujita, T.A. Hornberger, Y. Kitaoka, Y. Makanae, K. Nakazato, et al., The role of mTOR signalling in the regulation of skeletal muscle mass in a rodent model of resistance exercise, Sci. Rep. 6 (2016) 31142.
[64] P. Castets, S. Lin, N. Rion, S. Di Fulvio, K. Romanino, M. Guridi, et al., Sustained activation of mTORC1 in skeletal muscle inhibits constitutive and starvation-induced autophagy and causes a severe, late-onset myopathy, Cell Metab. 17 (5) (2013) 731–744.
[65] C.F. Bentzinger, K. Romanino, D. Cloetta, S. Lin, J.B. Mascarenhas, F. Oliveri, et al., Skeletal muscle-specific ablation of raptor, but not of rictor, causes metabolic changes and results in muscle dystrophy, Cell Metab. 8 (5) (2008) 411–424.
[66] C.S. Deane, D.J. Wilkinson, B.E. Phillips, K. Smith, T. Etheridge, P.J. Atherton, "Nutraceuticals" in relation to human skeletal muscle and exercise, Am. J. Physiol. Endocrinol. Metab. 312 (4) (2017) E282–E299.
[67] B. Gualano, G.G. Artioli, J.R. Poortmans, A.H. Lancha Jr., Exploring the therapeutic role of creatine supplementation, Amino Acids 38 (1) (2010) 31–44.
[68] S.R. Nash, B. Giros, S.F. Kingsmore, J.M. Rochelle, S.T. Suter, P. Gregor, et al., Cloning, pharmacological characterization, and genomic localization of the human creatine transporter, Recept. Channels 2 (2) (1994) 165–174.
[69] B. Banerjee, U. Sharma, K. Balasubramanian, M. Kalaivani, V. Kalra, N.R. Jagannathan, Effect of creatine monohydrate in improving cellular energetics and muscle strength in ambulatory Duchenne muscular dystrophy patients: a randomized, placebo-controlled 31P MRS study, Magn. Reson. Imaging 28 (5) (2010) 698–707.
[70] E. Hultman, K. Soderlund, J.A. Timmons, G. Cederblad, P.L. Greenhaff, Muscle creatine loading in men, J. Appl. Physiol. 81 (1) (1985) 232–237.
[71] T. Wallimann, M. Wyss, D. Brdiczka, K. Nicolay, H.M. Eppenberger, Intracellular compartmentation, structure and function of creatine kinase isoenzymes in tissues with high and fluctuating energy demands: the 'phosphocreatine circuit' for cellular energy homeostasis, Biochem. J. 281 (Pt 1) (1992) 21–40.
[72] R.V. Santos, R.A. Bassit, E.C. Caperuto, L.F. Costa, Rosa, The effect of creatine supplementation upon inflammatory and muscle soreness markers after a 30 km race, Life Sci. 75 (16) (2004) 1917–1924.
[73] J.S. Volek, N.D. Duncan, S.A. Mazzetti, R.S. Staron, M. Putukian, A.L. Gomez, et al., Performance and muscle fiber adaptations to creatine supplementation and heavy resistance training, Med. Sci. Sports Exerc. 31 (8) (1999) 1147–1156.
[74] A. Safdar, N.J. Yardley, R. Snow, S. Melov, M.A. Tarnopolsky, Global and targeted gene expression and protein content in skeletal muscle of young men following short-term creatine monohydrate supplementation, Physiol. Genomics 32 (2) (2008) 219–228.
[75] M.E. Powers, B.L. Arnold, A.L. Weltman, D.H. Perrin, D. Mistry, D.M. Kahler, et al., Creatine supplementation increases total body water without altering fluid distribution, J. Athletic Train 38 (1) (2003) 44–50.
[76] E.S. Rawson, J.S. Volek, Effects of creatine supplementation and resistance training on muscle strength and weightlifting performance, J. Strength Cond. Res. 17 (4) (2003) 822–831.
[77] M. Louis, J.R. Poortmans, M. Francaux, J. Berre, N. Boisseau, E. Brassine, et al., No effect of creatine supplementation on human myofibrillar and sarcoplasmic protein synthesis after resistance exercise, Am. J. Physiol. Endocrinol. Metab. 285 (5) (2003) E1089–E1094.
[78] K.M. Flanigan, Duchenne and Becker muscular dystrophies, Neurol. Clin. 32 (3) (2014) 671–688. viii.
[79] M.A. Tarnopolsky, D.J. Mahoney, J. Vajsar, C. Rodriguez, T.J. Doherty, B.D. Roy, et al., Creatine monohydrate enhances strength and body composition in Duchenne muscular dystrophy, Neurology 62 (10) (2004) 1771–1777.
[80] M. Louis, J. Lebacq, J.R. Poortmans, M.C. Belpaire-Dethiou, J.P. Devogelaer, P. Van Hecke, et al., Beneficial effects of creatine supplementation in dystrophic patients, Muscle Nerve 27 (5) (2003) 604–610.
[81] P.D. Chilibeck, M.J. Chrusch, K.E. Chad, K. Shawn Davison, D.G. Burke, Creatine monohydrate and resistance training increase bone mineral content and density in older men, J. Nutr. Health Aging 9 (5) (2005) 352–353.
[82] M.J. Chrusch, P.D. Chilibeck, K.E. Chad, K.S. Davison, D.G. Burke, Creatine supplementation combined with resistance training in older men, Med. Sci. Sports Exerc. 33 (12) (2001) 2111–2117.
[83] A.C. Passaquin, M. Renard, L. Kay, C. Challet, A. Mokhtarian, T. Wallimann, et al., Creatine supplementation reduces skeletal muscle degeneration and enhances mitochondrial function in mdx mice, Neuromuscul. Disord. 12 (2) (2002) 174–182.
[84] B. Gualano, V. DE Salles Painneli, H. Roschel, G.G. Artioli, M. Neves Jr., A.L. De Sa Pinto, et al., Creatine in type 2 diabetes: a randomized, double-blind, placebo-controlled trial, Med. Sci. Sports Exerc. 43 (5) (2011) 770–778.

[85] B. Op 't Eijnde, B. Urso, E.A. Richter, P.L. Greenhaff, P. Hespel, Effect of oral creatine supplementation on human muscle GLUT4 protein content after immobilization, Diabetes 50 (1) (2001) 18–23.
[86] L.J. van Loon, R. Murphy, A.M. Oosterlaar, D. Cameron-Smith, M. Hargreaves, A.J. Wagenmakers, et al., Creatine supplementation increases glycogen storage but not GLUT-4 expression in human skeletal muscle, Clin. Sci. (Lond.) 106 (1) (2004) 99–106.
[87] W.R. Fearon, The carbamido diacetyl reaction: a test for citrulline, Biochem. J. 33 (6) (1939) 902–907.
[88] K. Takeda, M. Machida, A. Kohara, N. Omi, T. Takemasa, Effects of citrulline supplementation on fatigue and exercise performance in mice, J. Nutr. Sci. Vitaminol. (Tokyo) 57 (3) (2011) 246–250.
[89] A. Callis, B. Magnan de Bornier, J.J. Serrano, H. Bellet, R. Saumade, Activity of citrulline malate on acid-base balance and blood ammonia and amino acid levels. Study in the animal and in man, Arzneimittelforschung 41 (6) (1991) 660–663.
[90] A.V. Hill, C. Long, H. Lupton, Muscular exercise, lactic acid, and the supply and utilisation of oxygen, Proc. R. Soc. Lond. Ser. B, Containing Papers Biol. Charact. 97 (681) (1924) 84–138.
[91] J. Perez-Guisado, P.M. Jakeman, Citrulline malate enhances athletic anaerobic performance and relieves muscle soreness, J. Strength Cond. Res. 24 (5) (2010) 1215–1222.
[92] B. Cunniffe, M. Papageorgiou, B. O'Brien, N.A. Davies, G.K. Grimble, M. Cardinale, Acute citrulline-malate supplementation and high-intensity cycling performance, J. Strength Cond. Res. 30 (9) (2016) 2638–2647.
[93] T. Suzuki, M. Morita, Y. Kobayashi, A. Kamimura, Oral L-citrulline supplementation enhances cycling time trial performance in healthy trained men: Double-blind randomized placebo-controlled 2-way crossover study, J. Int. Soc. Sports Nutr. 13 (2016) 6.
[94] D. Bendahan, J.P. Mattei, B. Ghattas, S. Confort-Gouny, M.E. Le Guern, P.J. Cozzone, Citrulline/malate promotes aerobic energy production in human exercising muscle, Br. J. Sports Med. 36 (4) (2002) 282–289.
[95] A.W. El-Hattab, J.W. Hsu, L.T. Emrick, L.J. Wong, W.J. Craigen, F. Jahoor, et al., Restoration of impaired nitric oxide production in MELAS syndrome with citrulline and arginine supplementation, Mol. Genet. Metab. 105 (4) (2012) 607–614.
[96] A.W. El-Hattab, A.M. Adesina, J. Jones, F. Scaglia, MELAS syndrome: Clinical manifestations, pathogenesis, and treatment options, Mol. Genet. Metab. 116 (1–2) (2015) 4–12.
[97] A.W. El-Hattab, L.T. Emrick, J.W. Hsu, S. Chanprasert, M. Almannai, W.J. Craigen, et al., Impaired nitric oxide production in children with MELAS syndrome and the effect of arginine and citrulline supplementation, Mol. Genet. Metab. 117 (4) (2016) 407–412.
[98] J.M. Wilson, R.P. Lowery, J.M. Joy, J.A. Walters, S.M. Baier, J.C. Fuller Jr, et al., beta-Hydroxy-beta-methylbutyrate free acid reduces markers of exercise-induced muscle damage and improves recovery in resistance-trained men, Br. J. Nutr. 110 (3) (2013) 538–544.
[99] A. Molfino, G. Gioia, F. Rossi Fanelli, M. Muscaritoli, Beta-hydroxy-beta-methylbutyrate supplementation in health and disease: a systematic review of randomized trials, Amino Acids 45 (6) (2013) 1273–1292.
[100] A.E. Knitter, L. Panton, J.A. Rathmacher, A. Petersen, R. Sharp, Effects of beta-hydroxy-beta-methylbutyrate on muscle damage after a prolonged run, J. Appl. Physiol. 89 (4) (1985) 1340–1344 (2000).
[101] J.S. Thomson, P.E. Watson, D.S. Rowlands, Effects of nine weeks of beta-hydroxy-beta-methylbutyrate supplementation on strength and body composition in resistance trained men, J. Strength Cond. Res. 23 (3) (2009) 827–835.
[102] M. Holecek, Beta-hydroxy-beta-methylbutyrate supplementation and skeletal muscle in healthy and muscle-wasting conditions, J. Cachexia Sarcopenia Muscle 8 (4) (2017) 529–541.
[103] P. Flakoll, R. Sharp, S. Baier, D. Levenhagen, C. Carr, S. Nissen, Effect of beta-hydroxy-beta-methylbutyrate, arginine, and lysine supplementation on strength, functionality, body composition, and protein metabolism in elderly women, Nutrition 20 (5) (2004) 445–451.
[104] J.C. Fuller Jr., S. Baier, P. Flakoll, S.L. Nissen, N.N. Abumrad, J.A. Rathmacher, Vitamin D status affects strength gains in older adults supplemented with a combination of beta-hydroxy-beta-methylbutyrate, arginine, and lysine: a cohort study, JPEN J. Parenter. Enteral Nutr. 35 (6) (2011) 757–762.
[105] F.W. Booth, M.J. Laye, Lack of adequate appreciation of physical exercise's complexities can pre-empt appropriate design and interpretation in scientific discovery, J. Physiol. 587 (Pt 23) (2009) 5527–5539.
[106] G. Singbartl, Adverse events of erythropoietin in long-term and in acute/short-term treatment, Clin. Investig. 72 (6 Suppl) (1994) S36–S43.
[107] F. Hartgens, H. Kuipers, Effects of androgenic-anabolic steroids in athletes, Sports Med. 34 (8) (2004) 513–554.
[108] M.S. Nieminen, M.P. Ramo, M. Viitasalo, P. Heikkila, J. Karjalainen, M. Mantysaari, et al., Serious cardiovascular side effects of large doses of anabolic steroids in weight lifters, Eur. Heart J. 17 (10) (1996) 1576–1583.
[109] S. Menon, J.L. Yecies, H.H. Zhang, J.J. Howell, J. Nicholatos, E. Harputlugil, Chronic activation of mTOR complex 1 is sufficient to cause hepatocellular carcinoma in mice, Sci. Signal 5 (217) (2012). ra24.
[110] S. Summermatter, G. Shui, D. Maag, G. Santos, M.R. Wenk, C. Handschin, PGC-1alpha improves glucose homeostasis in skeletal muscle in an activity-dependent manner, Diabetes 62 (1) (2013) 85–95.

7.2 Appendix B: BDNF is a mediator of glycolytic fiber-type specification in mouse skeletal muscle

Contribution: Martin Weihrauch conducted laser-capture microdissection of neuromuscular junctions (including animal sacrifice, sample preparations and cryosectioning) and qPCR experiments (pertaining to the LCM-samples), wrote the respective materials & methods part of the paper and assisted with tissue collection (brain/cerebellum).

PNAS

BDNF is a mediator of glycolytic fiber-type specification in mouse skeletal muscle

Julien Delezie[a], Martin Weihrauch[a], Geraldine Maier[a], Rocío Tejero[b], Daniel J. Ham[a], Jonathan F. Gill[a], Bettina Karrer-Cardel[a], Markus A. Rüegg[a], Lucía Tabares[b], and Christoph Handschin[a,1]

[a]Biozentrum, University of Basel, CH-4056 Basel, Switzerland; and [b]Department of Medical Physiology and Biophysics, School of Medicine, University of Seville, 41009 Seville, Spain

Edited by Louis M. Kunkel, Boston Children's Hospital, Harvard Medical School, Boston, MA, and approved June 24, 2019 (received for review January 11, 2019)

Brain-derived neurotrophic factor (BDNF) influences the differentiation, plasticity, and survival of central neurons and likewise, affects the development of the neuromuscular system. Besides its neuronal origin, BDNF is also a member of the myokine family. However, the role of skeletal muscle-derived BDNF in regulating neuromuscular physiology in vivo remains unclear. Using gain- and loss-of-function animal models, we show that muscle-specific ablation of BDNF shifts the proportion of muscle fibers from type IIB to IIX, concomitant with elevated slow muscle-type gene expression. Furthermore, BDNF deletion reduces motor end plate volume without affecting neuromuscular junction (NMJ) integrity. These morphological changes are associated with slow muscle function and a greater resistance to contraction-induced fatigue. Conversely, BDNF overexpression promotes a fast muscle-type gene program and elevates glycolytic fiber number. These findings indicate that BDNF is required for fiber-type specification and provide insights into its potential modulation as a therapeutic target in muscle diseases.

neurotrophic factor | myokine | oxidative fiber | neuromuscular junction | endurance exercise

Neurotrophins (NTs) are members of a subfamily of structurally related trophic factors that regulate the differentiation, survival, and function of neuronal cells by modulating the $p75^{NTR}$ receptor and members of the Trk family of receptor tyrosine kinases (1, 2). Besides the central nervous system, skeletal muscle is an abundant source of trophic factors during development (3, 4). In particular, NTs can be released from muscle fibers, acting on the nerve terminals of motor neurons (5, 6), in addition to using retrograde routes to be transported to the cell body (7, 8).

Inactivation or overexpression of NTs in mouse models demonstrates their broad involvement in neuromuscular physiology. For instance, chronic deprivation of the nerve growth factor leads to muscular dystrophy (9). Deficiency in NT-3 or its receptor TrkC decreases proprioceptive afferents and muscle spindles, resulting in severe movement defects (10, 11). Lack of NT-4/5 induces the disassembly of postsynaptic acetylcholine receptor (AChR) clusters in association with neurotransmission failure and decreased fatigue resistance (12).

Similar to these NT family members, the brain-derived neurotrophic factor (BDNF) also exerts diverse roles in the neuromuscular system. For example, BDNF regulates agrin-induced AChR clustering in cultured myotubes (13). Moreover, precursor and mature forms of BDNF influence the survival and innervation pattern of developing motor neurons by modulating both $p75^{NTR}$ and TrkB receptors (8, 14). Accordingly, mice heterozygous for TrkB display altered neuromuscular junction (NMJ) structure and function as well as muscle weakness and sarcopenia (6, 15). In contrast to BDNF of neuronal origin, the role of BDNF in muscle function is much less studied, in part due to controversial BDNF detection in this tissue (16). There is, however, evidence that BDNF is a contraction-induced myokine likely involved in autocrine and/or paracrine regulation of muscle fat metabolism (17). Moreover, specific loss of BDNF within the satellite cell niche affects early stages of the regenerative process after muscle cardiotoxin injury (18). However, no study to date has comprehensively investigated the potential contribution of skeletal muscle-derived BDNF to both muscle and NMJ physiology in the postnatal mouse in vivo.

Using functional, cellular, and molecular approaches, we show that mice lacking BDNF specifically in striated muscle fibers do not exhibit any developmental neuromuscular or metabolic deficits. Intriguingly, we discovered that loss of BDNF within muscle fibers induces structural and functional remodeling of the NMJ toward a slower phenotype. In line, our data indicate that muscle BDNF loss or gain of function is sufficient to decrease or increase, respectively, the proportion of types IIB and IIX muscle fibers along with a broad range of oxidative and glycolytic marker genes.

Results

BDNF Muscle Knockout Mice Show Altered Spontaneous Gait Behavior and Locomotion. To restrict the Cre-induced recombination of the *Bdnf* floxed allele to skeletal muscle cells, we used the human α-skeletal actin (HSA) promoter (19, 20). $Bdnf^{flox/flox}$;HSA-Cre mice (hereafter referred as muscle knockout [MKO]) were born at Mendelian ratios and exhibited an average lifespan comparable with their $Bdnf^{flox/flox}$ control (CTRL) littermates (CTRL: 833.1 ± 38.2 d vs. MKO: 880 ± 31.3 d; $n = 10$ per genotype; not significant).

Significance

The brain-derived neurotrophic factor (BDNF) is essential to promote neuronal differentiation, plasticity, and survival. Altered BDNF expression is associated with several pathologies, including neuropsychiatric and neurodegenerative disorders, cardiovascular diseases, diabetes, and motor neuron diseases. Although BDNF has been identified as a contraction-induced myokine, its involvement in muscle physiology is unclear. Using functional, cellular, and molecular approaches, we report here that the myokine BDNF regulates glycolytic muscle fiber-type identity. Our findings warrant additional studies to determine whether modulating the activity of BDNF represents an effective therapeutic strategy to delay or even prevent muscle wasting disorders in which the function of glycolytic musde fibers is compromised (e.g., in Duchenne muscular dystrophy, muscle insulin resistance).

Author contributions: J.D. and C.H. designed research; J.D., M.W., G.M., R.T., D.J.H., J.F.G., and B.K.-C. performed research; M.A.R. and L.T. contributed new reagents/analytic tools; J.D., R.T., and D.J.H. analyzed data; and J.D. and C.H. wrote the paper.

The authors declare no conflict of interest.

This article is a PNAS Direct Submission.

[1]To whom correspondence may be addressed. Email: christoph.handschin@unibas.ch.

This article contains supporting information online at www.pnas.org/lookup/suppl/doi:10.1073/pnas.1900544116/-/DCSupplemental.

Analysis of *Bdnf* transcript expression in 3-mo-old MKO mice revealed a ≤70% reduction in both oxidative and glycolytic skeletal muscle (Fig. 1*A* and *SI Appendix*, Fig. S1*A*). Interestingly, while *TrkB* levels were not affected by BDNF depletion, other NTs, such as *NT-3* and *NT-4/5*, show increased and decreased transcript expression, respectively, in the glycolytic gastrocnemius (GAS) muscle (*SI Appendix*, Fig. S1*A*). We, however, could not reveal changes in circulating BDNF; the latter was undetectable in mouse serum (*SI Appendix*, Fig. S1*B*) in agreement with previous studies (21, 22). Because BDNF is associated with fatty acid oxidation (17, 23, 24), we evaluated systemic and muscle metabolism of mice lacking muscle BDNF in a broad manner. MKO mice did not show an overt metabolic phenotype in terms of daily food intake (CTRL: 3.43 ± 0.11 g vs. MKO: 3.17 ± 0.26 g; $n = 5$ to 6; not significant), body, lean and fat mass, glucose tolerance, daily body temperature, VO_2 consumption, or energy substrate utilization (respiratory exchange ratio [RER]), which were all not significantly different from CTRL mice (*SI Appendix*, Fig. S1 *C–I*).

In line with unchanged whole-body lean mass, individual weights of different oxidative and glycolytic muscles were indistinguishable in BDNF MKO mice (*SI Appendix*, Fig. S1*E*). Basic histological evaluation of glycolytic tibialis anterior (TA) muscle revealed normal muscle structure (Fig. 1*B*). Using a telemetry system to record spontaneous, in-cage locomotion over a 10-d period, we observed that nighttime general locomotor activity was significantly reduced in MKO mice (Fig. 1*C*). A more detailed characterization of locomotor and gait behavior using the CatWalk XT system indicated that MKO gait velocity was slightly reduced as supported by parameters associated with walking speed (Fig. 1*D*). Overall, these data show that, even though spontaneous locomotion and walking speed are reduced in MKO mice, BDNF deletion is not linked to pathological changes in whole-body metabolism, body composition, and muscle mass and morphology.

Muscle-Specific BDNF Deletion Reduces Motor End Plate Volume in the Extensor Digitorum Longus Muscle. The BDNF-TrkB signaling pathway plays an essential role in the maturation and maintenance of the developing mammalian motor unit (6, 8, 13, 25). We thus investigated whether the locomotor phenotype of MKO mice was associated with NMJ abnormalities. We first evaluated the expression of transcripts playing a key role in the function and maintenance of the neuromuscular synapse and observed a significant reduction of the *Muscle-specific Kinase* (*MuSK*) and its downstream regulator *Docking Protein 7* (*Dok7*) in glycolytic muscles of MKO mice (Fig. 2*A* and *SI Appendix*, Fig. S2*A*). Of note, loss of MuSK abolishes synapse formation in mice (26). However, a closer examination of *MuSK* expression in subsynaptic regions—where it is preferentially expressed at the adult NMJ—did not reveal any significant reduction on BDNF deletion (*SI Appendix*, Fig. S2*A*). Moreover, MuSK protein showed a normal presence at synaptic sites, colocalizing with AChR clusters as in CTRL muscle (*SI Appendix*, Fig. S2*B*). Lastly, transcripts encoding for the α-and ε-AChR subunits were similarly enriched in the synaptic area of both genotypes (*SI Appendix*, Fig. S2*C*), further suggesting that molecules involved in NMJ maintenance are likely present at similar levels in adult MKO vs. CTRL muscles. Incidentally, transcript levels

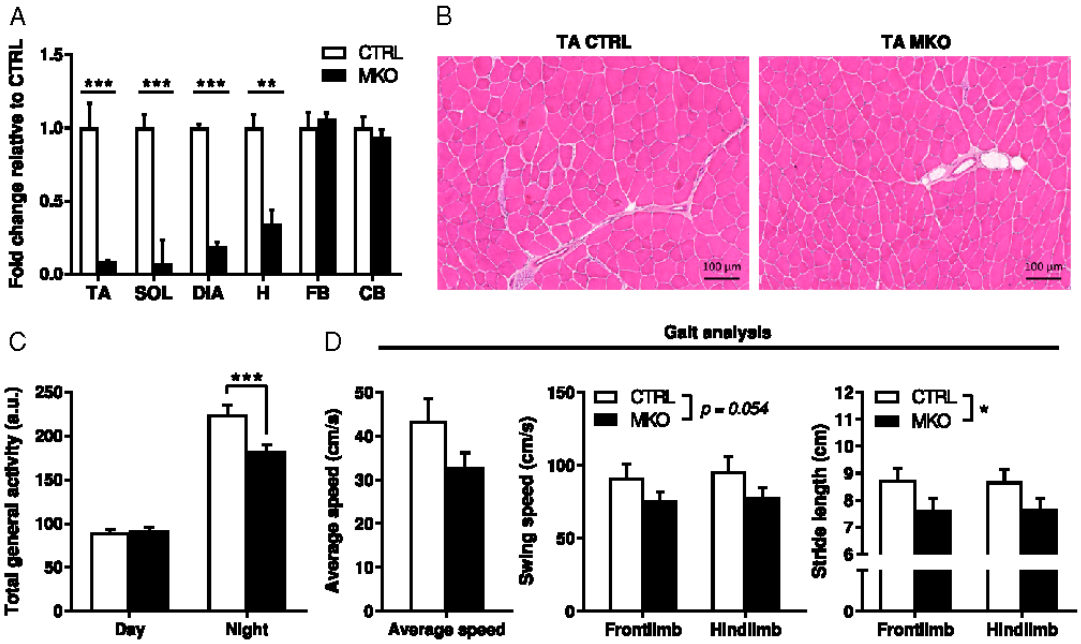

Fig. 1. BDNF MKO mice show altered spontaneous gait behavior and locomotion. (*A*) *Bdnf* gene expression in CTRL and BDNF MKO tissues. Expression values were determined by qPCR and normalized to *Hprt*. Data are shown as the average fold change ± SEM ($n = 3$ to 9 per genotype per tissue) relative to the expression in CTRL set to 1. CB, cerebellum; DIA, diaphragm; FB, forebrain; H, heart. (*B*) Histology of CTRL and MKO TA muscles as determined by hematoxylin and eosin staining. (Scale bar: 100 µm.) (*C*) Total gross locomotor activity ($n = 15$ per genotype, average of a 10-d period) and (*D*) gait locomotor parameters ($n = 8$ per genotype) of CTRL and MKO animals. Results are expressed as mean ± SEM. Unpaired Student's *t* test (*A* and *D*) and 2-way ANOVA followed by Sidak's multiple comparisons (*C* and *D*). $^*P < 0.05$; $^{**}P < 0.01$; $^{***}P < 0.001$.

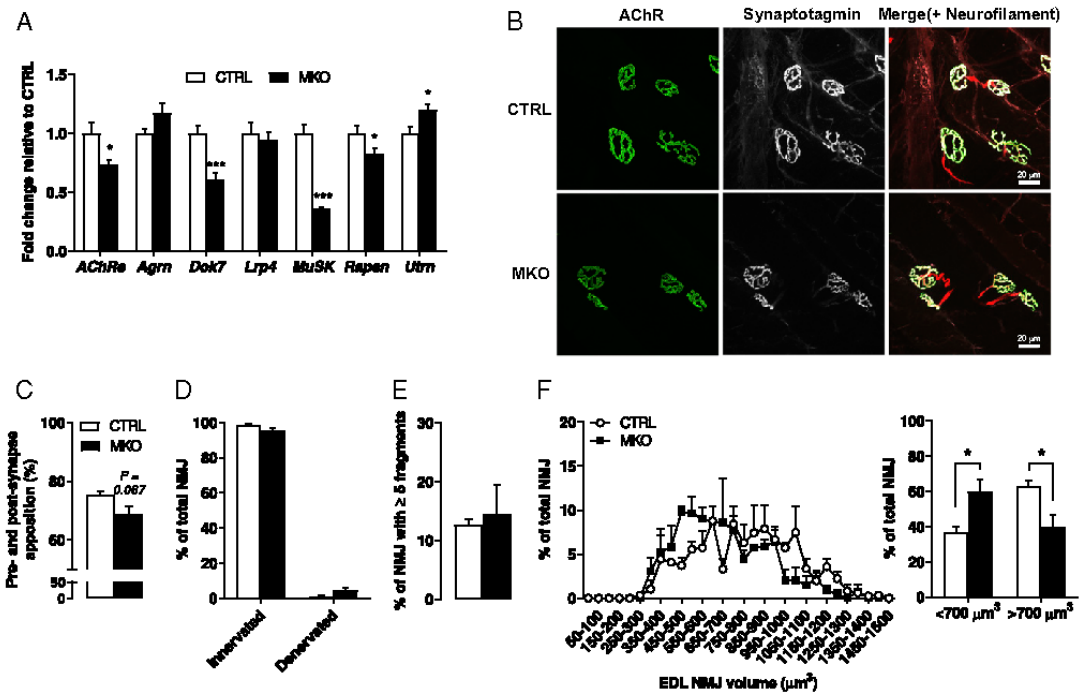

Fig. 2. Muscle-specific BDNF deletion reduces motor end plate size in the EDL muscle. (*A*) Gene expression in CTRL and BDNF MKO GAS muscles. Expression values were determined by qPCR and normalized to *Hprt*. Data are shown as the average fold change ± SEM ($n = 12$ per genotype) relative to the expression in CTRL set to 1. (*B*) Confocal microscopy images illustrating the apposition of both pre- and postsynaptic markers and the motor neuron innervation of EDL NMJs from CTRL and MKO mice. (Scale bar: 20 µm.) Quantification of (*C*) pre- and postsynapse apposition, (*D*) NMJ innervation, and (*E*) NMJ fragmentation. (*F*) NMJ volume distribution from CTRL and MKO EDL muscles (*Materials and Methods* has the number of NMJ analyzed per muscle per genotype). Results are expressed as percentage (mean ± SEM; $n = 4$ per genotype). Unpaired Student's *t* test (*A*, *C*, and *E*) and 2-way ANOVA followed by Sidak's multiple comparisons (*D* and *F*). $^{*}P < 0.05$; $^{***}P < 0.001$.

of *Bdnf* and *TrkB* were not enriched in microdissected synaptic regions of adult CTRL muscles (*SI Appendix*, Fig. S2*D*), hinting at synaptic and extrasynaptic functions of this signaling pathway.

We then examined the morphology of NMJs from the extensor digitorum longus (EDL)—a fast-twitch muscle used in rapid movements of hind limb digits—of CTRL and MKO animals by confocal microscopy. We used synaptotagmin, a synaptic vesicle-associated Ca^{2+} protein, as a presynaptic marker; α-bungarotoxin, a selective and potent ligand for AChR, to visualize the postsynaptic membrane; and an antineurofilament antibody to label motor nerve axons. Knockdown of muscle BDNF did not impair synapse structure in regard to presynaptic–postsynaptic apposition (Fig. 2 *B* and *C*). Similarly, no evidence of increased NMJ fragmentation and denervation was observed in MKO mice, indicating that muscle BDNF is not essential to maintain NMJ integrity (Fig. 2 *D* and *E*). Strikingly, however, lack of muscle BDNF led to a significant reduction of the motor end plate volume (Fig. 2*F*). Importantly, the reduction in NMJ volume was not associated with significant changes in the expression of $p75^{NTR}$ and both full-length and truncated forms of TrkB and TrkC in motor neurons and interneurons that lie in the lumbar portion of the spinal cord (*SI Appendix*, Fig. S2 *E–G*). Moreover, these receptors were not or only poorly detected in the GAS muscle (*SI Appendix*, Fig. S2 *E–G*), in keeping with their low expression levels postdifferentiation (16, 17, 27). In summary, muscle-specific ablation of BDNF does not affect NMJ apposition and integrity but evokes a shift in motor end plate size that is reminiscent of slow-type muscles (28).

Loss of BDNF Promotes Slow Contraction Velocity and Fatigue Resistance. We next assessed whether the morphological and molecular changes in the NMJs of MKO animals had any functional consequences on muscle contractile and fatigue properties and neuromuscular transmission. We first performed in situ measurements of TA muscle function in response to sciatic nerve stimulation. MKO muscles produced similar twitch and tetanic force as their CTRL counterparts (Fig. 3*A*, force frequency curve, and Fig. 3*E*, cross-sectional area [CSA]-normalized maximal twitch and tetanic forces), in line with in vivo measures of grip strength (*SI Appendix*, Fig. S2*J*). In contrast, time-to-peak tension and half-relaxation time were significantly longer in MKO mice (Fig. 3 *B–D*), indicating slower contraction velocities. Next, we studied force production during a fatigue protocol consisting of intermittent 100-Hz tetanic stimulations. After 1 min of repeated stimulation, contraction force started to drop faster in CTRL than in MKO TA muscles and remained lower until the end of the fatigue protocol (Fig. 3*F*). Consistent with fatigue resistance, BDNF knockout muscles recovered significantly faster than CTRL muscles, returning to ~95% of baseline peak force, while CTRL muscles reached ~84% of peak force 3 min after the fatigue protocol (Fig. 3*F*).

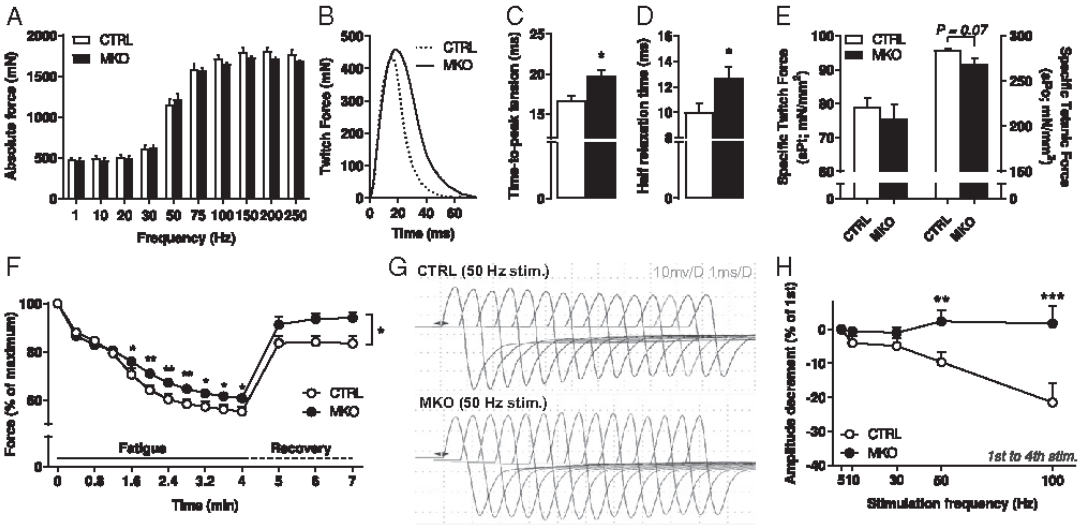

Fig. 3. Lack of BDNF promotes slow muscle contraction and enhances fatigue resistance. (*A*) In situ TA absolute muscle force frequency relationship as evoked by electrical sciatic nerve stimulation from CTRL ($n = 4$) and MKO ($n = 5$) mice. (*B*) Representative traces of twitch force from both genotypes. (*C*) Time-to-peak tension and (*D*) half-relaxation time. (*E*) CSA-normalized maximal twitch and tetanic forces. (*F*) Average curves showing the force decline during a 4-min muscle fatigue protocol and of muscle force recovery up to 3 min after fatigue. (*G*) Representative EMG traces from CTRL (*Upper*) and MKO (*Lower*) GAS muscle on 50-Hz stimulation of the sciatic nerve. (*H*) Average decrement in the amplitude of GAS CMAPs from 1st to 4th stimulation (5- to 50-Hz stimulation: $n = 9$ to 10 per genotype; 100-Hz stimulation: $n = 6$ per genotype). Results are expressed as percentage. Unpaired Student's *t* test (*C*–*E*) and 2-way ANOVA followed by Sidak's multiple comparisons (*A*, *F*, and *H*). $^*P < 0.05$; $^{**}P < 0.01$; $^{***}P < 0.001$.

To complement the in situ nerve–muscle stimulation experiments, we also evaluated in vivo evoked compound muscle action potentials (CMAPs) in the GAS muscle in response to supramaximal repetitive nerve stimulation using electromyography (EMG) as described previously (28). CMAPs did not significantly differ between genotypes over 15 consecutive stimuli at 5, 10, or 30 Hz (Fig. 3*H*). However, we found greater reductions of CMAPs at 50- and 100-Hz stimulation in CTRL than in MKO mice (Fig. 3 *G* and *H* and *SI Appendix*, Fig. S2*I*). Remarkably, while CMAPs dropped by ∼10 and ∼20% at 50- and 100-Hz stimulation, respectively, CMAPs reduction was completely absent after 4 stimulations in MKO mice (Fig. 3*H*). Lastly, to assess whether the changes in muscle contractile properties of MKO mice are associated with altered NMJ functionality, we evaluated both spontaneous and evoked neurotransmitter release using the levator auris longus (LAL)—a fast-twitch neck muscle—as described previously (29). Ex vivo electrophysiological recordings showed that the resting muscle membrane potential and both miniature end plate potential amplitude and frequency remained unaffected by muscle BDNF deletion (*SI Appendix*, Fig. S3 *A* and *B*, representative traces, and Tables S1 and S2). Likewise, there was no significant difference in the average amplitude of evoked neurotransmitter release, quantum content, and time constants between mouse groups (*SI Appendix*, Fig. S3 *C* and *D* and Table S3). Furthermore, short-term plasticity was indistinguishable between LAL NMJ synapses of CTRL vs. MKO animals (*SI Appendix*, Fig. S3 *E* and *F*). Together, these results indicate that glycolytic muscles lacking BDNF exhibit slower contractile properties and higher fatigue resistance in the absence of altered synaptic communication.

BDNF MKO Mice Show Improved Running Capacity. The change in NMJ morphology and the altered contractility in situ and using EMG collectively suggest a higher endurance performance. To test this, we first evaluated spontaneous wheel-running activity in both groups over a 7-d period. MKO mice exhibited a similar increase and overnight distribution of wheel activity as their CTRL littermates (*SI Appendix*, Fig. S4*A*). Because running performance as elicited by forced treadmill differs in many aspects from spontaneous mouse wheel-running activity, we then characterized the running capacity of MKO animals under dynamic treadmill exercise conditions. Untrained mice from both genotypes first performed a forced maximal running capacity test (i.e., $\dot{V}O_{2max}$ test) consisting of a speed increment of 2 m every 2 min at 15° inclination until exhaustion. In this strenuous exercise challenge, both genotypes demonstrated similar energy substrate utilization (RER) during the course of the experiment (*SI Appendix*, Fig. S4*B*). Furthermore, despite slightly higher $\dot{V}O_2$ consumption rates toward the end of the running exercise session, muscle BDNF deletion did not significantly improve maximal aerobic capacity (*SI Appendix*, Fig. S4 *C* and *D*). Moreover, plasma lactate accumulation—a marker of muscle metabolism and fatigue—was similar in both genotypes at exhaustion (*SI Appendix*, Fig. S4*E*). Nevertheless, MKO mice were able to run significantly longer than CTRL mice (713 vs. 519 m; $n = 9$ per genotype; $P = 0.044$) (*SI Appendix*, Fig. S4 *G* and *H*). Incidentally, expression of exercise- and NT-related genes in response to an acute bout of treadmill exercise as described above was similar in the GAS muscle of both mouse genotypes (*SI Appendix*, Fig. S4 *I* and *J*).

Mice that performed the $\dot{V}O_{2max}$ test were then subjected to an endurance-type protocol, during which animals ran from 20 to 100% of their maximal running speed. Evaluation of energy fuel utilization and oxygen consumption, specifically at moderate exercise intensities [i.e., 20 to 60% of maximal speed when muscle fat oxidation is at its highest (30, 31)] did not reveal any differences between genotypes (Fig. 4 *A* and *B*). Moreover, blood lactate levels were similarly increased in both genotypes at

exhaustion (Fig. 4*C*). Conversely, blood glucose values were significantly lower in MKO mice at exhaustion (Fig. 4*D*), which could result from their altered performance. Indeed, in line with their improved maximal running capacity, BDNF MKO animals demonstrated significantly greater endurance performance, running about 1.5 times the distance of CTRL mice (BDNF MKO: 2,708 m; CTRL: 1,862 m; $P = 0.015$) (Fig. 4 *F* and *G*). In summary, deletion of BDNF in mouse skeletal muscle confers greater resistance to fatigue during physical exercise without significantly affecting whole-body aerobic capacity and energy substrate utilization.

Lack of Muscle BDNF Promotes a Fast-to-Slow Transition in Glycolytic Muscles. Muscle fiber type and oxidative capacity are essential determinants of muscle contractile properties, endurance, and fatigue (32). Therefore, we assessed whether BDNF deletion was associated with a muscle fiber transformation. Fiber composition and CSA were unchanged in the oxidative soleus (SOL) muscle of MKO mice (*SI Appendix*, Fig. S5 *A–C*). In contrast, the proportion of type IIX fibers in both glycolytic TA and EDL muscles was significantly increased in MKO animals at the expense of type IIB fibers (Fig. 5 *A* and *B*). Importantly, type IIX fibers show characteristics intermediate to types IIA and IIB fibers (e.g., in terms of contraction velocities and resistance to fatigue as evaluated above) and succinate dehydrogenase activity—a mitochondrial enzyme involved in oxidative phosphorylation (33). Accordingly, we observed that muscles depleted of BDNF showed higher succinate dehydrogenase (SDH) activity-dependent staining (Fig. 5*C*). Of note, the higher proportion of type IIX fibers in both TA and EDL muscles of MKO mice was not associated with significant change in myofiber CSA (Fig. 5*D*).

To investigate whether other fiber type-specific genes were also affected by this transition from type IIB to IIX, we measured the expression of several key oxidative and glycolytic markers by qPCR. In line, the α-cardiac form of the actin gene (*Actc1*)—a major constituent of the contractile apparatus predominantly expressed in oxidative muscles (34)—was elevated in the absence of BDNF (Fig. 5*E*). Conversely, the glycolytic marker *troponin-C fast* (*Tnnc2*) and transcriptional regulators controlling glycolytic fiber identity, such as *Baf60c*/*Smarcd3* (35) and *Tbx15* (36), were down-regulated in MKOs (Fig. 5*E*). The higher proportion of type IIX fibers was, however, not associated with elevated expression of *Ppargc1b* (37) or increased mitochondrial transcript and mitochondrial DNA levels (*SI Appendix*, Fig. S5*D*). We also examined the level of transcripts encoding key sarcoplasmic calcium-regulatory proteins in muscles of MKO mice. In particular, the fast-type calcium-transporting ATPase *Atp2a1* (also called sarco/endoplasmic reticulum Ca^{2+}-ATPase 1 [*Serca1*]) was reduced, while the slow-type form *Atp2a2* (*Serca2*) was significantly increased (Fig. 5*F*). In contrast, both the fast-type calsequestrin 1 (*Casq1*) and the slow-type *Casq2* were elevated in the MKO animals (Fig. 5*F*). Additional transcripts encoding for regulators of fast fiber Ca^{2+} homeostasis (e.g., myoregulin [*Mrln*]—a repressor of SERCA activity expressed in fast fibers [38]—and ryanodine receptor [*RyR1*] and parvalbumin [*Pvalb*]—highly expressed in fast-contracting fibers that have a more developed sarcoplasmic reticulum [33]) equally showed significantly reduced expression levels in muscle cells depleted of BDNF (Fig. 5*F*). These results collectively demonstrate that muscle-derived BDNF depletion promotes a fast-to-slow transition in glycolytic muscles.

BDNF Overexpression Increases Fast-Type Gene Expression and Glycolytic Fibers. The effect of muscle BDNF deletion on fiber-type composition prompted us to investigate the consequence of enhanced BDNF expression in skeletal muscle of adult CTRL mice. To this aim, a plasmid-based gene delivery method was used to introduce either BDNF or an empty vector (EV) into the TA muscle by electroporation. *SI Appendix*, Fig. S6*A* depicts in vivo transfection efficiency of a pCAG-EGFP (enhanced green fluorescent protein) expression vector using our established parameters, demonstrating even muscle distribution of EGFP at 7 and 21 d postelectroporation. Importantly, when TA muscles

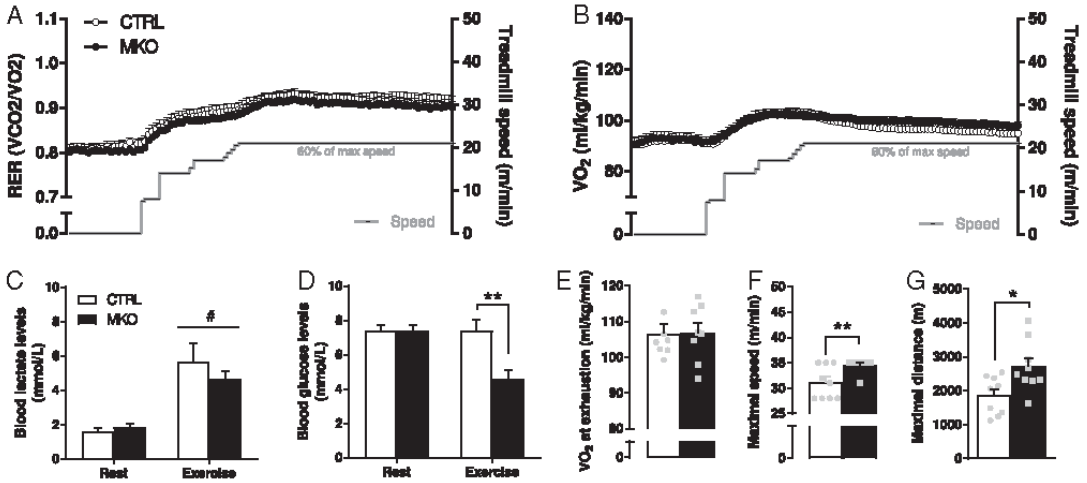

Fig. 4. BDNF MKO mice show improved running endurance capacity. (*A*) RER and (*B*) O_2 consumption as a function of speed in CTRL and MKO animals during endurance exercise challenge. Note that data in *A* and *B* are only depicted until a speed of 22 m/min (i.e., 60% of maximum speed). (*C*) Blood lactate and (*D*) glucose levels at rest and within 1 min after exhaustion. (*E*) Maximal O_2 consumption at exhaustion. (*F*) Maximal speed and (*G*) total distance reached at exhaustion. Results are expressed as mean ± SEM ($n = 9$ per genotype except in *A*, *B*, and *E*, where data from 1 CTRL and 1 MKO mouse could not be included due to O_2 artifacts during run acquisition). Unpaired Student's *t* test (*E–G*) and 2-way ANOVA followed by Sidak's multiple comparisons (*C* and *D*). $^*P < 0.05$; $^{**}P < 0.01$; $^{\#}$Significant difference ($P < 0.05$) between experimental conditions.

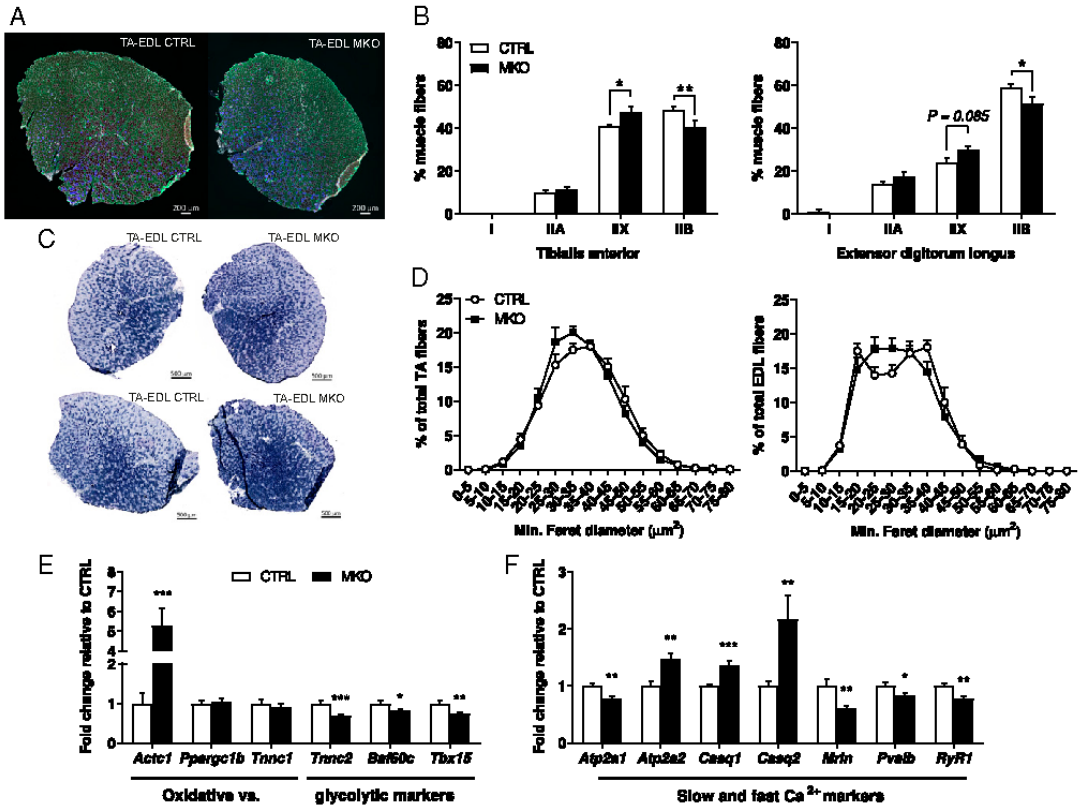

Fig. 5. Lack of BDNF leads to a type IIB to IIX transition in glycolytic muscles. (*A*) Representative fluorescence microscopy images illustrating the fiber-type composition in the TA-EDL muscle of CTRL and MKO animals. Corresponding color legend for fiber types: type I = red, type IIA = blue, type IIX = unstained (black), type IIB = green, and laminin = white. (Scale bar: 200 μm.) (*B*) Quantification of fiber-type content in (*Left*) TA and (*Right*) EDL muscles ($n = 5$ per genotype). Note that EDL and TA muscles were analyzed separately. (*C*) Representative SDH staining of TA-EDL muscles from different CTRL and MKO animals. (Scale bar: 500 μm.) (*D*) CSA based on minimal Feret's diameter of (*Left*) TA and (*Right*) EDL myofibers ($n = 5$ per genotype). Results are expressed as percentage (mean ± SEM). (*E* and *F*) Gene expression in CTRL and BDNF MKO GAS muscles. Expression values were determined by qPCR and normalized to *Hprt*. Data are shown as the average fold change ± SEM ($n = 12$ per genotype) relative to the expression in CTRL set to 1. Unpaired Student's *t* test (*E* and *F*) and 2-way ANOVA followed by Sidak's multiple comparisons (*B* and *D*). $^*P < 0.05$; $^{**}P < 0.01$; $^{***}P < 0.001$.

from CTRL mice were transfected with a BDNF-encoding vector, both pro- and mature forms of BDNF were detected 21 d after electrotransfer with 2 different antibodies (Fig. 6*A*). This clearly indicates that—alongside the drastic elevation of its transcript (Fig. 6*B*)—BDNF is further processed and cleaved in adult skeletal muscle.

Next, we found that BDNF elevation mirrored the consequences of BDNF deletion at the gene expression level. Specifically, there was a greater expression of glycolytic markers (e.g., *Serca1* and its coregulator *Mlm*) and of transcriptional mediators of fast fiber-type gene programs, such as *Baf60c* and *Tbx15* (Fig. 6 *B* and *C*). Because electroporation is known to produce significant damage in skeletal muscle leading to satellite cell activation and the formation of new fibers (39–41), we concomitantly determined myosin heavy-chain composition in both small new fibers (i.e., based on a CSA value < 20 μm^2), nearly absent in nonelectroporated TA muscle (Fig. 5*D*), and in larger fibers (CSA > 20 μm^2) of EV- and BDNF-electroporated muscles (Fig. 6*D*). Intriguingly, on BDNF overexpression, small myofibers had a significantly lower content of the type IIX myosin heavy-chain isoform alongside an elevation of the type IIB isoform (Fig. 6*E*). Thus, overexpression of BDNF is sufficient to induce fast-twitch markers and influence fiber-type composition in skeletal muscle.

Higher Muscle Mass, Strength, and Oxidative Fibers in Old BDNF MKO Mice. NMJ structure, muscle fiber type and contractile properties, fatigue resistance, and exercise capacity are all changed in young adult BDNF MKO animals. Incidentally, altered NT signaling at the neuromuscular interface is associated with the age-related decline of muscle mass and function (15, 16, 42). Moreover, there is an age-dependent decrease of both circulating BDNF and brain *TrkB* levels in humans (43, 44) and a likewise age-dependent reduction of both *Bdnf* and *TrkB* levels in the rodent brain (45–47). However, we could not find data on muscle *Bdnf* and *TrkB* expression in the aging context and have, therefore, compared their transcript levels in 6- vs. 24-mo-old CTRL animals. We did not find any change in regard to *Bdnf* and *TrkB* expression in the old muscle (Fig. 7*A*).

In a last set of experiments, we evaluated whether the lifelong deletion of muscle BDNF would further alter muscle physiology

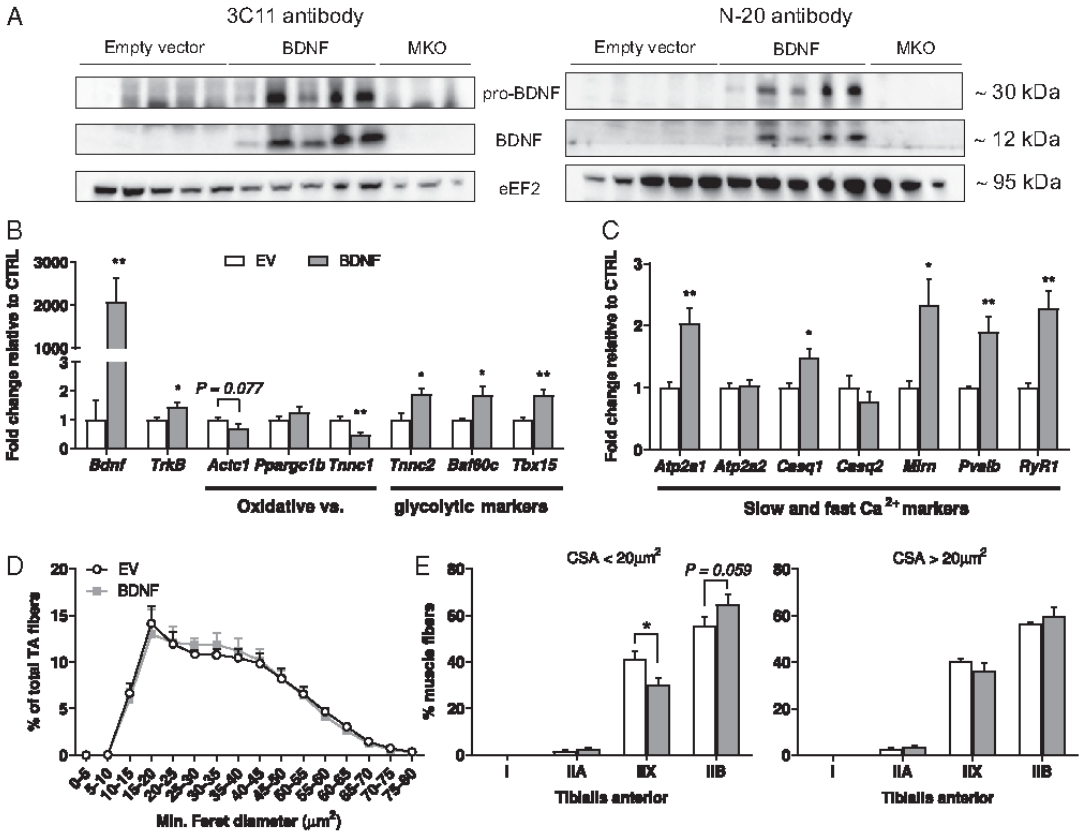

Fig. 6. BDNF influences skeletal muscle fiber-type specification. (*A*) Expression of BDNF protein in EV- and BDNF-electroporated TA muscles ($n = 5$ per condition) as determined by western blot. Note that muscle protein extracts from MKO animals were used as negative controls. (*B* and *C*) Gene expression in EV- and BDNF-electroporated TA muscles. Expression values were determined by qPCR and normalized to *Hprt*. Data are shown as the average fold change ± SEM ($n = 5$ per condition) relative to the expression in EV set to 1. (*D*) CSA based on minimal Feret's diameter of TA myofibers ($n = 5$ per genotype). (*E*) Fiber-type composition in small (*Left*) vs. large (*Right*) TA fibers ($n = 5$ per genotype). Results are expressed as percentage (mean ± SEM). Unpaired Student's *t* test (*B* and *C*) and 2-way ANOVA followed by Sidak's multiple comparisons (*E*). $^*P < 0.05$; $^{**}P < 0.01$.

in the aging context. Motor balance and coordination were unchanged in 24-mo-old MKO mice (Fig. 7 *B* and *C*). Likewise, old MKO animals demonstrated a running capacity comparable with their CTRL littermates (Fig. 7*D*). Old MKO mice, however, showed significantly higher grip strength in comparison with old CTRL mice (Fig. 7*E*). This was, furthermore, associated with significantly increased whole-body lean mass alongside elevated GAS and quadriceps hind limb muscle mass (Fig. 7 *F* and *G*). Finally, we found a higher SDH activity-dependent staining and a significantly increased proportion of type IIA fibers in TA muscles of 24-mo-old MKO mice (Fig. 7 *H* and *I*). Overall, these results suggest that lifelong expression of muscle BDNF is not required for the maintenance of neuromuscular function and that, conversely, the more oxidative phenotype of muscles lacking BDNF contributes to attenuation of some aspects of muscle aging.

Discussion

The trophic activity of BDNF and related NT family members is well recognized in the interaction between cells of the central nervous system (24, 48). In contrast, the regulation and function of BNDF in other cell types remains less understood. Here, we describe a hitherto unknown and surprising effect of skeletal muscle BNDF on the promotion of a fast-twitch glycolytic muscle fiber program using both loss- and gain-of-function approaches in vivo.

Our findings uncover BDNF as a myokine that promotes a glycolytic fiber phenotype; other factors, such as the insulin-like growth factor 2 (IGF2), have been associated with embryonic development of fast fibers (49), while IGF1 primarily promotes hypertrophy of fibers, with minimal effects on fiber-type distribution (50). In contrast, our data demonstrate that BDNF affects the gene program and fiber composition of glycolytic muscles without significantly altering muscle fiber CSA. It is, therefore, conceivable that BNDF cooperates with other factors (e.g., IGF1) in the adaptation of skeletal muscle to resistance training. Of note, the seemingly beneficial effect of muscle-specific deletion of BDNF on different parameters (e.g., fatigue resistance and endurance capacity) might be offset in other contexts. It thus will be interesting to test the performance of the BDNF MKO animals in other paradigms where adequate function of type IIB fibers is required (e.g., maximal strength or resistance

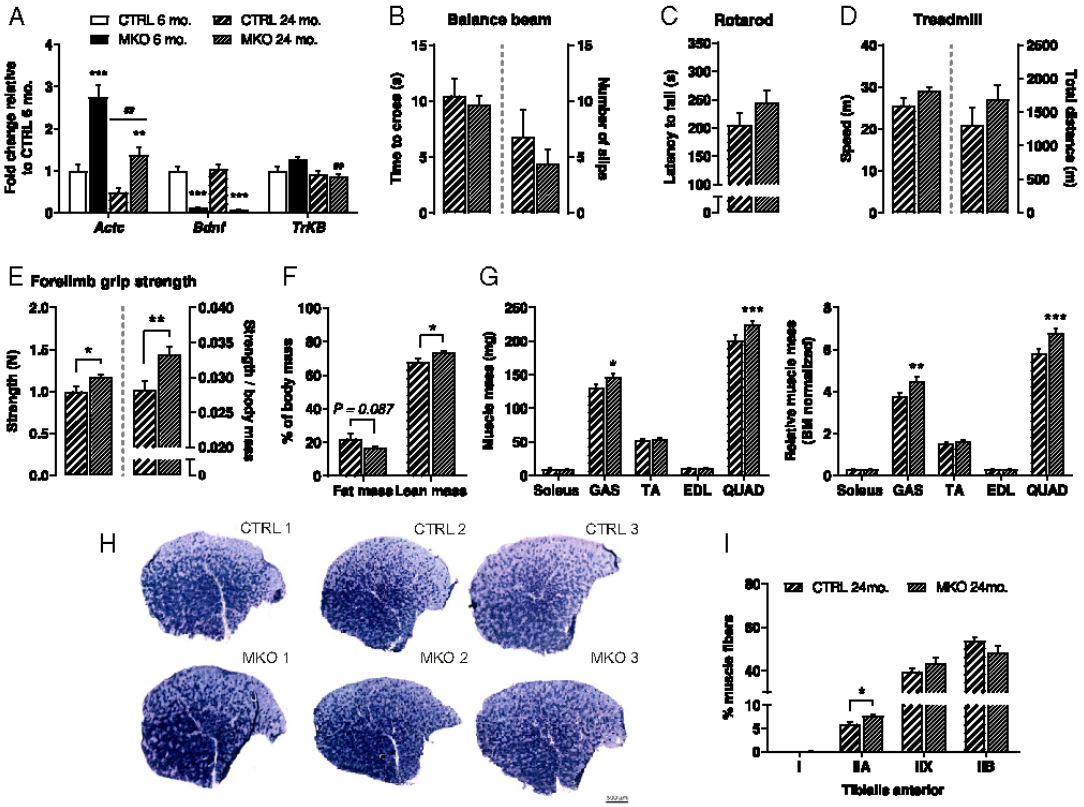

Fig. 7. The 24-mo-old BDNF MKO mice show higher muscle mass, grip strength, and oxidative fiber number. (*A*) Gene expression in young ($n = 6$ per genotype) and old ($n = 7$ to 9 per genotype) CTRL and BDNF MKO GAS muscles. Expression values were determined by qPCR and normalized to *Hprt*. Data are shown as the average foldchange ± SEM relative to the expression in young CTRL set to 1. (*B*) Balance beam (CTRL $n = 9$, MKO $n = 11$), (*C*) rotarod (CTRL $n = 9$, MKO $n = 12$), and (*D*) treadmill running data (CTRL $n = 8$, MKO $n = 9$). (*E*) Absolute and body mass-normalized forelimb muscle strength as determined by grip test (CTRL $n = 9$, MKO $n = 12$). Note that experiments were performed from the age of 23 mo and that some mice from this specific cohort spontaneously died between the start of our behavioral investigation and their euthanasia. (*F*) Normalized lean and fat mass and (*G*) absolute vs. normalized muscle mass from 24-mo-old CTRL ($n = 7$) and MKO ($n = 9$) animals just before euthanasia. QUAD, quadricep. (*H*) Representative SDH staining of TA muscles from different old CTRL and MKO animals. Note that sections with the same number originate from the same slide. (Scale bar: 500 μm.). (*I*) Evaluation of TA muscle fiber composition of old CTRL and MKO animals ($n = 6$ per genotype from randomly chosen muscles). Results are expressed as mean ± SEM. Unpaired Student's *t* test (*B*–*E*) and 2-way ANOVA followed by Sidak's multiple comparisons (*A*, *F*, *G*, and *I*). $^{*}P < 0.05$; $^{**}P < 0.01$; $^{***}P < 0.001$; $^{\#\#}$Significant difference ($P < 0.01$) between conditions.

exercise performance). Nevertheless, other pathological settings could profit from a reduction or ablation of muscle BNDF as evidenced by the improvement of lean mass, muscle weight, and grip strength in old mice.

Contrary to postnatal and whole-body disruption of TrkB (6, 15, 25), muscle-specific BDNF deletion did not adversely affect neuromuscular structure and function. Furthermore, even though we did not directly assess NMJ morphology and functionality in old MKO animals, the fact that these mice displayed similar, if not greater, muscle force, motor balance, and coordination likely rules out an essential role for postsynaptic BDNF expression in the lifelong maintenance of the motor unit. Finally, our observations of unchanged substrate utilization on BDNF deletion are contrasting with the proposed role of BDNF as an exercise-induced myokine to regulate fatty acid oxidation (17). Whether this difference stems from diverging effects of long-term deletion (these results) vs. the transient overexpression and the relatively modest induction of BDNF after acute exercise bouts (17) remains unclear. In any case, in contrast to its key function in other central and peripheral cells controlling energy homeostasis (23, 24), BDNF depletion did not alter systemic energy homeostasis. One limitation of this study, however, is the use of the HSA-Cre transgene to excise BDNF, leading to Cre expression from E9.5 in somitic cells committed to the myogenic lineage (19, 20). It thus would be interesting to initiate muscle BDNF deletion at a later stage to rule out the possibility of any developmental compensation (51).

Some of the characteristics of muscle lacking BDNF (e.g., higher SDH activity, slower contraction and relaxation times, and decreased fatigability rate) are found in endurance-trained muscle (52). However, MKO mice did not show increased spontaneous locomotor activity but rather, showed decreased spontaneous locomotor activity—as some other mouse models

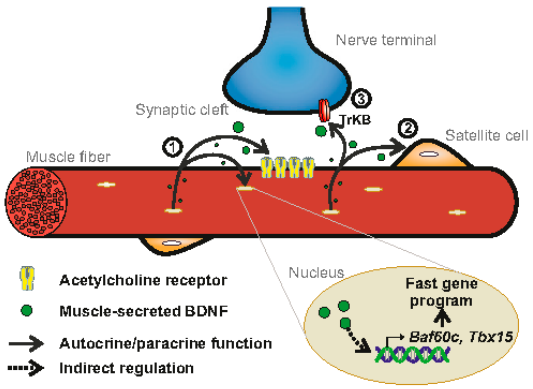

Fig. 8. Proposed model by which BDNF signaling regulates neuromuscular physiology. (*1*) BDNF could act as an autocrine factor to influence the expression of transcriptional regulators involved in fast-twitch muscle-specific gene expression or the expression of synaptic proteins involved in AChR clustering. (*2*) As a paracrine factor, BDNF could regulate the differentiation of satellite cells into slow vs. fast myofibers. (*3*) BDNF might also affect myofiber identity and motor end plate structure indirectly (e.g., by modulating the activity of the TrkB receptors present in nerve terminals of motor neurons).

exhibiting a slow-type muscle transition (36, 53)—ruling out physical activity as a primary cause of the fiber-type change. Intriguingly, there is a clear relationship between the expression of the fast IIB myosin isoform and BDNF during early postnatal development, when muscles are subjected to distinct programs of myosin isoform transitions influenced, for example, by functional demand or motor innervation (33, 54). For instance, the fast IIB myosin isoform rises in both mouse EDL and GAS muscles from day 5 until day 90 after birth (54). BDNF protein also gradually increases in glycolytic muscles of rodent neonates but not in the SOL (27, 55). Besides, combined administration of a ciliary neurotrophic factor (CNTF)–BDNF mixture after neonatal sciatic nerve crush injury can rescue a small fraction (i.e., 5%) of type IIB fibers in the EDL muscle (27). Mechanistically, it is not clear how BNDF controls the type IIB fiber program. Future studies will aim at elucidating the BDNF-activated signaling pathways that ultimately result in a transcriptional induction of *Baf60c* and *Tbx15*, 2 transcriptional regulators involved in fast-twitch muscle-specific gene expression (35, 36). BDNF might also affect these regulators indirectly [e.g., by modulating the activity of the TrkB receptors present in nerve terminals of motor neurons (5, 6)] to mediate morphological remodeling of the NMJ. In that regard, other approaches to overexpress BDNF [e.g., the tetracycline-inducible system (56)] could not only circumvent the significant changes induced by muscle electroporation but also, allow the careful functional and structural evaluation of the effect of muscle BDNF elevation at different developmental stages on the neuromuscular system. Finally, the role of extrinsic signals, such as muscle-derived BDNF, in influencing the commitment of myoblast nuclei to particular gene expression programs and thus, the differentiation of these cells into slow vs. fast myofibers needs additional investigation (Fig. 8).

In summary, we report here that BDNF is a myokine that regulates glycolytic muscle fiber-type identity. Muscle-specific loss of BDNF confers beneficial effects on endurance and mitigates loss of muscle mass and function in sarcopenia. Thus, strategies aimed at neutralizing muscle BDNF might be of interest in certain pathologies. Inversely, our findings of BNDF to promote type IIB fiber programs could be leveraged in diseases where the function of glycolytic muscle fibers is compromised or increased fast-twitch muscle fiber activity is desirable. For example, circulating BDNF levels are associated with type 2 diabetes (16, 57, 58), and chronic BDNF administration enhances glucose uptake in muscle cells (59), which could be, at least in part, mediated by a higher proportion of glycolytic type IIB muscle fibers. Moreover, BDNF may also modulate the glycolytic capabilities of muscle fibers by mechanisms similar to the fibroblast growth factor 21 myokine (60, 61). Lastly, in light of the susceptibility of certain muscle fibers to muscle diseases [e.g., Duchenne muscular dystrophy (62)] and the positive effect of essential determinants of fiber identity on muscle disease progression (63, 64), our findings warrant additional studies to determine whether modulating the activity of BDNF represents an effective therapeutic strategy to delay or even prevent muscle wasting disorders.

Materials and Methods

Animals. *HSA-Cre* transgenic mice were purchased from the Jackson Laboratory (stock no. 006149). $Bdnf^{flox/flox}$ mice were a gift from Yves-Alain Barde, Cardiff University, Wales, United Kingdom and have been previously characterized (ref. 65 has mutation and genotyping details). Mice were maintained on a C57BL/6J genetic background in the animal facility of the Biozentrum (University of Basel) in a temperature-controlled room (21 °C to 22 °C) under a 12:12-h light/dark cycle (lights on at 6:00 AM). Unless specifically mentioned, all experiments were performed in young adult male mice (3 to 4 mo old) housed in groups of 3 to 5 in standard cages with enrichment and free access to regular chow diet (3432; KLIBA NAFAG) and water. All experiments were performed in accordance with the principles of the Basel Declaration and with Federal and Cantonal Laws regulating the care and use of experimental animals in Switzerland as well as institutional guidelines of the Biozentrum and the University of Basel. The protocol with all methods described here was approved by the Kantonales Veterinäramt of the Kanton Basel-Stadt under consideration of the wellbeing of the animals and the 3R (replacement, reduction, and refinement) principle.

Statistical Analysis. No statistical methods were used to predetermine sample size. The *n* number used per genotype for each experiment is indicated in the figure legends. Data are expressed as mean ± SEM and were represented and analyzed with the GraphPad Prism 7.0 software. Comparisons between 2 groups were performed with unpaired Student's *t* test. For assessment between 2 independent variables, 2-way ANOVA was used followed by Sidak's multiple comparisons test if the interaction term was significant. A value of $P < 0.05$ was considered statistically significant. Symbols used to indicate the different degrees of statistical significance are as follow: $^{*}P < 0.05$, $^{**}P < 0.01$, and $^{***}P < 0.001$ between mouse genotypes and $^{\#}P < 0.05$ and $^{\#\#}P < 0.01$ between experimental conditions.

Details about body composition analysis; comprehensive laboratory animal monitoring system, glucose homeostasis, body temperature and locomotor activity recordings, gait analysis, indirect calorimetry coupled to treadmill exercise, repetitive nerve stimulation EMG, muscle force and fatigue measurements, muscle electroporation, tissue collection, enzyme-linked immunosorbent assay, histology and immunohistochemistry, slide imaging and image analysis, muscle RNA extraction and real-time qPCR, protein extraction and western blot, mitochondrial DNA number, laser capture microdissection, electrophysiology, behavioral phenotyping of old mice, and antibodies and reagents are provided in *SI Appendix, Supplementary Materials and Methods*. Primer pairs and TaqMan probes used in this study are listed in *SI Appendix*, Table S4.

ACKNOWLEDGMENTS. We thank the Imaging Core Facility of the Biozentrum for their technical help with imaging procedures and data analysis. We also thank Prof. Yves-Alain Barde (Cardiff University, Wales, United Kingdom) for providing the founder $Bdnf^{flox/flox}$ mice. L.T. is supported by Spanish Ministry of Economy and Competitiveness/European Regional Development Fund BFU2016-78934-P. The work in the laboratory of C.H. is funded by the Swiss National Science Foundation, European Research Council Consolidator Grant 616830-MUSCLE_NET, Swiss Cancer Research Grant KFS-3733-08-2015, the Swiss Society for Research on Muscle Diseases, SystemsX.ch, the Novartis Stiftung für Medizinisch-Biologische Forschung, and the University of Basel.

1. M. V. Chao, Neurotrophins and their receptors: A convergence point for many signalling pathways. *Nat. Rev. Neurosci.* **4**, 299–309 (2003).
2. E. J. Huang, L. F. Reichardt, Trk receptors: Roles in neuronal signal transduction. *Annu. Rev. Biochem.* **72**, 609–642 (2003).
3. G. Chevrel, R. Hohlfeld, M. Sendtner, The role of neurotrophins in muscle under physiological and pathological conditions. *Muscle Nerve* **33**, 462–476 (2006).
4. B. Kablar, M. A. Rudnicki, Development in the absence of skeletal muscle results in the sequential ablation of motor neurons from the spinal cord to the brain. *Dev. Biol.* **208**, 93–109 (1999).
5. N. García *et al.*, The interaction between tropomyosin-related kinase B receptors and presynaptic muscarinic receptors modulates transmitter release in adult rodent motor nerve terminals. *J. Neurosci.* **30**, 16514–16522 (2010).
6. M. Gonzalez *et al.*, Disruption of Trkb-mediated signaling induces disassembly of postsynaptic receptor clusters at neuromuscular junctions. *Neuron* **24**, 567–583 (1999).
7. L. B. Tovar-Y-Romo, U. N. Ramírez-Jarquín, R. Lazo-Gómez, R. Tapia, Trophic factors as modulators of motor neuron physiology and survival: Implications for ALS therapy. *Front. Cell. Neurosci.* **8**, 61 (2014).
8. V. E. Koliatsos, R. E. Clatterbuck, J. W. Winslow, M. H. Cayouette, D. L. Price, Evidence that brain-derived neurotrophic factor is a trophic factor for motor neurons in vivo. *Neuron* **10**, 359–367 (1993).
9. S. Capsoni, F. Ruberti, E. Di Daniel, A. Cattaneo, Muscular dystrophy in adult and aged anti-NGF transgenic mice resembles an inclusion body myopathy. *J. Neurosci. Res.* **59**, 553–560 (2000).
10. P. Ernfors, K. F. Lee, J. Kucera, R. Jaenisch, Lack of neurotrophin-3 leads to deficiencies in the peripheral nervous system and loss of limb proprioceptive afferents. *Cell* **77**, 503–512 (1994).
11. R. Klein *et al.*, Disruption of the neurotrophin-3 receptor gene trkC eliminates la muscle afferents and results in abnormal movements. *Nature* **368**, 249–251 (1994).
12. N. Belluardo *et al.*, Neuromuscular junction disassembly and muscle fatigue in mice lacking neurotrophin-4. *Mol. Cell. Neurosci.* **18**, 56–67 (2001).
13. D. G. Wells, B. A. McKechnie, S. Kelkar, J. R. Fallon, Neurotrophins regulate agrin-induced postsynaptic differentiation. *Proc. Natl. Acad. Sci. U.S.A.* **96**, 1112–1117 (1999).
14. H. S. Je *et al.*, ProBDNF and mature BDNF as punishment and reward signals for synapse elimination at mouse neuromuscular junctions. *J. Neurosci.* **33**, 9957–9962 (2013).
15. S. A. Kulakowski, S. D. Parker, K. E. Personius, Reduced TrkB expression results in precocious age-like changes in neuromuscular structure, neurotransmission, and muscle function. *J. Appl. Physiol.* **111**, 844–852 (2011).
16. K. Sakuma, A. Yamaguchi, The recent understanding of the neurotrophin's role in skeletal muscle adaptation. *J. Biomed. Biotechnol.* **2011**, 201696 (2011).
17. V. B. Matthews *et al.*, Brain-derived neurotrophic factor is produced by skeletal muscle cells in response to contraction and enhances fat oxidation via activation of AMP-activated protein kinase. *Diabetologia* **52**, 1409–1418 (2009).
18. C. Clow, B. J. Jasmin, Brain-derived neurotrophic factor regulates satellite cell differentiation and skeltal muscle regeneration. *Mol. Biol. Cell* **21**, 2182–2190 (2010).
19. M. Leu *et al.*, Erbb2 regulates neuromuscular synapse formation and is essential for muscle spindle development. *Development* **130**, 2291–2301 (2003).
20. M. Schwander *et al.*, β1 integrins regulate myoblast fusion and sarcomere assembly. *Dev. Cell* **4**, 673–685 (2003).
21. P. Chacón-Fernández *et al.*, Brain-derived neurotrophic factor in megakaryocytes. *J. Biol. Chem.* **291**, 9872–9881 (2016).
22. A. B. Klein *et al.*, Blood BDNF concentrations reflect brain-tissue BDNF levels across species. *Int. J. Neuropsychopharmacol.* **14**, 347–353 (2011).
23. S. Bathina, U. N. Das, Brain-derived neurotrophic factor and its clinical implications. *Arch. Med. Sci.* **11**, 1164–1178 (2015).
24. E. E. Noble, C. J. Billington, C. M. Kotz, C. Wang, The lighter side of BDNF. *Am. J. Physiol. Regul. Integr. Comp. Physiol.* **300**, R1053–R1069 (2011).
25. C. B. Mantilla *et al.*, TrkB kinase activity maintains synaptic function and structural integrity at adult neuromuscular junctions. *J. Appl. Physiol.* **117**, 910–920 (2014).
26. T. M. DeChiara *et al.*, The receptor tyrosine kinase MuSK is required for neuromuscular junction formation in vivo. *Cell* **85**, 501–512 (1996).
27. K. Mousavi, B. J. Jasmin, BDNF is expressed in skeletal muscle satellite cells and inhibits myogenic differentiation. *J. Neurosci.* **26**, 5739–5749 (2006).
28. A.-S. Arnold *et al.*, Morphological and functional remodelling of the neuromuscular junction by skeletal muscle PGC-1α. *Nat. Commun.* **5**, 3569 (2014).
29. R. Tejero, M. Lopez-Manzaneda, S. Arumugam, L. Tabares, Synaptotagmin-2, and -1, linked to neurotransmission impairment and vulnerability in Spinal Muscular Atrophy. *Hum. Mol. Genet.* **25**, 4703–4716 (2016).
30. J. Jeppesen, B. Kiens, Regulation and limitations to fatty acid oxidation during exercise. *J. Physiol.* **590**, 1059–1068 (2012).
31. J. A. Romijn *et al.*, Regulation of endogenous fat and carbohydrate metabolism in relation to exercise intensity and duration. *Am. J. Physiol.* **265**, E380–E391 (1993).
32. J. R. Zierath, J. A. Hawley, Skeletal muscle fiber type: Influence on contractile and metabolic properties. *PLoS Biol.* **2**, e348 (2004).
33. S. Schiaffino, C. Reggiani, Fiber types in mammalian skeletal muscles. *Physiol. Rev.* **91**, 1447–1531 (2011).
34. S. Schiaffino, C. Reggiani, Molecular diversity of myofibrillar proteins: Gene regulation and functional significance. *Physiol. Rev.* **76**, 371–423 (1996).
35. Z.-X. Meng *et al.*, Baf60c drives glycolytic metabolism in the muscle and improves systemic glucose homeostasis through Deptor-mediated Akt activation. *Nat. Med.* **19**, 640–645 (2013).
36. K. Y. Lee *et al.*, Tbx15 controls skeletal muscle fibre-type determination and muscle metabolism. *Nat. Commun.* **6**, 8054 (2015).
37. Z. Arany *et al.*, The transcriptional coactivator PGC-1β drives the formation of oxidative type IIX fibers in skeletal muscle. *Cell Metab.* **5**, 35–46 (2007).
38. D. M. Anderson *et al.*, A micropeptide encoded by a putative long noncoding RNA regulates muscle performance. *Cell* **160**, 595–606 (2015).
39. C. Trollet, D. Scherman, P. Bigey, "Delivery of DNA into muscle for treating systemic diseases: Advantages and challenges" in *Electroporation Protocols: Preclinical and Clinical Gene Medicine*, S. Li, Ed. (Humana Press, Totowa, NJ, 2008), pp. 199–214.
40. J. D. Schertzer, D. R. Plant, G. S. Lynch, Optimizing plasmid-based gene transfer for investigating skeletal muscle structure and function. *Mol. Ther.* **13**, 795–803 (2006).
41. M. J. Molnar *et al.*, Factors influencing the efficacy, longevity, and safety of electroporation-assisted plasmid-based gene transfer into mouse muscles. *Mol. Ther.* **10**, 447–455 (2004).
42. M. Gonzalez-Freire, R. de Cabo, S. A. Studenski, L. Ferrucci, The neuromuscular junction: Aging at the crossroad between nerves and muscle. *Front. Aging Neurosci.* **6**, 208 (2014).
43. K. I. Erickson *et al.*, Brain-derived neurotrophic factor is associated with age-related decline in hippocampal volume. *J. Neurosci.* **30**, 5368–5375 (2010).
44. M. J. Webster, M. M. Herman, J. E. Kleinman, C. Shannon Weickert, BDNF and trkB mRNA expression in the hippocampus and temporal cortex during the human lifespan. *Gene Expr. Patterns* **6**, 941–951 (2006).
45. M. Silhol, V. Bonnichon, F. Rage, L. Tapia-Arancibia, Age-related changes in brain-derived neurotrophic factor and tyrosine kinase receptor isoforms in the hippocampus and hypothalamus in male rats. *Neuroscience* **132**, 613–624 (2005).
46. E. Palomer *et al.*, Aging triggers a repressive Chromatin state at Bdnf promoters in hippocampal neurons. *Cell Rep.* **16**, 2889–2900 (2016).
47. F. Rage, M. Silhol, F. Binamé, S. Arancibia, L. Tapia-Arancibia, Effect of aging on the expression of BDNF and TrkB isoforms in rat pituitary. *Neurobiol. Aging* **28**, 1088–1098 (2007).
48. E. J. Huang, L. F. Reichardt, Neurotrophins: Roles in neuronal development and function. *Annu. Rev. Neurosci.* **24**, 677–736 (2001).
49. D. Merrick, T. Ting, L. K. Stadler, J. Smith, A role for Insulin-like growth factor 2 in specification of the fast skeletal muscle fibre. *BMC Dev. Biol.* **7**, 65 (2007).
50. A. C. Paul, N. Rosenthal, Different modes of hypertrophy in skeletal muscle fibers. *J. Cell Biol.* **156**, 751–760 (2002).
51. J. J. McCarthy, R. Srikuea, T. J. Kirby, C. A. Peterson, K. A. Esser, Inducible Cre transgenic mouse strain for skeletal muscle-specific gene targeting. *Skelet. Muscle* **2**, 8 (2012).
52. J. O. Holloszy, F. W. Booth, Biochemical adaptations to endurance exercise in muscle. *Annu. Rev. Physiol.* **38**, 273–291 (1976).
53. P. Klover, W. Chen, B.-M. Zhu, L. Hennighausen, Skeletal muscle growth and fiber composition in mice are regulated through the transcription factors STAT5a/b: Linking growth hormone to the androgen receptor. *FASEB J.* **23**, 3140–3148 (2009).
54. O. Agbulut, P. Noirez, F. Beaumont, G. Butler-Browne, Myosin heavy chain isoforms in postnatal muscle development of mice. *Biol. Cell* **95**, 399–406 (2003).
55. M. Nagano, H. Suzuki, Quantitative analyses of expression of GDNF and neurotrophins during postnatal development in rat skeletal muscles. *Neurosci. Res.* **45**, 391–399 (2003).
56. M. A. Grill *et al.*, Tetracycline-inducible system for regulation of skeletal muscle-specific gene expression in transgenic mice. *Transgenic Res.* **12**, 33–43 (2003).
57. K. S. Krabbe *et al.*, Brain-derived neurotrophic factor (BDNF) and type 2 diabetes. *Diabetologia* **50**, 431–438 (2007).
58. K. Marosi, M. P. Mattson, BDNF mediates adaptive brain and body responses to energetic challenges. *Trends Endocrinol. Metab.* **25**, 89–98 (2014).
59. M. Yamanaka *et al.*, Brain-derived neurotrophic factor enhances glucose utilization in peripheral tissues of diabetic mice. *Diabetes Obes. Metab.* **9**, 59–64 (2007).
60. F. L. Mashili *et al.*, Direct effects of FGF21 on glucose uptake in human skeletal muscle: Implications for type 2 diabetes and obesity. *Diabetes Metab. Res. Rev.* **27**, 286–297 (2011).
61. Y. Izumiya *et al.*, FGF21 is an Akt-regulated myokine. *FEBS Lett.* **582**, 3805–3810 (2008).
62. J. Talbot, L. Maves, Skeletal muscle fiber type: Using insights from muscle developmental biology to dissect targets for susceptibility and resistance to muscle disease. *Wiley Interdiscip. Rev. Dev. Biol.* **5**, 518–534 (2016).
63. C. Handschin *et al.*, PGC-1alpha regulates the neuromuscular junction program and ameliorates Duchenne muscular dystrophy. *Genes Dev.* **21**, 770–783 (2007).
64. V. Ljubicic *et al.*, Chronic AMPK activation evokes the slow, oxidative myogenic program and triggers beneficial adaptations in mdx mouse skeletal muscle. *Hum. Mol. Genet.* **20**, 3478–3493 (2011).
65. S. Rauskolb *et al.*, Global deprivation of brain-derived neurotrophic factor in the CNS reveals an area-specific requirement for dendritic growth. *J. Neurosci.* **30**, 1739–1749 (2010).

8 Acknowledgments

First, I would like to thank my supervisor Prof. Dr. Christoph Handschin for granting me the opportunity to perform my PhD thesis in his laboratory. You have supported and encouraged me to do my very best. You always had an open door and listened to each and every of my issues, provided critical feedback and helped me navigate the world of science. I would like to thank all of my present and former co-workers and lab members for their tremendous support and encouragement. I thank Dr. Shuo Lin, Dr. Daniel J. Ham, Dr. Perrine Castets and Dr. Anastasiya Börsch for their helpful advice and instruction. Very special thanks go to Dr. Fabienne Battilana, who shared the small lab with me for all of these years and honestly was the best lab mate I could have ever wished for. We shared all of the ups and downs a PhD brings with it, listened to great music together and we always had the best conversations, be it about life, science, or philosophy. Fabienne, I thank you for always making the atmosphere in and outside the lab the very best possible. Thanks for your support, your inputs, your criticism, and your advice! Special thanks go to Dr. Julien Delezie, who always provided honest and insightful feedback and really sparked my passion for science. I thank Dr. Regula Furrer and Dr. Joaquin Pérez-Schindler who helped me with my experiments and provided insightful inputs in and outside of meetings. I would also like to express my gratitude to the core facilities of the Biozentrum, especially the IMCF, PCF, Research IT, and the workshop, all of which provided me with tremendous help in my research efforts. Furthermore, I would like to thank the D-BSSE, especially Dr. Christian Beisel and Katja Eschbach for their help with all of my next-generation sequencing needs. I would like to thank Prof. Dr. Markus A. Rüegg and Dr. Mara Fornaro for joining my PhD advisory committee and providing critical feedback.

Special thanks goes to all my friends and family who supported me throughout my PhD, you made the bad times bearable and the good times even more enjoyable! Finally, I am grateful for all of the support, encouragement, and understanding of Dominique Keller, who accompanied me all throughout this exciting journey. Thank you for always being there for me. I would not have succeeded without you!